The Quantum and Stochastic Toolbox: xSPDE4

May 2, 2024

PRELIMINARY DOCUMENTATION

Centre for Quantum Science and Technology Theory, Swinburne University of Technology, Melbourne, Victoria, Australia.

Contents

1. Introduction

xSPDE is an eXtensible Stochastic Partial Differential Equation solver.

The xSPDE toolbox treats stochastic partial and ordinary differential equations, with applications in biology, chemistry, engineering, medicine, physics and quantum technologies. It computes statistical averages, including time-step and/or sampling error estimation. xSPDE can provide higher order convergence, Fourier spectra and probability densities. The toolbox has graphical output and χ^2 statistics, as well as weighted, projected, or forward-backward equations. It can generate input-output quantum spectra. All equations may have independent periodic, Dirichlet, and Neumann or Robin boundary conditions in any dimension, for any vector field component, and at either end of any interval.

xSPDE has functions that can numerically solve both ordinary and partial differential stochastic equations of any type, obtaining correlations, probabilities and averages. There are many equations of this type [1–5] in physics, chemistry, engineering, biology, medicine, and finance. The toolbox has a core treating stochastic differential equations, with averages, probability distributions and full error estimates. There are stochastic extensions treating applications to partial differential equations, projected equations, quantum stochastic equations, master equations and quantum phase-space simulations.

Previous applications are in physics and quantum technology [6–25], but the code has general applicability. The emphasis in xSPDE is on combining a simple user interface with a wide range of useful functions, including the essential features of averaging and global error estimates. The code enables an efficient use memory and parallelism, which is vital for large stochastic models, and it is able to be further extended if needed.

The extensible structure of the code-base permits drop-in replacements of the algorithms. Different simulations can be carried out sequentially. This models different stages in an experiment or simulated environment. It can be used with or without noise terms, and can use a range of either built-in or user defined integration algorithms. This user guide describes xSPDE4, which is an improved version of earlier toolboxes [26, 27].

xSPDE calculates and plots averages and probabilities of arbitrary functions of any number of complex or real fields, as well as Fourier transforms in time or space with any given dimensionality. Importantly, it gives error estimates for both the discretization and sampling error, but the algorithm, the step-size and the number of samples used is up to the user to control to obtain the required error levels.

Ordinary and stochastic differential equations of many types can be treated numerically [28, 29], including stochastic partial differential equations with space dependence [30]. Comparative χ^2 statistical tests are available. Additional libraries exist for projected, forward-backward, and weighted equations.

The algorithms included are designed to be useful and fast in many practical applications. Higher order convergence is obtained through order extrapolation. This allows higher-order convergence to be realized in a uniform way. More complex higher-order algorithms are known [29, 31], which can be included if preferred, as the code is extensible.

The code can be used interactively or in batch mode. All graphs, data, and input parameters, including default values, can be stored permanently using standard filetypes. It has a fully integrated graphics program, xGRAPH. This is able to handle data of any dimensions, with multiple types of graphical output, error-bars and comparisons.

xSPDE supports parallelism at both vector instruction and multiple core level using array and parallel loop syntax. This version is Octave/Matlab based. Matlab is a commercial product, GNU Octave [32] is free and open-source. They each have excellent user interfaces and reliable implementations. Full parallel operation currently requires the Matlab parallel toolbox.

Chapters 2 and 5 give background information. Readers who are simply interested in how to use the code can go directly to section 6.

Chapter 2 has definitions and notations for stochastic differential equations (SDEs). This is useful for understanding later sections. The section includes Ito and Stratonovich calculus, probability distributions and Fokker-Planck equations. It also explains and defines the Fourier input-output spectra used in quantum technology.

Chapter 5 gives the concepts of stochastic partial differential equations (SPDEs). It includes details of spectral methods and the interaction picture approach. It has an explanation of how Fourier transforms and discrete sine or cosine transforms are implemented. It also explains how boundary conditions can be implemented using finite differences.

Chapter 6 describes the numerical solution of SDEs with xSPDE. This includes an explanation of the user interface, how to input parameters and equations, how to define the output in terms of functional averages or probabilities, and how to define and access auxiliary fields and noises. This chapter uses the default algorithms, and a more detailed explanation is given in chapter 9.

In Chapter 8, the practical approach to solving stochastic partial differential equations with xSPDE is explained. The techniques used are an extension of the previous one, so a thorough understanding of chapter 6 is strongly recommended.

Chapter 9 outlines the integration algorithms used in the manual. It includes a number of extended integration libraries, applicable to more specialized problems. This chapter also outlines how integration errors, including time-step and stochastic errors, can be estimated and displayed.

Chapter 10 provides a reference for the details of the internals as well as a comprehensive explanation of the input parameters useful in xSPDE simulations. This explains how to create projects with separated computation and graphics, as well as workflow and data storage. It also provides an extensive description of the visualization aspects of xSPDE, using the integrated xGRAPH function, which includes an automatic 'cascade' of graphic output where high dimensional data is reduced to lower dimensional, visualizable data through projections.

Input parameters related to this are described as well. Data can also be graphed externally or stored for later analysis if preferred. Both average and raw trajectory data can be stored. However, the storage of raw data is generally not recommended, due to the large storage requirements. Additional examples in Chapter 11 demonstrate how to obtain parametric plots against input parameters. Plots of one component value against another can be graphed. A function that analyses convergence rates is also available.

Future implementations will include Julia versions, which are under development and testing.

See: **www.github.com/peterddrummond/xspde_matlab.** For those familiar with earlier versions, a list of the main xSPDE changes since the documentation of the previously published version (v3.44) [26, 27] is as follows:

1. Cell arrays for multiple variables with differing spatial grids
2. Error-checking outputs with both maximum and RMS error estimates
3. Quantum stochastic Schrödinger equations
4. Integration of master equations
5. Jump algorithms, in addition to Gaussian noise methods
6. DST and DCT spectral methods for SPDEs with non-zero boundaries

xSPDE is distributed with no guarantee, under an open-source license. Contributions and bug reports are welcome. An alternative approach to SPDEs [33, 34] is available in C++ at http://www.xmds.org/.

Part I.

Fundamental Theory

2. SDE theory

This chapter describes the basics of stochastic differential equation (SDE) theory, in order to explain the background to the numerical methods.

2.1. General form

A stochastic differential equation (SDE) is an equation with random noise terms. These were introduced by Langevin to treat small particles in fluids [3], and extended by Wiener, Ito and Stratonovich [35–37]. The theory and its applications to biology, chemistry, engineering, economics, physics, meteorology and other disciplines are treated in many texts [1, 2, 4, 38–40].

An ordinary stochastic differential equation in one time dimension is,

$$\frac{\partial \mathbf{a}}{\partial t} = \mathbf{A}\left(\mathbf{a}, t\right) + \underline{\mathbf{B}}\left(\mathbf{a}, t\right) \cdot \boldsymbol{\xi}(t)\,. \tag{2.1}$$

Here $\mathbf{a}$ is a real or complex vector, $\mathbf{A}$ is a vector function, $\underline{\mathbf{B}}$ a matrix function and $\mathbf{w}$ is usually a delta-correlated real Gaussian noise vector such that:

$$\left\langle \xi_i\left(t\right) \xi_j\left(t'\right) \right\rangle \quad = \quad \delta\left(t - t'\right) \delta_{ij}. \tag{2.2}$$

One can also have non-Gaussian noise or noise that is not delta-correlated. Although these are somewhat less commonly treated, these alternatives are often found in real applications.

2.1.1. Observables

In all cases, there are multiple independent trajectories, and one is interested in probabilistic averages, where the unweighted average of an observable $\mathbf{O}\left(\mathbf{a}\right)$, for N_s trajectories $\mathbf{a}^{(n)}$ is:

$$\left\langle \mathbf{O} \right\rangle_{N_s} \quad = \quad \frac{1}{N_s} \sum_n \mathbf{O}\left(\mathbf{a}^{(n)}\right). \tag{2.3}$$

In other types of stochastic equation [41, 42], there is a weight $\Omega\left(t\right)$ for each trajectory. This has an additional equation of motion, where:

$$\frac{\partial \Omega}{\partial t} = A_\Omega\left(\mathbf{a}, \Omega, t\right) + \underline{B}_\Omega\left(\mathbf{a}, \Omega, t\right) \cdot \boldsymbol{\xi}(t)\,. \tag{2.4}$$

The results for all mean values are then weighted by the term $\exp(\Omega(t))$, so that:

$$\langle \mathbf{O} \rangle_{\Omega} = \frac{\sum_n \mathbf{O}\left(\mathbf{a}^{(n)}\right) \exp\left(\Omega^{(n)}(t)\right)}{\sum_n \exp\left(\Omega^{(n)}(t)\right)}. \tag{2.5}$$

This expression reduces to the usual average if the weights are zero, i.e, $\Omega = 0$. Apart from the way that averages are treated, the weight can simply be regarded as an additional term in the stochastic differential equations. This simply means that one now has an equation with an extra random field, so that $\mathbf{a} \to [\mathbf{a}, \Omega]$, together with a modified expression for the averages. This, in fact, is how these equations are solved.

For reasons of efficiency, it is best to use "breeding" algorithms to treat these numerically. This replicates highly weighted trajectories with $\Omega^{(n)}(t) \gg 0$ and removes trajectories with $\Omega^{(n)} \ll 0$, that have negligible weight. The numerical method is described in section 9. The remainder of This chapter will focus on the most commonly treated case of unweighted, Gaussian, delta-correlated noise.

2.2. Stochastic calculus

In the case of delta-correlated noise, the trajectories are not differentiable. As a result, there are two main variants of stochastic calculus used to define the derivatives, called Ito or Stratonovich [1, 40], and xSPDE can be used for either type. The default algorithms are designed for Stratonovich cases, since this is just ordinary calculus. Ito calculus can be treated also, either using the directly applicable Euler method, or else by appropriate transformations to a Stratonovich form. One can also have a time-reversed or implicit Ito calculus [28], which is directly solved using an implicit Ito-Euler method.

A single step in time of duration Δt uses finite noises $\boldsymbol{\xi}$ which are defined to be delta-correlated in the small time-step limit, so that $\langle \xi_i \xi_j \rangle = \delta_{ij}/\Delta t$.

2.2.1. Types of stochastic calculus

The limits as $\Delta t \to 0$ are taken differently for the different types of stochastic calculus. Let $\mathbf{a}_0 = \mathbf{a}(t_0)$, $t_1 = t_0 + \Delta t$, $\mathbf{a}_1 = \mathbf{a}(t_1)$, $\bar{\mathbf{a}} = (\mathbf{a}_1 + \mathbf{a}_0)/2$, and $\bar{t} = t + \Delta t/2$, then the next step in time is:

- Ito calculus - uses **initial-time** derivative evaluations

$$\mathbf{a}_1 = \mathbf{a}_0 + \left[\mathbf{A}^{(I)}(\mathbf{a}_0, t_0) + \underline{\mathbf{B}}(\mathbf{a}_0, t_0) \cdot \boldsymbol{\xi}\right] \Delta t\ . \tag{2.6}$$

- Stratonovich calculus - uses **midpoint** derivative evaluations

$$\mathbf{a}_1 = \mathbf{a}_0 + \left[\mathbf{A}(\bar{\mathbf{a}}, \bar{t}) + \underline{\mathbf{B}}(\bar{\mathbf{a}}, \bar{t}) \cdot \boldsymbol{\xi}\right] \Delta t\,. \tag{2.7}$$

- Backward Ito calculus - uses **final-time** derivative evaluations

$$\mathbf{a}_1 = \mathbf{a}_0 + \left[\mathbf{A}^{(I+)}\left(\mathbf{a}_1, t_1\right) + \underline{\mathbf{B}}\left(\mathbf{a}_1, t_1\right) \cdot \boldsymbol{\xi}\right] \Delta t \ . \tag{2.8}$$

The drift term $\mathbf{A}$ is changed in Ito or implicit Ito calculus, if the noise coefficient B depends on the stochastic variable. Defining $\partial_n \equiv \partial/\partial a_n$ and using the Einstein convention of summing over repeated indices, one has the following relationships:

$$\begin{aligned} A_i^{(I)} &= A_i + \frac{1}{2} B_{jk} \partial_j B_{ik}, \\ A_i^{(I+)} &= A_i - \frac{1}{2} B_{jk} \partial_j B_{ik}. \end{aligned} \tag{2.9}$$

Methods used for solving stochastic equations depend on the type of stochastic calculus. The default methods used in xSPDE are for Stratonovich calculus. Other methods are available as well, for both forward and backward Ito calculus. Alternatively, one can use the conversion formulae to change the equation.

2.3. Stochastic equations with jumps

Many stochastic equations involve a discrete Poisson or jump process, which xSPDE can also solve. These are common in many fields, from financial modeling to open quantum systems. The fundamental noise is then a discrete jump or Poisson process, dN, which in our applications has the integer values 0 or 1.

Including this, a combined jump-diffusion Ito SDE can be written [43]:

$$\Delta \boldsymbol{a} = \left[\mathbf{A}\left(\mathbf{a}, t\right) + \underline{\mathbf{B}}\left(\mathbf{a}, t\right) \cdot \boldsymbol{\xi}(t)\right] \Delta t + \underline{\boldsymbol{C}}\left(\mathbf{a}, t\right) \cdot \Delta \boldsymbol{N}_{\lambda}(t), \tag{2.10}$$

where the $i-th$ jump process intensity is $\lambda_i\left(\mathbf{a}, t\right)$. This is defined such that:

$$\lambda_i\left(\mathbf{a}, t\right) = \lim_{\Delta t \to 0} \frac{1}{\Delta t} P(\Delta N_{i\lambda}(t) = 1). \tag{2.11}$$

Defining this general equation requires two additional parameters, $\underline{\boldsymbol{C}}\left(\mathbf{a}, t\right)$ and $\boldsymbol{\lambda}\left(\mathbf{a}, t\right)$, to specify the jump rate and its effect on the independent variable $\mathbf{a}$. Such equations are treated in the mathematics and numerical literature, but quantum physics applications require a variable jump rate, which is sometimes ignored.

Such equations are often specified in the Ito picture in the usual mathematical literature. The fact that $\underline{\boldsymbol{C}}\left(\mathbf{a}, t\right)$ and $\boldsymbol{\lambda}\left(\mathbf{a}, t\right)$ can depend on the field $\mathbf{a}$ means that the equations do not follow standard calculus, just as with continuous SDE equations.

2.4. Interaction picture

The interaction picture allows one to eliminate linear terms in the time derivatives. It is especially useful for stochastic partial differential equations, but it is applicable to stochastic equations as well. Suppose there are linear terms $\underline{\mathbf{L}}$, so that $\mathbf{A}\left(\mathbf{a}, t\right) = \mathbf{A}_1\left(\mathbf{a}, t\right) + \underline{\mathbf{L}} \cdot \mathbf{a}$, where $\underline{\mathbf{L}}$ is a constant matrix. The interaction picture defines local variables $\tilde{\mathbf{a}}$ for the fields $\mathbf{a}$.

It is convenient to introduce an abbreviated notation as:

$$D(\mathbf{a}) = \mathbf{A}_1(\mathbf{a}, t) + \underline{\mathbf{B}}(\mathbf{a}, t) \cdot \mathbf{w}(t), \tag{2.12}$$

so that one can write the differential equation as:

$$\frac{\partial \mathbf{a}}{\partial t} = D(\mathbf{a}) + \underline{\mathbf{L}} \cdot \mathbf{a}. \tag{2.13}$$

2.4.1. Linear propagator

Next, we define a linear propagator. This is given formally by:

$$\underline{\mathbf{P}}(\Delta t) = \exp(\Delta t \underline{\mathbf{L}}). \tag{2.14}$$

where $\Delta t = t - \bar{t}$, and $\bar{t}$ is the interaction picture origin. Transforming the field $\mathbf{a}$ to an interaction picture is achieved on defining:

$$\tilde{\mathbf{a}} = \underline{\mathbf{P}}^{-1}(\Delta t)\, \mathbf{a}. \tag{2.15}$$

As a result, the equation of motion is:

$$\frac{\partial \tilde{\mathbf{a}}}{\partial t} = D\left(\underline{\mathbf{P}}(\Delta t)\, \tilde{\mathbf{a}}\right). \tag{2.16}$$

This removes linear terms, which can cause stiffness in the equations, increasing the discretization error. Given the case of a completely linear ODE or SDE, the trajectory solutions will be exact up to round-off errors.

2.5. Probability distributions

Stochastic equations generate trajectories distributed with a probability density $P(\mathbf{a})$. These can be defined as an average and hence can be evaluated stochastically, since:

$$P(\mathbf{a}') = \left\langle \delta(\mathbf{a}' - \mathbf{a}) \right\rangle. \tag{2.17}$$

Here $\langle .. \rangle \equiv \langle .. \rangle_\infty$ is the infinite ensemble limit of the average over many trajectories. The probability can be shown to follow a Fokker-Planck equation (FPE) with positive semi-definite diffusion matrix, [1, 44]:

$$\frac{\partial P}{\partial t} = \mathcal{L}P = \left[-\partial_n A_n^{(I)} + \frac{1}{2} \partial_n \partial_m B_{nk} B_{mk} \right] P, \tag{2.18}$$

where the differential operators act on all terms to their right.

2.5.1. Distribution averages

The average of any observable $\mathbf{O}(\mathbf{a})$ is obtained either by averaging over the stochastic trajectories numerically, or by analytic calculations, using:

$$\langle \mathbf{O} \rangle = \int \mathbf{O}(\mathbf{a}) P(\mathbf{a}) d\mathbf{a}. \tag{2.19}$$

The dynamics of an observable or moment follows an adjoint equation, where $\tilde{\mathcal{L}}$ is the adjoint of $\mathcal{L}$:

$$\left\langle \frac{\partial \mathbf{O}}{\partial t} \right\rangle = \left\langle \tilde{\mathcal{L}} \mathbf{O} \right\rangle, \tag{2.20}$$

where:

$$\left\langle \tilde{\mathcal{L}} \mathbf{O} \right\rangle = \left\langle \left[A_n^{(I)} \partial_n + \frac{1}{2} B_{nk} B_{mk} \partial_n \partial_m \right] \mathbf{O} \right\rangle. \tag{2.21}$$

This equation allows the time-evolution of averages to be calculated analytically in simple cases, given an initial distribution. However, in more complex cases, a numerical simulation of the stochastic equations is more practical, and this can be carried out with xSPDE or other software.

2.6. Example: random walk

The first example of an SDE is the simplest possible stochastic equation or Wiener process:

$$\dot{a} = w(t). \tag{2.22}$$

This has the solution that

$$a(t) = a(0) + \int_0^t w(\tau) d\tau, \tag{2.23}$$

which means that the initial mean value does not change in time:

$$\langle a(t) \rangle = \langle a(0) \rangle. \tag{2.24}$$

2.6.1. Variance solution

The noise correlation is non-vanishing from Eq (2.2), so the variance must increase with time:

$$\begin{aligned} \left\langle a^2(t) \right\rangle &= \left\langle a^2(0) \right\rangle + \int_0^t \int_0^t \left\langle w(\tau) w\left(\tau'\right) \right\rangle d\tau d\tau' \\ &= \left\langle a^2(0) \right\rangle + \int_0^t \int_0^t \delta\left(\tau - \tau'\right) d\tau d\tau'. \end{aligned} \tag{2.25}$$

Integrating the delta function gives unity, which means that the second moment and the variance both increase linearly with time:

$$\begin{aligned}\left\langle a^2(t)\right\rangle &= \left\langle a^2(0)\right\rangle + \int_0^t d\tau \\ &= \left\langle a^2(0)\right\rangle + t. \end{aligned} \tag{2.26}$$

The probability follows an elementary diffusion equation:

$$\frac{\partial P}{\partial t} = \frac{1}{2}\frac{\partial^2 P}{\partial a^2}\,, \tag{2.27}$$

which is an example of Eq (2.18). From this equation and using Eq (2.20), the first two corresponding moment equations in this case are

$$\begin{aligned}\frac{\partial}{\partial t}\langle a\rangle &= \left\langle \frac{1}{2}\frac{\partial^2}{\partial a^2}a \right\rangle = 0 \\ \frac{\partial}{\partial t}\left\langle a^2\right\rangle &= \left\langle \frac{1}{2}\frac{\partial^2}{\partial a^2}a^2 \right\rangle = 1. \end{aligned} \tag{2.28}$$

These differential equations are satisfied by the solutions obtained directly from the stochastic equations, namely Eq (2.24) and Eq (2.26).

2.7. Probability densities

The Wiener process with an arbitrary noise strength has the stochastic equation:

$$\dot{a} = bw(t)\,. \tag{2.29}$$

The probability density satisfies the Fokker-Planck equation for diffusion,

$$\frac{\partial P}{\partial t} = \frac{b^2}{2}\frac{\partial^2}{\partial a^2}P\,. \tag{2.30}$$

Then, if x initially is Gaussian distributed, this has a Gaussian distribution at time t with:

$$P(a) = \frac{1}{\sqrt{2\pi\sigma^2(t)}}\exp\left[-\frac{(a-\bar{a}(t))^2}{2\sigma^2(t)}\right]. \tag{2.31}$$

Here:

$$\begin{aligned}\bar{a}(t) &= \bar{a}(0) \\ \sigma^2(t) &= \sigma^2(0) + b^2 t. \end{aligned} \tag{2.32}$$

2.7.1. Distributions of functions

Any function of the stochastic variables has a corresponding probability density. For example, the distribution of a^2 has a χ^2 distribution with a single degree of freedom, such that if $y = (a - \bar{a}(t))^2 / \sigma^2(t)$, then:

$$P(y) = \frac{1}{\sqrt{2\pi y}} \exp\left[-\frac{y}{2}\right]. \tag{2.33}$$

Hence:

$$P\left(a^2\right) = \frac{1}{|a - \bar{a}(t)| \sqrt{2\pi\sigma^2(t)}} \exp\left[-\frac{(a - \bar{a}(t))^2}{2\sigma^2(t)}\right]. \tag{2.34}$$

More generally, it is often not known what the exact analytic solutions are, and a numerical solution is employed. This can either use the stochastic equation directly, or the Fokker-Planck equation, although it is generally difficult to scale this to many variables or to partial differential equations,

That is why we focus on the stochastic equation approach here, which can be used to numerically calculate either the mean values or the probability distributions in general cases.

2.8. Fourier transforms

Frequency spectra have many uses, especially for understanding the steady-state fluctuations of any physical system in the presence of noise, typically either thermal or quantum-mechanical, although the noise could have other sources.

The time-domain spectral definition used here is:

$$\begin{aligned} \tilde{a}(\omega) &= \frac{1}{\sqrt{2\pi}} \int e^{i\omega t} a(t) dt \\ a(t) &= \frac{1}{\sqrt{2\pi}} \int e^{-i\omega t} \tilde{a}(\omega) d\omega. \end{aligned} \tag{2.35}$$

As a simple example, a sinusoidal oscillation in the form

$$a(t) = \cos(\omega_0 t). \tag{2.36}$$

between $t = -T/2$ and $t = T/2$ has a Fourier transform given by:

$$\begin{aligned} \tilde{a}(\omega) &= \frac{1}{2\sqrt{2\pi}} \int_{-T/2}^{T/2} \left[e^{i(\omega-\omega_0)t} + e^{i(\omega+\omega_0)t}\right] dt \\ &= \frac{T}{2\sqrt{2\pi}} \left[sinc\left((\omega - \omega_0)\frac{T}{2}\right) + sinc\left((\omega + \omega_0)\frac{T}{2}\right)\right]. \end{aligned} \tag{2.37}$$

2.8.1. Discrete Fourier transforms

While exact in this analytic case, the definition above is impractical for numerical calculations. In taking measurements and doing simulations, one has a discrete set of data-points. Assuming the samples are at fixed intervals, the best one can do in practical cases is a discrete Fourier transform, with samples $\bar{a}(\bar{t}_j)$ that are defined as integrals over each small interval dt:

Let $\bar{a}(\bar{t}_j)$ be the average over a small time interval:

$$\bar{a}(\bar{t}_j) = \int_{t_j}^{t_j+dt} a(t)dt\,, \tag{2.38}$$

then to a good approximation as $dt \to 0$, provided ω_n is not too large,

$$\begin{aligned}\tilde{a}(\omega_n) &= \frac{\Delta t}{\sqrt{2\pi}} \sum_{j=1}^{N} e^{i\omega_n \bar{t}_j} \bar{a}(\bar{t}_j) \\ \bar{a}(\bar{t}_j) &= \frac{\Delta \omega}{\sqrt{2\pi}} \sum_{n=1}^{N} e^{-i\omega_n \bar{t}_j} \tilde{a}(\omega_n)\,.\end{aligned} \tag{2.39}$$

These also form an invertible pair provided that $\Delta t \Delta\omega = 2\pi/N$. As well as being more practical, this is very efficient due to the fast Cooley-Tukey (FFT) algorithm [45], allowing computation on time-scales of $O\left(N \ln N\right)$ rather than $O\left(N^2\right)$ as one might expect.

When taking Fourier transforms in the time-domain, xSPDE does a time-averaging of all fields over the current time-step, using the available coarse and fine time-samples. This is done by averaging the field before and after the stochastic time-step. The methods used for this are described in greater detail in Section (6.7).

2.9. Quantum phase-space

One useful application of stochastic equations is in quantum technologies, where stochastic methods are generally much more scalable than other methods [46,47]. This approach started when Schrödinger [48] pointed out that quantum oscillators can have classical equations. Wigner, Moyal and Glauber extended this to other systems [49–51]. In lasers and quantum optics [2, 52–54], it is used to obtain SDEs for quantum systems coupled to reservoirs.

For the case of bosons, any M-mode quantum density matrix $\hat{\rho}$ may be written in a unified quantum phase-space form as:

$$\hat{\rho} = \int d^{2M}\boldsymbol{\alpha} d^{2M}\boldsymbol{\beta} P_\sigma\left(\boldsymbol{\alpha},\boldsymbol{\beta}\right) \hat{\Lambda}_\sigma\left(\boldsymbol{\alpha},\boldsymbol{\beta}\right), \tag{2.40}$$

where P_σ is the σ-ordered phase-space distribution function, and $\boldsymbol{\alpha} = [\alpha_1, \ldots \alpha_M]$. The basis, $\hat{\Lambda}_\sigma$, is a Gaussian function of annihilation and creation operators ([55]), whose

variance depends on σ. This is defined as the variance of $\alpha\beta$ due to vacuum fluctuations, in the operator ordering of the representation.

For clarity, we hats like $\hat{a}$ are used here to indicate operators that do not commute with each other, as opposed to stochastic variables like α that do commute. For any given operator ordering, it is always possible to find a probability distribution such that the expectation of an operator product equals the stochastic variable correlations [56].

2.9.1. Positive-P representation

The above expansion leads to different statistics and noise terms depending on the operator ordering. For example, in the normally ordered positive P-representation where $\sigma = 0$, the operator basis is

$$\hat{\Lambda}\left(\boldsymbol{\alpha},\boldsymbol{\beta}\right) \equiv \frac{\left|\boldsymbol{\alpha}\right\rangle \left\langle \boldsymbol{\beta}^{*}\right|}{\left\langle \boldsymbol{\beta}^{*}\right| \left.\boldsymbol{\alpha}\right\rangle}. \tag{2.41}$$

Here $\boldsymbol{\beta} = \boldsymbol{\alpha}^{\dagger} \sim \hat{\boldsymbol{a}}^{\dagger}$ is a stochastic variable conjugate in the mean to $\boldsymbol{\alpha}^{*}$. Any quantum state has a positive representation of this type [57], and normally ordered coherence functions are moments of the distribution with:

$$\left\langle \hat{a}_{m_1}^{\dagger} \ldots \hat{a}_{m_n} \right\rangle = \int d^{2M}\boldsymbol{\alpha} d^{2M}\boldsymbol{\beta} \left[\beta_{m_1} \ldots \alpha_{m_n}\right] P\left(\boldsymbol{\alpha},\boldsymbol{\beta}\right). \tag{2.42}$$

The Glauber-Sudarshan representation used in laser physics is obtained for $\boldsymbol{\beta} = \boldsymbol{\alpha}^{*}$, so that the two variables are exactly conjugate:

$$\hat{\rho} = \int d^{2M}\boldsymbol{\alpha} P\left(\boldsymbol{\alpha}\right) \left|\boldsymbol{\alpha}\right\rangle \left\langle \boldsymbol{\alpha}\right|. \tag{2.43}$$

In this case, the total number of stochastic variables is halved, but nonclassical squeezed or entangled states cannot be represented as a positive distribution. Two additional frequently utilized representations are the Wigner ($\sigma = 1/2$) and Husimi ($\sigma = 1$) representations, characterized by symmetric ordering and anti-normal ordering, respectively. These also have a classical phase-space with $\boldsymbol{\beta} = \boldsymbol{\alpha}^{*}$.

2.9.2. Master equations

The dynamics of a quantum system coupled to a reservoir is described by a master equation. In the Markovian (high-frequency) limit, the general quantum master equation for a dissipative quantum system with damping rates Γ_j is

$$\begin{aligned}\frac{\partial\hat{\rho}}{\partial t} = &\frac{1}{i\hbar}\left[\hat{H}_{sys},\hat{\rho}\right] + \sum_{j}\Gamma_j\left(\bar{n}_j+1\right)\left(2\hat{A}_j\hat{\rho}\hat{A}_j^{\dagger} - \hat{A}_j^{\dagger}\hat{A}_j\hat{\rho} - \hat{\rho}\hat{A}_j^{\dagger}\hat{A}_j\right)\\ &+ \sum_{j}\Gamma_j\bar{n}_j(2\hat{A}_j^{\dagger}\hat{\rho}\hat{A}_j - \hat{A}_j\hat{A}_j^{\dagger}\hat{\rho} - \hat{\rho}\hat{A}_j\hat{A}_j^{\dagger}),\end{aligned} \tag{2.44}$$

where Γ_j is a damping rate for reservoir couplings to the operator $\hat{A}_j$, $\bar{n}_j$ is the finite temperature reservoir occupation, and the typical damping operators are:

Damping operator ($\hat{A}_j$)	Γ_j	Physical interpretation
$\hat{a}_j$	γ_j	Linear amplitude loss (units s^{-1})
$\hat{a}_j^\dagger$	g_j	Linear amplitude gain (units s^{-1})
$\hat{a}_j^\dagger \hat{a}_j$	γ_j^p	Phase decay rate gain (units s^{-1})
$\hat{a}_j^2$	$\kappa_j/2$	nonlinear amplitude loss (units s^{-1}).

Table 2.1.: Typical types of quantum damping term

The operator equations are mapped to differential equations with the equivalences:

$$\begin{aligned}
\hat{a}_n^\dagger \hat{\rho} &\rightarrow \left[\beta_n + (\sigma - 1)\frac{\partial}{\partial \alpha_n}\right] P_\sigma \\
\hat{a}_n \hat{\rho} &\rightarrow \left[\alpha_n + \sigma \frac{\partial}{\partial \beta_n}\right] P_\sigma \\
\hat{\rho}\hat{a}_n &\rightarrow \left[\alpha_n + (\sigma - 1)\frac{\partial}{\partial \beta_n}\right] P_\sigma \\
\hat{\rho}\hat{a}_n^\dagger &\rightarrow \left[\beta_n + \sigma \frac{\partial}{\partial \alpha_n}\right] P_\sigma \,.
\end{aligned} \tag{2.45}$$

The operator mappings give a differential equation. If it has a second-order positive-definite form it is a Fokker-Planck equation equivalent to an SDE, or an SPDE for quantum fields [58]. The noise can be additive or multiplicative, depending on the problem. Not all cases give stable FPE equations [59], and truncation is required for the Wigner representation if the Hamiltonian is nonlinear [60].

The total noise includes internal quantum noise generated from the Hamiltonian term $\hat{H}_{sys}$, as well as reservoir noise terms generated from the coupling to the reservoir operators, which is proportional to Γ_j. There is a similar behavior in classical systems, except that these correspond to a high-temperature limit, and in most cases only have external reservoir noise from thermal fluctuations.

2.10. Damped harmonic oscillator

As an example, take the damped quantum harmonic oscillator. This has the Hamiltonian $H = \omega_0 \hat{a}^\dagger \hat{a}$. If damping is added, it obeys the master equation

$$\begin{aligned}
\frac{d\hat{\rho}}{dt} = \frac{-i}{\hbar}[\omega_0 \hat{a}^\dagger \hat{a}, \rho] + \gamma\,(1+\bar{n})\,(2\hat{a}\rho\hat{a}^\dagger - \hat{a}^\dagger\hat{a}\rho - \rho\hat{a}^\dagger\hat{a}) \\
+ \gamma\bar{n}(2\hat{a}^\dagger\rho\hat{a} - \hat{a}\hat{a}^\dagger\rho - \rho\hat{a}\hat{a}^\dagger).
\end{aligned} \tag{2.46}$$

This leads to a random walk in a complex space [1, 2],

$$\begin{aligned}\frac{d\alpha}{dt} &= -\left(\gamma + i\omega_0\right)\alpha + \sqrt{2\gamma\left(\sigma + \bar{n}\right)}\zeta(t)\\ \frac{d\beta}{dt} &= -\left(\gamma - i\omega_0\right)\beta + \sqrt{2\gamma\left(\sigma + \bar{n}\right)}\zeta^*(t),\end{aligned} \tag{2.47}$$

where the noise is complex and $\zeta(t) = \left(w_1(t) + iw_2(t)\right)/\sqrt{2}$. The correlations are

$$\begin{aligned}\left\langle \zeta(t)\left(\zeta(t')\right)^*\right\rangle &= \delta\left(t - t'\right)\\ \left\langle \zeta(\omega)\left(\zeta\left(\omega'\right)\right)^*\right\rangle &= \delta\left(\omega - \omega'\right).\end{aligned} \tag{2.48}$$

2.10.1. Wigner representation

In the zero temperature Wigner case with γ =1, $\sigma = 1/2$, and in a rotating frame so that $\omega_0 = 0$, the probability follows the Fokker-Planck equation:

$$\frac{\partial P}{\partial t} = \left[\frac{\partial}{\partial\alpha_x}\alpha_x + \frac{\partial}{\partial\alpha_y}\alpha_y + \frac{1}{4}\left(\frac{\partial^2}{\partial\alpha_x^2} + \frac{\partial^2}{\partial\alpha_y^2}\right)\right]P, \tag{2.49}$$

which is an example of Eq (2.18). Ignoring terms that vanish or can be obtained from symmetry, the first corresponding moment equations in each of the real and imaginary directions are

$$\begin{aligned}\frac{\partial}{\partial t}\left\langle\alpha_x\right\rangle &= \left\langle -\alpha_x\frac{\partial}{\partial\alpha_x}\alpha_x\right\rangle = -\left\langle\alpha_x\right\rangle\\ \frac{\partial}{\partial t}\left\langle\alpha_x\alpha_y\right\rangle &= \left\langle -\left(\alpha_x\frac{\partial}{\partial\alpha_x} + \alpha_y\frac{\partial}{\partial\alpha_y}\right)\alpha_x\alpha_y\right\rangle = -\left\langle\alpha_x\alpha_y\right\rangle\\ \frac{\partial}{\partial t}\left\langle\alpha_x^2\right\rangle &= \left\langle\left(-\alpha_x\frac{\partial}{\partial\alpha_x} + \frac{1}{4}\frac{\partial^2}{\partial\alpha_x^2}\right)\alpha_x^2\right\rangle = \frac{1}{2} - 2\left\langle\alpha_x^2\right\rangle.\end{aligned} \tag{2.50}$$

The steady-state is therefore a Gaussian distribution with $\left\langle\alpha_{x,y}\right\rangle = 0$, $\left\langle\alpha_x\alpha_y\right\rangle = 0$ and $\left\langle\alpha_{x,y}^2\right\rangle = 1/4$. One can use an initial condition of $\alpha = (v_1 + iv_2)/2$, with $\left\langle v_i^2\right\rangle = 1/2$, in order to replicate the steady state, which is a Gaussian with$\left\langle\alpha_x\right\rangle = \left\langle\alpha_y\right\rangle = 0$ and$\left\langle\alpha_x^2\right\rangle = \left\langle\alpha_y^2\right\rangle = 1/4$.

2.10.2. Internal spectrum

Neglecting any boundary terms, the equation in frequency space is:

$$-i\omega\tilde{\alpha}(\omega) = -\tilde{\alpha}(\omega) + \tilde{\zeta}(\omega). \tag{2.51}$$

For sufficiently long times, the solution in frequency space - where $\omega = 2\pi f$ is the angular frequency - is therefore given by:

$$\tilde{\alpha}\left(\omega\right) = \frac{\tilde{\zeta}(\omega)}{1 - i\omega}. \tag{2.52}$$

The expectation value of the noise spectrum, $\left\langle |\tilde{\alpha}(\omega)|^2 \right\rangle$ in the long time limit, is:

$$\begin{aligned} \left\langle |\tilde{\alpha}(\omega)|^2 \right\rangle &= \frac{1}{2\pi\left(1+\omega^2\right)} \int\int e^{-i\omega(t-t')} \left\langle \zeta(t)\zeta^*(t') \right\rangle dtdt' . \\ &= \frac{T}{2\pi\left(1+\omega^2\right)}. \end{aligned} \tag{2.53}$$

This equation can also be used for some classical problems, which correspond to the high-temperature limit of $\bar{n} \gg 1$.

2.11. Input-output spectra

The spectrum of an internal field variable is not the one that is usually measured. An important application of stochastic equations is therefore in calculating output, measured spectra of lasers, quantum optics, opto-mechanics and quantum circuits [53, 61]. These have the feature that the measured output spectrum may also include noise from reflected fields at the input/output ports. If the quantum noise term in the Heisenberg equations for a cavity operator $\hat{a}_c$ is given by: $\dot{\hat{a}}_c \sim .. + \sqrt{2\gamma}\hat{a}_{in}(t)$, then the corresponding operator input-output relations are $\hat{a}_{out}(t) + \hat{a}_{in}(t) = \sqrt{2\gamma}\hat{a}_c$.

In quantum phase-space for the case of the harmonic oscillator or similar systems, $\alpha_{in} = \sqrt{\sigma + \bar{n}}\zeta$ is the noise term in the Langevin equation. The output fields α_{out} that are measured are given by:

$$\alpha_{out} = \sqrt{2\gamma}\alpha - \alpha_{in}. \tag{2.54}$$

Hence one must include in the spectrum both the internal mode variables and the noise terms themselves. Solving for the spectra, one obtains auxiliary fields with

$$\begin{aligned} \tilde{\alpha}_{in}(\omega) &= \sqrt{\sigma + \bar{n}}\tilde{\zeta}(\omega) \\ \tilde{\alpha}_{out}(\omega) &= \sqrt{2\gamma}\tilde{a}(\omega) - \sqrt{\sigma + \bar{n}}\tilde{\zeta}(\omega). \end{aligned} \tag{2.55}$$

In summary, it is the output fields that are amplified and measured. Hence one must be able to compute the spectra of the output fields for experimental comparisons. These have the additional feature that they include the reservoir noise $\tilde{\zeta}(\omega)$, evaluated at the same time as the field is evaluated, since the reservoir noise is the input here. In xSPDE these are called *auxfields*.

2.11.1. Steady-state result

Consider the example of Section (2.10), in the Wigner representation case with $\gamma = 1$, $\sigma = 1/2$ and $\bar{n} = 0$. Over long time-scales, so that one is in the steady state, the solution for $\tilde{a}_{out}$ is that:

$$\begin{aligned} \tilde{\alpha}_{out}(\omega) &= \sqrt{2}\left[\frac{1}{1-i\omega} - \frac{1}{2}\right]\tilde{\zeta}(\omega) \\ &= \frac{1}{\sqrt{2}}\left[\frac{1+i\omega}{1-i\omega}\right]\tilde{\zeta}(\omega). \end{aligned} \tag{2.56}$$

This gives the following expectation values:

$$\left\langle \tilde{\alpha}_{out}(\omega)\left(\tilde{\alpha}_{out}(\omega)\left(\omega'\right)\right)^{*}\right\rangle = \frac{1}{2}\delta\left(\omega-\omega'\right)$$
$$\left\langle \tilde{\alpha}_{in}(\omega)\left(\tilde{\alpha}_{in}(\omega)\left(\omega'\right)\right)^{*}\right\rangle = \frac{1}{2}\delta\left(\omega-\omega'\right). \tag{2.57}$$

These are the expectation values of the zero temperature quantum fluctuations in the input and output channels. This means that the harmonic oscillator in its ground state is in equilibrium with an external vacuum field reservoir, also in its ground state. However, from Eq (2.53), the internal spectral correlations of the harmonic oscillator are modified by the coupling.

While this is a simple result, exactly the same general type of behavior occurs in more sophisticated cases. These may include many coupled modes with nonlinearities. Additional or auxiliary fields that depend both on noise terms and internal stochastic variables are required. The soluble case given above is a useful test case, and it is treated numerically later in the manual.

3. Quantum master equations

This chapter describes the quantum theory used in xSPDE, to explain the background to the open system methods available.

3.1. Master equations

The density matrix master equation is basic to quantum theory. It has a memory requirement that scales as $e^{2\lambda M}$ for M modes, where $\lambda = \ln(N_{max})$, and N_{max} is the dimension of the Hilbert space of a single mode. This becomes exponentially difficult to solve numerically as $M \to \infty$.

The master equation treated here and elsewhere is repeated for reference purposes. It has the standard Lindblad form that:

$$\dot{\rho} = \mathcal{L}_J \rho \tag{3.1}$$

$$= -i\left[\hat{H}, \rho\right] + \sum_{j=1}^{J} \gamma_j \left(2\hat{L}_j \rho \hat{L}_j^\dagger - \hat{L}_j^\dagger \hat{L}_j \rho - \rho \hat{L}_j^\dagger \hat{L}_j\right) \tag{3.2}$$

Here, $\mathcal{L}_J$ is the total super-operator for J terms,H is the reversible system Hamiltonian, L_j are J operators that couple the system to the dissipative reservoir, and γ_j is the decay rate. The dissipative operators can be further classified by type n and mode index k, including vector indices if needed.

Provide that ρ is normalized, the expectation values of observables $\hat{O}$ are given by:

$$\left\langle \hat{O} \right\rangle = Tr\left(\rho \hat{O}\right) \tag{3.3}$$

The definitions used here mean that for the case of linear damping with $\hat{L} = \hat{a}$, the rate γ is the amplitude decay rate. This abstract notation does not include the effects of finite temperatures, which are explained below.

The rate is written explicitly here. This is useful for xSPDE inputs, which use standard dimensionless operators. Alternative approaches include combining the rate with the operator [**?**], implying $\gamma = 1$. Others use a rate constant $\kappa = 2\gamma$, i.e., the number decay rate. Some combine *this* with the operator, defining $\hat{c}_j = \sqrt{2\gamma_j}\hat{L}_j$, giving a fourth operator convention.

Including finite temperature reservoir occupation numbers $\bar{n}_j$ explicitly, the quantum

Damping operator ($\hat{A}_j$)	Γ_j	Physical interpretation
$\hat{a}_j$	γ_j	Linear amplitude loss (units s^{-1})
$\hat{a}_j^\dagger$	g_j	Linear amplitude gain (units s^{-1})
$\hat{a}_j^\dagger \hat{a}_j$	γ_j^p	Phase decay rate gain (units s^{-1})
$\hat{a}_j^2$	$\kappa_j/2$	nonlinear amplitude loss (units s^{-1}).

Table 3.1.: Typical types of quantum damping term

master equation with damping rates Γ_j is

$$\frac{\partial \hat{\rho}}{\partial t} = -i\left[\hat{H}, \hat{\rho}\right] + \sum_j \Gamma_j \left(\bar{n}_j + 1\right)\left(2\hat{A}_j \hat{\rho} \hat{A}_j^\dagger - \hat{A}_j^\dagger \hat{A}_j \hat{\rho} - \hat{\rho} \hat{A}_j^\dagger \hat{A}_j\right) + \sum_j \Gamma_j \bar{n}_j (2\hat{A}_j^\dagger \hat{\rho} \hat{A}_j - \hat{A}_j \hat{A}_j^\dagger \hat{\rho} - \hat{\rho} \hat{A}_j \hat{A}_j^\dagger) \,, \tag{3.4}$$

where Γ_j is a zero temperature damping rate for reservoir couplings to the operator $\hat{A}_j$, $\bar{n}_j$ is the finite temperature reservoir occupation. In the numerical toolbox, the finite-temperature reservoirs are included explicitly as a separate Lindblad term.

3.1.1. Bosonic Hilbert spaces

The operators available in xSPDE include multimode bosonic operators $\hat{a}_j$. For these, typical damping operators are:

3.1.2. Qubit Hilbert spaces

Additionally, xSPDE includes finite Hilbert spaces, focusing on $SU(2)$ or qubit cases. Operators available are: $\hat{\sigma}_m^x$,$\hat{\sigma}_m^y$,$\hat{\sigma}_m^z$, together with quantum logic gates: hadamard, controlled-not, phase and $\pi/8$. These can be combined to give a complete set of logic gates, allowing a simulation of quantum computers.

Using the master-equation toolbox, one can also include decoherence and loss. As usual, this is limited by exponential growth in the Hilbert space dimension, but the stochastic Schrödinger equation and related methods improve memory efficiency compared to the full density matrix.

3.2. Stochastic Schrödinger equation (SSE)

A stochastic Schrödinger equation (SSE) is an equation with noise terms used to solve a dissipative master equation by random sampling, and was originally developed for applications in quantum foundations [**?**,**?**,**?**]. It has the advantage over a master equation that for large numbers of modes it uses less storage. This requires $e^{\lambda M}$complex numbers for the storage of an $M-$mode quantum system, compared to $\sim e^{2\lambda M}$ for the master equation, where $\lambda = \log_e(N)$ for an N-level local Hilbert space. This is exponentially

large, but the memory required is less than with a density matrix equation, doubling the number of modes that are accessible. The drawback is that many parallel trajectories must be averaged in order to give a low final sampling error.

An SSE can also be regarded in certain cases as providing a direct simulation of the measurement process, which means that the information recorded in a simulation is similar to the information measured in a quantum experiment. This requires a suitable choice of the method, sometimes called an "unraveling" and the stochastic integration algorithm. Different unravellings mean different measurements and different convergence rates.

There are many versions of the SSE, which use different normalization, different random noises or different types of stochastic calculus. Noises can be real or complex, and either continuous or with discrete jumps. These are different "unravellings", and correspond physically to distinct measurement devices and outcomes. They also have different sampling errors.

Compared to phase-space expansions, the SSE method has the problem that storage requirements are exponential in the system size, although it may have lower sampling errors for high nonlinearities. This limits mode numbers to $10-50$, depending on the size of the Hilbert space per mode and the computational resources. The approach is most useful for small mode numbers, especially for large nonlinearities.

3.2.1. Normalized Ito SSE

A widely used form of the continuous noise, normalized SSE is as follows [**?**], in the Ito calculus:

$$\begin{aligned} d\left|\Psi\right\rangle = & \left\{-i\hat{H}+\sum_{j}\gamma_{j}\left(2\left\langle \hat{L}_{j}^{\dagger}\right\rangle _{\Psi}\hat{L}_{j}-\left\langle \hat{L}_{j}^{\dagger}\right\rangle _{\Psi}\left\langle \hat{L}_{j}\right\rangle _{\Psi}-\hat{L}_{j}^{\dagger}\hat{L}_{j}\right)\right\}\left|\Psi\right\rangle dt\\ & +\sum_{j}\sqrt{2\gamma_{j}}\Delta\hat{L}_{j}\left|\Psi\right\rangle d\xi_{j}. \end{aligned} \tag{3.5}$$

where $\Delta\hat{L}_{j}=\hat{L}_{j}-\left\langle \hat{L}_{j}\right\rangle _{\Psi}$, and

$$\begin{aligned} \left\langle d\xi_{j}^{*}d\xi_{k}\right\rangle &= \delta_{jk}dt.\\ \left\langle d\xi_{j}d\xi_{k}\right\rangle &= 0. \end{aligned} \tag{3.6}$$

A more general form of the normalized SSE [**?**] in the Ito calculus is:

$$\begin{aligned} d\left|\Psi\right\rangle = & \left\{-i\hat{H}+\sum_{j}\gamma_{j}\left(2\left\langle \hat{L}_{j}^{\dagger}\right\rangle _{\Psi}\hat{L}_{j}-\left\langle \hat{L}_{j}^{\dagger}\right\rangle _{\Psi}\left\langle \hat{L}_{j}\right\rangle _{\Psi}-\hat{L}_{j}^{\dagger}\hat{L}_{j}\right)\right\}\left|\Psi\right\rangle dt\\ & +\sum_{jn}\sqrt{2\gamma_{j}}\Delta\hat{L}_{j}\left|\Psi\right\rangle \alpha_{jn}d\zeta_{jn}. \end{aligned} \tag{3.7}$$

where we require that $\sum_n |\alpha_{jn}|^2 = 1$, and

$$\left\langle d\zeta_{jn}(t)\, d\zeta_{km}\left(t'\right)\right\rangle = \delta_{jk}\delta_{nm}dt. \tag{3.8}$$

One can also include a unitary transformation, which we set to a delta function for simplicity. When there is one noise per decay channel, then $\alpha_j(t) = e^{i\phi_j}$, where ϕ_j is arbitrary. If there are two noises, then one can choose $\alpha_{j1}(t) = 1/\sqrt{2}$, and $\alpha_{j2}(t) = i/\sqrt{2}$, giving a complex noise SDE, with $\xi_j = (\zeta_1 + i\zeta_2)/\sqrt{2}$, as above.

This can be written for $|\Psi\rangle \to \Psi_\nu$, and $d\zeta_{jn} \to dw_\sigma$, as:

$$d\psi_\mu = A_\mu dt + B_{\mu\sigma}dw_\sigma$$

3.3. Stratonovich equations

To obtain standard calculus for an SSE, one must transform to the Stratonovich equation. This form of stochastic calculus allows integration algorithms that often give lower errors [28]. There are also higher order methods for Ito equations, but these have greatly increased complexity. Here we derive the Stratonovich correction [1, 37], which is obtained with $\hat{L}_j|\Psi\rangle \to L_{j\mu\nu}\Psi_\nu$ so that $\left\langle \hat{L}_j^\dagger \right\rangle_\Psi = \sum_{\sigma\rho} \Psi_\sigma^* L_{j\rho\sigma}^* \Psi_\rho$.

For complex noise as in Eq (3.6), the Stratonovich drift is given by:

$$A_\mu = A_\mu^{(I)} - \frac{1}{2}\sum_{j\nu} B_{\nu j}^* \partial_\nu^* B_{\mu j}. \tag{3.9}$$

On taking matrix elements in an orthogonal basis, and defining:

$$\Delta L_{j\mu\nu} = L_{j\mu\nu} - \delta_{\mu\nu}\sum_{\sigma\rho}\Psi_\rho^* L_{j\rho\sigma}\Psi_\sigma, \tag{3.10}$$

one has:

$$\begin{aligned} B_{\mu j} &= \sqrt{2\gamma_j}\Delta L_{j\mu\beta}\Psi_\beta \\ B_{\mu j}^* &= \sqrt{2\gamma_j}\Psi_\beta^* \Delta L_{j\mu\beta}^*. \end{aligned} \tag{3.11}$$

On differentiating one therefore obtains:

$$\begin{aligned} \partial_\nu^* B_{\mu j} &= \sqrt{2\gamma_j}\sum_\beta \left[-\Psi_\beta \partial_\nu^*\left(\delta_{\mu\beta}\sum_{\sigma\rho}\Psi_\rho^* L_{j\rho\sigma}\Psi_\sigma\right)\right] \\ &= \sqrt{2\gamma_j}\left[-\Psi_\mu \sum_\sigma L_{j\nu\sigma}\Psi_\sigma\right]. \end{aligned} \tag{3.12}$$

The Stratonovich correction is given by:

$$\begin{aligned}-\frac{1}{2}\sum_{\nu,j}B^*_{\nu j}\partial^*_\nu B_{\mu j} &= -\sum_j \gamma_j \sum_{\nu,\alpha}\Psi^*_\alpha \Delta L^*_{j\nu\alpha}\left[-\Psi_\mu \sum_\sigma L_{j\nu\sigma}\Psi_\sigma\right]\\ &= \sum_j \gamma_j \left[\sum_{\nu\sigma\alpha}\Psi^*_\alpha\left(L^*_{j\nu\alpha}-\delta_{\nu\alpha}\left\langle \hat{L}^\dagger_j\right\rangle_\Psi\right)L_{j\nu\sigma}\Psi_\sigma\right]\Psi_\mu\\ &= \sum_j \gamma_j\left[\left\langle \hat{L}^\dagger_j\hat{L}_j\right\rangle_\Psi - \left\langle \hat{L}^\dagger_j\right\rangle_\Psi\left\langle \hat{L}_j\right\rangle_\Psi\right]\Psi_\mu. \end{aligned} \tag{3.13}$$

In summary, the complex Ito SSE can be transformed to a nonlinear Stratonovich stochastic differential equation which locally preserves normalization for zero step-size [**?**]. This is called the quantum state diffusion model:

$$\begin{aligned}\frac{d\left|\Psi\right\rangle}{dt} &= \left(-i\hat{H}+\sum_j\gamma_j\left(2\gamma_j\Delta\hat{L}_j\left\langle\hat{L}^\dagger_j\right\rangle_\Psi-\Delta\left[\hat{L}^\dagger_j\hat{L}_j\right]\right)\right)\left|\Psi\right\rangle\\ &+\sum_j\sqrt{2\gamma_j}\xi_j\Delta\hat{L}_j\left|\Psi\right\rangle\end{aligned} \tag{3.14}$$

where:

$$\left\langle \xi_k\left(t\right)\xi^*_j\left(t'\right)\right\rangle = \delta_{kj}\delta\left(t-t'\right). \tag{3.15}$$

Here, $\Delta\hat{L}_j \equiv \hat{L}_j - \left\langle\hat{L}_j\right\rangle_\Psi$ and the equation uses Stratonovich calculus. This preserves the norm of the wave-function. Suppose the Stratonovich form has a dissipative term $\Delta\hat{\mathcal{L}}_s$, where

$$\frac{d\left|\Psi\right\rangle}{dt} = \left\{\Delta\hat{\mathcal{L}}_s - i\hat{H}\right\}\left|\Psi\right\rangle \tag{3.16}$$

Since it is a Stratonovich equation, one can use ordinary calculus rules. Only dissipative terms can change the norm, and:

$$\begin{aligned}\frac{d}{dt}\left\langle\Psi\right|\left.\Psi\right\rangle &= \left\langle\Delta\left(\hat{\mathcal{L}}_s+\hat{\mathcal{L}}^\dagger_s\right)\right\rangle_\psi\\ &= \left\langle\hat{\mathcal{L}}_s+\hat{\mathcal{L}}^\dagger_s\right\rangle_\psi - \left\langle\hat{\mathcal{L}}_s+\hat{\mathcal{L}}^\dagger_s\right\rangle_\psi = 0\end{aligned} \tag{3.17}$$

For Ito equations, the trajectories have a norm error that grows with time. While there are projective methods to prevent this, the result has higher step-size errors [62].To obtain observables, one must use the "double" expectation indicating a quantum and stochastic mean, where the wave-functions $\left|\Psi\right\rangle$ are normalized, and have all the same weight:

$$\left\langle O\right\rangle \equiv \left\langle\left\langle\Psi\right|O\left|\Psi\right\rangle\right\rangle_\xi. \tag{3.18}$$

Integrating this equation is best carried out with a projection at each time-step to prevent the normalization changing, as derived elsewhere [62]. This is implemented automatically within xSPDE.

3.3.1. Real noise Stratonovich equation

For the real noise case, the correction term is:

$$A_\mu = A_\mu^{(I)} - \frac{1}{2}\sum_{\sigma\nu}\left(B_{\nu\sigma}\partial_\nu + B^*_{\nu\sigma}\partial^*_\nu\right)B_{\mu\sigma}, \tag{3.19}$$

where $B_{\mu j} = \sqrt{2\gamma_j}\Delta L_{j\mu\beta}\Psi_\beta$. Taking $n = 1$ and $j = \sigma$, the conjugate correction is given above and is independent of α_j. The first term is obtained from differentiation of the noise matrix:

$$B_{\mu j} = \alpha_j\sqrt{2\gamma_j}\Delta L_{j\mu\beta}\Psi_\beta. \tag{3.20}$$

hence one obtains that:

$$\partial_\nu B_{\mu j} = \sqrt{2\gamma_j}\alpha_j\left[\Delta L_{j\mu\nu} - \sum_\beta \delta_{\mu\beta}\left[\Psi^*_\rho L_{j\rho\nu}\right]\Psi_\beta\right]. \tag{3.21}$$

The additional correction is as follows:

$$\begin{aligned}-\frac{1}{2}\sum_{\nu j}B_{\nu j}\partial_\nu B_{\mu j} &= -\sum_{\nu j}\gamma_j\alpha_j^2\left[\Delta L_{j\mu\nu} - \Psi^*_\rho L_{j\rho\nu}\Psi_\mu\right]\Delta L_{j\nu\sigma}\Psi_\sigma \\ &= -\sum_{\nu j}\gamma_j\alpha_j^2\left(\Delta L_{j\mu\nu}\Delta L_{j\nu\sigma}\Psi_\sigma - \left[\Psi^*_\rho L_{j\rho\nu}\Delta L_{j\nu\sigma}\Psi_\sigma\right]\Psi_\mu\right).\end{aligned} \tag{3.22}$$

Written in operator/wave-function terminology, the real correction $|\delta A^r\rangle$is

$$\begin{aligned}|\delta A^r\rangle &= -\sum_{\nu j}\gamma_j\alpha_j^2\left(\left[\Delta\hat{L}_j\Delta\hat{L}_j\right] - \left\langle\hat{L}_j\Delta\hat{L}_j\right\rangle_\Psi\right)|\Psi\rangle \\ &= -\sum_{\nu j}\gamma_j\alpha_j^2\left(\left[\hat{L}_j^2 - 2\hat{L}_j\left\langle\hat{L}_j\right\rangle_\Psi + \left\langle\hat{L}_j\right\rangle_\Psi^2\right] - \left\langle\hat{L}_j^2\right\rangle_\Psi + \left\langle\hat{L}_j\right\rangle_\Psi^2\right)|\Psi\rangle \\ &= \sum_{\nu j}\gamma_j\left(2\Delta\hat{L}_j\left\langle\alpha_j^2\hat{L}_j\right\rangle_\Psi - \Delta\left[\alpha_j^2\hat{L}_j^2\right]\right)|\Psi\rangle.\end{aligned} \tag{3.23}$$

Combining both terms, and defining $\hat{X}_j = \hat{L}_j^\dagger + \alpha_j^2\hat{L}_j$, one obtains a result known in the literature [63] for the case $\alpha = 1$;

$$\begin{aligned}\frac{d|\Psi\rangle}{dt} &= \left\{-iH + \sum_j\gamma_j\left(2\left\langle\hat{X}_j\right\rangle_\Psi\Delta\hat{L}_j - \Delta\left[\hat{X}_j\hat{L}_j\right]\right)\right\}|\Psi\rangle \\ &\quad + \sum_j\sqrt{2\gamma_j}\Delta\hat{L}_j|\Psi\rangle\,\alpha_j\zeta_j(t)\end{aligned} \tag{3.24}$$

As with the complex noise case, this is explicitly norm-preserving since the dissipative terms have zero quantum mean values for every noise realization. This generic result reduces to the complex case if one sets$\hat{X}_j = \hat{L}_j^\dagger$ and $\alpha_j\zeta_j \to \xi_j$.

3.3.2. Stochastic master equation (SME)

There is a density matrix version of this equation. It is derived using the product rule, since the above equation is in the Stratonovich calculus. It is useful for measurements when only some measurements are being monitored. One can divide the dissipative operators into U unconditional and C conditional terms that are being monitored:

$$\frac{d\rho}{dt} = \left\{ \mathcal{L}_U \rho + \left[\sum_{j=1}^{C} \gamma_j \left(2 \left\langle \hat{X}_j \right\rangle_\rho \Delta \hat{L}_j - \Delta \left[\hat{X}_j \hat{L}_j \right] \right) \rho + h.c \right] \right\} + \sum_{j=1}^{C} \sqrt{2\gamma_j} \left[\Delta \hat{L}_j \rho \alpha_j \zeta_j (t) + h.c. \right] \tag{3.25}$$

where:

$$\left\langle \zeta_k (t) \zeta_j \left(t' \right) \right\rangle = \delta_{kj} \delta \left(t - t' \right). \tag{3.26}$$

The operator X is defined as $\hat{X}_j = \hat{L}_j^\dagger + \alpha_j^2 \hat{L}_j$ for real measurements with real noise, and reduces to the complex case if one sets $\hat{X}_j = \hat{L}_j^\dagger$ and $\alpha_j \zeta_j \to \xi_j$. The observable z_j measured with efficiency η then gives an output of $z_j = \sqrt{2\eta\gamma_j} \left\langle \hat{X}_j \right\rangle_\rho + \xi_j^*$. The remaining $J - C$ operators are included in $\mathcal{L}_U$.

3.4. Monte Carlo wave-function method

The Monte Carlo or quantum jump method is another approach to solve a master equation. The master equation treated here has the form given in Eq (3.1).

3.4.1. Integer noise

A jump SSE is obtained by using an Ito stochastic differential equation with real noise, in the form:

$$d|\phi\rangle = \left\{ -i\hat{H} - \sum_j \gamma_j \left[\hat{L}_j^\dagger \hat{L}_j - \left\langle \hat{L}_j^\dagger \hat{L}_j \right\rangle \right] \right\} |\phi\rangle \, dt + \sum_j \left(\hat{L}_j / \sqrt{\left\langle \hat{L}_j^\dagger \hat{L}_j \right\rangle} - 1 \right) |\phi\rangle \, dN_j, \tag{3.27}$$

where the real integer noise $dN = [0, 1]$ has correlations of:

$$\langle dN_j (t) \rangle = 2\gamma_j \left\langle \hat{L}_j^\dagger \hat{L}_j \right\rangle dt. \tag{3.28}$$

In any interval dt, dN is unity with probability $p = 2\gamma_j \left\langle \hat{L}_j^\dagger \hat{L}_j \right\rangle dt$, and zero otherwise.

To generate integer noise, one first obtains a random real number r where $0 < r < 1/dt$. From this, one can choose $dN = 1$ if $r < 2\gamma_j \left\langle \hat{L}_j^\dagger \hat{L}_j \right\rangle$.

3.4.2. MCWF method

In the MCWF method, state vectors evolve according to an effective Hamiltonian,

$$H_e = H - i \sum_m \gamma_m L_m^\dagger L_m \,, \tag{3.29}$$

punctuated by quantum jumps

$$|\psi\rangle \to L_m |\psi\rangle \,, \tag{3.30}$$

where L_m is one of the possible operators in the master equation. At each step in time, the system will either evolve according to the non-Hermitian Hamiltonian Eq. (3.29) or undergo a jump operation, depending on the jump probability ΔP.

A sequence of quantum jumps or photo-counts giving total counts $\boldsymbol{c} = c_1, \ldots c_M$ is obtained. For times when there is no jump,

$$\dot{\psi}_c = -i \hat{H}_e \psi_c. \tag{3.31}$$

Jumps occur at random times given by choosing random numbers r_m such that $0 < r_m < 1/\Delta t$, where r_m determines the jump probability for the $m - th$ process.

The jump changes counts so that $c_j \to c_j + 1$. Afterwards, one resets ρ_c after an infinitesimal time ϵ so that

$$|\psi\left(t_c + \epsilon\right)\rangle = \frac{|\psi_j\rangle}{\sqrt{\langle\psi_j|\,\psi_j\rangle}}. \tag{3.32}$$

The MCWF algorithm is presented in the numerical section.

3.4.3. Monte-Carlo master equations

Monte Carlo master equation theory [?, ?, ?, ?, ?, 64] implements the Copenhagen model for measurement as a sequential wave-function projections. It treats dissipative evolution whose average behavior is given by a master equation, where if there is one decay channel $\hat{L}_j$ per mode M:

$$\frac{d\rho}{dt} = -i \left[\hat{H}, \rho\right] + \sum_{j=1}^{M} \gamma_j \left(2\hat{L}_j \rho \hat{L}_j^\dagger - \left[\hat{L}_j^\dagger \hat{L}_j, \rho\right]_+ \right). \tag{3.33}$$

An equivalent sequence of quantum jumps or photo-counts giving total counts $\boldsymbol{c} = c_1, \ldots c_M$ is described by a conditional density matrix equation, which is a nonlinear Ito discrete SDE in the form:

$$d\rho = -i \left[\hat{H}_e \rho - \rho \hat{H}_e^\dagger\right] dt + \sum_j \left(\frac{\hat{L}_j \rho \hat{L}_j^\dagger}{\left\langle \hat{L}_j^\dagger \hat{L}_j \right\rangle} - \rho \right) dN_j \tag{3.34}$$

,

where the effective Hamiltonian $\hat{H}_e$ is non-hermitian:

$$\hat{H}_e = H - i\sum_{j=1}^{M}\gamma_j\left[\hat{L}_j^\dagger\hat{L}_j - \left\langle\hat{L}_j^\dagger\hat{L}_j\right\rangle\right]$$

and the real integer noise $dN_j = [0,1]$ has correlations of:

$$\langle dN_j(t)\rangle = 2\gamma_j\left\langle\hat{L}_j^\dagger\hat{L}_j\right\rangle dt. \tag{3.35}$$

In any interval dt, dN is unity with probability $p = 2\gamma_j\left\langle\hat{L}_j^\dagger\hat{L}_j\right\rangle dt$, and zero otherwise. This is not a standard Lindblad form due to the nonlinear terms, but it conserves probabilities, and has an average behavior that corresponds to the full master equation.

Jumps occur at times given as above by choosing random numbers r_j in $[0, 1/dt]$ such that $dN = 1$ if

$$r_j < 2\gamma_j\left\langle\hat{L}_j^\dagger\hat{L}_j\right\rangle. \tag{3.36}$$

The Ito density matrix equation can be integrated by integrating the deterministic part over a small time interval, then deciding whether or not to jump. A jump changes detector counts so $c_j \to c_j + 1$. One must correspondingly project ρ after an infinitesimal time to give the new density matrix, given by the discontinuous jump $d\rho_N$, where

$$d\rho_N = \sum_j\left(\frac{\hat{L}_j\rho\hat{L}_j^\dagger}{\left\langle\hat{L}_j^\dagger\hat{L}_j\right\rangle} - \rho\right)dN_j. \tag{3.37}$$

3.5. Examples

We now consider examples of linear and nonlinear dissipative operators.

3.5.1. Linear master equation

The standard case of linear losses in quantum optics, gives:

$$L = a \tag{3.38}$$

The corresponding master equation is;

$$\dot{\rho} = 2a\rho a^\dagger - a^\dagger a\rho - \rho a^\dagger a. \tag{3.39}$$

This leads to a linear decay in amplitude and occupation number:

$$\begin{aligned}\langle\dot{n}\rangle &= Tr\left[\left(2a\rho a^\dagger a^\dagger a - n^2\rho - \rho n^2\right)\right]\\ &= 2Tr\left[\rho a^{\dagger 2}a^2 - n^2\rho\right]\\ &= 2Tr\left[\rho\left(n^2 - n\right) - n^2\rho\right]\\ &= -2\langle n\rangle.\end{aligned} \tag{3.40}$$

The effect of the operator on the state expansion is

$$\begin{aligned} |\phi\rangle &= \sum_n \phi_n |n\rangle \\ a|n\rangle &= \sqrt{n}\,|n-1\rangle \\ a^\dagger |n\rangle &= \sqrt{n+1}\,|n+1\rangle \\ a^\dagger a |n\rangle &= n|n\rangle . \end{aligned} \tag{3.41}$$

Therefore for a number state expansion of the density operator:

$$\begin{aligned} \langle a\rangle &= \sum_{nm} \phi_j^* \langle m|\phi_n a|n\rangle \\ &= \sum_{nm} \phi_j^* \langle m|\phi_n \sqrt{n}|n-1\rangle \\ &= \sum_{n=0}^{\infty} \phi_n^* \phi_{n+1}\sqrt{n+1}. \end{aligned} \tag{3.42}$$

also, for the conjugate,

$$\left\langle a^\dagger \right\rangle = \sum_{n=1}^{\infty} \phi_n^* \phi_{n-1}\sqrt{n}. \tag{3.43}$$

3.5.2. Linear stochastic equation

This is the simplest case:

$$\begin{aligned} \frac{d|\phi\rangle}{dt} &= \sum_n \left(-a^\dagger a + a\xi\right)\phi_n |n\rangle \\ &= \sum_n \left(-n|n\rangle + \sqrt{n}|n-1\rangle\,\xi\right)\phi_n. \end{aligned} \tag{3.44}$$

Taking matrix elements, one obtains:

$$\frac{d\phi_j}{dt} = \sqrt{m+1}\phi_{m+1}\xi - m\phi_j$$

3.5.3. Normalized, nonlinear stochastic equation

$$\begin{aligned} \frac{d|\phi\rangle}{dt} &= \sum_n \left(\left[\left\langle a^\dagger a\right\rangle - a^\dagger a\right] + [a - \langle a\rangle]\left[\xi + 2\left\langle a^\dagger\right\rangle\right]\right)\phi_n|n\rangle \\ &= \sum_n \left(\left[\langle n\rangle - n\right]|n\rangle + \left[\xi + 2\left\langle a^\dagger\right\rangle\right]\left[\sqrt{n}|n-1\rangle - \langle a\rangle|n\rangle\right]\right)\phi_n \end{aligned}$$

Taking matrix elements,

$$\frac{d\phi_j}{dt} = \left[\xi + 2\left\langle a^\dagger\right\rangle\right]\left[\sqrt{m+1}\phi_{m+1} - \langle a\rangle\,\phi_j\right] + [\langle n\rangle - m]\,\phi_j. \tag{3.45}$$

3.5.4. Nonlinear absorber

The next case of nonlinear two-photon losses in quantum optics, gives:

$$L = a^2$$

where we recall that:

$$\begin{aligned} |\phi\rangle &= \sum_n \phi_n |n\rangle \\ a^2 |n\rangle &= \sqrt{n\,(n-1)}\,|n-2\rangle \\ a^{\dagger 2} |n\rangle &= \sqrt{(n+1)\,(n+2)}\,|n+2\rangle \\ a^{\dagger 2} a^2 |n\rangle &= n\,(n-1)\,|n\rangle \end{aligned}$$

3.5.5. Master equation

The quantum expectations in a pure state are given by:

$$\begin{aligned} \left\langle a^2 \right\rangle &= \sum_{nm} \phi_j^* \langle m| \phi_n a^2 |n\rangle \\ &= \sum_{nm} \phi_j^* \langle m| \phi_n \sqrt{n(n-1)}\,|n-2\rangle \\ &= \sum_{n=0}^{\infty} \phi_n^* \phi_{n+2} \sqrt{(n+2)(n+1)} \end{aligned}$$

The diagonal master equation in a number state basis is therefore:

$$\dot{\rho}_n = -2n(n-1)\rho_n + 2(n+1)(n+2)\rho_{n+2}.$$

This equation is generated automatically using the master equation quantum method in the numerical toolbox.

3.6. Quantum networks

The xSPDE numerical code can solve for output observables obtained after a linear transformation of a multi-mode quantum input state $\hat{\rho}^{(\mathrm{in})}$. The mode transformation is generated by a linear photonic network of generalized beam-splitters and phase delays. This acts as an M-mode interferometer such that output modes are linear combinations of each input mode.

Without losses, the network itself is defined by an $M \times M$ unitary matrix $\boldsymbol{U}$. Physically, this corresponds to the interference of input photons that generates large amounts of entanglement due to the exponential number of paths available to photons.

In the ideal, lossless case, one has:

$$\hat{a}_i^{(\text{out})} = \sum_{j=1}^{M} U_{ij} \hat{a}_j^{(\text{in})}, \tag{3.46}$$

where $\hat{a}_i^{(\text{in})}$ and $\hat{a}_j^{(\text{out})}$ are the input and output annihilation operators for modes i, j respectively.

Practically, losses in the network are commonplace, thus causing the experimental transmission matrix to be non-unitary. Therefore, lossy networks are denoted by the transmission matrix $\boldsymbol{T}$. Not every input channel needs to have an input. In these cases, $N \subset M$ represents the number of input modes, thus changing the unitary to an $N \times M$ transmission matrix.

These give a different transformation law, where:

$$\hat{a}_i^{(\text{out})} = \sum_{j=1}^{N} T_{ij} \hat{a}_j^{(\text{in})} + \sum_{j=1}^{M} B_{ij} \hat{b}_j^{(\text{in})}, \tag{3.47}$$

Here, the M operators $\hat{b}_i^{(\text{in})}$are noise operators. These are necessary to conserve the operator commutation relations. They comprise inputs from the reservoirs that cause losses, as well as the $M - N$ vacuum inputs at unused ports. They are independent commuting operators, whose reservoirs are all in a vacuum state.

Due to the need to conserve commutators, we know that for both inputs and outputs:

$$\begin{aligned} [\hat{a}_i, \hat{a}_j] &= 0 \\ \left[\hat{a}_i, \hat{a}_j^\dagger\right] &= \delta_{ij}. \end{aligned} \tag{3.48}$$

Applying this to the outputs, considering a vacuum state input, and taking expectation values, gives

$$\begin{aligned} \delta_{ij} &= \left\langle \left[\hat{a}_i^{(\text{out})}, \hat{a}_j^{\dagger(\text{out})}\right] \right\rangle \\ &= \sum_k \left(T_{ik} T_{jk}^* + B_{ik} B_{jk}^*\right). \end{aligned} \tag{3.49}$$

Next, we can define a new $M \times M$ matrix

$$\boldsymbol{D} = \boldsymbol{B}\boldsymbol{B}^\dagger = \boldsymbol{I} - \boldsymbol{T}\boldsymbol{T}^\dagger. \tag{3.50}$$

This is hermitian, since $\boldsymbol{D}^\dagger = \boldsymbol{D}$, and so has a diagonal representation as $D = \tilde{U}\lambda^2\tilde{U}^\dagger$, for some unitary matrix $\tilde{U}$. We assume that the transmission matrix $\boldsymbol{T}$ is lossy, so that $\boldsymbol{D}$ is positive definite and λ is real, representing absorption rather than gain.

3.7. Quantum input states

The input state is defined in a number of ways depending on the desired distribution one wishes to sample from. If each input mode is independent, $\hat{\rho}^{(\text{in})}$ is a product of input states.

To sample from the permanent, inputs are single photon Fock states such that

$$\hat{\rho}^{(\text{in})} = \prod_{j=1}^{M} |1\rangle_j \langle 1|_j \,, \tag{3.51}$$

where $|1\rangle_j = a_j^\dagger |0\rangle$.

To sample from the Hafnian or Torontonian, the input is a product of single-mode pure squeezed vacuum states

$$\hat{\rho}^{(\text{in})} = \prod_{j=1}^{M} |r_j\rangle \langle r_j| \,, \tag{3.52}$$

where $\boldsymbol{r} = [r_1, \ldots, r_M]$ is the squeezing vector and

$$\begin{aligned} |r_j\rangle &= \hat{S}(r_j) |0\rangle \\ &= \exp\left(r_j \frac{(a_j^\dagger)^2}{2} - r_j \frac{\hat{a}_j^2}{2} \right) |0\rangle \,, \end{aligned} \tag{3.53}$$

is the squeezed vacuum state where we have assumed the squeezed phase is zero.

Currently, xSPDE can only generate input squeezed states and thermal states as outlined below. Other inputs are possible, since the positive P-representation and Q-representation are complete, positive representations, and can be added through user customization.

3.7.1. Pure squeezed states

For a single-mode, squeezed vacuum states are generated by applying the squeezing operator $\hat{S}(r)$ onto a vacuum state. As is clear from the operator definition Eq.(3.53), where we drop the j subscript for the single-mode case, squeezed vacuum states always generate even numbers of photons.

The mean photon number $\bar{n} = \langle \hat{a}^\dagger \hat{a} \rangle$ and coherence $m = \left\langle (\hat{a})^2 \right\rangle$ can be derived using the relations

$$\begin{aligned} \hat{S}^\dagger(r) \hat{a} \hat{S}(r) &= \hat{a} \cosh(r) - \hat{a}^\dagger \sinh(r) \\ \hat{S}^\dagger(r) \hat{a}^\dagger \hat{S}(r) &= \hat{a}^\dagger \cosh(r) - \hat{a} \sinh(r), \end{aligned} \tag{3.54}$$

where the mean photon number is

$$\begin{aligned} \bar{n} &= \left\langle \hat{a}^\dagger \hat{a} \right\rangle \\ &= \langle r| \hat{a}^\dagger \hat{a} |r\rangle \\ &= \langle 0| \hat{S}^\dagger(r) \hat{a}^\dagger \hat{a} \hat{S}(r) |0\rangle \\ &= \sinh^2(r), \end{aligned} \tag{3.55}$$

whilst the coherence is

$$\begin{aligned} m &= \left\langle (\hat{a})^2 \right\rangle \\ &= \langle r| \hat{a}\hat{a} |r\rangle \\ &= \langle 0| \hat{S}^\dagger(r)\hat{a}\hat{a}\hat{S}(r) |0\rangle \\ &= \sinh(r)\cosh(r). \end{aligned} \tag{3.56}$$

For pure squeezed states, the coherence and photon number are related via $m^2 - \bar{n} = \bar{n}^2$.

The superposition of only even Fock states becomes clearer when expanding the squeezed state in terms of Fock states as

$$|r\rangle = \frac{1}{\sqrt{\cosh(r)}} \sum_{n=0}^{\infty} \frac{\sqrt{(2n)!}}{2^n n!} \tanh^n(r) |2n\rangle , \tag{3.57}$$

where $n = 0, 1, 2, \ldots$ is the number of photons. From the above Fock state expansion the photon number distribution for the squeezed vacuum state is

$$\begin{aligned} P_{2n} &= \frac{1}{\cosh(r)} \frac{(2n)!}{(n!)^{2n} 2^{2n}} (\tanh(r))^{2n}, \\ P_{2n+1} &= 0, \end{aligned} \tag{3.58}$$

with variance $\sigma_n^2 = 2\bar{n}(\bar{n}+1) = \bar{n}(1+\cosh(2r_j))$.

Squeezed states are minimum uncertainty states and are therefore defined entirely by their quadrature variances. Using the quadrature operators

$$\begin{aligned} \hat{x} &= \hat{a} + \hat{a}^\dagger \\ \hat{y} &= -i \left(\hat{a} - \hat{a}^\dagger \right), \end{aligned} \tag{3.59}$$

which obey the commutation relation $[\hat{x}_j, \hat{y}_k] = 2i\delta_{jk}$, the normally ordered x-quadrature variance is obtained as

$$\begin{aligned} \left\langle : (\Delta\hat{x})^2 : \right\rangle &= \left\langle \hat{x}^2 \right\rangle \\ &= 2(n+m) \\ &= e^{2r} - 1, \end{aligned} \tag{3.60}$$

whilst the normally ordered y-quadrature variance is

$$\begin{aligned} \left\langle : (\Delta\hat{y})^2 : \right\rangle &= \left\langle \hat{y}^2 \right\rangle \\ &= 2(n-m) \\ &= e^{-2r} - 1. \end{aligned} \tag{3.61}$$

All the results derived here are also valid for multiple modes, denoted by the subscript j, given each mode is independent as is the case in optical networks. Currently, xSPDE can simulate pure and thermalized squeezed states as well as classical thermal state inputs into the network. This is achieved using a model for thermal squeezed states which alters the multi-mode input coherence $m(r_j)$ as $\tilde{m}(r_j) = (1-\epsilon)m(r_j)$ whilst keeping the input photon number $n(r_j) = \bar{n}_j$ unchanged. This allows one to interpolate between pure thermal, $\epsilon = 1$, and pure squeezed, $\epsilon = 0$, states.

3.7.2. Squeezed thermal states

Thermal states are classical states with fluctuations larger than the vacuum limit such that their quadrature variances are $\langle : (\Delta\hat{x})^2 : \rangle = \langle : (\Delta\hat{y})^2 : \rangle$.

In terms of Fock states, the thermal state density matrix is

$$\hat{\rho} = \frac{1}{1+\bar{n}} \sum_{n=0}^{\infty} \left(\frac{\bar{n}}{1+\bar{n}} \right)^n |n\rangle \langle n| , \tag{3.62}$$

which gives the well known photon number distribution

$$P(n) = \frac{\bar{n}^n}{(\bar{n}+1)^{n+1}}. \tag{3.63}$$

Thermal states can be used to generate squeezed thermal states with initial occupation n_{th}, which gives [**?**]:

$$\begin{aligned} \bar{n} =& n_{th} + (2n_{th}+1)\sinh^2(r) \\ \tilde{m} =& (2n_{th}+1)\sinh(r)\cosh(r) . \end{aligned} \tag{3.64}$$

In the thermalized case, the relationship between coherence and photon number is modified, since to eliminate r one must use the relationship that

$$\begin{aligned} \frac{\tilde{m}^2}{(2n_{th}+1)^2} &= \sinh^2(r)\left(1+\sinh^2(r)\right) \\ &= \frac{\bar{n}-n_{th}}{(2n_{th}+1)} \left(1 + \frac{\bar{n}-n_{th}}{(2n_{th}+1)} \right) \end{aligned}$$

Therefore:

$$\begin{aligned} \tilde{m}^2 &= (\bar{n}-n_{th})(1+\bar{n}+n_{th}) \\ &= \bar{n} + \bar{n}^2 - \left(n_{th}^2 + n_{th}\right) . \end{aligned} \tag{3.65}$$

Squeezed thermal states are used as a test case, since one can define the saturating, or click, detectors in terms of the photon number and coherence as explained below.

3.8. Photon counting

Photonic networks employed as quantum computers aim to sample from an output state whose distribution corresponds to the $\#P$-hard matrix permanent, Hafnian or Torontonian distributions. Which output probability is sampled depends on the input states to the network, with Fock states corresponding to the permanent and squeezed states corresponding to the Hafnian or Torontonian distributions, where the difference between these distributions comes from the detector used.

The sampled distribution not only depends on the input state but also the detector type. When photon-number resolving (PNR) detectors are used one samples either the permanent, given the input is a Fock state, or the Hafnian distribution for a squeezed state input. The Torontonian corresponds to the use of saturating, or click, detectors with squeezed state inputs.

Output samples from linear networks consist of photon count patterns. The j-th detector records $c_j = 0, 1, 2, \ldots$ photon counts, with a specific output pattern being denoted by the count vector $\boldsymbol{c}$.

From standard photon counting theory, the projection operator for observing $c_j = 0, 1, 2, \ldots$ counts is denoted by

$$\hat{p}_j(c_j) = \frac{1}{c_j!} : (\hat{n}'_j)^{c_j} e^{-\hat{n}'_j} :, \tag{3.66}$$

where $: \cdots :$ denotes normal ordering and $\hat{n}'_j = a_j^{\dagger(\text{out})} a_j^{(\text{out})}$ is the output photon number.

For PNR detectors, which can discriminate between photon numbers, each detector is defined by the above projector, with the projection operator for a specific output pattern given as

$$\hat{P}(\boldsymbol{c}) = \bigotimes_{j=i}^{M} \hat{p}_j(c_j). \tag{3.67}$$

The expectation value of the PNR pattern projection operator corresponds to the Hafnian

$$\text{Haf} = \left\langle \hat{P}(\boldsymbol{c}) \right\rangle, \tag{3.68}$$

which is $\#P$-hard to compute at large M.

Click detectors saturate for more than one count at a detector. Therefore, outputs are binary with $c_j = 1$ denoting a detection event, even if multiple photons hit the same detector, and $c_j = 0$ is no detection event. From Eq.(3.66), the click projection operator is obtained by summing over all $c_j > 0$ counts such that

$$\begin{aligned} \hat{\pi}(1) =: \sum_{c_j > 0} \frac{(\hat{n}'_j)^{c_j}}{c_j!} e^{-\hat{n}'_j} : \\ = 1 - e^{-\hat{n}'_j}, \end{aligned} \tag{3.69}$$

which gives the standard saturating detector projection operator

$$\hat{\pi}_j(c_j) =: e^{-\hat{n}'_j} \left(e^{\hat{n}'_j} - 1\right)^{c_j} : . \tag{3.70}$$

The projection operator for an pattern output is then similarly defined as

$$\hat{\Pi}(\boldsymbol{c}) = \bigotimes_{j=i}^{M} \hat{\pi}_j(c_j), \tag{3.71}$$

where the expectation value corresponds to the Torontonian distribution

$$\mathrm{Tor} = \left\langle \hat{\Pi}(\boldsymbol{c}) \right\rangle . \tag{3.72}$$

3.8.1. Exact outputs

To test photon count distributions, xSPDE uses a modified version of the click probabilities which can be computed exactly in the limit of a unit transmission matrix.

Using the thermal state photon number distribution Eq.(3.63), one obtains the click distributions:

$$\begin{aligned} \pi(0) = P(0) &= \frac{1}{\bar{n}+1} \\ \pi(1) = 1 - \pi(0) &= \frac{\bar{n}}{\bar{n}+1}. \end{aligned} \tag{3.73}$$

Substituting the thermal squeezed state modified photon number the probability of a vacuum state is [**?**]:

$$\begin{aligned} \pi(0) &= \frac{1}{n_{th}+1} \left(1 + \frac{2n_{th}+1}{(n_{th}+1)^2} \sinh^2(r)\right)^{-(1/2)} \\ &= \left(\bar{n} - n_{th} + (n_{th}+1)^2\right)^{-(1/2)} \\ &= \left(1 + \bar{n} + n_{th} + n_{th}^2\right)^{-(1/2)} \\ &= \left((1+\bar{n})^2 - \tilde{m}^2\right)^{-(1/2)} . \end{aligned}$$

Hence, by using known results for a photon number distribution of a squeezed thermal state [**?**], combined with the definitions of $\bar{n}$ and $\tilde{m}$, the probability of a vacuum state and a non-vacuum or click state are:

$$\begin{aligned} \langle \hat{\pi}(0) \rangle &= \frac{1}{\sqrt{(1+\bar{n})^2 - \tilde{m}^2}} \\ \langle \hat{\pi}(1) \rangle &= 1 - \frac{1}{\sqrt{(1+\bar{n})^2 - \tilde{m}^2}}. \end{aligned} \tag{3.74}$$

3.9. Intensity correlations

We now explain two types of measurable correlations: Glauber intensity correlations and grouped correlations, also referred to as a grouped count probabilities (GCPs).

Intensity correlation simulations can only be performed on photon number operator observables. Therefore, although they are valid for determining photon number probabilities in click experiments, they correspond directly to PNR detector outputs. Meanwhile GCPs are only valid for click detectors. Although methods are available which convert PNR detectors to click detectors, direct binning methods for PNR outputs will be included in a sequential updates.

Glauber's n-th order intensity correlation is defined as

$$G^{(n)}(c_j) = \left\langle : (\hat{n}'_j)^{c_j} \dots (\hat{n}'_M)^{c_M} : \right\rangle, \tag{3.75}$$

where $n = \sum c_j$ is the correlation order. Multi-mode Glauber correlations determine the probability of detecting n photons at n modes.

The normal ordering requirement causes all creation operators to the right and all annihilation operators to the left. For example, the second-order correlation

$$G^{(2)} = \left\langle a_1^{\dagger(\text{out})} a_2^{\dagger(\text{out})} a_2^{(\text{out})} a_1^{(\text{out})} \right\rangle, \tag{3.76}$$

corresponds to detecting one photon at mode 1 and one at mode 2.

Upon reordering using the standard Bose commutation relations Eq.(3.48), one obtains

$$G^{(2)} = \left\langle a_1^{\dagger(\text{out})} a_2^{(\text{out})} \right\rangle \left\langle a_2^{\dagger(\text{out})} a_1^{(\text{out})} \right\rangle + \left\langle a_1^{\dagger(\text{out})} a_1^{(\text{out})} \right\rangle \left\langle a_2^{\dagger(\text{out})} a_2^{(\text{out})} \right\rangle. \tag{3.77}$$

The first term describes non-local correlations which is the interference of photons between detectors, whilst the second term describes the photon intensity at a detector or local correlations.

If the mean number of photons is small, such that a detector will only ever observe one photon, the intensity correlation becomes a coincidence count

$$P_N = \left\langle \prod_j \hat{n}'_j \right\rangle, \tag{3.78}$$

as we assume photons do not interfere at detectors, removing non-local correlations.

3.9.1. Grouped correlations

Grouped count probabilities (GCPs) are the main observable correlation implemented by xSPDE and are only valid for click detectors.

GCPs are defined as

$$\mathcal{G}_{\boldsymbol{S}}^{(n)}(\boldsymbol{m}) = \left\langle \prod_{j=1}^{d} \left[\sum_{\sum c_i = m_j} \hat{\Pi}_{S_j}(\boldsymbol{c}) \right] \right\rangle, \tag{3.79}$$

where $\boldsymbol{m} = (m_1, \ldots, m_d)$ are the observed grouped counts in d-dimensions and $\boldsymbol{S} = (S_1, S_2, \ldots)$ is a vector of disjoint subsets of $\boldsymbol{M} = (M_1, M_2, \ldots)$ modes.

Each grouped count is obtained by summing over binary patterns $m_j = \sum_i^M c_i$. Therefore, grouped counts contain k bins, with each bin corresponding to the total number of clicks in each pattern. In one-dimension, GCPs are the probability of observing m counts in any pattern with $n = M$ and $S = \{1, \ldots, M\}$. This observable is called total counts.

For larger dimensions, each grouped count sums over detector outputs for a subset of modes only such that $m_j = \sum_i^{M/d} c_i$. The modes in each subset are denoted in the vector $\boldsymbol{S}$. For example, in two-dimensions one has subsets $\boldsymbol{S} = (S_1, S_2)$ which contain modes

$$\begin{aligned} S_1 &= \left\{1, \ldots, \frac{M}{2}\right\} \\ S_2 &= \left\{\frac{M+2}{2}, \ldots, M\right\}. \end{aligned} \tag{3.80}$$

The output GCP is then a joint probability of observing $m_1 = \sum_{i=1}^{M/2} c_i$ and $m_2 = \sum_{i=M/2+1}^{M} c_i$ grouped counts with $k = (M/2+1)^2$ total bins.

The implied segregation of output modes in the two-dimensional example above is that S_1 will always contain the first M/d modes, S_2 the next $M/d + 1 \to 2M/d$ modes, and so on for larger dimensions. However, there is no practical restriction on the output modes each subset can contain.

Therefore, by randomly permuting each binary pattern we can change the output modes that are contained in each subset giving

$$\frac{\binom{M}{M/d}}{d} = \frac{M!}{d(M/d)!(M - M/d)!}, \tag{3.81}$$

possible ways of generating $m_1, \ldots, m_d$ grouped counts without repeating a specific permutation.

For example, when $M = 4$ and $d = 2$, including the standard division, there are 3 different orderings of outputs modes with subsets

$$\begin{aligned} \boldsymbol{S} &= (S_1, S_2) = (\{1,2\}, \{3,4\}), \\ \boldsymbol{S} &= (S_1, S_2) = (\{1,3\}, \{2,4\}), \\ \boldsymbol{S} &= (S_1, S_2) = (\{1,4\}, \{2,3\}). \end{aligned} \tag{3.82}$$

Each permutation generates a different correlation, where we assume the commutation of GCP probabilities with subsets $(\{1,3\}, \{2,4\}) = (\{2,4\}, \{1,3\})$.

This permutation only changes the multidimensional GCP simulations, as in the total count case all modes are contained in the same subset $S = \{1, \ldots, M\}$. This is also

the case when simulating marginal probabilities, which are obtained by setting $n < M$ such that $M - n$ inputs are ignored. The first-order marginal, $n = 1$, is called the click correlation, $\langle \hat{\pi}_j(1) \rangle$, and determines the probability of observing a click at the j-th detector.

4. Quantum phase-space

4.1. Introduction

Orthogonal basis methods are not scalable to large numbers of mode, because the Hilbert space dimension grows exponentially with the number of modes. If one solves the quantum equations in an orthogonal basis, the memory and CPU time grows rapidly. Hence, large quantum systems are inaccessible.

Instead, a useful application of stochastic equations is in phase-space expansions, where stochastic methods are often more scalable than other methods [46, 47]. There are trade-offs, and this often may require further approximations.

The advantage is that the phase-space distribution can be sampled using random sampling, where each sample in phase-space requires a polynomial amount of storage, typically growing linearly with the number of modes. It is usually relatively straightforward to estimate sampling errors.

This approach started when Schrödinger [48] pointed out that quantum oscillators can have classical equations. This was extended to other systems [49–51], especially including lasers and quantum optics [2, 52–54].

For the case of bosons, any M-mode quantum density matrix $\hat{\rho}$ may be written in a unified quantum phase-space form as:

$$\hat{\rho} = \int d\boldsymbol{\phi} P_{\sigma}\left(\boldsymbol{\phi}\right) \hat{\Lambda}_{\sigma}\left(\boldsymbol{\phi}\right), \tag{4.1}$$

where P_{σ} is the σ-ordered phase-space distribution function, and $\boldsymbol{\phi}$ is the phase-space. The basis, $\hat{\Lambda}_{\sigma}$, is a Gaussian function of annihilation and creation operators ([55]), whose variance depends on σ. This is defined as the mean occupation of vacuum fluctuations, in the operator ordering of the representation.

Commonly utilized classical phase-space representations, where $\boldsymbol{\phi} = \boldsymbol{\alpha} = [\alpha_1, \ldots \alpha_M]$ are the Glauber-Sudarshan, ($\sigma = 0$), Wigner ($\sigma = 1/2$) and Husimi ($\sigma = 1$) representations, characterized by symmetric ordering and anti-normal ordering, respectively. One can also use nonclassical representations, which have a larger than classical phase-space.

For clarity, hats like $\hat{a}$ are used here to indicate operators that do not commute with each other, as opposed to stochastic variables like α that do commute. For any given operator ordering, it is always possible to find a probability distribution such that the expectation of an operator product equals the stochastic variable correlations [56].

4.2. Phase-space sampling

The outputs in phase-space are continuous real or complex variables whose stochastic moments are equal to moments of the experimental distributions, apart from sampling errors due to finite numbers of experimental and theoretical counts. This assumes that the parameters are precisely known, and do not have noise or fluctuations.

4.2.1. Glauber P-representation

The M-mode Glauber diagonal P-representation expands the density matrix as a sum of diagonal coherent state projectors

$$\hat{\rho} = \int P(\boldsymbol{\alpha}) \left|\boldsymbol{\alpha}\right\rangle \left\langle\boldsymbol{\alpha}\right| d^{2M}\boldsymbol{\alpha}, \tag{4.2}$$

where the distribution $P(\boldsymbol{\alpha})$ is a positive and non-singular distribution over multimode coherent state amplitudes $\boldsymbol{\alpha} = [\alpha_1, \ldots, \alpha_M]$ for classical states.

The diagonal P-representation breaks down for certain quantum states, giving non-positive and singular distributions. This is due to the lack of off-diagonal coherent state amplitudes needed to represent such nonclassical superpositions.

4.2.2. Positive P-representation

Part of a family of generalized P-representations developed to extend Glauber's diagonal P-representation to quantum states [**?**], the normally ordered positive-P representation always generates a non-singular and positive distribution for any quantum state. The trade-off is that it is non-unique, which can lead to a growing sampling error for nonlinear Hamiltonians.

The density matrix is defined as an expansion over a multidimensional subspace of the complex plane:

$$\hat{\rho} = \iint P(\boldsymbol{\alpha}, \boldsymbol{\beta}) \hat{\Lambda}(\boldsymbol{\alpha}, \boldsymbol{\beta}) \mathrm{d}^{2M}\boldsymbol{\alpha} \mathrm{d}^{2M}\boldsymbol{\beta}, \tag{4.3}$$

where $P(\boldsymbol{\alpha}, \boldsymbol{\beta})$ is the positive-P distribution over coherent state amplitudes $\boldsymbol{\alpha}, \boldsymbol{\beta}$. The off-diagonal coherent state projector

$$\hat{\Lambda}(\boldsymbol{\alpha}, \boldsymbol{\beta}) = \frac{\left|\boldsymbol{\alpha}\right\rangle \left\langle\boldsymbol{\beta}^*\right|}{\left\langle\boldsymbol{\beta}^* | \boldsymbol{\alpha}\right\rangle}, \tag{4.4}$$

doubles the classical phase-space dimension, allowing off-diagonal amplitudes $\boldsymbol{\beta} \neq \boldsymbol{\alpha}^*$ to exist.

One can restrict the distribution to a classical phase-space with $\boldsymbol{\beta} = \boldsymbol{\alpha}^*$, in which case the diagonal P-representation is obtained as a special case of the positive P-representation via the substitution $P(\boldsymbol{\alpha}, \boldsymbol{\beta}) = P(\boldsymbol{\alpha})\delta(\boldsymbol{\alpha}^* - \boldsymbol{\beta})$. However, for squeezed states, this will lead to the singular behavior that is already known.

Moments of the positive-P distribution are equivalent to normally ordered operator moments

$$\left\langle \hat{a}_{j_1}^\dagger, \ldots, \hat{a}_{j_n} \right\rangle = \langle \beta_{j_1}, \ldots, \alpha_{j_n} \rangle_P$$
$$= \iint P(\boldsymbol{\alpha}, \boldsymbol{\beta}) [\beta_{j_1}, \ldots, \alpha_{j_n}] \mathrm{d}^{2M}\boldsymbol{\alpha} \mathrm{d}^{2M}\boldsymbol{\beta}, \tag{4.5}$$

where $\langle \ldots \rangle$ denotes a quantum expectation value and $\langle \ldots \rangle_P$ is the positive-P probability average.

4.2.3. Wigner representation

The diagonal P-representation is unsuitable to simulate squeezed or entangled states, but there are classical phase-space distributions with positive distributions for quantum states. These are the symmetrically ordered Wigner representation and anti-normally ordered Q-function. They are more suitable for different types of detection, as they lead to large sampling errors when used for normally-ordered detectors.

The M-mode Wigner representation is defined as the Fourier transform of the symmetrically ordered characteristic function such that

$$W(\boldsymbol{\alpha}) = \frac{1}{\pi^{2M}} \int \mathrm{d}^2\boldsymbol{z} \mathrm{Tr} \left\{ \hat{\rho} e^{i\boldsymbol{z}(\hat{a}-\boldsymbol{\alpha}) + i\boldsymbol{z}^*(\hat{a}^\dagger - \boldsymbol{\alpha}^*)} \right\}, \tag{4.6}$$

where Tr $\{\ldots\}$ is the trace and $\boldsymbol{z}$ is a complex vector.

Although the Wigner function always exists as a real-valued function on phase-space for the density operator, or any other hermitian operator, the resulting probability distribution need not be positive. This is why the Wigner distribution is referred to as a quasi-probability. For thermal and squeezed states, the Wigner distribution is positive.

The Wigner function is directly applicable to symmetrically ordered operator products. Symmetric ordering, denoted $\{\ldots\}_{sym}$, is the average over all possible combinations of creation and annihilation operators, for example

$$\{\hat{a}^\dagger a\}_{sym} = \frac{1}{2}(\hat{a}\hat{a}^\dagger + \hat{a}^\dagger\hat{a}) \tag{4.7}$$

$$\{\hat{a}^\dagger \hat{a}^2\}_{sym} = \frac{1}{3}(\hat{a}^2\hat{a}^\dagger + \hat{a}\hat{a}^\dagger\hat{a} + \hat{a}^\dagger\hat{a}^2). \tag{4.8}$$

This ordering requirement makes applications to normally ordered detectors both cumbersome, as one must reorder all operators to normal order, and inaccurate, as seen from Eq.(4.7), where the expectation value of the symmetrically ordered number operator becomes

$$\left\langle \{\hat{a}^\dagger a\}_{sym} \right\rangle = |\alpha|^2 + \frac{1}{2}. \tag{4.9}$$

Therefore, the Wigner function adds half a quantum of vacuum noise per mode, causing a rapid increase sampling errors, making the Wigner function unsuitable for simulations of photon counting probabilities.

However, the Wigner function is ideal for simulating squeezed state quadrature operators, as these are measured via homodyne detectors which are symmetrically ordered.

4.2.4. Q-function

The standard form of the anti-normally ordered M-mode Q-function is

$$Q(\boldsymbol{\alpha}) = \frac{1}{\pi^M} \langle \boldsymbol{\alpha}|\hat{\rho}|\boldsymbol{\alpha}\rangle \,, \tag{4.10}$$

and, like the Wigner function, can be expressed as the Fourier transform of the anti-normally ordered characteristic function.

The Q-function distribution is always positive but is only defined for anti-normally ordered operator products with moments being obtained as

$$\begin{aligned} \left\langle \hat{a}_{j_1}, \ldots, \hat{a}^\dagger_{j_n} \right\rangle &= \left\langle \alpha_{j_1}, \ldots, \alpha^*_{j_n} \right\rangle_Q \\ &= \int Q(\boldsymbol{\alpha}) [\alpha_{j_1}, \ldots, \alpha^*_{j_n}] \mathrm{d}^{2M}\boldsymbol{\alpha}, \end{aligned} \tag{4.11}$$

where $\langle \ldots \rangle_Q$ denotes a Q-distribution average.

However, like the Wigner function, operators must be reordered for applications to normally ordered detectors. Using the standard bosonic commutation relations, Eqs.(3.48), the expectation value of the number operator is

$$\left\langle \{a\hat{a}^\dagger\}_{anti} \right\rangle = |\alpha|^2 + 1. \tag{4.12}$$

The Q-function adds a quantum of vacuum noise per mode, generating the largest increase in sampling errors of any phase-space representation when used to simulate normally ordered detectors. This accumulation of vacuum noise for multimode networks rapidly causes the Q-function to become inaccurate for simulating linear networks.

4.2.5. σ-ordering

The amount of vacuum noise added by each representation can be used to define the operator ordering parameter σ, where $\sigma = 0$ corresponds to normal ordering, $\sigma = 1/2$ symmetric ordering and $\sigma = 1$ anti-normal ordering.

The ability to define a common ordering scheme arises from writing the Wigner and Q-function distributions as convolutions of the positive P-representation

$$P_\sigma(\boldsymbol{\alpha}) = \frac{1}{(\pi\sigma)^M} \int P(\boldsymbol{\alpha}_0, \boldsymbol{\beta}_0) e^{-(\boldsymbol{\alpha}-\boldsymbol{\alpha}_0)(\boldsymbol{\alpha}^*-\boldsymbol{\beta}_0)/\sigma} \mathrm{d}^{2M}\boldsymbol{\alpha} \mathrm{d}^{2M}\boldsymbol{\beta}, \tag{4.13}$$

where $P_\sigma(\boldsymbol{\alpha})$ is a σ-ordered representation, $P(\boldsymbol{\alpha}_0, \boldsymbol{\beta}_0)$ is the positive-P distribution and $\boldsymbol{\alpha}_0, \boldsymbol{\beta}_0$ are used to denote the normal ordered nonclassical phase-space variables whilst $\boldsymbol{\alpha}, \boldsymbol{\alpha}^*$ denotes a classical phase-space which is valid for $\sigma = 1/2, 1$.

Operator moments for any ordering can now be obtained via

$$\left\langle \left\{ \hat{a}_{j_1}^\dagger, \ldots, \hat{a}_{j_n} \right\}_\sigma \right\rangle = \left\langle \alpha_{j_1}^*, \ldots, \alpha_{j_n} \right\rangle_\sigma$$
$$= \int P_\sigma(\boldsymbol{\alpha}) [\alpha_{j_1}^*, \ldots, \alpha_{j_n}] \mathrm{d}^{2M}\boldsymbol{\alpha}. \tag{4.14}$$

4.3. Operator mappings

In phase-space methods, it is convenient to define $\beta = \alpha^*$ in a classical phase-space, to give a unified notation. The operator equations are then mapped to differential equations with the equivalences:

$$\begin{aligned}
\hat{a}_n^\dagger \hat{\rho} &\rightarrow \left[\beta_n + (\sigma - 1) \frac{\partial}{\partial \alpha_n} \right] P_\sigma \\
\hat{a}_n \hat{\rho} &\rightarrow \left[\alpha_n + \sigma \frac{\partial}{\partial \beta_n} \right] P_\sigma \\
\hat{\rho} \hat{a}_n &\rightarrow \left[\alpha_n + (\sigma - 1) \frac{\partial}{\partial \beta_n} \right] P_\sigma \\
\hat{\rho} \hat{a}_n^\dagger &\rightarrow \left[\beta_n + \sigma \frac{\partial}{\partial \alpha_n} \right] P_\sigma \,.
\end{aligned} \tag{4.15}$$

The operator mappings give a differential equation. If it has a second-order positive-definite form it is a Fokker-Planck equation equivalent to an SDE, or an SPDE for quantum fields [58]. The noise can be additive or multiplicative, depending on the problem. Not all cases give stable FPE equations [59], and truncation is required for the Wigner representation if the Hamiltonian is nonlinear [60].

The total noise includes internal quantum noise generated from the Hamiltonian term $\hat{H}_{sys}$, as well as reservoir noise terms generated from the coupling to the reservoir operators, which is proportional to Γ_j. There is a similar behavior in classical systems, except that these correspond to a high-temperature limit, and in most cases only have external reservoir noise from thermal fluctuations.

4.4. Damped harmonic oscillator

As an example, take the driven and damped quantum harmonic oscillator. This has the Hamiltonian

$$\hat{H}/\hbar = i\mathcal{E}\left(\hat{a}^\dagger - \hat{a}\right) + \omega_0 \hat{a}^\dagger \hat{a}. \tag{4.16}$$

. If damping is added, it obeys the master equation

$$\begin{aligned}
\frac{d\hat{\rho}}{dt} = &-i[i\left(\mathcal{E}\hat{a}^\dagger - \mathcal{E}^*\hat{a}\right) + \omega_0 \hat{a}^\dagger \hat{a}, \rho] + \gamma\left(1 + \bar{n}\right)\left(2\hat{a}\rho\hat{a}^\dagger - \hat{a}^\dagger\hat{a}\rho - \rho\hat{a}^\dagger\hat{a}\right) \\
&+ \gamma\bar{n}(2\hat{a}^\dagger\rho\hat{a} - \hat{a}\hat{a}^\dagger\rho - \rho\hat{a}\hat{a}^\dagger).
\end{aligned} \tag{4.17}$$

This leads to a random walk in a complex space [1, 2],

$$\begin{aligned}\frac{d\alpha}{dt} &= \mathcal{E} - (\gamma + i\omega_0)\,\alpha + \sqrt{2\gamma\,(\sigma+\bar{n})}\zeta(t)\\ \frac{d\beta}{dt} &= \mathcal{E}^* - (\gamma - i\omega_0)\,\beta + \sqrt{2\gamma\,(\sigma+\bar{n})}\zeta^*(t),\end{aligned} \tag{4.18}$$

where the noise is complex and $\zeta(t) = (w_1(t) + iw_2(t))/\sqrt{2}$. The correlations are

$$\begin{aligned}\left\langle \zeta(t)\left(\zeta(t')\right)^*\right\rangle &= \delta\left(t-t'\right)\\ \left\langle \zeta(\omega)\left(\zeta\left(\omega'\right)\right)^*\right\rangle &= \delta\left(\omega-\omega'\right).\end{aligned} \tag{4.19}$$

4.4.1. Wigner representation

In the undriven, zero temperature Wigner case with γ =1, $\sigma = 1/2$, and in a rotating frame so that $\omega_0 = 0$, the probability follows the Fokker-Planck equation:

$$\frac{\partial P}{\partial t} = \left[\frac{\partial}{\partial\alpha_x}\alpha_x + \frac{\partial}{\partial\alpha_y}\alpha_y + \frac{1}{4}\left(\frac{\partial^2}{\partial\alpha_x^2} + \frac{\partial^2}{\partial\alpha_y^2}\right)\right]P, \tag{4.20}$$

which is an example of Eq (2.18). Ignoring terms that vanish or can be obtained from symmetry, the first corresponding moment equations in each of the real and imaginary directions are

$$\begin{aligned}\frac{\partial}{\partial t}\left\langle\alpha_x\right\rangle &= \left\langle -\alpha_x\frac{\partial}{\partial\alpha_x}\alpha_x\right\rangle = -\left\langle\alpha_x\right\rangle\\ \frac{\partial}{\partial t}\left\langle\alpha_x\alpha_y\right\rangle &= \left\langle -\left(\alpha_x\frac{\partial}{\partial\alpha_x} + \alpha_y\frac{\partial}{\partial\alpha_y}\right)\alpha_x\alpha_y\right\rangle = -\left\langle\alpha_x\alpha_y\right\rangle\\ \frac{\partial}{\partial t}\left\langle\alpha_x^2\right\rangle &= \left\langle\left(-\alpha_x\frac{\partial}{\partial\alpha_x} + \frac{1}{4}\frac{\partial^2}{\partial\alpha_x^2}\right)\alpha_x^2\right\rangle = \frac{1}{2} - 2\left\langle\alpha_x^2\right\rangle.\end{aligned} \tag{4.21}$$

The steady-state is therefore a Gaussian distribution with $\langle\alpha_{x,y}\rangle = 0$, $\langle\alpha_x\alpha_y\rangle = 0$ and $\left\langle\alpha_{x,y}^2\right\rangle = 1/4$. One can use an initial condition of $\alpha = (v_1 + iv_2)/2$, with $\left\langle v_i^2\right\rangle = 1/2$, in order to replicate the steady state, which is a Gaussian with$\langle\alpha_x\rangle = \langle\alpha_y\rangle = 0$ and$\left\langle\alpha_x^2\right\rangle = \left\langle\alpha_y^2\right\rangle = 1/4$.

4.4.2. Internal spectrum

Neglecting any boundary terms, the equation in frequency space is:

$$-i\omega\tilde{\alpha}(\omega) = -\tilde{\alpha}(\omega) + \tilde{\zeta}(\omega). \tag{4.22}$$

For sufficiently long times, the solution in frequency space - where $\omega = 2\pi f$ is the angular frequency - is therefore given by:

$$\tilde{\alpha}\left(\omega\right) = \frac{\tilde{\zeta}(\omega)}{1 - i\omega}. \tag{4.23}$$

The expectation value of the noise spectrum, $\left\langle |\tilde{\alpha}(\omega)|^2 \right\rangle$ in the long time limit, is:

$$\begin{aligned} \left\langle |\tilde{\alpha}(\omega)|^2 \right\rangle &= \frac{1}{2\pi\left(1+\omega^2\right)} \int\int e^{-i\omega(t-t')} \left\langle \zeta(t)\zeta^*(t') \right\rangle dtdt' . \\ &= \frac{T}{2\pi\left(1+\omega^2\right)}. \end{aligned} \tag{4.24}$$

This equation can also be used for some classical problems, which correspond to the high-temperature limit of $\bar{n} \gg 1$.

4.5. Stochastic gauge expansion

In this approach, the density matrix is expanded as a weighted integral over coherent state projection operators:

$$\rho\left(t\right) = \int d\boldsymbol{\phi} P\left(t,\boldsymbol{\phi}\right) \Lambda\left(\boldsymbol{\phi}\right). \tag{4.25}$$

Here, in the stochastic gauge method [**?**], $\boldsymbol{\phi} \equiv [\Omega, \boldsymbol{\alpha}, \boldsymbol{\beta}]$, where $\boldsymbol{\alpha}, \boldsymbol{\beta}$ are each M-dimensional complex numbers, and Ω is a real or complex weight. The operator basis Λ is defined using un-normalized coherent states $\|\boldsymbol{\alpha}\rangle$, so that:

$$\Lambda\left(\boldsymbol{\phi}\right) = \Omega \left\|\boldsymbol{\alpha}\right\rangle \left\langle \boldsymbol{\beta}^* \right\| e^{-\boldsymbol{\alpha}\cdot\boldsymbol{\beta}}. \tag{4.26}$$

There are standard identities available, namely:

$$\begin{aligned} \hat{a}_j \Lambda &= \alpha_j \Lambda \\ \hat{a}_j^\dagger \Lambda &= \left[\partial/\partial\alpha_j + \beta_j\right] \Lambda \\ \Lambda \hat{a}_j^\dagger &= \beta_j \Lambda \\ \Lambda \hat{a}_j &= \left[\partial/\partial\beta_j + \alpha_j\right] \Lambda \\ 0 &= \left[\Omega\partial/\partial\Omega - 1\right] \Lambda \\ 0 &= \partial^2/\partial\Omega^2 \Lambda \end{aligned} \tag{4.27}$$

The hermiticity of ρ means that every $\boldsymbol{\phi}$ has a conjugate $\boldsymbol{\phi}^*$ of equal weight, so the integral is sampled in pairs $\boldsymbol{\phi}_s$ and $\boldsymbol{\phi}_s^*$, corresponding to a sum over $\mathcal{S}$ samples of the real part of Λ:

$$\rho_c\left(t\right) = \lim_{\mathcal{S}\to\infty} \frac{1}{\mathcal{S}} \sum_s \Re\Lambda\left(\boldsymbol{\phi}_s\left(t\right)\right). \tag{4.28}$$

Operator averages are obtained through defining a *weighted* average as the infinite ensemble limit of a sum of trajectories:

$$\left\langle f\left(\boldsymbol{\phi}\right)\right\rangle \equiv \lim_{\mathcal{S}\to\infty} \left\langle f\left(\boldsymbol{\phi}\right)\right\rangle_{\mathcal{S}}. \tag{4.29}$$

Here, for hermitian operators,

$$\langle f(\boldsymbol{\phi})\rangle_{\mathcal{S}} \equiv \frac{1}{\mathcal{S}}\sum_{s}\Re\left[\Omega_s f(\boldsymbol{\phi}_s)\right], \tag{4.30}$$

with the approximation of taking only a finite number of samples $\mathcal{S}$. For example, the quantum average particle number $\langle\hat{n}_j\rangle_Q$ is obtained on taking a weighted average of $n_{js}\equiv\alpha_{js}\beta_{js}$:

$$\langle\hat{n}_j\rangle_Q = \langle n_j\rangle. \tag{4.31}$$

Individual trajectory photon numbers $\Re(\Omega_s n_{js})$ can be negative, although their large-$\mathcal{S}$ average is non-negative. These trajectories correspond to Schrodinger cat superpositions, causing mixtures of positive and negative 'effective' photon numbers. Such behavior is impossible in the diagonal Glauber-Sudarshan representation, where for a probabilistic distribution, only classical photon statistics occur [**?**, **?**].

4.5.1. MCPS

The Monte-Carlo density matrix equations can be solved with a positive-P phase-space representation, in which the density matrix is expanded as above. While it does not involve exponential storage, there is a sampling error with this method. One can term this approach MCPS.

As an application of the MCPS method we now treat the case of photodetector counts, where $\hat{L}_j = \hat{a}_j$ is the annihilation operator for mode j. The evolution only occurs through losses, which describes the ideal case for photo-detection, and is simplest to treat in detail.

We assume all photodetectors have identical efficiency γ. The non-Hermitian Hamiltonian evolution leads to an anti-commutator, so that, if $\tau = 2\gamma t$

$$\frac{d\rho_c}{d\tau} = -\frac{1}{2}\int d\boldsymbol{\phi}P(t,\boldsymbol{\phi})\sum_j\left[\hat{a}_j^\dagger\hat{a}_j - \langle\hat{n}_j\rangle, \Lambda(\boldsymbol{\phi})\right]_+. \tag{4.32}$$

Using standard identities together with partial integration gives a first order partial differential equation for $P(\boldsymbol{\phi})$, and hence ensures that the probability remains normalized:

$$\dot{P}(\boldsymbol{\phi}) = \sum_j\frac{1}{2}\left[\frac{\partial}{\partial\alpha_j}\alpha_j + \frac{\partial}{\partial\beta_j}\beta_j + 2\Omega\frac{\partial}{\partial\Omega}\Delta n_j(\boldsymbol{\phi})\right]P(\boldsymbol{\phi}), \tag{4.33}$$

where $\Delta n_j(\boldsymbol{\phi}) \equiv \alpha_j\beta_j - \langle\hat{n}_j\rangle = n_j - \langle n_j\rangle$. Because the coherent states are eigenstates of $\hat{a}$, the density matrix jump in Eq (3.37) is

$$d\rho \equiv \sum_j\int d\boldsymbol{\phi}\frac{\Delta n_j}{\bar{n}_j}P(\boldsymbol{\phi})\Lambda(\boldsymbol{\phi})\,dN_j. \tag{4.34}$$

4.5.2. Sampled trajectory equations

The equations only involve $n_j = \alpha_j \beta_j$, so we transform to these variables. The sampled probability of a jump dN_j in channel j is $p_j = \langle n_j \rangle \, d\tau$. This gives a change in trajectory weights so that, for sampled calculations, the jump maps $\Omega_s \to \Omega_s + d\Omega_s$ where:

$$d\omega_s = \sum_j \frac{\Delta n_{js}}{\langle n_j \rangle} dN_{js}. \tag{4.35}$$

This leads to a combined equation for the time-evolution of sample trajectories,

$$\begin{aligned} dn_{js} &= -n_{js} d\tau \\ d\Omega_s &= \Omega_s \sum_j \left(-d\tau + \frac{dN_{js}}{\langle n_j \rangle} \right) \Delta n_{js}, \end{aligned}$$

Consider a moving frame transformation, and a compensated jump variable with zero mean:

$$\begin{aligned} \tilde{n}_j(\tau) &= n_{j0}(0) \, e^{\tau} \\ dN_j^c &= dN_j - \langle n_j \rangle \, d\tau \end{aligned}$$

Hence, there are now only $\mathcal{S}$ stochastic variables, with equation

$$d\Omega_s(\tau) = \Omega_s \sum_j \frac{dN_{js}^c}{\langle \tilde{n}_j \rangle} \Delta \tilde{n}_{js}$$

As a further transformation, let

$$\begin{aligned} \chi &= 1 - e^{-\tau} \\ d\chi &= e^{-\tau} d\tau \end{aligned}$$

so that if the probability of a jump in $d\tilde{N}_j$ is $\tilde{p}_j$:

$$\begin{aligned} \tilde{p}_j &= \langle n_j \rangle \, d\tau = \langle \tilde{n}_j \rangle \, d\chi \\ d\tilde{N}_j^c &= d\tilde{N}_j - \langle \tilde{n}_j \rangle \, d\chi \end{aligned}$$

In a step of $d\chi$ there is a time-independent probability of:

$$\begin{aligned} d\Omega_s(\chi) &= \Omega_s \sum_j \frac{d\tilde{N}_{js}^c}{\langle \tilde{n}_j \rangle} \Delta \tilde{n}_{js} \\ &= \Omega_s \sum_j c_j(\mathbf{\Omega}) \, d\tilde{N}_j^c \end{aligned}$$

Numerically, this can be treated using an Euler method,

$$\Omega_s^{(n+1)} = \Omega_s^{(n)} \left(1 + \sum_j c_j \left(\mathbf{\Omega}^{(n)} \right) d\tilde{N}_j^c \right).$$

Hence, a weight Ω_s with a positive relative number Δn_{js} decays if unobserved, but grows if a jump is observed. This is because a large number is more probable if a jump is observed, and less probable otherwise. The opposite behavior is found with a negative relative number Δn_{js}. Every term eventually is in a vacuum state, and no further decay is possible.

4.6. Input-output spectra

The spectrum of an internal field variable is not the one that is usually measured. An important application of stochastic equations is therefore in calculating output, measured spectra of lasers, quantum optics, opto-mechanics and quantum circuits [53, 61]. These have the feature that the measured output spectrum may also include noise from reflected fields at the input/output ports. If the quantum noise term in the Heisenberg equations for a cavity operator $\hat{a}_c$ is given by: $\dot{\hat{a}}_c \sim .. + \sqrt{2\gamma}\hat{a}_{in}(t)$, then the corresponding operator input-output relations are $\hat{a}_{out}(t) + \hat{a}_{in}(t) = \sqrt{2\gamma}\hat{a}_c$.

In quantum phase-space for the case of the harmonic oscillator or similar systems, $\alpha_{in} = \sqrt{\sigma + \bar{n}}\zeta$ is the noise term in the Langevin equation. The output fields α_{out} that are measured are given by:

$$\alpha_{out} = \sqrt{2\gamma}\alpha - \alpha_{in}. \tag{4.36}$$

Hence one must include in the spectrum both the internal mode variables and the noise terms themselves. Solving for the spectra, one obtains auxiliary fields with

$$\begin{aligned} \tilde{\alpha}_{in}(\omega) &= \sqrt{\sigma + \bar{n}}\tilde{\zeta}(\omega) \\ \tilde{\alpha}_{out}(\omega) &= \sqrt{2\gamma}\tilde{a}(\omega) - \sqrt{\sigma + \bar{n}}\tilde{\zeta}(\omega). \end{aligned} \tag{4.37}$$

In summary, it is the output fields that are amplified and measured. Hence one must be able to compute the spectra of the output fields for experimental comparisons. These have the additional feature that they include the reservoir noise $\tilde{\zeta}(\omega)$, evaluated at the same time as the field is evaluated, since the reservoir noise is the input here. In xSPDE these are called *auxfields*.

4.6.1. Steady-state result

Consider the example of Section (4.4), in the Wigner representation case with $\gamma = 1$, $\sigma = 1/2$ and $\bar{n} = 0$. Over long time-scales, so that one is in the steady state, the solution for $\tilde{a}_{out}$ is that:

$$\begin{aligned} \tilde{\alpha}_{out}(\omega) &= \sqrt{2}\left[\frac{1}{1 - i\omega} - \frac{1}{2}\right]\tilde{\zeta}(\omega) \\ &= \frac{1}{\sqrt{2}}\left[\frac{1 + i\omega}{1 - i\omega}\right]\tilde{\zeta}(\omega). \end{aligned} \tag{4.38}$$

This gives the following expectation values:

$$\left\langle \tilde{\alpha}_{out}(\omega)\left(\tilde{\alpha}_{out}(\omega)\left(\omega'\right)\right)^{*}\right\rangle = \frac{1}{2}\delta\left(\omega-\omega'\right)$$
$$\left\langle \tilde{\alpha}_{in}(\omega)\left(\tilde{\alpha}_{in}(\omega)\left(\omega'\right)\right)^{*}\right\rangle = \frac{1}{2}\delta\left(\omega-\omega'\right). \tag{4.39}$$

These are the expectation values of the zero temperature quantum fluctuations in the input and output channels. This means that the harmonic oscillator in its ground state is in equilibrium with an external vacuum field reservoir, also in its ground state. However, from Eq (4.24), the internal spectral correlations of the harmonic oscillator are modified by the coupling.

While this is a simple result, the same general type of behavior occurs in more sophisticated cases. These may include many coupled modes with nonlinearities. Additional or auxiliary fields that depend both on noise terms and internal stochastic variables are required. The soluble case given above is a useful test case, and it is treated numerically later in the manual.

4.7. Sampling methods in phase-space

The section outlines the sampling methods used to simulate output distributions and perform comparisons with either experimental data, or exact tests.

4.7.1. Input-output samples

To simulate quantum networks in phase-space, one must first generate initial stochastic samples. This is achieved using the σ-ordering scheme as stochastic samples for any Gaussian input state in any representation are generated following:

$$\alpha_j = \frac{1}{2}\left(\Delta_{\sigma x_j} w_j + i\Delta_{\sigma y_j} w_{j+M}\right)$$
$$\beta_j = \frac{1}{2}\left(\Delta_{\sigma x_j} w_j - i\Delta_{\sigma y_j} w_{j+M}\right), \tag{4.40}$$

where $\langle w_j w_k\rangle = \delta_{jk}$ are real Gaussian noises and

$$\Delta^2_{\sigma x_j} = 2(n_j + \sigma + \tilde{m}_j)$$
$$\Delta^2_{\sigma y_j} = 2(n_j + \sigma - \tilde{m}_j), \tag{4.41}$$

are thermal squeezed state quadrature variances which are altered from the pure squeezed state definitions Eqs. (3.60) and (3.61).

For normally ordering, the input amplitudes $\boldsymbol{\alpha}, \boldsymbol{\beta}$ are converted to outputs as

$$\boldsymbol{\alpha}' = \boldsymbol{T}\boldsymbol{\alpha}$$
$$\boldsymbol{\beta}' = \boldsymbol{T}^{*}\boldsymbol{\beta}, \tag{4.42}$$

which follows from Eq.(3.46). However for non-normally ordered methods, additional vacuum noise arising from the reservoir modes must be included.

This is achieved using a hermitian decoherence matrix

$$\boldsymbol{D} = \boldsymbol{I} - \boldsymbol{T}^{\dagger}\boldsymbol{T}, \tag{4.43}$$

with decomposition $\boldsymbol{D} = \boldsymbol{U}\boldsymbol{\lambda}^2\boldsymbol{U}^{\dagger}$ where $\boldsymbol{B} = \boldsymbol{U}\boldsymbol{\lambda}\boldsymbol{U}^{\dagger}$ is the matrix square root and $\boldsymbol{\lambda}$ is a diagonal, positive matrix. The output amplitudes when $\sigma > 0$ are then obtained as

$$\boldsymbol{\alpha}' = \boldsymbol{T}\boldsymbol{\alpha} + \sqrt{\frac{\sigma}{2}}\boldsymbol{B}(\boldsymbol{u} + i\boldsymbol{v}), \tag{4.44}$$

where $\boldsymbol{\beta}' = \boldsymbol{\alpha}'^{*}$ as we are in a classical phase-space.

4.7.2. Grouped correlations computation

GCPs are readily simulated in phase-space using the positive-P representation by replacing the normally ordered projection operator Eq.(3.70) with the positive-P observable

$$\pi_i(c_i) =: e^{-n_i'}\left(e^{n_i'} - 1\right)^{c_i}, \tag{4.45}$$

where $n_i' = \alpha_i'\beta_i'$ is the output photon number.

The summation over exponentially many patterns implemented by GCPs (see Eq.(3.79) is simulated using a multidimensional inverse discrete Fourier transform

$$\begin{aligned}\tilde{\mathcal{G}}_{\boldsymbol{S}}^{(n)}(\boldsymbol{k}) &= \left\langle \prod_{j=1}^{d} \bigotimes_{i\in S_j} \left(\pi_i(0) + \pi_i(1)e^{-ik_j\theta_j}\right) \right\rangle_P, \\ \mathcal{G}_{\boldsymbol{S}}^{(n)}(\boldsymbol{m}) &= \frac{1}{\prod_j (M_j+1)} \sum_{\boldsymbol{k}} \tilde{\mathcal{G}}_{\boldsymbol{S}}^{(n)}(\boldsymbol{k}) e^{i\sum k_j\theta_j m_j},\end{aligned} \tag{4.46}$$

where $\theta_j = 2\pi/(M_j+1)$ and $k_j = 0, \ldots, M_j$.

The Fourier transform removes all patterns which don't contain $\boldsymbol{m}$ counts, in doing this the Fourier transform simulates all possible correlations generated in a network. This reduces an otherwise computationally complex task into a highly efficient and scalable one, allowing comparisons to be performed on experimental correlations of any order.

5. SPDE theory

This chapter describes the basics of stochastic partial differential equation (SPDE) theory, in order to explain the background to the numerical methods.

5.1. SPDE definitions

A stochastic partial differential equation or SPDE is defined in both time t and one or more space dimensions $\mathbf{x}$. We suppose there are d total space-time dimensions. The space-time coordinate is denoted as $\mathbf{r} = \left(r^1, \ldots r^d\right) = (t, \mathbf{x}) = (t, x, y, z, ...)$.

The stochastic partial differential equation solved is written in differential form as

$$\frac{\partial \mathbf{a}}{\partial t} = \mathbf{A}\left[\nabla, \mathbf{a}, \mathbf{r}\right] + \underline{\mathbf{B}}\left[\nabla, \mathbf{a}, \mathbf{r}\right] \cdot \mathbf{w}(\mathbf{r}) + \mathbf{L}\left[\nabla, \mathbf{a}, \mathbf{r}\right] \cdot \mathbf{a}. \tag{5.1}$$

Here, $\mathbf{a} = [a_1, \ldots a_f]$ is a real or complex vector field, $\mathbf{A}$ is a vector function of fields and space and $\underline{\mathbf{B}}$ a matrix function. The new feature is that terms can now include the operator ∇, which is a differential term in a real space $\mathbf{x}$. The exact structure of these terms is important, and not all such equations have well-behaved solutions [65, 66].

In many common cases, the noise term $\mathbf{w}$ is delta-correlated in time and space:

$$\left\langle w_i\left(\mathbf{r}\right) w_j\left(\mathbf{r}'\right)\right\rangle \quad = \quad \delta\left(t - t'\right)\delta\left(\mathbf{x} - \mathbf{x}'\right)\delta_{ij}. \tag{5.2}$$

One can also have noise with a finite correlation length defined by a noise correlation function $N_{ij}\left(\mathbf{x} - \mathbf{x}'\right)$ in space so that:

$$\left\langle w_i\left(\mathbf{r}\right) w_j\left(\mathbf{r}'\right)\right\rangle \quad = \quad \delta\left(t - t'\right)N_{ij}\left(\mathbf{x} - \mathbf{x}'\right). \tag{5.3}$$

It is even possible to have noise with a finite correlation time. Currently, these are not directly treated in xSPDE, although user definitions of this are possible by adding a customized noise function.

Additionally, the initial field has a probability distribution. In most examples, we suppose that this initial random field distribution can be generated as a function of Gaussian distributed initial random fields $\mathbf{v}\left(\mathbf{x}\right)$, where:

$$\left\langle v_i\left(\mathbf{x}\right) v_j\left(\mathbf{x}'\right)\right\rangle = \delta\left(\mathbf{x} - \mathbf{x}'\right)\delta_{ij}. \tag{5.4}$$

However, it is also possible that the initial random fields are also not delta-correlated, so that

$$\left\langle v_i\left(\mathbf{x}\right) v_j\left(\mathbf{x}'\right)\right\rangle = R_{ij}\left(\mathbf{x} - \mathbf{x}'\right). \tag{5.5}$$

Both finite correlation length and delta-correlated noise and random terms can be used in xSPDE simulations, with finite correlation lengths defined through a Fourier transform method.

5.2. Boundary conditions

There are three types of boundaries that are commonly used. They are specified independently for each space dimension $j = 2, \ldots d$, field component $i = 1, \ldots f$, and lower or upper location $\ell = 1, 2$. Each has a specific boundary type. These are described with a numerical code bt, as:

Dirichlet (specified value, $bt = 1$): $a_i\left(r^1, r^2, \ldots \hat{r}^j_\ell, \ldots\right) = f_{ij\ell}\left(\mathbf{r}, \mathbf{a}\right)$.

Periodic ($bt = 0$): $a_i\left(r^1, r^2, \ldots \hat{r}^j_\ell, \ldots\right) = a_i\left(r^1, r^2, \ldots \hat{r}^j_{3-\ell}, \ldots\right)$.

Robin/Neumann (specified derivative, $bt = -1$): $\frac{\partial}{\partial r^j} a_i\left(r^1, r^2, \ldots \hat{r}^j_\ell, \ldots\right) = g_{ij\ell}\left(\mathbf{r}, \mathbf{a}\right)$.

The coordinates $\hat{r}^j_\ell = \left(r^j_1, r^j_2\right)$ are locations where boundary conditions are enforced. There are five types of boundary *combinations* of these for each dimension and field variable. Note that the boundary type can change the error stability properties of an equation. The most general boundaries can only be specified using finite differences currently, as the spectral method boundary types are more limited.

Periodic boundaries can't be combined with other types, as this defines both boundaries:

a) periodic-periodic- P-P: "0,0"

b) Dirichlet-Dirichlet- D-D: "1,1"

c) Robin-Robin- R-R: "-1,-1"

d) Robin-Dirichlet- R-D: "-1,1"

e) Dirichlet-Robin- D-R: "1,-1"

Just as with the derivative term, each of these types can change with dimension and field component. Specified field or derivative values can be any user-defined functions of space, time, and field amplitude or simply have fixed values. Currently, all combinations of boundaries can be treated in xSPDE using finite difference derivatives. Spectral methods are restricted to periodic or zero Dirichlet/Neumann boundary conditions.

5.3. Spatial grid and boundaries

The location of the boundary at $\hat{r}_\ell^j$ is important in solving (S)PDEs, especially if high accuracy is required, or if field values at the boundary are needed.

Suppose the spatial grid spacing is Δx and the number of grid points in a particular dimension d is $points(d) = N$, then the maximum range from the first to last computed point is:

$$R = (N-1)\Delta x = ranges(d). \tag{5.6}$$

Noting that $\mathbf{r} = (t, \mathbf{x})$, and $\Delta\mathbf{r} = (\Delta t, \Delta\mathbf{x})$,this means that the space-time points for an origin vector $\boldsymbol{O}$are at:

$$r_i = O_i + (i-1)\Delta r_i. \tag{5.7}$$

There are two slightly different spatial boundary locations used in xSPDE, depending on the type of boundary conditions specified, as follows:

5.3.1. Periodic boundary

For the default case of a periodic boundary, the logical boundary location is arbitrary. The indices are arranged as though on a circle from $1 : N$. It is useful to suppose the boundary is simultaneously at $\hat{r}_1^j = r_1^j - \Delta r^j/2$ and at $\hat{r}_2^j = r_{N_j}^j + \Delta r^j/2$. Neither upper or lower logical 'boundary' is at a grid point. The effective range of the domain is $R^j + \Delta r^j$, due to this displaced boundary.

Only the values at N points are computed, and one must regard the point where the periodicity is enforced as interpolating between the last and first point.

5.3.2. Non-periodic boundary

For the case of a non-periodic boundary, including Dirichlet, Robin and Neumann boundary conditions, the indices are in a line from $1 : N$. The lower and upper lower boundaries are at $\hat{r}_1^j = r_1^j$ and at $\hat{r}_2^j = r_{N_j}^j$. In some PDE methods the logical boundaries are outside the grid boundaries, but that is not the case here. Unlike the periodic case, boundaries are enforced at the first and last point.

This is different to what is found in most trigonometric transform software, but this approach allows for a unified treatment of multiple types of algorithm. For finite difference derivatives at the boundaries, this leads to the usual result that the central difference approximation to the second derivative is of first order (in Δr) at the boundaries, while it is of second order elsewhere.

With spectral methods, the derivative boundaries are obtained with a combination of an interaction picture transform and additional polynomial terms. For simplicity, only linear, even order space derivatives are included in the linear propagator for the interaction picture (see 5.5), which means that other space derivatives must be included using finite differences.

5.4. Multidimensional walk

The simplest example of an SPDE is the multidimensional Wiener process:

$$\dot{a} = w(t, \mathbf{x}) \,. \tag{5.8}$$

This has a solution that is identical in appearance to an SDE:

$$a\left(t, \mathbf{x}\right) = a\left(0, \mathbf{x}\right) + \int_0^t w\left(\tau, \mathbf{x}\right) d\tau. \tag{5.9}$$

Just as for an SDE, this means that the initial mean value does not change in time:

$$\left\langle a\left(t, \mathbf{x}\right)\right\rangle = \left\langle a\left(0, \mathbf{x}\right)\right\rangle . \tag{5.10}$$

Since there are no spatial derivatives here, boundary values are not important. One can regard this as having periodic boundaries, which by the xSPDE conventions means that no boundary conditions are enforced - since periodic boundaries do not alter computed values when there are no derivatives.

5.4.1. Variance solution

The noise correlation is non-vanishing from Eq (2.2), so the variance must increase with time:

$$\begin{aligned} \left\langle a^2\left(t, \mathbf{x}\right)\right\rangle &= \left\langle a^2\left(0, \mathbf{x}\right)\right\rangle + \int_0^t \int_0^t \left\langle w\left(\tau, \mathbf{x}\right) w\left(\tau', \mathbf{x}\right)\right\rangle d\tau d\tau' \\ &= \left\langle a^2\left(0, \mathbf{x}\right)\right\rangle + \delta^{d-1}\left(0\right) \int_0^t \int_0^t \delta\left(\tau - \tau'\right) d\tau d\tau'. \end{aligned} \tag{5.11}$$

Integrating the temporal delta function gives unity. The spatial delta-function is replaced by $1/\Delta V$ in a discretized lattice calculation at points $\mathbf{x}_j$ with cell volume $\Delta V = \prod \Delta x_j$, which means that the second moment and the variance both increase linearly with time:

$$\left\langle a^2\left(t, \mathbf{x}_j\right)\right\rangle = \left\langle a^2\left(0, \mathbf{x}_j\right)\right\rangle + t/\Delta V. \tag{5.12}$$

The probability on the lattice for observing lattice field values a_j follows an elementary diffusion equation:

$$\frac{\partial P}{\partial t} = \frac{1}{2\Delta V} \sum_j \frac{\partial^2 P}{\partial a_j^2} \,, \tag{5.13}$$

which is an example of Eq (2.18). From this equation and using Eq (2.20), the first two corresponding moment equations in this case are

$$\begin{aligned} \frac{\partial}{\partial t} \left\langle a_j \right\rangle &= \left\langle \frac{1}{2} \frac{\partial^2}{\partial a_j^2} a_j \right\rangle = 0 \\ \frac{\partial}{\partial t} \left\langle a_j^2 \right\rangle &= \left\langle \frac{1}{2\Delta V} \frac{\partial^2}{\partial a_j^2} a_j^2 \right\rangle = \frac{1}{\Delta V}. \end{aligned} \tag{5.14}$$

These differential equations are satisfied by the solutions obtained directly from the stochastic equations, but as one can see, the coupling between the lattice points provides more interesting behavior. This requires derivative terms such as Laplacians.

5.5. Interaction picture

To treat Laplacians, spectral or interaction-picture methods can be very efficient, with much lower errors and much faster run-times. This is because they do not have the stability problems of finite difference methods when treating higher-order derivatives, which allows much larger time-steps to be used.

To explain the interaction picture algorithm, SPDEs often contain terms which are linear in the field variables $\mathbf{a}$, including derivative operators acting on $\mathbf{a}$. This can be treated exactly using an *interaction picture*, which leads to dramatically reduced time-step errors and higher stability [30, 67], by using a spectral method to compute derivatives. These methods are also very useful in non-stochastic PDEs.

In summary, the interaction picture provides a means to solve for linear space-derivative terms in the propagation in an efficient way. This is based on introducing local variables $\tilde{\mathbf{a}}$ for the field variables $\mathbf{a}$. It is convenient for the purposes of describing such interaction picture methods to introduce an abbreviated notation as:

$$\mathcal{D}\left[\mathbf{a}, \mathbf{r}\right] = \mathbf{A}\left[\nabla, \mathbf{a}, \mathbf{r}\right] + \underline{\mathbf{B}}\left[\nabla, \mathbf{a}, \mathbf{r}\right] \cdot \mathbf{w}(\mathbf{r}) \tag{5.15}$$

Hence, we can write the differential equation as:

$$\frac{\partial \boldsymbol{a}}{\partial t} = \mathcal{D}\left[\mathbf{a}, \mathbf{r}\right] + \underline{\mathbf{L}}\left[\boldsymbol{\nabla}\right] \cdot \boldsymbol{a}. \tag{5.16}$$

Here $\underline{\mathbf{L}}\left[\boldsymbol{\nabla}\right]$ should include the highest order derivatives, as these have the largest eigenvalues, but lower-order derivative terms may occur in the other terms.

5.5.1. Linear propagator

Next, we define a linear propagator. This is given formally by:

$$\mathcal{P}\left(t, \bar{t}\right) = \exp\left(\Delta t \underline{\mathbf{L}}\left[\boldsymbol{\nabla}\right]\right). \tag{5.17}$$

where $\Delta t = t - \bar{t}$, $\bar{t}$ is the interaction picture origin, and the notation includes setting boundary values. Transforming the field $\mathbf{a}$ to an interaction picture is achieved on defining:

$$\tilde{\mathbf{a}} = \mathcal{P}^{-1}\left(t, \bar{t}\right) \mathbf{a}. \tag{5.18}$$

As a result, the equation of motion is:

$$\frac{\partial \tilde{\mathbf{a}}}{\partial t} = \mathcal{D}\left[\mathcal{P}\left(t, \bar{t}\right) \tilde{\mathbf{a}}, t\right]. \tag{5.19}$$

This allows an SPDE to be treated with transformations using Fourier or discrete sine/cosine transforms. Our implementation uses a diagonal linear operator L without

space-dependence. The linear operator can have any derivative in the periodic case, but only even order derivatives in the Dirichlet and Neumann case.

As well as the linear term, derivatives and nonlinear functions that are not tractable with spectral methods can appear in the residual term $\mathcal{D}[\mathbf{a}, \mathbf{r}]$, where they are treated using finite difference techniques. As a result, while the interaction picture does not handle all possible derivative terms, it also does not restrict them from being used elsewhere in the equations.

Other methods exist in the literature. Improved convergence properties are obtained for some problems in a spectral picture using an exact solution of a linear part of the drift term [68, 69], or stochastic noise terms [70], as well as the Laplacian terms. The xSPDE code has user-definable functions that can be adapted to include these.

5.6. Fourier transforms

It is often useful to transform a field to implement the interaction picture, or to extract nonlocal correlation properties in space. The Fourier transforms or spectrum definitions used in xSPDE are given by the symmetric Fourier transform definition:

$$\begin{aligned}\tilde{a}(\mathbf{k}) &= \mathcal{F}(a(\mathbf{x})) \\ &= \frac{1}{[2\pi]^{(d-1)/2}} \int e^{-i\mathbf{k}\cdot\mathbf{x}} a(\mathbf{x}) d\mathbf{x}\,. \end{aligned} \tag{5.20}$$

The inverse Fourier transform is the function:

$$\begin{aligned} a(\mathbf{x}) &= \mathcal{F}^{-1}(\tilde{a}) \\ &= \frac{1}{[2\pi]^{(D-1)/2}} \int e^{i\mathbf{k}\cdot\mathbf{x}} \tilde{a}(\mathbf{k}) d\mathbf{k}\,. \end{aligned} \tag{5.21}$$

In simulations, this is not combined with any time (or space) averaging as in the temporal Fourier transforms. The reason for this is that the interaction picture transformations must be invertible, which is the case for a point-based discrete Fourier transform.

5.6.1. Normalization

During propagation, we define temporary internal fields $A(\mathbf{k_n})$, that are normalized using FFT conventions:

$$\begin{aligned} A(\mathbf{k_n}) &= \sum_{j_2=1}^{N_2} \cdots \sum_{j_d=1}^{N_d} e^{-i\mathbf{k}_n\cdot\mathbf{x_j}} a(\mathbf{x_j}) \\ a(\mathbf{x_j}) &= \frac{1}{\prod_{k=2}^{D} N_k} \sum_{n_2=1}^{N_2} \cdots \sum_{n_D=1}^{N_D} e^{i\mathbf{k_n}\cdot\mathbf{x_j}} A(\mathbf{k_n})\,. \end{aligned} \tag{5.22}$$

Otherwise, for graphical and output averages, we define Fourier transforms using physics and mathematics conventions:

$$\tilde{a}\left(\mathbf{k_n}\right) = \prod_{d=2}^{D}\left[\frac{\Delta x_d}{\sqrt{2\pi}}\right]\sum_{j_2=1}^{N_2}\cdots\sum_{j_d=1}^{N_D} e^{-i\mathbf{k}_n\cdot\mathbf{x_j}} a\left(\mathbf{x_j}\right)$$
$$a\left(\mathbf{x_j}\right) = \prod_{d=2}^{D}\left[\frac{\Delta k_d}{\sqrt{2\pi}}\right]\sum_{n_2=1}^{N_2}\cdots\sum_{n_d=1}^{N_D} e^{i\mathbf{k_n}\cdot\mathbf{x_j}} \tilde{a}\left(\mathbf{k_n}\right) . \tag{5.23}$$

Note that this rescaling is consistent, because

$$\Delta x_d \Delta k_d = \frac{2\pi}{N_d}. \tag{5.24}$$

5.7. Trigonometric transforms

Taking the interaction picture approach, we now consider other types of boundary conditions, which we initially assume here are either a zero field (Dirichlet) or a zero derivative (Neumann). We will only treat cases of even order derivatives, which do not change the trigonometric function. Any odd order derivatives are taken to be included in the finite difference ($\mathcal{D}$) term.

5.7.1. Zero boundary cases

In the spectral transform method in one space dimension, with zero boundaries, one uses a trigonometric function, $T\left(kx\right) = T_1 \sin\left(kx\right) + T_2 \cos\left(kx\right)$ to expand as:

$$a_i\left(t,x\right) = \sum_n a_{i,n}(t) T(k_{i,n}x), \tag{5.25}$$

The discrete inverse transform allows evaluation at sample points x_j, in order to satisfy the boundary conditions:

$$a_{i,n}(t) = \sum_j a_i(t,x_j)\tilde{T}(k_n x_j), \tag{5.26}$$

The trigonometrical function is defined such that:

$$\partial_x^{2p} T(kx) = \left(-k^2\right)^p T(kx). \tag{5.27}$$

The propagated equation is exactly soluble for the sampled points, since for each component

$$\begin{aligned}\mathcal{L}\cdot a(t,x_j) &= \sum_{ijn} \mathcal{L} a_n(t) T(k_n x_j),\\ &= -\sum_{ijnp} L_p\left(-k_n^2\right)^p a_n(t) T(k_n x_j)).\end{aligned} \tag{5.28}$$

Hence,

$$a_n(t) = \exp\left(\sum L_p \left(-k_n^2 t\right)^p t\right) a_n(0). \tag{5.29}$$

This is an exact solution, provided the initial condition has the given expansion. This of course is usually an approximation itself, which should be checked by changing the grid. There are no other approximations made on the transverse derivative. Provided the k values are the same, this propagator is identical for all types of trigonometric and Fourier transforms.

As explained in (5.2), there are five boundary combinations that are possible in each dimension and field component. Each has a corresponding xSPDE boundary type and spectral integrator. Each boundary type is specified to depend on the space dimension and the field component, as well as having boundary values depending on time and any field value.

Currently, all can be treated in xSPDE using finite differences, and each type of boundary also has a spectral method that preserves the boundary requirement. In principle one can define the trigonometric transforms to correspond to whole symmetries whose boundary is at a grid point, as used in xSPDE, or half symmetries which are halfway between two grid points.

All spectral methods used in xSPDE make use of boundaries at a grid point, in order to compute the relevant terms, which means that there is greater compatibility with the finite difference methods, when the boundaries are at the grid points. Differential equations can also have first order terms, which currently require using either finite differences or periodic boundaries.

It is possible to compute first-order derivatives with spectral methods, but these turn sine transforms into cosine transforms. This is not compatible with trigonometric interaction picture transformations used in XSPDE. As a result, any odd-order derivative terms must be computed using finite differences in all cases , except for the periodic case, where either method can be used.

In summary, spectral transforms can all be implemented using fast FTT, discrete sine (DST) or cosine (DCT) transforms. The spectral method used is specific to the boundary type. The definitions used here correspond to the standard definitions [71,72], except for one-based indexing, normalisation, and extra points at the boundaries, explained below.

5.7.2. Finite boundary values

For the case of finite boundaries, a combination of trigonometric and polynomial functions are used to expand the fields, so that:

$$\begin{aligned} a_i(t,x) &= b_i(t,x) + u_i(t,x) \\ &= b_i(t,x) + \sum_n u_{i,n}(t) T(k_{i,n} x), \end{aligned} \tag{5.30}$$

Here, the functions $b_i(t,x)$ are inhomogeneous polynomial terms specified to satisfy the nonvanishing boundary conditions such that:

$$\dot{b} = \mathcal{L} \cdot b, \tag{5.31}$$

while the trigonometric expansion simply has to satisfy the equation with zero boundaries.

5.8. Transforms and boundaries

For Dirichlet or Neumann/Robin boundaries, the following expansion can be employed in each dimension. We only describe one space dimension for simplicity with:

$$u = \sum_{n=1}^{\infty} \left[S_n \sin\left(k_n x\right) + C_n \cos\left(k_n x\right) \right] e^{\sum L_p \left(-k_n^2\right)^p t}, \tag{5.32}$$

where k_n, C_n, S_n are chosen to satisfy the initial and boundary conditions. Boundaries are taken, for the purposes of explanation, as being from $x = 0$ to $x = R$. This is not the case in the actual code, which can treat arbitrary boundary locations due to the use of the optional *origins* input to change the origin.

Unlike fast Fourier transform (FFT) definitions, there are multiple distinct trigonometric transforms . These are generally labeled DST-(n) and DCT-(n), where $n = I..IV$. They correspond to distinct boundary combinations, as explained below.

Suppose there are N computational grid-points. For the spatial grid (1-based), this corresponds to $x_n = (n-1)\,\Delta x$, $n = 1, ..., N$ with $\Delta x = \frac{R}{N-1}$, so we have $x_1 = 0$ and $x_N = R$, as elsewhere in the manual.

In carrying out a discrete transform on N_T points, with standard trigonometric transform definitions of N_T, there are **less** transform grid points required if some boundary values are defined due to Dirichlet boundaries, hence $N_T < N$. This is because xSPDE stores the full computational range, N, *with* boundary values.

Sometimes one may wish to refer to the corresponding periodic Fourier transform size, N_{FT}. This is $N_{FT} = 2N_T = 2\,(N-1)$, except for DST-I , when it is $N_{FT} = 2(N_T+1) = 2\,(N-1)$.

An unnormalized inverse gives the original array multiplied by $N_{FT}/4 = (N-1)\,/2$, where $N_{FT} = 2\,(N-1)$ is the periodic size, so our definitions include a normalisation of $\sqrt{2/\,(N-1)}$. HereN_T, the number of points in the standard DST/DCT definitions, differs from **both** the xSPDE computation grid size N that includes both boundaries, and also from the periodic size, which always includes one (periodic) boundary.

Our notation is based on standard discrete sine and cosine transform definitions. Here we use $1-$based indices throughout. For all coordinates, including these examples of discrete Fourier transforms, with an origin at $\boldsymbol{r} = 0$ and an integration range of $\boldsymbol{R}$, we define:

$$\begin{aligned} r_n^d &= (n-1)\,\Delta r^d. \\ \Delta r^d &= R^d/(N^d - 1). \end{aligned} \tag{5.33}$$

If we regard the transforms as having arguments of form $k_j \cdot r_n$, the momentum spacings

given below are such that:

$$\Delta k = \frac{\pi}{R}$$
$$\Delta x \Delta k = \frac{\pi}{N-1}. \tag{5.34}$$

The internal momentum definitions used in the propagator calculations are therefore different to those used in external graphs and in periodic boundary cases.

The following lists the trigonometric transforms required to obtain the transform $\tilde{u}_k$ from u_n, and vice-versa, for the four non-periodic boundary types in each dimension and field index.

5.8.1. D-D case: Discrete map (DST-I)

Let $u(0) = u_1 = 0$, and $u(R) = u_N = 0$. The discrete representation of u is:

Forward transform: DST-I

$$\tilde{u}_k = \sqrt{\frac{2}{N-1}} \sum_{n=2}^{N-1} u_n \sin\left(\pi \frac{(k-1)(n-1)}{N-1}\right). \tag{5.35}$$

Inverse transform: DST-I

$$u_n = \sqrt{\frac{2}{N-1}} \sum_{k=2}^{N-1} \tilde{u}_k \sin\left(\pi \frac{(k-1)(n-1)}{N-1}\right). \tag{5.36}$$

The forward transform does **not** require the values at the end-points of $n = 1$ and $n = N$, which are set to zero in this case. This is implicit in the sine expansion, since $\sin(\mathrm{n}\pi) = 0$. Second derivatives are proportional to $(k-1)^2$.

5.8.2. R-R case: Discrete map (DCT-I)

Let $u'(0) = 0$, and $u'(R) = 0$. The discrete representation of u is:

Forward transform: DCT-I

$$\tilde{u}_k = \sqrt{\frac{2}{N-1}} \left(\frac{1}{2}\left(u_1 + (-1)^{n-1} u_N\right) + \sum_{n=2}^{N-1} u_n \cos\left(\pi \frac{(k-1)(n-1)}{N-1}\right)\right). \tag{5.37}$$

Inverse transform: DCT-I

$$u_n = \sqrt{\frac{2}{N-1}} \left(\frac{1}{2}\left(\tilde{u}_1 + (-1)^{n-1} \tilde{u}_N\right) + \sum_{k=2}^{N-1} \tilde{u}_k \cos\left(\pi \frac{(k-1)(n-1)}{N-1}\right)\right). \tag{5.38}$$

The forward transform requires the values at the end-points of $n = 1$ and $n = N$, which are not zero in this case. It is equal (up to a factor) to a discrete Fourier transform of $2(N-1)$ real numbers u_n with even symmetry about $n = 1$ and $n = N$. As a result, the equivalent discrete derivatives at both the end-points are zero. Second derivatives are proportional to $(k-1)^2$.

5.8.3. D-R case: Discrete map (DST-II/III)

Let $u(0) = 0$, and $u'(R) = 0$. The discrete representation of u is:

Forward transform: DST-III

$$\tilde{u}_k(t) = \sqrt{\frac{2}{N-1}} \left((-1)^{(n-1)} u_N/2 + \sum_{n=2}^{N-1} u_n \sin\left[\frac{\pi}{N-1} \left(k - \frac{1}{2} \right) (n-1) \right] \right). \quad (5.39)$$

Inverse transform: DST-II

$$u_n = \sqrt{\frac{2}{N-1}} \left(\sum_{k=1}^{N-1} \tilde{u}_k(t) \sin\left[\frac{\pi}{N-1} \left(k - \frac{1}{2} \right) n \right] \right). \quad (5.40)$$

The forward transform does **not** require the value at $n = 1$, which is zero in this case. This is implicit in the sine expansion, since $\sin(\mathrm{n}\pi) = 0$. This transform implies a boundary condition that is odd around $n = 1$, and even around $n = N$. Second derivatives are proportional to $(k - 1/2)^2$.

5.8.4. R-D case Discrete map (DCT-II/III)

Take $u'(0) = u(R) = 0$. The discrete representation of u is:

Forward transform: DCT-III

$$\tilde{u}_k = \sqrt{\frac{2}{N-1}} \left(u_1/2 + \sum_{n=2}^{N-1} u_n \cos\left[\frac{\pi}{N-1} \left(k - \frac{1}{2} \right) (n-1) \right] \right). \quad (5.41)$$

Inverse transform: DCT-II

$$u_n = \sqrt{\frac{2}{N-1}} \sum_{k=1}^{N} \tilde{u}_k \cos\left[\frac{\pi}{N-1} \left(k - \frac{1}{2} \right) (n-1) \right]. \quad (5.42)$$

The forward transform does not require the value at $n = N$, which is zero in this case. This transform implies a boundary condition that is even around $n = 1$, and odd around $n = N$. Second derivatives are proportional to $(k - 1/2)^2$.

5.9. Frequency or momentum grid

The frequency or momentum grid spacing is defined for all *output* graphs and periodic Fourier transforms as

$$\Delta k = \frac{2\pi}{N\Delta x}. \tag{5.43}$$

The internal momentum grid spacing used can differ from this, depending on the transforms used in the interaction picture. As explained above in Section (5.8), the internal momenta for trigonometric transforms are:

$$\Delta k = \frac{\pi}{(N-1)\,\Delta x}. \tag{5.44}$$

This is because the xSPDE algorithms allow the use of a sequence of interaction pictures. Each successive interaction picture is referenced to $t = t_n$, for the n-th step starting at $t = t_n$, so $\boldsymbol{a}_I(t_n) = \boldsymbol{a}(t_n) \equiv \boldsymbol{a}_n$. It is also possible to solve stochastic partial differential equations in xSPDE using explicit derivatives, but this is less efficient.

A discrete Fourier transform (DFT) using a fast Fourier transform method is employed for the interaction picture (IP) transforms used with periodic boundaries. This is normalized differently to the graphed Fourier transforms, but the difference is not computationally significant. However, the Δk used internally changes with the precise type of trigonometric transform used in other cases.

In one dimension, the DFT is usually defined by a sum over indices starting with zero, rather than the Matlab convention of one. Hence, if $\tilde{m} = m - 1$:

$$A_{\tilde{n}} = \mathcal{F}(a) = \sum_{\tilde{m}=0}^{N-1} a_{\tilde{m}} \exp\left[-2\pi i \tilde{m}\tilde{n}/N\right]. \tag{5.45}$$

For periodic boundaries, the IP Fourier transform can be written in terms of an FFT as

$$\boldsymbol{A}(\boldsymbol{k_n}) = \prod_j \left[\sum_{\tilde{m}_j} \exp\left[-i\,(dk_j dx_j)\,\tilde{m}_j\tilde{n}_j\right]\right]. \tag{5.46}$$

The inverse FFT Fourier transforms divide by the correct factors of $\prod_j N_j$ to ensure invertibility. Due to the periodicity of the exponential function, negative momenta are obtained if we consider an ordered lattice such that:

$$\begin{aligned} k_j &= (j-1)\Delta k \;\; (j \leq N/2) \\ k_j &= (j-1-N)\Delta k \;\; (j > N/2) \end{aligned}. \tag{5.47}$$

This Fourier transform is then multiplied by the appropriate factor to propagate in the interaction picture, then an inverse Fourier transform is applied. While it is not scaled for interaction picture transforms, an additional scaling factor is applied to obtain transformed fields in any averages for output plots.

In other words, in the averages

$$\tilde{a}_n = \frac{\Delta x}{\sqrt{2\pi}} A_{\tilde{n}'}. \tag{5.48}$$

where the indexing change indicates that graphed momenta are stored from negative to positive values. For plotted frequency spectra a **positive** sign is used in the frequency exponent of the transform to frequency space, to agree with common physics conventions.

5.10. Derivatives

5.10.1. Spectral derivatives

For spectral derivatives in the interaction picture, we define $D_x(k)$ to obtain a derivative. To explain, one integrates by parts:

$$D_x^p \tilde{\boldsymbol{a}}(\boldsymbol{k}) = [ik_x]^p \tilde{\boldsymbol{a}}(\boldsymbol{k}) = \frac{1}{(2\pi)^{d/2}} \int d\boldsymbol{x} e^{-i\boldsymbol{k}\cdot\boldsymbol{x}} \left[\frac{\partial}{\partial x}\right]^p \boldsymbol{a}(\boldsymbol{x}). \tag{5.49}$$

This means, for example, that to calculate a one dimensional space derivative in a Fourier interaction picture routine, one uses:

$$\nabla_x \to D_x. \tag{5.50}$$

Here Dx is an array of momenta in cyclic order in dimension d as defined above, suitable for an FFT calculation. The imaginary i is not needed to give the correct sign, as it is included in the derivative array. In two dimensions, a full two-dimensional Laplacian is:

$$\boldsymbol{\nabla}^2 = \nabla_x^2 + \nabla_y^2 \to D_x^2 + D_y^2. \tag{5.51}$$

Then, on inverting the transform

$$\left[\frac{\partial}{\partial x}\right]^p \boldsymbol{a}(\boldsymbol{x}) = \frac{1}{(2\pi)^{d/2}} \int d\boldsymbol{x} e^{i\boldsymbol{k}\cdot\boldsymbol{x}} [D_x(\boldsymbol{k})]^p \tilde{\boldsymbol{a}}(\boldsymbol{k}). \tag{5.52}$$

5.10.2. Finite difference derivatives

For calculating derivatives using finite differences, the following central differencing method is used, away from the boundaries:

$$\nabla_x a(x_i) \to \frac{1}{2\Delta x} [a(x_{i+1}) - a(x_{i-1})]$$

$$\nabla_x^2 a(x_i) \to \frac{1}{\Delta x^2} [a(x_{i+1}) - 2a(x_i) + a(x_{i-1})]. \tag{5.53}$$

This raises the question of how to calculate derivatives at the boundary, for example at the lower boundary x_1, where $a(x_0)$ is not known, and similarly at the upper

boundary. The answer depends on the boundary type [73], and is obtained by extending the boundary to additional points $a(x_0)$ and $a(x_{N+1})$ that are assumed to extend the boundary condition:

Periodic: $a(x_0) = a(x_N)$

$$\nabla_x a(x_1) \to \frac{1}{2\Delta x}\left[a(x_2) - a(x_N)\right]$$

$$\nabla_x^2 a(x_1) \to \frac{1}{\Delta x^2}\left[a(x_2) - 2a(x_2) + a(x_N)\right]. \tag{5.54}$$

Dirichlet: $\tilde{a}(x_1)$ **specified:** $a(x_0) = \tilde{a}(x_1)$

$$\nabla_x a(x_1) \to \frac{1}{2\Delta x}\left[a(x_2) - \tilde{a}(x_1)\right]$$

$$\nabla_x^2 a(x_1) \to \frac{1}{\Delta x^2}\left[a(x_2) - \tilde{a}(x_1)\right]. \tag{5.55}$$

Robin/Neumann: $\tilde{a}'(x_1)$ **specified:** $a(x_0) = a(x_2) - 2\tilde{a}'(x_1)\Delta x$

$$\nabla_x a(x_1) \to \tilde{a}'(x_1)$$

$$\nabla_x^2 a(x_1) \to \frac{2}{\Delta x^2}\left[a(x_2) - a(x_1) - \tilde{a}'(x_1)\Delta x\right]. \tag{5.56}$$

In all cases the boundary value is evaluated as part of the derivative evaluation, so it can be a nonlinear function of $\mathbf{a}$.

Part II.

Numerical Toolboxes

6. SDE toolbox

This chapter describes how to use the xSPDE numerical toolbox to solve an SDE to obtain and graph averages, spectra or probability distributions.

6.1. Using xSPDE

Stochastic equations generally require numerical solutions. To obtain them, xSPDE has a parameter structure, p, that defines both the equations and numerical parameters. The equations are defined as user functions with arguments *(fields..,noises.., parameters)*.

ALl input parameters are all passed to functions in the structure p. Complete details of the xSPDE input parameters are given in 10.7.3. There are default options that allow one to reduce the required parameter inputs and functions to just the important ones. The three most essential user-specified functions are listed below:

Label	Arguments	Purpose
initial	(w, p)	**Function to initialize fields**
deriv	$(a, ..w, ..p)$	**Stochastic derivative**
observe	$(a, .., p)$	**Observable function**

To run xSPDE, an Octave or Matlab environment is needed. A Julia option will be available in future. The current xSPDE distribution includes the toolbox: *xspde.mltbx*, or a folder: xSPDE, with:

- simulation (xSIM) and graphics (xGRAPH) functions.
- xAMPLES: examples that can also be used as templates
- xDOC: contains the current documentation

xSPDE can be run interactively as a script, or as a function in batch mode, either at a local workstation or on a remote cluster. Data can be either plotted immediately, or saved then plotted later. To simulate a stochastic equation interactively, first check that the xSPDE toolbox is installed.

If you have the toolbox file, *xspde.mltbx***, just open it and click on** *install***.** Otherwise the Octave/Matlab path must point to the xSPDE folder and subfolders. If you have the folders, but not the toolbox, proceed as follows:

- Click on the Octave/Matlab HOME tab (top left), then Set Path
- Click on Add with Subfolders

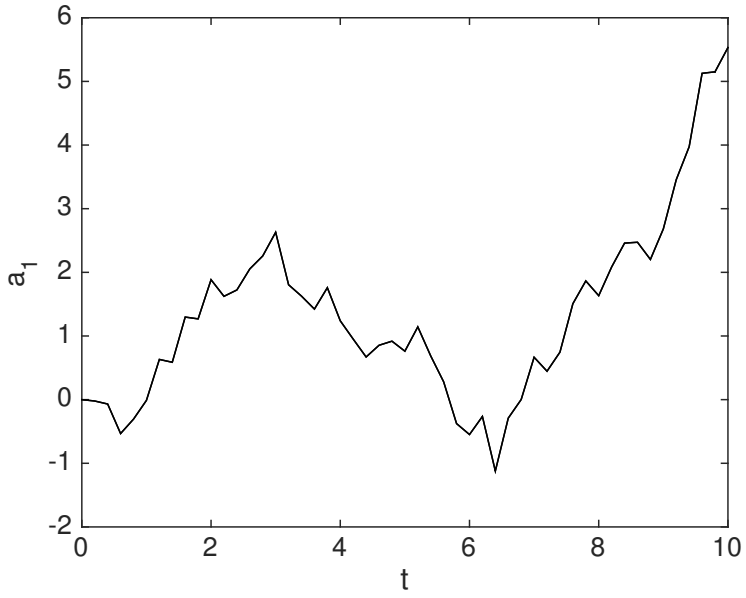

Figure 6.1.: *The simplest example: a random walk.*

- Find the xSPDE folder in the drop-down menu, and select it , then save the path.

Type *clear* to clear old data, and enter the inputs and functions into the command window interactively. For more advanced cases, it is best to create a function that calls xSPDE. There are many examples listed in this manual, and there are more in the xAMPLES folder. Any of these can be used as templates for building your own simulation code.

6.1.1. Wiener process

To solve for a single trajectory of Eq (2.22) with xSPDE, only two lines are needed:

```
p.deriv = @(a,w,p) w;
xspde(p);
```

Here *p.deriv* defines the time derivative $\dot{a}$ in the input parameter structure *p,* while w is a delta-correlated Gaussian noise generated internally. There are no other parameters, so default values are used for *initial*, *observe*, as well as the points and timesteps. This produces the graph shown in Fig (6.1), for a single trajectory.

At the end of the run, xSPDE reports the RMS errors. There are discretization, sampling and comparison errors, all normalized by the maximum observable value, unless compared to a result of zero. In the present simulation, the discretization or step error is about 10^{-16}, due to round-off. This is just a single trajectory, but more can be added.

6.1.2. General derivatives

All important xSPDE procedures use functions. Functions can be specified inline, which is the simplest, or externally. The last argument of more complex xSPDE functions is the parameter structure. An example already introduced is the derivative function, labeled *p.deriv*.

For example, consider the stochastic differential equation,

$$\frac{da}{dt} = -ga + w. \tag{6.1}$$

The corresponding derivative code definition is:

```
p.deriv = @(a,w,p) - p.G*a + w;
```

This code defines the function handle *p.deriv*, which gives the derivative function, da/dt. In this example, it simply returns the derivative, in terms of the variable a, loss parameter $p.G$, and stochastic noise term w. This user specified inline function is known internally by the function handle *p.deriv*.

Inside a complete xSPDE simulation input with a parameter values, it would look like:

```
p.G = 0.25;
p.deriv = @(a,w,p) - p.G*a + w;
xspde(p);
```

External function handles can also be used. They are useful for complex functions with more internal logic. A typical script first defines parameters and function specifications, in a structure, then runs the simulation code with the parameter structure as an input, as follows:

```
p.[label1] = [parameter1];
...
p.[label2] = [parameter2];
p.deriv = @(a,w,p) [derivative];
xspde(p);
```

Note the following points to remember:

- `p.`[*label*1] = [*parameter*1] defines a parameter in the structure p.
- There are many possible inputs, which all have default values.
- You don't have to save the data if you want an immediate plot.
- The notation `p.deriv` =@(`a`, `w`, `p`) [*derivative*] defines a function, da/dt.
- In this example, `a` is the stochastic variable, `w` the random noise, p a structure.
- Other labels can be used instead of *(a,w,p)* if preferred.

6.2. Input parameters

All xSPDE simulations use a structure for input data. Most functions also require a parameter structure, combining the data input with additional internal parameters. Any naming convention will do for either structure, as long as you are consistent.

User-defined parameters can be added freely. To ensure that there is no clash with internal variables, it is best if user defined parameters start with a capital letter.

The xSPDE inputs have default values, which are used if the input values are omitted. If you only need the first element of a vector or array, just input the value required. Parameters can be output with the verbose switch, `p.verbose`. This has four levels of output: −1,0, 1 or 2, with `p.verbose=0` as default, giving final error reports. To get more progress details and individual errors, use `p.verbose=1`. To eliminate almost everything, use `p.verbose=-1`. For maximum information, including all the internal parameter values, use;

```
p.verbose = 2;
```

While this level of detail is not usually needed, it can be useful to print out all the internal parameters and default values to understand how the program operates.

6.2.1. Simulation parameters table

The most common xSPDE input parameters used to define the equations in a simulation, together with their default values are:

Label	Type	Default value	Description
fields	integer vector	1	Number of stochastic *fields*
noises	integer vector	1	Number of *noises*
name	string	' '	Simulation *name*
deriv	function	0	The stochastic *deriv*ative
initial	function	0	Function to *initial*ize variables
method	function	[see 9]	Integration *method*
ensembles	integer vector	[1,1,1]	Stochastic *ensemble* sizes
ranges	real vector	[10]	Time and space *ranges*
points	integer vector	[51]	Output lattice *points* in [t,x,y,z,..]
steps	integer	[1]	Intermediate *steps* per time point
observe{*n*}	function	*a*	*Observ*able function for averages
compare{*n*}	function	*0*	*Compar*ison function for averages
binranges{*n*}{*m*}	vector	[0]	*Bin*ning *ranges* for probabilities

A more detailed explanation of these parameters is found below, and a complete table is given in section 10.3.

6.2.2. Graphics parameters

The generated average data can be graphed using any graphics editors, or else using the internal xGRAPH function defined for this purpose. An xSPDE simulation can return many different averages. These are defined in a cell array with indices in braces. The index is used to address the output data produced.

For each index, one can define parameters that define the quantity stored, together with corresponding graphics outputs. Some commonly used options are:

Label	Type	Default value	Description
olabels{*n*}	string	*'a'*	Observable label
transverse{*n*}	integer	0	Transverse slices in time
transforms{*n*}	vector	0	Set to 1 for Fourier transforms in time
scatters{*n*}	integer	0	Set to s for s scatter plots in the observable

The full definition of the options is given in the user guide in sections 10.3.1 and **??**, although most will be clear from examples.

6.3. Fields and noises

Stochastic variables in an SDE are *fields*, stored in a real or complex matrix, $a(i, j)$. Here, i is an internal field index, while e is the ensemble index.

fields gives the range of the first internal index. This is the total number of SDE variables or fields. It has a default value of $fields = 1$.

ensembles allows multiple trajectories to be integrated. This has up to three components. The first component, *ensembles(1),* gives a vector of local trajectories, so $e = 1, \ldots ensembles(1)$. The two other ensemble values specify serial or parallel processing, as explained below.

noises are noise dimensions, similar to *fields*, and used as $w(i, j)$, where the first noise index has *noises* components. The default value is $noises = fields$.

In the example above, we could add the fields, dimensions, ensembles and noises:

```
p.fields = 1;
p.dimensions = 1;
p.noises = 1;
p.ensembles = 1;
```

As these are all default values, this is superfluous in a simple case. The full definition of ensembles as a vector is given below, and in some cases uses the parallel toolbox in Matlab.

6.3.1. Initial values, points and ranges

Initial values are required to define any differential equation, and in a numerical calculation one must also have a defined lattice.

initial The initial value is defined by a function *p.initial*. This must return either an initial vector of size *fields*, or else a random array of size $fields \times ensembles(1)$. The default function simply returns zero.

inrandoms are initial random number dimensions, similar to *fields*, and used as $v(i,j)$, where the first random dimension has *randoms* components. The default value is $randoms = noises$. Specifies the first argument of the function $p.initial(v,p)$ as a real Gaussian noise vector v with unit variance. The same noise is used when error-checking, so that changes are from the step-size, not from random fluctuations.

points The number of integration points. The default setting is currently 51.

steps The number of integration steps used for each output time-step. The default is 1.

ranges The total integration range in each dimension, the first element being the maximum integration time T. The default setting is currently 10.

6.3.2. Observables

observe is a cell array of functions of stochastic fields, each defining an average. xSPDE expects a (named or anonymous) function that takes two parameters, namely the field matrix a and the input structure p. The function must return a real or complex array, where the first index is used for a vector observable. xSPDE then averages over the last index, to calculate the observable.
To plot the variance, for example:

```
p.observe{1} = @(a,p) (a(1,:)-mean(a,2)).^2;
```

rawdata By setting *p.rawdata=1* (see section 10.3.1), one can also store every trajectory including both fine and coarse time-step values, and but this is very memory-intensive for large simulations.

olabels is cell array of the output labels associated with each average, although one can also define additional functional transformation of the averages to be graphed and label them.

Observables are computed as a two-dimensional packed array, then unpacked for storage, giving an array of dimension $(d1, dspacetime, ensembles(1))$. Here $d1$ is the local observable dimension, so $d1 = 1$ for a scalar observable. The space-time dimension is $dspacetime = 1$ for an SDE, otherwise a vector for a SPDE, and $ensembles(1)$ is the size of the ensemble of trajectories computed in each processor. Once data is averaged internally over $ensembles(1)$, further transforms of the averages are available.

6.3.3. Using the dot

All equations entered in xSPDE utilize the Matlab syntax. This is designed to handle scientific or mathematical matrix and array-based formulae. It has features to simplify matrix or array equations which often require a 'dot' or a 'colon'.

- Stochastic variables in xSPDE are matrices or arrays, where the last index is used to treat parallel stochastic trajectories, for greater efficiency. This requires use of the 'dot' notation to perform multiplication inside equations.
- To multiply vectors, matrices or arrays element-wise, like $a_{ij} = b_{ij}c_{ij}$, the notation $a = b. * c$ indicates that all the elements are multiplied. This is used to speed up calculations in parallel.
- An equation in xSPDE can apply to many stochastic trajectories in parallel. Using the dot shortens the equation, and it also means that a fast parallel arithmetic will be used. The same principle holds for larger arrays with spatial lattices, treated in in section 8.
- Broadcasting occurs if one or more dimensions has a unit size. For example, arrays of size (1,100) and (6,1) can be added or multiplied to give a (6,100) matrix.
- A formula may require addressing the first index - which is the field component - and treating all the other elements in parallel. To do this in a compact way, one may use the notation $a(n,:)$, which indicates that all the subsequent index elements are being addressed as well.
- This will "flatten" a spatial array into a matrix, in which case it is better to include space indices.

In summary, whenever a formula combines multiplication operations over spatial lattices or ensembles, **USE THE DOT**.

6.4. Advanced random walk

We now return to the random walk, but with some more advanced features:

$$\dot{a} = w(t)\,, \tag{6.2}$$

This is integrated numerically and graphed with $N = points(1)$ points. The first point stored is the initial value, so there are $N-1$ integration steps, of length $dt = ranges(1)/(N-1)$. Numerical graphs have discrete steps, and more detail is obtained if more time steps are used. The default value is $N = 51$, which is predefined in the $xpreferences$ file. This is adjustable by the user. It can also be changed for a simulation, by inputting a new value of $points$.

6.4.1. Simple xSPDE example

Unless you type *clear* first, any changes to the input structure are additive; so in the exercises you should get the combination of all the previous structure inputs as well as your new input.

- **Run the complete xSPDE script of Example 1 in Matlab.**

It is simple to cut and paste from an electronic file to the command window. Be careful; pasting can cause subtle changes that may require correction. Some generated characters may be invalid input characters, and these will need retyping if this occurs.

You should get the output in Fig (6.1).

- **What do you see if you average over** 10000 **trajectories ?**

```
p.ensembles = 10000;
xspde(p);
```

- **What do you see if you plot the mean square distance? Note that variances should increase linearly with** t**.**

```
p.observe = @(a,p) a.^2;
p.olabels = '<a^2>';
xspde(p);
```

- **What if you add a force that takes the particle back to the origin?**

$$\dot{a} = -a + w(t)\,, \tag{6.3}$$

```
p.deriv = @(a,w,p) -a+w;
xspde(p);
```

The corresponding Fokker-Planck equation from Eq (2.18) is:

$$\frac{\partial P(a)}{\partial t} = \left[\frac{\partial}{\partial a} + \frac{1}{2}\frac{\partial^2}{\partial a^2}\right] P(a)\,. \tag{6.4}$$

It is easy to verify that inserting this dynamical equation into Eq (2.20) gives the result:

$$\frac{\partial}{\partial t}\left\langle a^2\right\rangle = 1 - 2\left\langle a^2\right\rangle \tag{6.5}$$

- Solve for $\left\langle a^2(t)\right\rangle$ and use xSPDE to compare the numerical and analytic solutions. The current time is accessible as the parameter $p.t$. Can you explain the graph differences?

6.5. Probability binning

It is possible to graph probability densities of real observables instead of averages, if *p.ensembles* is large. This is achieved by inputting the observable number and binning range:

$$p.binranges\{n\} = \{oa : ostep : ob\}; \tag{6.6}$$

If present, this returns probability density of the n-th observable $o\{n\}$, through binning into ranges of width *ostep* around the centers of each bin, starting at *oa*, and ending at *ob*. The simulation returns a result of $1/ostep$ in the $j-th$ bin if the trajectory is inside the bin, so that $o(j) - ostep/2 < o < o(j) + ostep/2$, and zero otherwise. This gives a probability density on output, plotted against time. Note that on graphing, an extra dimension is added for the variable o. The probability density at *ntimes* equally spaced simulation times can be plotted with *p.transverse*$\{n\}$=*ntimes*.

The probability can be plotted for any *observe* function of the stochastic variable.

6.5.1. Multivariate probabilities

The probability density is multivariate for vector observables. This is possible because the binning ranges are stored in a cell array, which may contain several bin vectors. If the observable $o\{n\}$ is two-dimensional, then one can input:

$$p.binranges\{n\} = \{oa(1) : ostep(1) : ob(1), oa(2) : ostep(2) : ob(2)\}; \tag{6.7}$$

On graphing, *two* extra dimensions are added for the variable o in this case. The graphics program *xGRAPH* will attempt to graph them, but it is limited by graphical visualization constraints. In general, an arbitrary observable dimension is possible, but this is also limited by the sampling and memory, since the number of samples per bin will decrease rapidly with dimensionality.

The graphics program extracts slices and windows of probabilities if required. To plot the probabilities of two observables, one for a range of $-5:5$ and the other for 0:25 for a range of 0:1, add the following inputs before the *xsim* or *xspde* command:

```
p.binranges{1} = {-5:0.25:5};
p.binranges{2} = {0:0.5:25};
```

In the case of a two-dimensional probability density, plotted against time, there are a total of four graphics dimensions. That is, one dimension for time, two for the observable dimensions, and one for the probability itself. One can also plot how the probability density changes in space for the case of a stochastic partial differential equation, as described in section 8.

6.6. Auxiliary fields and noises

In some problems, it is useful to access the noise terms, or functions of the noises and their correlations with the fields at the same time. This is handled in xSPDE with auxiliary fields or *auxfields.* These are fields that are functions of noise terms and the integrated fields. The number of these is defined in the input structures using the parameter *p.auxfields,* which is arbitrary.

Auxiliary fields are calculated using a function *p.define,* which is similar to *p.deriv*, except that it returns the current value of the auxiliary field, not the derivative. These fields are defined as the *average* over the previous step in time of the auxiliary function, including the noise term. This is essential in calculating spectra, in order to eliminate systematic errors in Fourier transforms.

More details on this are given in Section (6.7). To access the auxiliary fields, one can compute any observable average using a *p.observe* function as usual, or else store the *raw* trajectories including auxiliary fields by setting *p.rawdata=1.* In either case, the auxiliary fields are appended to the integrated fields by adding extra cells.

6.6.1. Outputting the noise

As a simple example, suppose one wishes to calculate the noise terms and compare them with the field trajectories in a simple Wiener process. Since there is now an extra cell for the auxiliary field in the define function, it is passed as an additional field argument to the observe function. The following code can be used:

```
clear
p.auxfields = 1;
p.deriv = @(a,w,p) w;
p.define = @(a,w,p) w;
p.observe = @(a,x,p) [a;x];
p.olabels = {'a, w'};
xspde(p);
```

The observe function calculates both rows of the output array, including the auxiliary field which is defined as the noise term and plotted as a dashed line. There is no ensemble averaging, and hence no ensemble error-bars in the example. This is because because no ensembles were specified in the input parameters. Similarly, there are no time-step error-bars for this observable, because the fine and coarse noises are equal to each other after time averaging.

The result that is plotted is therefore the coarse noise, whose correlation time equals the time step. This is plotted below in Fig (6.2), which plots the same Wiener process as before, except adding the driving noise term as well. The standard deviation of the noise in a single step here is $\sqrt{1/dt}$, where $1/dt = 50/10 = 5$ for the default range of 10 and default time points of 51. Note that noise terms do not converge at small time-steps for delta-correlated noise, even when the integrated stochastic process does converge.

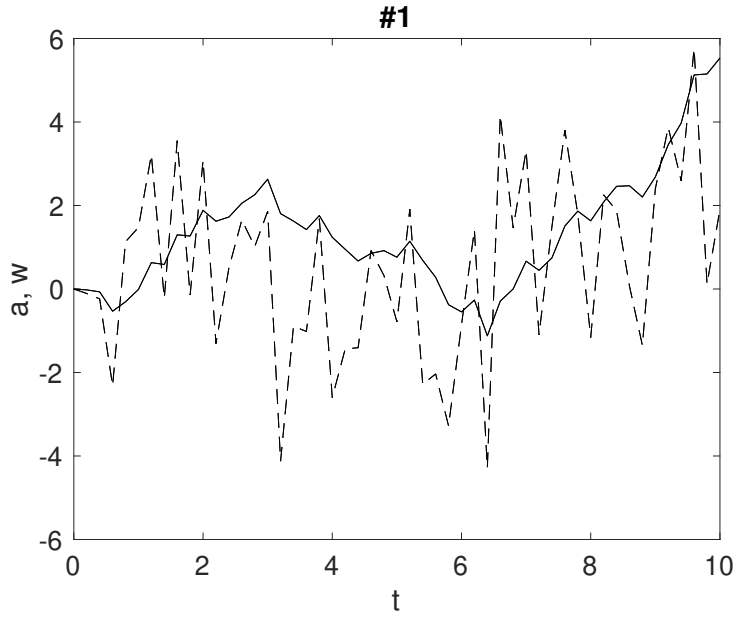

Figure 6.2.: *A single trajectory of a random walk, with the noise terms w graphed using dashed lines, and the integrated variable a plotted as the solid line.*

This is why it is necessary to choose to plot one or the other, or else to time-average to obtain a converged result.

If multiple steps are used, only the noise during the last step prior to the time-point is plotted.

6.7. Time-domain spectra

To get an output from a temporally Fourier transformed field, set $transforms\{n\} = 1$ for the observable (n) you need to calculate in transform space. This parameter is a cell array. It can have a different value for every observable and for every dimension in space-time, if you have space dimensions as well.

To obtain spectra from Eq (2.38) with greater accuracy, all fields are must be averaged internally. The code will use trapezoidal integration in time over the integration interval, to give the average midpoint value. This employs the same interval for fine and coarse integration, to allow comparisons for error-checking. After this, the resulting step-averaged fields are then Fourier transformed.

In the simplest case of just one internal step, with no error-checking, this means that the field used to calculate a spectrum is:

$$\bar{a}_j = \left(a_j + a_{j+1}\right)/2, \tag{6.8}$$

which corresponds to the time in the spectral Fourier transform of:

$$\bar{t}_j = \left(t_j + t_{j+1}\right)/2. \tag{6.9}$$

Note that if any temporal Fourier transform is specified, all the field variables are time-averaged over a step. This is not strictly necessary, but it means that there is a reduced code complexity for cases where there is a Fourier transform for some but not all variables. As described above, the auxiliary variables are always time-averaged to allow error-checking, so there is no change for these.

6.7.1. Error-checking

For an error-checking calculation with two internal *steps*, there are three successive valuations: a_j, $a_{j+1/2}$, a_{j+1}. In this case, for spectral calculations one averages according to:

$$\bar{a}_j = \left(a_j + 2a_{j+1/2} + a_{j+1}\right)/4. \tag{6.10}$$

In addition, one must define the noise terms, both for error-checking and for output, since spectral calculations in quantum input-output theory include noise terms as well as fields. The noise term used to calculate a spectrum involving $\bar{a}_j$ is w_j. A coarse noise term is set equal to the average of two successive fine noise terms:

$$\bar{w}_1 = \frac{1}{2}\left(w_1 + w_{1/2}\right). \tag{6.11}$$

The time integral is carried out numerically as a sum which has $N = points(1)$ time points of interval dt. In xSPDE, $dt = T/(N-1)$, where $T = ranges(1)$. The effective integration time for the Fourier transform time integrals is

$$T_{eff} = Ndt = 2\pi/d\omega \tag{6.12}$$

When there are larger numbers of steps from using the internal *steps* parameter, there are more points to Fourier transform. These additional frequencies are computed while carrying out the Fourier transform, but only N low frequency points are saved. The unused high frequency results are not stored or plotted, to conserve memory.

6.8. Examples

6.8.1. Complex damped spectrum

Consider the spectrum of Eq (6.3), with a complex noise,

$$\left\langle w\left(t\right) w^*\left(t'\right)\right\rangle = \delta\left(t - t'\right), \tag{6.13}$$

a random initial equation near the equilibrium value, and a range of $t = 100$, with 640 points. Here there are two real noises.

The input parameters are given below. There are parallel operations here, for ensemble averaging, so we **USE THE DOT**.

```
clear
p.points = 640;
p.ranges = 100;
p.noises = 2;
p.ensembles = 10000;
p.initial = @(v,p) (v(1,:)+1i*v(2,:))/sqrt(2);
p.deriv = @(a,w,p) -a + w(1,:)+1i*w(2,:);
p.observe = @(a,p) a.*conj(a);
p.transforms = 1;
p.olabels = '|a(\omega)|^2';
xspde(p);
```

Note that *p.transforms = 1* tells xSPDE to Fourier transform the field over the time coordinate before averaging, to give a spectrum. Both *observe* and *transforms* could be cell arrays, but the this is not needed with a single observable. The first argument v of the *initial* function is a random field, used to initialize the stochastic variable.

To define as many observables as you like, use a Matlab cell array;

```
p.observe{1} = ..;
p.observe{2} = ..;
```

To learn more, try the following:

- **Simulate over a range of $t = 200$. What changes do you see? Why?**
- **Change the equation to the laser noise equations introduced in the next section (Laser quantum noise). Why is the spectrum much narrower?**

6.8.2. Laser amplification noise

Laser quantum noise is commonly modeled [52–54] using SDEs in a normally ordered quantum phase-space representation. Consider a model for the quantum noise of a single mode laser as it turns on, near threshold:

$$\dot{a} = ga + bw(t) \tag{6.14}$$

where the noise is complex, $w = (w_1 + iw_2)$, so that:

$$\left\langle w(t)w^*(t')\right\rangle = 2\delta\left(t - t'\right) . \tag{6.15}$$

Here the coefficient b describes the quantum noise of the laser, and is inversely proportional to the equilibrium photon number.

Try the following, noting that you should type *clear* first when starting new simulations.

- **Solve for the case of $g = 0.1$, $b = 0.01$**

Most lasers have more than 100 photons and hence much less noise than this.

For this exercise, small error-bars will display on the graph. These are calculated from the difference between using steps of size dt and steps of size $dt/2$. They only appear if greater than a minimum relative size, typically 1% of the graph size, which can be set by the user.

```
clear
p.noises = 2;
p.observe = @(a,p) abs(a)^2;
p.olabels = '|a|^2';
p.deriv = @(a,w,p) a + 0.01*(w(1)+1i*w(2));
xspde(p);
```

6.8.3. Saturated laser noise

Consider the case where the laser saturates to a steady state:

$$\dot{a} = \left(1 - |a|^2\right) a + bw(t) \tag{6.16}$$

To learn how to use the function inputs, try the following:

- **Solve for the saturated laser case**

You should get the output graph in Fig (6.3).

```
p.deriv = @(a,w,p) (1-abs(a)^2)*a+0.01*(w(1)+1i*w(2));
xspde(p);
```

6.8.4. Financial calculus

A well-known Ito-type stochastic equation is called the Black-Scholes equation [74], used to price financial options. It describes the fluctuations in a stock or commodity value:

$$da = \mu a\, dt + a\sigma\, dw, \tag{6.17}$$

where $\langle dw^2 \rangle = dt$. As the noise is multiplicative, the equation is different in Ito and Stratonovich calculus. The corresponding Stratonovich equation, as used in xSPDE for the standard default integration routine is:

$$\dot{a} = \left(\mu - \sigma^2/2\right) a + a\sigma w(t). \tag{6.18}$$

An interactive xSPDE script in Matlab is given below with an output graph in Fig (6.4). This is for a startup with a volatile stock having $\mu = 0.1$, $\sigma = 1$. The spiky behavior is typical of multiplicative noise, and also of the more risky stocks in the small capitalization portions of the stock market.

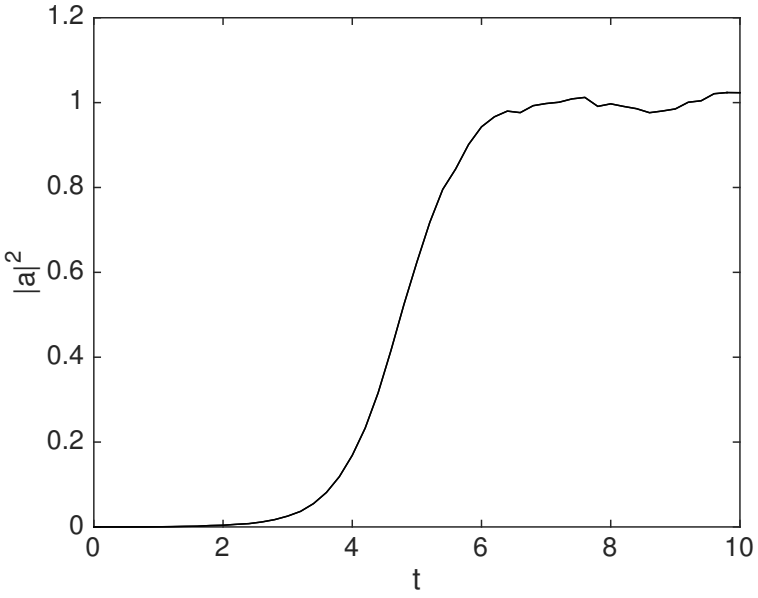

Figure 6.3.: *Simulation of the stochastic equation describing a laser turning on.*

```
clear
p.initial = @(v,p) 1;
p.deriv = @(a,w,p) -0.4*a+a.*w;
xspde(p);
```

Here *p.initial* describes the initialization function. The first argument of $@(v,p)$ is v, an initial random variable with unit variance. *The error-bars are estimates of step-size error.* Errors can be reduced by using more time-steps.

To learn more, try the following:

- **Solve for a more mature stock having** $\mu = 0.1$, $\sigma = 0.1$**.**

6.8.5. Nonlinear quantum simulation

This example involves a full nonlinear quantum phase-space simulation using the positive-P representation described in Sec (2.9), in which the two variables are only conjugate in the mean. This allows quantum superpositions of coherent states to be represented, or in fact any state, including squeezed or entangled states in more general cases.

A simple example is the nonlinear driven quantum subharmonic generator - for example, an opto-mechanical, superconducting or nonlinear optical medium in a driven cavity [75–78]. This is derived from the Hamiltonian for a resonant, coupled two-mode nonlinear interferometer, with $\hat{a}_2$ driven externally at twice the frequency of $\hat{a}_1$:

$$\hat{H} = i\hbar\left[\frac{\kappa}{2}\hat{a}_2\hat{a}_1^{\dagger 2} + \mathcal{E}_2\hat{a}_2^{\dagger} - h.c.\right] \tag{6.19}$$

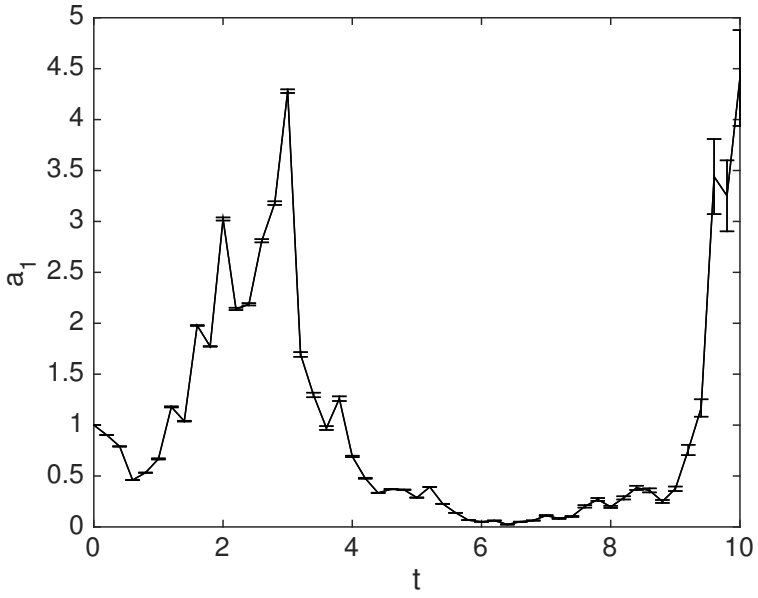

Figure 6.4.: *Simulation of the Black-Scholes equation describing stock prices.*

After including losses in both modes in the positive P-representation, assuming zero temperature reservoirs, and adiabatically eliminating α_2 with $\gamma_2 \gg \gamma_1$, one has the following Ito equation:

$$\begin{aligned}\frac{d\alpha_1}{dt} &= -\gamma_1\alpha_1 + \alpha_1^\dagger\frac{\kappa\epsilon_2}{\gamma_2}\left[1-\frac{\kappa}{2\epsilon_2}\alpha_1^2\right] + \sqrt{\frac{\kappa\epsilon_2}{\gamma_2}-\frac{\kappa^2}{2\gamma_2}\alpha_1^2}w_1(t)\\ \frac{d\alpha_1^\dagger}{dt} &= -\gamma_1\alpha_1^\dagger + \alpha_1\frac{\kappa\epsilon_2}{\gamma_2}\left[1-\frac{\kappa}{2\epsilon_2}\alpha_1^{\dagger 2}\right] + \sqrt{\frac{\kappa\epsilon_2}{\gamma_2}-\frac{\kappa^2}{2\gamma_2}\alpha_1^{\dagger 2}}w_1(t)\end{aligned} \tag{6.20}$$

Rescaling the fields so that $\alpha_1 = a_1\sqrt{n_c}$, $\alpha_1^\dagger = a_2\sqrt{n_c}$, where $n_c = \frac{2\epsilon_2}{\kappa}$, then rescaling time by letting $\tau = \frac{\kappa\epsilon_2}{\gamma_2}t$, defining $c = \frac{\gamma_1\gamma_2}{\kappa\epsilon_2}$, and using Eq (**??**) to transform from an Ito to a Stratonovich equation gives:

$$\begin{aligned}\frac{da_1}{d\tau} &= -(c-\frac{1}{2n_c})a_1 + a_2\left[1-a_1^2\right] + \frac{1}{\sqrt{n_c}}\sqrt{1-a_1^2}w_1(\tau)\\ \frac{da_2}{d\tau} &= -(c-\frac{1}{2n_c})a_2 + a_1\left[1-a_2^2\right] + \frac{1}{\sqrt{n_c}}\sqrt{1-a_2^2}w_2(\tau)\ ,\end{aligned} \tag{6.21}$$

where w_1, w_2 are delta-correlated real Gaussian noises.

There is a bistable region, which leads to a discrete time symmetry breaking. The solution in the steady-state is

$$P = \left(1-a_1^2\right)^{cn_c-1}\left(1-a_2^2\right)^{cn_c-1}e^{2n_ca_1a_2} \tag{6.22}$$

The integration manifold is the region of real a_1, a_2, such that $a_1^2 \leq 1$, $a_2^2 \leq 1$. There are two physically possible metastable values of the amplitudes. The physically observed quantity is the amplitude and number:

$$\langle \hat{a} \rangle = \langle a_1 + a_2 \rangle \sqrt{\frac{n_c}{2}}$$
$$\langle \hat{n} \rangle = n_c \langle a_1 a_2 \rangle . \tag{6.23}$$

Parameters that show bistable behavior on reasonable time-scales of $T = 100$ are $c = 0.6$, $n_c = 4$. To learn more, try the following:

- **Simulate the nonlinear oscillator by creating a file, say,** $NonlinearQ.m$
- **Can you observe quantum tunneling in the bistable regime?**
- **Do you see transient Schrödinger 'cat states' with a negative** $n = \alpha_1\alpha_2$ **value?**

A negative value of $\alpha_1\alpha_2$ is evidence for a quantum superposition! For experimental comparisons, one would measure correlation functions and spectra. These calculations require long time scales, `p.ranges`, to observe tunneling, and of order 100 time steps per plotted time point, `p.steps`, to maintain good accuracy in the quantum simulations.

For lower damping and large nonlinearity, other methods should be used, as the stochastic equations can become unstable in this limit.

The model is a simplified version of more recent quantum technologies used to investigate Schrödinger cat formation in superconducting quantum circuits [79], and the CIM machine used to solve NP-hard optimization problems with photonic circuits [80–82], although there are greater complexities in both these cases.

Similar methods can also be used to investigate quantum and chemical non-equilibrium phase transitions [83], tunneling in open systems [84], quantum entanglement [85], Einstein-Podolsky-Rosen paradoxes [86,87], Bell violations [88,89], and many other problems treated in the literature [2, 53].

6.8.6. Kubo project

To get started on more complex programs, we next simulate the Kubo oscillator, which is an oscillator with a random frequency:

$$\dot{a} = iaw. \tag{6.24}$$

Exercises

- Simulate the Kubo oscillator using a file, $Kubo.m$, with two ensemble levels to allow sampling error estimates. The error vector *error* gives the total time-step error plus the sampling error.
- Increase the first ensemble size to check how it modifies the sampling errors.

```
function [error] = Kubo()
p.name = 'Kubo oscillator';
p.ensembles = [400,16];
p.initial = @(v,p) 1;
p.deriv = @(a,w,~) 1i*a.*w;
p.olabels = {'<a_1>'};
p.file = 'kubo.mat';
[error,~,~,~] = xsim(p);
xgraph(p.file);
end
```

This function generates a data file, `kubo.mat`. If you run this twice without deleting the earlier file, you will get a warning and the old file will be moved to a backup filename, `kubo_1.mat`, to protect the earlier data. Note that xGRAPH will graph the data in the most recent file saved.

You can also include modified graphics parameters as a second input when running `xGRAPH,` just in case the first graphs you generate need further changes.

6.9. Hints

- When first using xSPDE, it is a good idea to run the batch test script, *Batchtest*.
- *Batchtest* uses the Matlab parallel toolbox installation. If you have no license for this, omit the third ensemble setting.
- To create a project file, it is often easiest to start with an existing example function using a similar equation: see the xAMPLES folder.
- Graphics parameters can be included in the xSIM inputs to modify graphs.
- Comparison functions can be included if you want to compare with analytic results.
- Chapters 10 and **??** list the input parameters.

7. Quantum toolbox

This chapter describes how to use the xSPDE numerical toolbox to solve quantum dynamical problems.

Techniques for master equations and stochastic Schrödinger equations (SSEs) are similar to those for an SDE, except for specific equations that generate the derivatives, and a projected version of the stochastic method.

The fundamental master equation solved has the Markovian form:

$$\dot{\rho} = -i\left[\hat{H}, \rho\right] + \sum_j \gamma_j \left(2\hat{L}_j \rho \hat{L}_j^\dagger - \hat{L}_j^\dagger \hat{L}_j \rho - \rho \hat{L}_j^\dagger \hat{L}_j\right), \tag{7.1}$$

where: $j = [j_1, j_2(, j_3)]$. Here j_1 is an index that gives the type of damping operator, j_2 is a mode index, and j_3 is an optional second mode index.

7.1. Wave-functions and density matrices

The quantum toolbox in xSPDE has three methods for representing open quantum systems, which allow the treatment of Hilbert spaces of increasing dimensionality:

1. Density matrices with sparse operators
2. Stochastic wave-functions with sparse operators
3. Stochastic wave-functions with functional operators

There is a speed/memory tradeoff here. The lowest numbered methods are typically faster, but use more memory. In the second two cases, one can use either a method using functions for operators, or else a sparse matrix method, which requires the operators to be stored in memory. The wave-function equations describe decoherence through stochastic methods, so each of these two approaches can treat coupling to reservoirs, up to the limits of time and memory constraints.

When using sparse methods, the multimode index $\boldsymbol{n}$ is packed into the first single index n. This is automatic for density matrices, but it is optional for stochastic wave-function calculations, which can use either sparse or full vectors. While sparse methods are useful for storing operators, these require memory, which must be allocated when the matrices are generated. This can be minimized by only generated the operators that are needed, rather than all possible ones.

Less memory is required if the operators' effect on the wave-function are calculated only when needed. This is a function call strategy, It is currently available for stochastic

wave-function calculations only. It is slower than using sparse matrices, but it is more scalable. Currently, this approach is not available for density matrix equations.

The different approaches have areas of applicability that depend on the Hilbert space dimension, as explained below.

7.1.1. Number-state methods

Algorithms for either wave-functions or density matrices, are selected by choosing two parameters, *quantum* and *sparse*. If *sparse* is omitted, the default is $sparse = 0$.

p.quantum = 1, p.sparse = 0 - this is used to treat a full wave-function, $psi(\boldsymbol{n}, e)$, Here, $\boldsymbol{n} = n_1, \ldots n_m$ is a wave-function index index, while e is an ensemble index for random ensembles, if used. Operators are treated as functions, so there are no operator matrices stored. This minimizes the overall memory requirement.

p.quantum = 1, p.sparse = 1 - this is used to treat a packed wave-function, $psi(n, e)$, Here, n is a wave-function index index, which is a packed version of the vector index $\boldsymbol{n}$, while e is an ensemble index for random ensembles. Operators are treated as sparse matrices, so these must be stored. This increases the overall memory usage but is somewhat faster.

p.quantum = 2, p.sparse = 1 - this is used to treat a packed density matrix, $rho(n, \ell)$, Here, n and ℓ are density matrix indices, which are packed version of the vector index $\boldsymbol{n}$. Operators are treated as sparse matrices. Due to the storage requirements of a density matrix, this uses the most memory, and is the fastest. There is no vector ensemble here.

7.1.2. Independent cells

If one wishes to combine results from independent quantum systems, or from classical and quantum subsystems, the relevant parameters can be input as successive cell variables, together with any other toolbox inputs that are required. This allows, as an example, implementation of the Maxwell-Bloch equations, togther with arbitrary numbers of independent quantum systems like molecules and atoms.

7.2. Input parameters

Input parameters are stored in a structure which is input to the *xSPDE* program. This is a superset of the parameters already defined. In the definitions below, the structure name is omitted. but we normally use p in the examples. For example, to specify a quantum wave-function method, one would use $quantum = 1$, as explained already. The input parameters can be chosen not just in terms of the problem itself, but also to suit the computational hardware that is available.

Not that while the *quantum* toolbox and *phase* toolbox share common parameters listed below, but they are distinct toolboxes, and one must choose to use either one or the other by setting $quantum > 0$ or $phase > 0$.

7.2.1. Common parameters

modes gives the number of modes, hence $modes = 3$ defines a 3 mode quantum system,. This can be given implicitly through nmax.

ensembles(1) gives a vector of trajectories, $e = 1, \ldots ensembles(1)$. This is fast, but increases memory use. It is not used for density matrices.

ensembles(2) gives the number of series repeats for stochastic ensembles. It is always available, but slower.

ensembles(3) gives the number of parallel repeats for stochastic ensembles. It is useful for multicore processors with fast memory.

jump selects either a stochastic differential equation ($jump = 0$), the default, or a stochastic jump equation ($jump = 1$).

noises noise dimensions, set automatically for the built-in quantum methods.

points The number of integration points in time for data outputs. The default setting is 51.

steps The integration steps used per time-step, used to reduce time-step errors. The default is 1.

ranges The total integration range in time. The default setting is10.

initial The initial state is given by a function *initial*. This returns a column vector of size $fields \times 1$ or $fields \times ensembles(1)$, for wave-functions, or else of size $fields \times fields$ for density matrix calculations. The default is the state with the first level occupied.

inrandoms are initial random number dimensions. They specify the first argument of the function $initial(v, p)$ as a real Gaussian noise vector v with unit variance and length *inrandoms*. These are used for an initially decoherent, randomized wave-function.

The internal variable *fields* is used to specify the dimension of the integrated variables, and is automatically set.

7.2.2. Quantum parameters

quantum is the type of problem: $quantum = 1$ for a wave-function, $quantum = 2$ for a density matrix.

sparse indicates sparseness: if $sparse = 1$, sparse matrices are used to store operators. The default is $sparse = 0$.

nmax is the Hilbert dimension per mode. If this is a vector, the dimension can be varied.

mk... is a make function to generate sparse operators where required, eg, **mkbose**.

operator: If *sparse = 0*, an operator is a function with inputs of the mode index (or indices), and the wave-function *psi*. Operators acting on multiple modes may have two or more indices. The function O_k returns a wave-function $\hat{O}_k |\psi\rangle$.

sparse_operator: When *sparse = 1*, operators are sparse matrices. This is faster, but uses more memory.

Hamiltonian: the function $H(psi, p)$ returns a wave-function $\hat{H} |\psi\rangle$, if *sparse = 0*. Otherwise, if *sparse = 1*, it is an operator function $H(p)$ that returns a sparse matrix.

The following defaults are used to simplify input:

- If *modes* is not specified, it is equal to the length of *nmax*.
- If *modes* and *nmax* are not specified the default is a single qubit*: modes=1* , *nmax=2*.
- If the *nmax* vector is shorter than *modes*, the last value of *nmax* is repeated as necessary.

7.3. Dissipative parameters

In order to explain the terminology for dissipative input, the following list is useful. There are some differences that depend on whether one uses sparse matrices or functional operators. In the list below, n is the channel index for the dissipative operators. One channel index can generate any number of mode operators of the same type.

L{n}: this is a cell array of dissipative functions. The first argument is the mode index, k, or a vector of two indices, $[k_1, k_2]$, and the last argument p is the parameter structure.

@(k,p) is used for sparse operators, and returns a sparse matrix $\hat{L}_k$.

@(k,psi) is used for operator functions, returning $\hat{L}_k |\psi\rangle$.

Conjugate operators: for functions, a conjugate is returned if the index or indices is negative.

gamma{n}(p): This is a cell array of functions for every type of damping process. Cell array indices return a vector or matrix of damping rates for each type of Lindblad operator.

alpha{n}(k): This is a cell array of noise amplitude vectors or matrices for each type of damping process with real noises. If **alpha** is zero, which is the default, a complex noise is used.

measure: This gives the number of measured channel operators.

Note that:

- Operators may have one or two mode indices.
- Functional operators are slower than sparse operators for small Hilbert spaces.
- Only the required index combinations are accessed by the Lindblad functions, reducing storage.

7.4. Functional operators

These are linear functions that act on the quantum wave-function. New ones can readily be added. They reduce memory requirements, which is an advantage for large Hilbert spaces, where storing even sparse operators can require large quantities of memory.

The xSPDE code includes internal functions for bosonic and spin operators. The predefined operators also return auxiliary quantities used in dissipative equations if required, as they have variable input and output lists.

7.4.1. Bosonic operators

Label	Inputs	Output(s)
a	(m, psi)	$\hat{a}_m \left\|\psi\right\rangle$
$a2$	(m, psi)	$\hat{a}_m^2 \left\|\psi\right\rangle$
n	$([m_1 \left(, m_2\right)], psi)$	$\hat{a}_{m_1}^\dagger \hat{a}_{m_2} \left\|\psi\right\rangle$

Operators have scalar or vector indices. For a complete description, see (10.5.1).

7.4.2. Qubit and Pauli spin operators

The following set of operators are used for spin chain evolution.

Label	Inputs	Output(s)
sx	(m, psi)	$\hat{\sigma}_m^x \left\|\psi\right\rangle$
sy	(m, psi)	$\hat{\sigma}_m^y \left\|\psi\right\rangle$
sz	(m, psi)	$\hat{\sigma}_m^z \left\|\psi\right\rangle$
$sx2$	$([m_1, m_2], psi)$	$\hat{\sigma}_{m_1}^x \hat{\sigma}_{m_2}^x \left\|\psi\right\rangle$
$sy2$	$([m_1, m_2], psi)$	$\hat{\sigma}_{m_1}^y \hat{\sigma}_{m_2}^y \left\|\psi\right\rangle$
$sz2$	$([m_1, m_2], psi)$	$\hat{\sigma}_{m_1}^z \hat{\sigma}_{m_2}^z \left\|\psi\right\rangle$

7.4.3. Qubit gate operators

The following operators can be used to implement quantum logic gates, in addition to the standard Pauli operators. These assume qubit or two-state qubit logic in each mode.

Label	Inputs	Output(s)
cx	$([m_1, m_2], psi)$	Controlled Not
ha	(m, psi)	Hadamard
p8	(m, psi)	$\pi/8$
ph	(m, psi)	Phase

7.5. Sparse operators

The xSPDE code includes internal functions to generate operators. These are either sparse or full. Sparse operators are generated if needed requiring a *mk* function call to create the required index combinations, before they are used.

7.5.1. Sparse bosonic operators: mkbose

These are a cell array of annihilation operators, generated using *mkbose.*

Label	Indices	Meaning
a	$\{m\}$	$\hat{a}_m$
a'	$\{m\}$	$\hat{a}_m^\dagger$

p.a = mkbose((list,) p) Returns a cell array of annihilation operators defined either at all modes, if there is no *list,* or at the listed mode locations. Here *list* is a vector of integers, *p* is the parameter structure.

7.6. Observe, expect, output and compare

There are four types of possible outputs. The *observe* and *compare* functions are computed during the time-evolution, so that the entire wave-function doesn't need to be stored in time, reducing the storage needs. Additional functional transformations for either can be used as well, called *output* functions. Finally, a *compare* function allows comparison plots.

observe is a cell array of *any* stochastic function. xSPDE expects a (named or anonymous) function that takes two parameters, namely the wave-function *psi* or density matrix ρ, and the input structure *p*. The function return a real or complex matrix of dimension $(\ell, ensembles(1))$, where ℓ indexes a vector observable. xSPDE then averages over the second index, to calculate the observable. This allows an average of any type.

expect is a cell array of operators defining a quantum expectation value. For full matrices, *expect* is a (named or anonymous) function that takes two inputs, the wave-function *psi* and the structure *p*. For sparse matrices, the *expect* function returns a matrix. xSPDE internally averages over both the quantum and stochastic degrees of freedom to calculate the observable.

To plot the mean number in mode $m = 1$, using:
a) the number operator $\hat{n} = \hat{a}^\dagger \hat{a}$ with sparse operators:

```
p.expect{1} = @(p) p.a{1}'*p.a{1};
```

b) the number operator $\hat{n} = \hat{a}^\dagger \hat{a}$, with function calls:

```
p.expect{1} = @(psi,p) n(1,psi);
```

output All *observe* and *expect* results are stored. Transformations of both can be introduced. These may include multiple averages and/or different times. These are called the *output* functions. Default *outputs* pass through *observe* and *expect* results with no change. Defined outputs, like *p.output{1}*, replace the defaults, or add new outputs. Graphed data uses the *outputs*, which include sampling errors if *ensembles* are used, and step-size errors if *checks* is turned on.

compare Comparison functions can be used to obtain comparison graphs and differences.

The output numbering that is used is the **same** for all four types of function. This can lead to overwriting, with the precedence that *output*>*expect*>*observe*. To prevent overwriting, use different cell-indices. Compare functions are plotted independently, as an extra line on an existing graph, so they don't overwrite, and can be compared with any of *output, expect, observe.*

7.7. SSE derivative

The SSE derivative terms are calculated from $SSE(a, w, p)$ for solving Eq 3.14. The equation can be solved by any *method* for a Stratonovich SDE. Projective normalization is automatic for the standard *methods* of xSPDE.

7.8. Solving with the MCWF method

At each time step in the numerical simulation with the MCWF method, the jump probability ΔP is first calculated. This is carried out by computing the jump probability per unit time of each jump operator L_m in the master equation, which is given by

$$\Delta P_m = 2\gamma_m \langle \psi(t)|L_m^\dagger L_m|\psi(t)\rangle \,. \tag{7.2}$$

The calculated jump rate ΔP_m is then compared with a uniform, randomly generated number r_m between zero and $1/\Delta t$. If $\Delta P_m > r_m$, the state then undergoes the given jump. As $\Delta t \to 0$, a jump in any given step become increasingly rare.

After this, the state vector evolves according to the non-hermitian Hamiltonian H_{eff} in Eq. (3.29) as follows:

$$\frac{d}{dt}|\psi(t)\rangle = -iH_{eff}|\psi(t)\rangle \tag{7.3}$$

This differential equation is solved by a midpoint or Runge-Kutta algorithm, or others available. These steps are repeated till the final time step, and they constitute a single trajectory. Many trajectories are taken to compute the expectation values for the observables of interest.

For error-checking, fine step results are checked against a coarse step with a noise given by $r_c = \min(r_1, r_2)$, so that the coarse jump occurs if a jump takes place in either fine step. This allows errors due to step-size to be accurately estimated by comparing the fine and coarse step-size results, just as with continuous noise.

The MCWF algorithm described above is carried out simply by setting $p.jump = 1$. No further inputs from the user are required. All other parameters are input exactly the same way as in the SSE numerical simulation.

8. SPDE toolbox

This chapter describes how to simulate a PDE or SPDE, including choosing spectral or finite difference methods and specifying boundary conditions.

8.1. SPDE parameters

A stochastic partial differential equation or $SPDE$ for a complex vector field is defined in both time t and space dimension(s) $\mathbf{x}$. The total *dimensions* includes both time and space. To solve a stochastic partial differential equation xSPDE involves a similar procedure to the case of the SDE, covered in section 6.

The numerical solutions require additional parameters to define the spatial grid, and to define the linear transformations in an interaction picture, if spectral methods are used. The SPDE input parameters extend those already introduced in (6.2.1). Some new and extended parameters are listed in the table below:

Label	Type	Typical value	Description
dimensions	integer	2	Space-time dimensions
linear{*c*}	function	@(p) p.Dx	Linear interaction picture function
ranges	real vector	[10,10,...]	Ranges in time and space
transforms{*c,d*}	integer vector	$[1, 0, 1, ..]$	Space-time transform switch
points{*c*}	integer vector	[51,35,..]	Output lattice points in [t,x,y,z,..]
origins	real vector	[0,-5,..]	Space-time integration origin
boundaries{*c,d*}	integer array	$[0, 0; 0, 0; ..]$	Boundary type per field index
boundval{*c,d*}	cell array	$\{0, 0; 0, 0; ..\}$	Boundary value per field index
boundfun	function	@(a,c,d,p) ...	Boundary value function

Setting *dimensions* > 1 defines an (S)PDE as opposed to an ordinary (S)DE. In the xSPDE implementation, the space-time *dimensions* are unlimited, but large space-time dimensions become memory-intensive and slow. There is a practical limit of less than ten space-time dimensions with current digital computers, owing to exponential growth of memory and corresponding CPU time requirements at large space dimensionality.

The cell index c can be omitted in cell arguments like *boundval*{*c,d*} if there is only one field cell. Using *boundval* will only specify boundary values that are static in time. These can be any combinations of Dirichlet and/or Neumann/Robin. Using *boundfun* allows boundary values that can vary in time or are dynamic functions of the field cells. Definitions of *boundfun* have four arguments, with the first one a field cell array.

8.1.1. Initial conditions

Initial conditions are set at the initial time of $t = O_1$ with a user-defined function so that:

$$a(O_1) = initial(v, p) \tag{8.1}$$

The *initial* function includes initial random fields $v = \left[v^x, v^k\right]$. Their correlations are either delta correlated or spatially correlated. To allow this, the input parameter *randoms* is a vector such that: $randoms(1)$ is the number of delta-correlated random fields, v^x, and $randoms(2)$ is the number of correlated random fields, v^k. All random fields in the *initial* function, even if correlated using filters in momentum space, are transformed to position space before use. If there is no filtering, v^x and v^k have the same correlations.

8.2. Multidimensional Wiener process

To solve for a single four-dimensional trajectory with three space dimensions, as in Eq (5.8) , just type in:

```
p.dimensions = 4;
p.deriv = @(a,w,p) w;
xspde(p);
```

Here *p.deriv* defines the time derivative $\dot{a}$ in the input parameter structure *p,* while w is a delta-correlated Gaussian noise generated internally. Apart from the dimensions, there are no other parameters, so default values are used. This produces the graph shown in Fig (8.1), which gives a single trajectory using the default lattice settings.

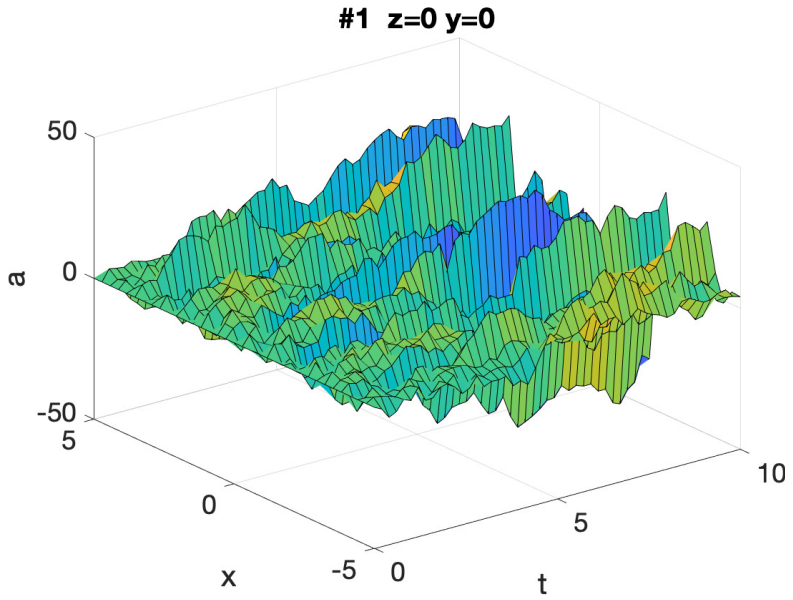

Figure 8.1.: *A multidimensional random walk of a three-dimensional field projected onto* $y = z = 0$.

For more interesting problems than this, more parameters are needed, as explained next.

8.2.1. Example with additional damping term

As another very simple example, consider the SPDE

$$\frac{\partial a}{\partial t} = -\frac{1}{4}a + x \cdot w \tag{8.2}$$

The system has one spatial dimension, or $d = 2$ space-time dimensions, one field and one noise variable. We suppose that the initial noise variance is Gaussian, with:

$$a(0, x) = 10v(x). \tag{8.3}$$

We want to consider $10,000$ stochastic trajectories per sub-ensemble with10 sub-ensembles. We will set the origin for x to 0. The variable a will be initialized as delta-correlated in space with a gaussian standard deviation on the lattice of $\sigma = 10/\sqrt{\Delta V}$. As our observable, we consider the second moment of a.

This is simulated through the following xSPDE code:

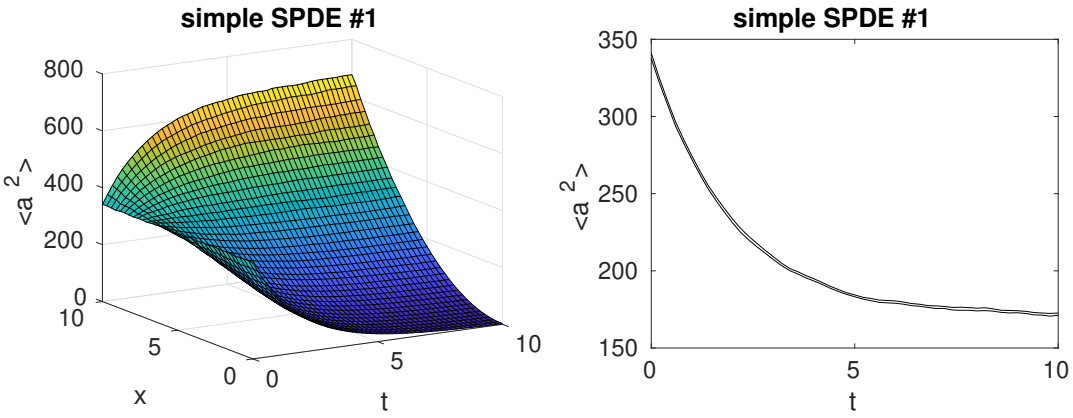

Figure 8.2.: *Example: simple SPDE output graphs.*

```
clear;
p.name = 'simple SPDE';
p.dimensions = 2;
p.ensembles = [10000,10];
p.origins = [0,0];
p.noises = 1;
p.initial = @(v,p) 10*v;
p.observe = @(a,~) a.^2;
p.olabels = '<a^2>';
p.deriv = @(a,w,p) -0.25*a + p.x .* w;
xspde(p);
```

With this input, Matlab produces two output graphs:

The second graph shows the time evolution for x at the mid-point, $x = 5$. The variances are larger than they would be in the SDE case, where one might expect an initial variance of $\langle a^2(0)\rangle = 100$. The reason for this is that the initial noise random and noise fields are replaced by a lattice with a variance of $1/\Delta V$. In the default case, this causes an increase in the local noise.

8.3. Transverse lattice

8.3.1. SPDE spatial lattice

Stochastic variables in an SPDE are stored in a cell array that can include one or more real or complex arrays, $a(f, \mathbf{i}, e)$. Here f is the internal field index, $\boldsymbol{i}$ is a $d-1$ dimensional spatial lattice index for d space-time dimensions, and e is the ensemble index. For a cell array of multiple fields, a, b, c .., these must each have either the same number of points or one point per dimension. When specifying the spatial lattice, one must define:

dimensions The dimensionality in time and space. The default is an SDE: $d = 1$.

points The number of integration points. The default is $\mathbf{N} = [51, 35, 35..]$. This can be a cell index for multiple fields, provided the indices are compatible for broadcasting, eg $points = \{[35, 25], [35, 1]\}$. This allows dynamic boundary fields to be input.

ranges The integration ranges in each dimension. The default is $\mathbf{R} = [10, 10, 10..]$. This is the same for all cells.

origins The origins of the space-time integration domains. By default, the origin is $O(1) = 0$ for the time coordinate and $\mathbf{O} = -\mathbf{R}/2$ for the space coordinates ($\mathbf{R}$ is the *ranges* variable) such that the spatial grid is symmetric around $\mathbf{r} = 0$.

There is an important restriction, which is that the first field should have the maximum number of points in each dimension.

The spatial points in the n-th dimension are at $r\{n\} = O(n), O(n) + dx(n), \ldots O(n) + R(n)$, so the spacing for $N(n)$ points is $dx(n) = R(n)/(N(n) - 1)$. For periodic boundaries, the boundaries where fields and derivatives are equal are at $O(n) - dx(n)/2$ and $O(n) + R(n) + dx(n)/2$. For other boundary types, the boundary values are defined at the first and last points.

8.3.2. Field indices

In the functions *deriv*, *initial* and *observe*, the field and noise variables a and w have extended dimensionality compared to the 1-dimensional case, to index the transverse lattice. The indices are $a(f, \mathbf{i}, e)$, where the:

field index f corresponds to the field index for a and the noise index for w.

intermediate indices $\mathbf{i}$, which are absent in the 1-dimensional case, correspond to the spatial grid and have the same structure. For example, in the case with *dimensions = 3*, indicating one time index and two spatial dimension, $\mathbf{i}$ corresponds to the two space indices.

last index e corresponds to the stochastic trajectory.

For storing space coordinates like $p.x$, the first and last index are $f = e = 1$. Where Fourier transforms are used internally, the momentum arrays have zero momentum as the first index to follow standard discrete Fourier transform conventions. This is changed to a symmetric convention in all stored graphics data outputs that are functions of moentum space.

8.3.3. Integrals and averages

There are functions available in xSPDE for spatial grid averages and integrals, to handle the spatial grid. These are ***Ave*** and ***Int,*** which are used to calculate observables for plotting. They operate in parallel over the lattice dimensions, by taking a vector or

scalar quantity, for example a single field component, and returning an average or a space integral. In each case the first argument is the field, the second argument is a vector defining the type of operation, and the last argument is the parameter structure. If there are two arguments, the operation vector is replaced by its default value.

Integrals over the spatial grid allow calculation of global quantities. To take an integral over the spatial grid, use the xSPDE function *Int* with arguments *(o, [dx,] p)*.

This function takes a scalar or vector quantity *o*, and returns a trapezoidal space integral over selected dimensions with vector measure *dx*. If $dx(j) > 0$ an integral is taken over dimension *j*. Dimensions are labelled from *j = 1,2,3 ...* as in all xSPDE standards. Time integrals are ignored at present. Integrals are returned at all lattice locations. To integrate over an entire lattice, set *dx = p.dx*, otherwise set *dx(j) = p.dx(j)* for selected dimensions *j*.

If momentum-space integrals are needed, first use the *transforms* switch to make sure that the field is Fourier transformed before being averaged, and input *dk* instead of *dx*.

Spatial grid averages can be used to obtain stochastic results with reduced sampling errors if the overall grid is homogeneous. An average is carried out using the builtin xSPDE function *Ave()* with arguments *(o, [av,] p)*.

This takes a vector or scalar field or observable, defined on the lattice, and returns an average over the spatial lattice. The input is a field *a* or observable *o*, and an optional averaging switch *av*. If $av(j) > 0$, an average is taken over dimension *j*. Space dimensions are labelled from *j = 2,3...* as elsewhere. If the *av* vector is omitted, the average is taken over all space directions.

8.4. Spectral operators

Using a linear spectral operator in an SPDE gives better accuracy, and allows use of the interaction picture. This is included automatically for all built-in xSPDE algorithms, provided the *linear* function is defined in the parameter structure. Variables $p.D\{i\}$ (with placeholders $p.Dx, p.Dy, p.Dz$ for the first 3 spatial dimensions) provide access to the derivative operator. Higher-order derivatives are found through potentiating $p.Dx$ accordingly.

For example, the 2-dimensional Laplacian operator

$$\nabla^2 = \frac{\partial^2}{\partial x^2} + \frac{\partial^2}{\partial y^2} \tag{8.4}$$

corresponds to a linear differential operator specified as:

$$p.linear = @(p)\ \ p.Dx.^2 + p.Dy^2; \tag{8.5}$$

For a comprehensive list of variables accessible through the *p*-structure, refer to sec. 10.7.3.

As explained in section 5.9, the general equation solved can be written in differential form as

$$\frac{\partial \mathbf{a}}{\partial t} = \mathbf{A}\left[\mathbf{a}\right] + \underline{\mathbf{B}}\left[\mathbf{a}\right] \cdot \mathbf{w}(t) + \underline{\mathbf{L}}\left[\nabla, \mathbf{a}\right] . \tag{8.6}$$

The linear function L can be input either inside the derivative function using finite difference operators described below, or as a separate *linear* function, to allow for an interaction picture in which case:

$$\underline{\mathbf{L}}\left[\nabla, \mathbf{a}\right] = \underline{\mathbf{L}}\left[\nabla\right] \mathbf{a} . \tag{8.7}$$

This depends on momentum space coordinates, which involves Fourier transforms so that no space dependence is allowed. It is also possible to use finite differences, in which case the derivative terms are included as part of the derivative function *deriv*.

The usual FFT spectral methods require periodicity, and may have either even or odd linear derivatives. The four other boundary combinations must be used with an interaction picture derivative that only has even powers of linear derivatives. Odd derivatives and nonlinear derivative terms can also be included by using finite difference derivatives in the *deriv* functions.

The field $p.x$ is provided by the parameter structure, and corresponds to the variable x in Eq (8.2). All parameters are preceded by the structure label, p. For two or three space dimensional problems, x, y, z are placeholders for $r\{2\}, r\{3\}, r\{4\}$, and spatial variables of even higher dimensional problems can be accessed through $r\{n\}$.

Note that where numerical labels or indices are used, the convention is that time is the first dimension.

8.4.1. One space-dimensional example

A famous partial differential equation is an exactly soluble equation for a soliton, the nonlinear Schrödinger equation (NLSE):

$$\frac{da}{dt} = \frac{i}{2}\left[\nabla^2 a - a\right] + ia\left|a\right|^2 . \tag{8.8}$$

Together with the initial condition that $a(0, x) = sech(x)$, this has a soliton, an exact solution that doesn't change in time:

$$a(t, x) \quad = \quad sech(x). \tag{8.9}$$

The spatial integral is simply:

$$\int sech(x)dx \quad = \quad \pi. \tag{8.10}$$

An xSPDE code that solves this is given below, together with code that compares the numerical solution with the exact solutions for the soliton and the integral:

```
p.name = 'NLS soliton';
p.dimensions = 2;
p.initial = @(v,p) sech(p.x);
p.deriv = @(a,~,p) 1i*a.*(conj(a).*a);
p.linear = @(p) 0.5*1i*(p.Dx.^2-1.0);
p.olabels = {'a(x)','\int a(x) dx'};
p.observe{2} = @(a,p) Int(a, p);
p.compare{1} = @(p) sech(p.x);
p.compare{2} = @(p) pi;
e = xspde(p);
```

Due to finite boundaries and discrete spatial lattice, the agreement is not perfect. The errors can be reduced by increasing the range of the integration domain and improving the resolution with more points.

8.4.2. Two space-dimensional example

As another example, consider the two-dimensional nonlinear stochastic equation, with periodic boundary conditions:

$$\frac{\partial a}{\partial t} = \nabla^2 a\left(\mathbf{x},t\right) + a\left(\mathbf{x},t\right) - a\left(\mathbf{x},t\right)^3 + \eta\left(\mathbf{x},t\right). \tag{8.11}$$

Using the interaction picture allows for the absorption of both the Laplacian and the first-order term by the *p.linear* parameter, which results in

```
...
p.linear = @(p) (p.Dx.^2+p.Dy.^2) + 1;
p.deriv = @(a,w,~) -a.^3 + w;
xspde(p);
```

With this input, Matlab produces two output graphs:

8.5. Finite differences

Instead of using the interaction picture, xSPDE also has finite difference methods for direct differentiation. These derivatives are obtained through function calls $D1$ and $D2$ respectively for first and second derivatives, which use a fixed grid spacing. As elsewhere, they can be replaced by user-written functions if preferred. Generally they require smaller steps in time than spectral methods, when used to define the derivative.

8.5.1. Finite difference first derivatives

The code to take a first order spatial derivative with finite difference methods is carried out using the xSPDE function *D1()* with arguments *(o, [dir, ind, c] p)*.

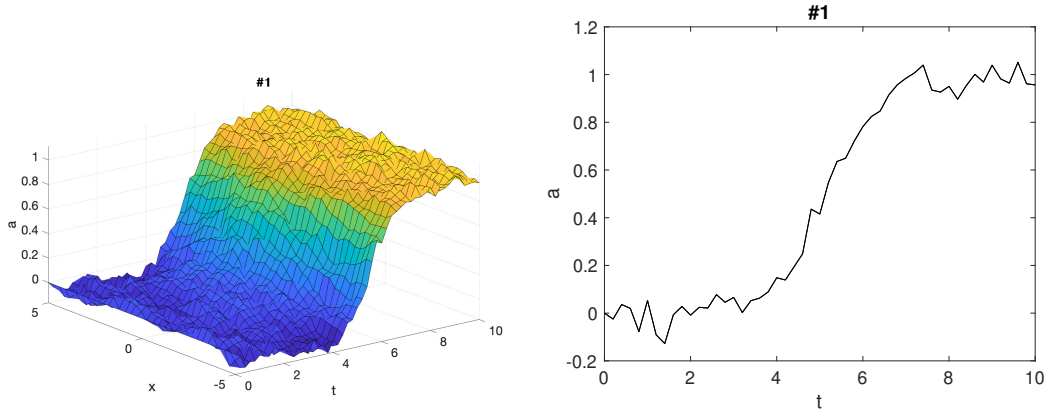

Figure 8.3.: *Two space-dimensional example graphs.*

This takes a scalar or vector *o* and returns a first derivative in an axis direction *dir*. Set *dir = 2* for an x-derivative, *dir = 3* for a y-derivative, and so on. Time derivatives are ignored at present. Derivatives are returned at all lattice locations.

If the direction is omitted, an x-derivative is returned. The next optional input is *ind,* which is a vector of one or more field indices that are differentiated. If it is omitted, all indices are differentiated. If there are Robin/Neumann

These derivatives can be used both in calculating propagation and in calculating observables. The boundary condition is set by the *boundaries* input. Any boundary of any dimension, cell or index can be made periodic, which is the default, or Neumann, or Robin/Dirichlet.

8.5.2. Finite difference second derivatives

The code to take a second order spatial derivative with finite difference methods is carried out using the xSPDE *D2* function with arguments *(o, [dir,] p).*

This takes a scalar or vector *o* and returns the second derivative in axis direction *dir*. Set *dir = 2* for an x-derivative, *dir = 3* for a y-derivative and so on. All other properties are exactly the same as *D1.*

Without using the interaction picture, the stochastic equation of Eq (8.11) is specified in xSPDE using finite differences as

```
p.dimensions = 3;
p.steps = 50;
p.deriv = @(a,w,p) D2(a,2,p)+D2(a,3,p)+a - a.^3 +...
w/10;
xspde(p);
```

This gives the same result as with the linear propagator, although requiring smaller step-sizes for numerical stability, with an output graph shown in Fig (8.4). Note that

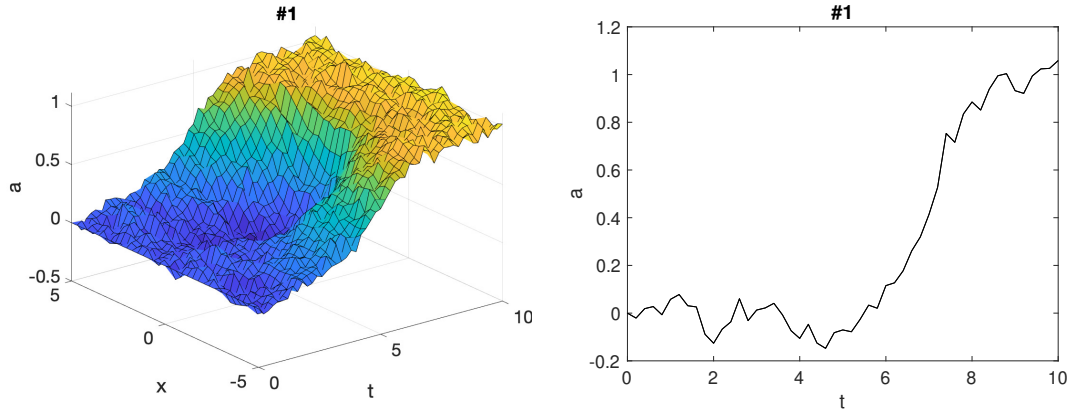

Figure 8.4.: *Two space-dimensional example graphs, direct differentiation.*

the parameters and noises are slightly different!

8.6. Boundary conditions

8.6.1. Transverse boundaries

Transverse boundary conditions must be given for all partial differential equations. Common transverse *boundary types* are of three types: Neumann (specified derivative), periodic, or Dirichlet (specified field). These are obtained using $boundaries\{c,d\} = -1, 0, 1$, which is specified for each cell c, space dimension $d > 1$, field index i and boundary j.

If *boundaries* are omitted for any dimension the default is 0, which gives periodic boundaries in that dimension for all field indices, and permits the use of Fourier transforms and an interaction picture as described above.

The value of $boundaries\{c,d\}$ is a matrix whose column index (i) is the field index, and whose row index (j) is given by $j = 1, 2$ for the lower and upper boundary type respectively.

Spatial derivatives or other functions linking different spatial points can be specified either in the functionals $\boldsymbol{A}[\mathbf{a},\mathbf{r}]$, $\underline{\mathbf{B}}[\mathbf{a},\mathbf{r}]$ or else in the *linear* function, provided the derivative terms are linear functions of the fields. Use of the *linear* function allows an interaction picture algorithm, with increased efficiency. The *linear* function is currently only available with periodic boundary conditions.

The default boundary conditions are periodic. The implicit setting of this is that periodicity is enforced such that $a(o_i - dx_i/2) = a(o_i + r_i + dx_i/2)$, which is the usual discrete Fourier transform requirement.

Otherwise, the differential equation boundaries are specified at $a(o_i)$, $a(o_i + r_i)$, using the cell-array input $boundaries\{c,d\}(i,j)$, which is defined per field cell, space dimension $(d = 2, 3..)$, field index $(i = 1, 2..)$ and boundary $j = (1, 2)$. Here $d > 1$ is the transverse dimension, not including time, which only has an initial condition.

In summary the available boundary types are:

Neumann: For specified *derivative* boundaries, $boundaries\{c,d\}(i,j) = -1$

Periodic: For *periodic* boundaries, $boundaries\{c,d\}(i,j) = 0$

Dirichlet: For specified *field* boundaries, $boundaries\{c,d\}(i,j) = 1$

These are specified in a cell array: $boundaries\{c,d\}(i,1)$ sets the lower boundary type in dimension d, for the i *-th* field component while $boundaries\{c,d\}(i,2)$ gives the upper boundary type. Each space dimension, variable and boundary is set independently. In xSPDE, the equations are always initial value problems in time, so the time dimension boundary specification for $d = 1$ is not included.

Example: boundary types in a 2-dimensional PDE Suppose there is one field cell with two field indices, and mixed boundaries in space: Dirichlet for a lower boundary at $x = 0$, and and Neumann for an upper boundary at $x = 1$, for the first field $a(1,:)$, with the opposite combination in the second field component, $a(2,:)$, hence

```
p.boundaries{2} = [1,-1;-1,1];
```

The field cell index is $c = 1$, which can be omitted here.

8.6.2. Transverse boundary values

For non-vanishing, specified boundary conditions, the boundary values can be entered either using $boundval\{c,d\}(a,p)$, if they are constant in time, \or else, if they are dynamical, the function $boundfun(a,c,d,p)$ is specified. This returns the boundary values used for the fields or derivatives in a particular cell c and dimension $d > 1$ as an array of dimension $b(\mathbf{j},e)$), where $\mathbf{j} = i,\mathbf{k}$.

Here a is the current field cell array, $i = j_1$ is the field index, and $\mathbf{k}$ is the space index, where j_d is the index of the dimension whose boundary values are specified. For this dimension, only two values are needed: $j_d = 1,2$ for the lower and upper boundary values, which could either be field values or their derivatives. An ensemble index e is also needed if the boundary values are stochastic.

Boundary values can be a function of both the fields (a) and internal variables like the current time (t). These may have stochastic initial values at $t = 0$ which are calculated only once. In such cases the boundary values must first be initialized, so the routine $boundfun(a,c,d,p)$ is first internally initialized with time $t < origin(1)$, and with random Gaussian values in the input field a. These are delta-correlated in space, i.e., with the same definition as "inrandoms". The xSDPE program stores the returned values b for the boundaries in an internal cell array, $boundval\{c,d\}$, for later use if required.

The default boundary value is zero, if not specified.

NOTE: Current xSPDE code requires finite-difference methods to be used with *boundval* or *boundfun*. **Spectral methods use the default boundary conditions, apart from Dirichlet-Dirichlet cases.**

8.6.3. Example: boundaries in a 2-dimensional PDE

Suppose there are two fields, and we wish to set boundary values.

We take boundary values as Dirichlet for $x = 0$ and Neumann for $x = 1$ in field variable 1, and Neumann for $x = 0$ and Dirichlet for $x = 1$ in field variable 2. Suppose the boundary values are different from the default values of $a = 0$, $\partial_x a = 0$, so that:

$$\begin{aligned} a_1\left(x=0\right) &= 1, \\ \partial_x a_1\left(x=1\right) &= a_1\left(x=1\right). \\ \partial_x a_2\left(x=0\right) &= -a_2\left(x=0\right) \\ a_2\left(x=1\right) &= -1. \end{aligned} \tag{8.12}$$

These are set in the following code:

```
p.boundfun = @mybfun
p.boundaries{2} = [1,-1;-1,1];
...
function b = mybfun(a,~,~,p)
% b = mybfun(a,c,d,p) calculates boundary values
b(1,2,:)  = a(1,end,:);
b(2,1,:)  = -a(2,end,:);
b(1,1,:)  = 1+0*a(1,end,:);
b(2,2,:)  = -1+0*a(1,end,:);
end
```

8.6.4. Transverse plots

A number of plots at equally spaced points in time can be generated through. For example, adding the line below creates 3 time-sliced plots at $t = 0, 5, 10$:

```
p.transverse{1} = 3;
```

8.7. Output transforms

For graphical output, Fourier transforms involve a sum over the lattice points using a discrete Fourier transform at the lattice points x_i, so that:

$$\tilde{a}(\omega_i, \mathbf{k}_i) = \frac{dtd\mathbf{x}}{[2\pi]^{d/2}} \sum_{j_1 \ldots j_d} \exp\left[i\left(\omega_{i_1} t_{j_1} - \mathbf{k_i} \cdot \mathbf{x_j}\right)\right] a(t_{j_1}, \mathbf{x_j}) \tag{8.13}$$

The momenta k_i have an interval of

$$dk_i = \frac{2\pi}{n_i dx_i} \tag{8.14}$$

with k_i values given for even n by:

$$k_i = \left(1 - \frac{n_i}{2}\right) dk_i, \ldots \frac{n_i}{2} dk_i \tag{8.15}$$

and for odd n by:

$$k_i = \frac{1 - n_i}{2} dk_i, \ldots \frac{n_i - 1}{2} dk_i \tag{8.16}$$

Once Fourier transformed, the *observe* function can be used to take any further functions or combinations of Fourier transformed fields prior to averaging. Important points to keep in mind are as follows:

- Fourier transforms are specified for the k-th *observe* function independently of all other functions, by specifying $transforms\{k\} = [\ell_{1,} \ldots \ell_{d,}]$.
- Here $\ell_j = 0, 1$ is a logical switch, set to to $\ell_j = 1$ if the $j - th$ dimension requires a Fourier transform, and $\ell_j = 0$ if there is no Fourier transform.
- The internal fields $p.k\{1\}, \ldots p.k\{d\}$ are available for use in making functions of momentum for use with observations.
- In propagation calculations, the momentum lattice values start with $k = 0, \ldots$, following standard Matlab and FFT conventions.
- For storing and graphing, momentum lattice values are reordered to start with $k = -k_{max}, \ldots$, following standard graphics and mathematical conventions.

8.8. Initial random fields

Fourier transforms are available for use both on initial random values and on noise fields during time-evolution. This is controlled by the second element of *randoms* and *noises*, respectively.

When $randoms(1) > 0$, an initial random field $\mathbf{v}^x$ is generated with delta-correlations in x-space. When $randoms(2) > 0$, an initial random field $\tilde{\mathbf{v}}^k$ is generated with delta-correlations in k-space. This can be filtered with a user-specified filter function to give $\tilde{\mathbf{v}}^{kf}$, then inverse Fourier transformed to give v^k. Both random fields are passed to the *initial* function as an extended vector $\left[v^x, v^k\right]$, for field *initialization* in space.

There is a user specified filter function available, to modify random fields $\tilde{v}^k$, that are delta-correlated in momentum space using a filter function, '*rfilter*' so that $v_i^{kf}(\mathbf{k}) = f_i^{(r)}\left(\mathbf{v}^k(\mathbf{k})\right)$, before being used. The corresponding correlations are:

$$\begin{aligned}
\left\langle v_i^x(\mathbf{x})\, v_j^x\left(\mathbf{x}'\right)\right\rangle &= \delta\left(\mathbf{x} - \mathbf{x}'\right)\delta_{ij} \sim \frac{1}{\Delta V}\delta_{\mathbf{x},\mathbf{x}'}\delta_{ij} \\
\left\langle \tilde{v}_i^k(\mathbf{k})\, \tilde{v}_j^k\left(\mathbf{k}'\right)\right\rangle &= \delta\left(\mathbf{k} - \mathbf{k}'\right)\delta_{ij} \sim \frac{1}{\Delta K}\delta_{\mathbf{k},\mathbf{k}'}\delta_{ij} \\
\left\langle \tilde{v}_i^{kf}(\mathbf{k})\, \tilde{v}_j^{kf}\left(\mathbf{k}'\right)\right\rangle &= \left\langle f_i^{(r)}\left(\tilde{\mathbf{v}}^k(\mathbf{k})\right) f_j^{(r)}\left(\tilde{\mathbf{v}}^k\left(\mathbf{k}'\right)\right)\right\rangle .
\end{aligned} \tag{8.17}$$

Note that on a lattice, we replace the Dirac continuous delta-function by a discrete Kronecker delta function scaled by an inverse volume element either in space (ΔV) or momentum (ΔK) . The xSPDE Fourier transforms are given by a symmetric Fourier transform, so that if we inverse Fourier-transform the $k-$space *inrandoms*, without filtering, then:

$$v^k(\mathbf{x}) = \frac{1}{[2\pi]^{(d-1)/2}} \int e^{i\mathbf{k}\cdot\mathbf{x}} \tilde{v}^k(\mathbf{k}) d\mathbf{k} \tag{8.18}$$

These have random initial values that are real and delta-correlated in space, so that:

$$\left\langle v^x(\mathbf{x})\, v^x\left(\mathbf{x}'\right)\right\rangle = \delta\left(\mathbf{x}-\mathbf{x}'\right). \tag{8.19}$$

The corresponding noises in position space are correlated according to:

$$\begin{aligned}\left\langle v^k(\mathbf{x})\left(v^k\left(\mathbf{x}'\right)\right)^*\right\rangle &= \frac{1}{[2\pi]^{(d-1)}} \int e^{i(\mathbf{k}\cdot\mathbf{x}-\mathbf{k}'\cdot\mathbf{x}')} \left\langle \tilde{v}^k(\mathbf{k})\, \tilde{v}^k\left(\mathbf{k}'\right)\right\rangle d\mathbf{k} d\mathbf{k}' \\ &= \frac{1}{[2\pi]^{(d-1)}} \int e^{i(\mathbf{x}-\mathbf{x}')\cdot\mathbf{k}} d\mathbf{k} \\ &= \delta\left(\mathbf{x}-\mathbf{x}'\right). \end{aligned} \tag{8.20}$$

Similarly, if we don't conjugate the k-noise, then:

$$\left\langle v^k(\mathbf{x})\, v^k\left(\mathbf{x}'\right)\right\rangle = \delta\left(\mathbf{x}+\mathbf{x}'\right). \tag{8.21}$$

However, if we define $\tilde{v}^c(\mathbf{k}) = \left[\tilde{v}_1^k(\mathbf{k}) + i\tilde{v}_2^k(\mathbf{k})\right]/\sqrt{2}$, then we obtain complex noise that is only delta correlated when conjugated.

$$\begin{aligned}\left\langle v^c(\mathbf{x})\left(v^c\left(\mathbf{x}'\right)\right)^*\right\rangle &= \delta\left(\mathbf{x}-\mathbf{x}'\right) \\ \left\langle v^c(\mathbf{x})\, v^c\left(\mathbf{x}'\right)\right\rangle &= 0. \end{aligned} \tag{8.22}$$

This is obtainable with the x-space noise as well, but the utility of the k-space noise is that it can be filtered to have nonlocal correlations in space if required.

During propagation in time, $\mathbf{w} = \left[\mathbf{w}^x, \mathbf{w}^k\right]$ are real noise fields that are delta-correlated in space-time. They are calculated in an analogies way, except with an additional factor of $1/\sqrt{dt}$ because they are delta correlated in time as well.There is a user specified scaling function available, to take random noises w^k in momentum space that are then scaled using a filter function, '*nfilter*' so that $w_i^{kf}(\mathbf{k}) = f_i^{(n)}\left(\mathbf{w}^k(\mathbf{k})\right)$, before being used:

$$\begin{aligned}\left\langle w_i^x(t,\mathbf{x})\, w_j^x\left(t,\mathbf{x}'\right)\right\rangle &= \delta\left(\mathbf{x}-\mathbf{x}'\right)\delta\left(t-t'\right)\delta_{ij} \\ \left\langle \tilde{w}_i^k(t,\mathbf{k})\, \tilde{w}_j^k\left(t,\mathbf{k}'\right)\right\rangle &= \delta\left(\mathbf{k}-\mathbf{k}'\right)\delta\left(t-t'\right)\delta_{ij} \\ \left\langle \tilde{w}_i^{kf}(t,\mathbf{k})\, \tilde{w}_j^{kf}\left(t',\mathbf{k}'\right)\right\rangle &= \left\langle f_i^{(n)}\left(\tilde{\mathbf{w}}^k(t,\mathbf{k})\right) f_j^{(n)}\left(\tilde{\mathbf{w}}^k\left(t',\mathbf{k}'\right)\right)\right\rangle. \end{aligned} \tag{8.23}$$

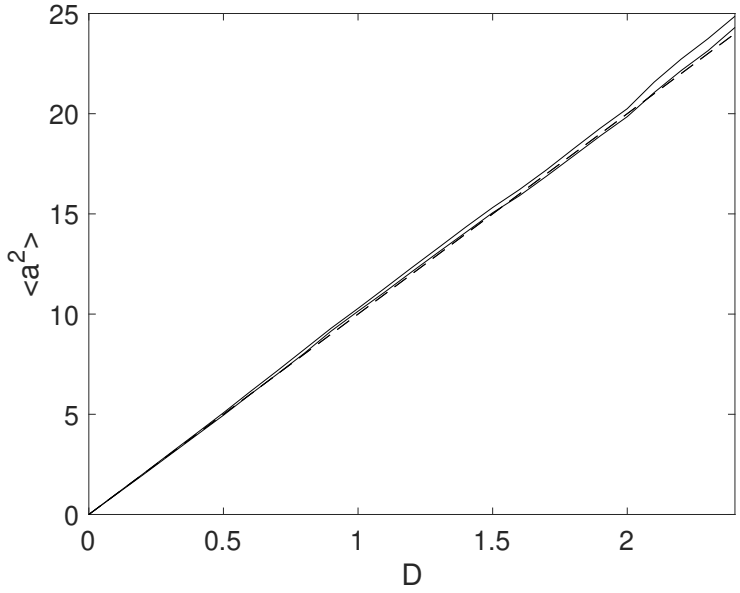

Figure 8.5.: *Scanned parameter output with a variable diffusion, for the case of a pure Wiener process, $\dot{a} = Bw(t)$. Exact value is the dashed line.*

8.9. Scanned parameter plots

Since xSIM is a function that can be called, plots of results against simulation parameters are possible. This requires repeated calls to xSIM with different parameter values, together with data storage in an xGRAPH compatible form, and a call to xGRAPH. If different random seeds are required, the seed needs to be reset in each call. The relevant axes points plotted, labels and the values of scanned parameters also need to be input.

The simulation function xSIM uses the last data array index, c, to store the data values and up to two corresponding errors. This takes up three index values. A value of $c = 4$ is used to store comparison data, and its errors if there are any in $c = 5, 6$. This can be used for exact results, approximations, or experimental data.

8.9.1. Example: Scanned diffusion

As an example, consider the simplest possible stochastic equation, with a scanned diffusion:

$$\dot{a} = Bw(t)\,. \tag{8.24}$$

The equation is integrated over the interval $t = 0 : 10$, with $a = 0$ initially, using 10^4 trajectories to give an expected error of around $\pm 1\%$. The variance of a at $t = 10$ is plotted as a function of $D = B^2$, then compared to an exact value. The result is in Fig (8.5). The corresponding code is given as well.

```
function e = WienerScan()
p.name = 'Wiener process';
p.ensembles = [1000,10];
p.points = 12;
p.deriv = @(a,z,p) z*p.B;
p.observe = @(a,p) a.^2;
p.olabels = {'<a^2>'};
p.glabels{1} = {'D'};
scanpoints = 25;
data{1}{1} = zeros(1,scanpoints,4);
for j = 1:scanpoints
  p.seed = j;
  p.B = sqrt((j-1)*0.1);
  [e,data1,input,~] = xsim(p);
  data{1}{1}(1,j,1:3) = data1{1}{1}(1,p.points,:);
  xk{1}{1}(j) = p.B^2;
  D(j) = p.B^2;
end
data{1}{1}(1,:,4) = input.ranges(1)*D(:);
input.xk = xk;
input.axes{1}{1} = 1:scanpoints;
xgraph(data,input);
end
```

Here *p.deriv* defines the time derivative function $\dot{a}$, with w being the delta-correlated Gaussian noise that is generated internally.

8.10. SPDE examples

8.10.1. Gaussian diffraction

Free diffraction and absorption of a Gaussian wave-function in $d-1 = s$ space dimensions, is given by the partial differential equation (PDE):

$$\frac{da}{dt} = -\frac{\gamma}{2}a + \frac{i}{2}D\nabla^2 a. \tag{8.25}$$

The corresponding stochastic partial differential equation (SPDE) includes additional noise, so that:

$$\frac{da}{dt} = -\frac{\gamma}{2}a + \frac{i}{2}D\nabla^2 a + bw(t,x). \tag{8.26}$$

The xSPDE spectral definition in space is:

$$\tilde{a}(t,\mathbf{k}) = \frac{1}{[2\pi]^{s/2}}\int e^{i\mathbf{k}\cdot\mathbf{x}}a(t,\mathbf{x})d\mathbf{x}\,. \tag{8.27}$$

Together with the initial condition that $a(0,x) = exp(-|\mathbf{x}|^2/2)$, this has an exact solution for the diffracted intensity with $b = 0$, in either ordinary space or momentum space:

$$\begin{aligned} |a(t,\mathbf{x})|^2 &= \frac{1}{\left(1+(Dt)^2\right)^{s/2}} exp\left(-|\mathbf{x}|^2/\left(1+(Dt)^2\right)-\gamma t\right) \\ |\tilde{a}(t,\mathbf{k})|^2 &= exp\left(-|\mathbf{k}|^2-\gamma t\right). \end{aligned} \tag{8.28}$$

Exercises

- Simulate Gaussian diffraction in three dimensions using an xSPDE function
- Check your results against the exact solution
- The example below stores data in a standard HDF5 file.

```
function [e] = Gaussian()
p.dimensions = 4;
p.initial = @(v,p) exp(-0.5*(p.x.^2+p.y.^2+p.z.^2));
p.linear = @(p) 1i*0.05*(p.Dx.^2+p.Dy.^2+p.Dz.^2);
p.observe = @(a,p) a.*conj(a);
p.olabels = '|a(x)|^2';
p.file = 'Gaussian.h5';
p.images = 4;
e = xsim(p);
xgraph(p.file);
end
```

- **Add an additive complex noise of $0.01(w_1 + iw_2)$ to the Gaussian differential equation, then replot with an average over 100 samples.**
- Work out the exact solution and repeat the comparisons.

Note that for this, you'll need to add: $p.deriv = @(a,w,p)\ ..+0.01*(w(1,:)+i*w(2,:))$

8.10.2. Stochastic Ginzburg-Landau

Including two space dimensions, or space-time dimensions of $d = 3$, an example of a SPDE is the stochastic Ginzburg-Landau equation. This describes symmetry breaking. The system develops a spontaneous phase which varies spatially as well. The model is used to describe lasers, magnetism, superconductivity, superfluidity and particle physics:

$$\dot{a} = \left(1-|a|^2\right)a + bw(t) + c\nabla^2 a \tag{8.29}$$

where

$$\left\langle w(x)w^*(x')\right\rangle = 2\delta\left(t-t'\right)\delta\left(x-x'\right). \tag{8.30}$$

The following new ideas are introduced for this problem:

1. `dimensions` **is the space-time dimension.**
2. **The** 'dot' **notation used for parallel operations over lattices**.
3. `linear` **is the linear operator - a Laplacian in these cases.**
4. `images` **produces movie-style images at discrete time slices.**
5. `Dx` **indicates a derivative operation,** $\partial/\partial x$**.**
6. $-5 < x < 5$ **is the default xSPDE coordinate range in space.**

Exercises

1. **Solve the stochastic G-L equation for** $b = 0.001$ **and** $c = 0.01i$**.**
2. **Change to a real diffusion so that** $c = 0.1$**.**

In the first case, you should get the output graphed in Fig (8.6) .

```
clear;
p.name = 'Extended laser gain equation';
p.noises = 2;
p.dimensions = 3;
p.steps = 10;
p.linear = @(p) 1i*0.01*(p.Dx.^2+p.Dy.^2);
p.observe = @(a,~) abs(a).^2;
p.images = 6;
p.olabels = '|a|^2';
p.deriv = @(a,w,~) (1-abs(a(1,:).^2)).*a(1,:)+...
                 0.001*(w(1,:)+1i*w(2,:));
xspde(p)
```

Here the notation $a(1,:)$ means that the operation is repeated over all values of the subsequent indices, which are the two spatial lattice indices in this case.

8.10.3. NLS soliton

The famous nonlinear Schrödinger equation (NLSE) is:

$$\frac{da}{dt} = \frac{i}{2}\left[\nabla^2 a - a\right] + ia\left|a\right|^2. \tag{8.31}$$

Together with the initial condition that $a(0,x) = sech(x)$, this has a soliton [90], an exact solution that doesn't change in time:

$$a(t,x) \quad = \quad sech(x). \tag{8.32}$$

The Fourier transform at $k = 0$ is simply:

$$\tilde{a}(t,0) \quad = \quad \frac{1}{\sqrt{2\pi}}\int sech(x)dx = \sqrt{\frac{\pi}{2}}. \tag{8.33}$$

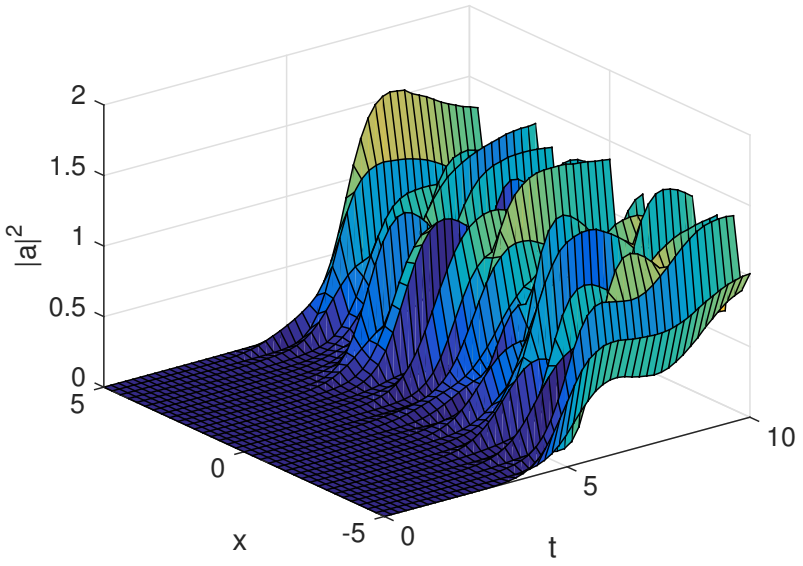

Figure 8.6.: *Simulation of the stochastic equation describing symmetry breaking in two dimensions. Spatial fluctuations are caused by the different phase-domains that interfere. The graph obtained here is projected onto the $y = 0$ plane.*

Exercises

- **Solve the NLSE for a soliton using a function instead of a script, then include an additive complex noise of $0.01(w_1 + iw_2)$ to the differential equation, and plot again with an average over 1000 samples.**

8.10.4. Planar noise

The next example is growth of thermal noise of a two-component complex field in a plane, given by the equation

$$\frac{d\mathbf{a}}{dt} = \frac{i}{2}\nabla^2\mathbf{a} + \mathbf{w}(t,x). \tag{8.34}$$

where ζ is a delta-correlated complex noise vector field:

$$w_j(t,\mathbf{x}) = \left[w_j^{re}(t,\mathbf{x}) + i\zeta_j^{im}(t,\mathbf{x})\right]/\sqrt{2}, \tag{8.35}$$

with the initial condition that the initial noise is delta-correlated in position space

$$a(0,\mathbf{x}) = \zeta^{(in)}(\mathbf{x}) \tag{8.36}$$

where:

$$\zeta^{(in)}(\mathbf{x}) = \left[\zeta^{re(in)}(\mathbf{x}) + i\zeta^{im(in)}(\mathbf{x})\right]/\sqrt{2} \tag{8.37}$$

This has an exact solution for the noise intensity in either ordinary space or momentum space:

$$\begin{aligned} \left\langle |a_j(t,\mathbf{x})|^2 \right\rangle &= (1+t)/dV \\ \left\langle |\tilde{a}_j(t,\mathbf{k})|^2 \right\rangle &= (1+t)/dV_k \\ \langle \tilde{a}_1(t,\mathbf{k})\,\tilde{a}_2^*(t,\mathbf{k})\rangle &= 0. \end{aligned} \tag{8.38}$$

Here, the noise is delta-correlated, and dV, dV_k are the cartesian space and momentum space lattice cell volumes, respectively. Suppose that $n = n_x n_y$ is the total number of spatial points, and there are $n_{x(y)}$ points in the x(y)-direction, so then:

$$\begin{aligned} dV &= dxdy \\ dV_k &= dk_x dk_y = \frac{(2\pi)^2}{ndV}. \end{aligned} \tag{8.39}$$

In the simulations, two planar noise fields are propagated, one using delta-correlated noise, the other with noise transformed to momentum space to allow filtering. This allows use of finite correlation lengths when needed, by including a frequency filter function that is used to multiply the noise in Fourier-space. The Fourier-space noise variance is the square of the filter function.

The first noise index, $p.noises(1)$, indicates how many noise fields are generated, while $p.noises(2)$ indicates how many of these are spatially correlated, via Fourier transform, filter and inverse Fourier transform. These appear to the user as additional noises, so the total is $p.noises(1)+p.noises(2)$. The filtered noises have a finite correlation length. They are correlated with the first $p.noises(1)$ x-space noises they are generated from, as this can be useful.

Exercises

- **Solve the planar noise growth equation**

```
function [e] = Planar()
p.name = 'Planar noise growth';
p.dimensions = 3;
p.fields = 2;
p.ranges = [1,5,5];
p.steps = 2;
p.noises = [2,2];
p.ensembles = [10,4,4];
p.initial = @Initial;
p.deriv = @Da;
p.linear = @Linear;
p.observe = @(a,p) a(1,:).*conj(a(1,:));
p.olabels = '<|a_1(x)|^2>';
p.compare = @(p) [1+p.t]/p.dv;
p.images = 4;
e = xspde(p);
end

function a0 = Initial(v,p)
a0(1,:)  = (v(1,:)+1i*v(2,:))/sqrt(2);
a0(2,:)  = (v(3,:)+1i*v(4,:))/sqrt(2);
end

function da = Da(a,w,p)
da(1,:)  = (w(1,:)+1i*w(2,:))/sqrt(2);
da(2,:)  = (w(3,:)+1i*w(4,:))/sqrt(2);
end

function L = Linear(p)
lap = p.Dx.^2+p.Dy.^2;
L(1,:)  = 1i*0.5*lap(:);
L(2,:)  = 1i*0.5*lap(:);
end
```

- **Add a decay rate of $-a$ to the differential equation, then plot again**
- **Add growth and nonlinear saturation terms**

8.10.5. Gross-Pitaevskii equation

The next example is a stochastic Gross-Pitaevskii (GP) equation [91] in two dimensions,

$$\frac{da}{dt} = \frac{i}{2}\nabla^2 a - ia(V(r) - i\kappa(r) + |a|^2) + \epsilon\eta \tag{8.40}$$

where η is a correlated complex noise vector field:

$$\eta(t, \mathbf{x}) = w_1(t, \mathbf{x}) + iw_2(t, \mathbf{x}), \tag{8.41}$$

with the initial condition that the initial random field and the noise are both filtered in momentum space

$$a(0, \mathbf{x}) = a_0(\mathbf{x}) + \epsilon\zeta^{(in)}(\mathbf{x}) \tag{8.42}$$

where:

$$\zeta^{(in)}(\mathbf{x}) = v_1(\mathbf{x}) + iv_2(\mathbf{x}) \tag{8.43}$$

We add a Gaussian filter in momentum space for both the initial random field and noise so that, if $\tilde{w}(\mathbf{k})$ is a delta-correlated noise in momentum space:

$$\begin{aligned} w(\mathbf{k}) &= \tilde{w}(\mathbf{k}) \exp\left(-|\mathbf{k}|^2\right) \\ v(\mathbf{k}) &= \tilde{v}(\mathbf{k}) \exp\left(-|\mathbf{k}|^2\right) \end{aligned} \tag{8.44}$$

This allows use of finite correlation lengths when needed, by including a frequency filter function that is used to multiply the noise in Fourier-space. The Fourier-space noise variance is the square of the filter function.

The first noise index, $p.noises(1)$, indicates how many noise fields are generated that are delta-correlated in x, while $p.noises(2)$ indicates how many of these are spatially correlated, via Fourier transform, filter and inverse Fourier transform. These appear to the user as additional noises, so the total is $p.noises(1) + p.noises(2)$. The filtered noises have a finite correlation length.

Exercises

- **Solve the stochastic GP equation** (8.40)**, with a noise coefficient of** $b = 0.1$**,** $V = 0.01\,|\mathbf{x}|^2$, $\kappa = 0.001\,|\mathbf{x}|^4$**, and a stored output data file.**

```
function [e] = GPE()
p.name = 'GPE';
p.dimensions = 3;
p.points = [101,64,64];
p.ranges = [1,20,20];
p.noises = [0,2];
p.rfilter = @(w,p) w.*exp(-p.kx.^2-p.ky.^2);
p.nfilter = @(v,p) v.*exp(-p.kx.^2-p.ky.^2);
b = @(xi) .1*(xi(1,:,:)+1i*xi(2,:,:));
p.initial = @(v,p) (p.x+1i*p.y)./(1+10*(p.x.^2 +...
p.y.^2))+b(v);
V = @(p) 0.01*(p.x.^2 + p.y.^2)-0.001*1i*(p.x.^2 +...
p.y.^2).^2;
p.deriv = @(a,w,p) -1i*a.*(V(p)+conj(a).*a)+b(w);
p.linear = @(p) 0.5*1i*(p.Dx.^2+p.Dy.^2);
p.observe{1} = @(a,p) a.*conj(a);
p.images = {2};
p.imagetype = {2};
p.olabels = {'|a|^2'};
p.file = 'GPE.mat';
e = xsim(p);
xgraph(p.file,p);
end
```

8.10.6. Characteristic equation

The next example is the characteristic equation for a traveling wave at constant velocity [92]. It is included to illustrate what happens at periodic boundaries, when Fourier-transform methods are used for propagation. There are a number of methods known to prevent this effect, including addition of absorbers - called apodization - at the boundaries. The equation is:

$$\frac{da}{dt} + \frac{da}{dx} = 0. \tag{8.45}$$

Together with the initial condition that $a(0,x) = sech(2x+5)$, this has an exact solution that propagates at a constant velocity:

$$a(t,x) \quad = \quad sech(2(x-t)+5). \tag{8.46}$$

The time evolution at $x = 0$ is simply:

$$a(t,0) \quad = \quad sech(2(t-5/2)). \tag{8.47}$$

Exercises

- **Solve the characteristic equation given above, noting the effects of periodic boundaries.**

```
function [e] = Characteristic()
p.name = 'Characteristic';
p.dimensions = 2;
p.initial = @(v,p) sech(2.*(p.x+2.5));
p.deriv = @(a,z,p) 0*a;
p.linear = @(p) -p.Dx;
p.olabels = {'a_1(x)'};
p.compare = @(p) sech(2.*(p.t-2.5));
e = xspde(p);
end
```

- **Recalculate with the opposite velocity, and a new exact solution.**

8.10.7. Nonlinear Anderson localization

A random potential *prevents* normal wave-packet spreading in quantum-mechanics. This is Anderson localization [93]: a famous property of quantum mechanics in a random potential. A typical experimental method is to confine an ultra-cold Bose-Einstein condensate (BEC) in a trap, then release the BEC in a random external potential produced by a laser [94]. The expansion rate of the BEC is reduced by the Anderson localization due to the random potential. Physically, the observable quantity is the particle density $n = |\psi|^2$, but there is a complication, which is that there are nonlinearities from atomic scattering [95].

This can be treated either using a Schrodinger equation with a random potential, at low density, or using the Gross-Pitaevskii (GP) equation to include atom-atom interactions at the mean field level. In this example of a problem where strong localization occurs, the general equations are:

$$\frac{\partial \psi}{\partial t} = \frac{1}{i\hbar}\left[-\frac{\hbar^2}{2m}\nabla^2 + V(\mathbf{r}) + g\left|\psi\right|^2\right]\psi. \tag{8.48}$$

In calculations, it is best to use a dimensionless form by rescaling coordinates and fields. A simple way to simulate this with xSPDE is to treat ψ as a scaled field $a(1)$, and to assume the random potential field $V(\mathbf{r})$ as caused by interactions with second random field $|a(2)|^2$. This has the advantage that it is similar to the actual experiment and allows one to treat time-dependent potentials as well, if desired.

With the rescaling, this simplifies to:

$$\frac{\partial a_1}{\partial \tau} = i\left[\frac{\partial}{\partial \zeta^2}^2 - \left|a_2\right|^2 - \left|a_1\right|^2\right]a_1. \tag{8.49}$$

A convenient initial condition is to use:

$$\begin{aligned} a_1 &= a_0 \exp(-\zeta^2) \\ \left\langle a_2(\zeta) a_2(\zeta')\right\rangle &= v\delta\left(\zeta - \zeta'\right). \end{aligned} \tag{8.50}$$

Exercise

- **Solve Schrodinger's equation without a random potential, to observe expansion.**
- **Include a random potential v, to observe localization.**
- **Experiment with nonlinear terms and higher dimensions.**

The GP equation is a mean field approximation; this is still not a full solution of the many-body problem! Also, the experiments are more complicated than this, and actually observe the momentum distribution.

Part III.

Methods, API and Examples

9. Stochastic methods and errors

This chapter describes the methods available, and how to add custom algorithms.

9.1. Introduction to algorithms

Stochastic, partial and ordinary differential equations are central to numerical mathematics. Ordinary differential equations have been known in some form ever since calculus was invented. There are an extraordinary number of algorithms used to solve these equations. This chapter provides an overview of the included algorithms.
xSPDE has six built-in choices of algorithm, with defaults. All built-in methods have an interaction picture and can be used with any space dimension, including $dimensions = 1$, which is an ordinary stochastic equation. All can be used with stochastic or with non-stochastic equations, and with order extrapolation.
For stochastic equations, the Euler method requires an Ito form of stochastic equation, the implicit Euler method requires an implicit Ito form, while the others should be used with the Stratonovich form of calculus. Each is chosen to be able to use an interaction picture to take care of exactly soluble linear terms.

The default methods will solve most DE, SDE, PDE and SPDE problems reliably, but other ones can be included if needed.

9.1.1. Standard methods

The standard xSIM algorithms given below are available for ODEs, PDEs, SDEs and SPDEs. More advanced algorithms for specialized cases are described in section 9.

For stochastic differential equations, which are non-differentiable, the usual rules of calculus do not apply because stochastic noise is non-differentiable. It has fluctuations proportional to $1/\sqrt{dtdV}$, for noise defined on a lattice with temporal cell-size dt and spatial cell-size dV. Hence, the usual differentiability and smoothness properties required to give high-order convergence for standard Runge-Kutta methods are simply not present. Instead, xSPDE has a built-in extrapolation to zero step-size for high-order stochastic convergence.

Many more complex higher order algorithms for stochastic integration exist but are not included in the current xSPDE distribution, and users are encouraged to contribute their favorite methods.

We note here that there are multiple error sources possible. SDE/SPDE errors are often dominated by the sampling error, not discretization. In addition, all convergence theorems only apply to the limit of zero step-size. One may be very far from this regime

in a given practical calculation. Analytic error estimates also have prefactors which are hard to calculate. However, xSPDE can numerically estimate both the discretization and sampling error for any given average observable.

9.1.2. Advanced methods

Three more advanced method libraries are included here, namely *weighted*, *projected* and *forward-backward* stochastic differential equations. If you have a favorite algorithm that is not included, user-defined algorithms and libraries can be added. The existing methods are listed below, and the corresponding .m-files can be used as a model.

Define the routine, for example "myalgorithm.m", set $p.method = @myalgorithm$, then adjust the input value of *ipsteps* and *order* if these need be changed to a new value. The interaction-picture transform, *prop*, can also be changed if the built-in choice is not sufficient.The xSPDE algorithms available currently treat

- ordinary (and partial) differential equations
- stochastic differential equations
- stochastic partial differential equations
- weighted stochastic differential equations
- projected stochastic differential equations,
- forward-backward stochastic differential equations

Some of the more advanced features of the libraries require additional input parameters. In particular:

backfields is used for forward-backward stochastic equations, describing backward time components. These are described in the *Forward-backward* section. Note that **fields** is still used, and it gives the total number of forward+backward fields.

auxfields gives the number of auxiliary fields. These have a functional definition (*defines*) that includes both a field and noise variable, as needed for spectral observables. Cell index numbers i greater than the maximum field cells access the auxiliary fields in the *observe* function.

9.2. General differential form

The general equation treated is given in differential form as

$$\frac{\partial \boldsymbol{a}}{\partial t} = \boldsymbol{A}\left[\boldsymbol{\nabla}, \boldsymbol{a}, t\right] + \underline{\mathbf{B}}\left[\boldsymbol{\nabla}, \boldsymbol{a}, t\right] \cdot \boldsymbol{\zeta}(t) + \underline{\mathbf{L}}\left[\boldsymbol{\nabla}\right] \cdot \boldsymbol{a}. \tag{9.1}$$

It is convenient for the purposes of describing interaction picture methods, to introduce an abbreviated notation as:

$$\mathcal{D}\left[\mathbf{a}, t\right] = \boldsymbol{A}\left[\boldsymbol{a}, t\right] + \underline{\mathbf{B}}\left[\boldsymbol{a}, t\right] \cdot \boldsymbol{\zeta}(t). \tag{9.2}$$

Hence, we can rewrite the differential equation in the form:

$$\frac{\partial \boldsymbol{a}}{\partial t} = \mathcal{D}\left[\mathbf{a}, t\right] + \underline{\mathbf{L}}\left[\boldsymbol{\nabla}\right] \cdot \boldsymbol{a}. \tag{9.3}$$

9.2.1. Linear propagator

Next, we define a linear propagator. This is given formally by:

$$\mathcal{P}\left(\Delta t\right) = \exp\left(\Delta t \underline{\mathbf{L}}\left[\boldsymbol{\nabla}\right]\right). \tag{9.4}$$

Typically, but not necessarily, this is evaluated in Fourier space, where it is a diagonal term in the momentum vector conjugate to the transverse space coordinate. It involves a Fourier transform, multiplication by a function of momentum, and an inverse Fourier transform. For simplicity, the stochastic noise is assumed constant throughout the interval dt. The reader is referred to the literature for more details.

It is simple to add your own algorithm if you prefer a different one. Note that if they use an interaction picture, then *ipsteps* must be given explicitly to specify the interaction picture duration, where *ipsteps* gives the number of sequential propagator steps in time required for the method.

9.3. Standard methods

The standard methods are listed below. All of these can be used with any equation: ODE, SDE, PDE or SPDE, either with or without a linear interaction picture term. The basic equation used here is:

$$\frac{\partial \tilde{\mathbf{a}}}{\partial t} = \mathcal{D}\left[\mathcal{P}\left(t, \tilde{t}\right)\tilde{\mathbf{a}}, t\right] = \tilde{\mathcal{D}}\left[\tilde{\mathbf{a}}, t\right].$$

9.3.1. Euler: Ito-Euler

This is an explicit Ito-Euler method using an interaction picture. While traditional, it is not generally recommended. If it is used, very small step-sizes will generally be necessary to reduce errors to a usable level. This is because it is is only convergent to first order deterministically and tends to have large errors.

It is designed for use with an Ito form of stochastic equation. It requires one IP transform per step ($p.ipsteps = 1$). Choosing the origin of the interaction picture at $\tilde{t} = t_n$, one has $\mathbf{a}_n \equiv \tilde{\mathbf{a}}_n$, so:

$$\Delta\tilde{\mathbf{a}}_{n+1} = \tilde{\mathbf{a}}_{n+1} - \tilde{\mathbf{a}}_n = \Delta t \mathcal{D}\left[\mathbf{a}_n, t_n\right]$$

To get the next time point at $t = t_{n+1} = t_n + \Delta t$, one calculates:

$$\begin{aligned} \Delta\tilde{\mathbf{a}}_{n+1} &= \Delta t \mathcal{D}\left[\mathbf{a}_n, t_n\right] \\ \mathbf{a}_{n+1} &= \mathcal{P}\left(\Delta t\right) \cdot \left[\mathbf{a}_n + \Delta\tilde{\mathbf{a}}_{n+1}\right] \end{aligned} \tag{9.5}$$

9.3.2. Implicit: implicit Ito-Euler

This is a fully implicit Ito-Euler method using an interaction picture. It is more robust, though slower, than the explicit form. If it is used, very small step-sizes will generally be necessary to reduce errors to a usable level.

This is because it is is only convergent to first order, and therefore tends to have large errors. It is designed for use with an implicit Ito form of stochastic equation. Note that this implies double the usual Stratonovich correction!

It requires one IP transform per step (*p.ipsteps* = 1). Choosing the origin of the interaction picture at $\tilde{t} = t_{n+1}$, one has $\mathbf{a}_{n+1} \equiv \tilde{\mathbf{a}}_{n+1}$, so:

$$\Delta\tilde{\mathbf{a}}_{n+1} = \tilde{\mathbf{a}}_{n+1} - \tilde{\mathbf{a}}_n = \Delta t\mathcal{D}\left[\mathbf{a}_{n+1}, t_n\right]$$

Starting from time $t = t_n$, to get the next time point at $t = t_{n+1} = t_n + \Delta t$, one calculates, using iteration to get the implicit result of the next time-point:

$$\begin{aligned} \bar{\mathbf{a}}^{(0)} &= \mathcal{P}\left(t_{n+1}, t_n\right) \cdot \left[\mathbf{a}_n\right] \\ \bar{\mathbf{a}}^{(i)} &= \bar{\mathbf{a}}^{(0)} + \Delta t\mathcal{D}\left[\bar{\mathbf{a}}^{(i-1)}, t_{n+1}\right] \\ \mathbf{a}_{n+1} &= \tilde{\mathbf{a}}_{n+1} = \bar{\mathbf{a}}^{(iter)} \end{aligned} \tag{9.6}$$

Here the result of $\bar{\mathbf{a}}^{(iter)}$ is obtained after a fixed number of iterations of $\bar{\mathbf{a}}^{(i)}$.

9.3.3. MP: Midpoint

This is a semi-implicit midpoint method using an interaction picture. It gives good results for stochastic and stochastic partial differential equations. It is convergent to second order in time for deterministic equations and for stochastic equations with commuting noise. It is strongly convergent and robust. It requires two half-length IP transforms per step (*p.ipsteps* = 2).

To get the next time point, one calculates a midpoint derivative iteratively at time to get the next time point at $t = t_{n+1/2} = t_n + \Delta t/2$, to give an estimated midpoint field $\bar{\mathbf{a}}^{(i)}$, usually with four iterations. The number of iterations can be changed:

$$\begin{aligned} \bar{\mathbf{a}}^{(0)} &= \mathcal{P}\left(t_{n+1/2}, t_n\right) \cdot \left[\mathbf{a}_n\right] \\ \bar{\mathbf{a}}^{(i)} &= \bar{\mathbf{a}}^{(0)} + \frac{\Delta t}{2}\mathcal{D}\left[\bar{\mathbf{a}}^{(i-1)}, t_{n+1/2}\right] \\ \mathbf{a}_{n+1} &= \mathcal{P}\left(t_{n+1}, t_{n+1/2}\right) \cdot \left[2\bar{\mathbf{a}}^{(iter)} - \bar{\mathbf{a}}^{(0)}\right] \end{aligned} \tag{9.7}$$

This is the default method for stochastic cases.

9.3.4. MPadapt: adaptive midpoint

This is an implicit midpoint method using an interaction picture, together with an adaptive technique for integrating highly nonlinear equations. At low amplitudes it is

identical to the standard midpoint method. For amplitudes $|a_i|^2$ above a critical value, *p.adapt*, the amplitude is inverted and propagated using the differential equation for its inverse.

Initially a switch p is set to 1 for low amplitudes, and -1 for high amplitudes. To get the next time point, one calculates a midpoint derivative iteratively at time to get the next time point at $t = t_{n+1/2} = t_n + \Delta t/2$, to give an estimated midpoint field $\bar{\mathbf{a}}^{(i)}$, as above, but with the derivative modified to give the derivative of a_i^p:

$$\begin{aligned}
\bar{\mathbf{a}}^{(0)} &= \mathcal{P}\left(t_{n+1/2}, t_n\right) \cdot [\mathbf{a}_n] \\
\tilde{\mathbf{a}}^{(0)} &= \mathbf{a}_n^p \\
\tilde{\mathbf{a}}^{(i)} &= \tilde{\mathbf{a}}^{(0)} + \frac{\Delta t}{2} p \left[\tilde{\mathbf{a}}^{(i-1)}\right]^{1-p} \left(\mathcal{D}\left[[\tilde{\mathbf{a}}^{(i-1)}]^p, t_{n+1/2}\right]\right) \\
\mathbf{a}_{n+1} &= \mathcal{P}\left(t_{n+1}, t_{n+1/2}\right) \cdot \left[2\tilde{\mathbf{a}}^{(iter)} - \tilde{\mathbf{a}}^{(0)}\right]^p
\end{aligned} \tag{9.8}$$

9.3.5. RK2: second order Runge-Kutta

This is a second order Runge-Kutta method using an interaction picture. It is convergent to second order in time for non-stochastic equations, and for stochastic equations with additive noise, but otherwise it is first order. It often has higher errors than midpoint methods. It requires two IP transforms per step, but each is a full time-step long ($p.ipsteps = 1$). The basic RK2 method is defined by:

$$\begin{aligned}
\tilde{\mathbf{a}}^{(1)} &= \tilde{\mathbf{a}}_n + \Delta t \tilde{\mathcal{D}}\left[\tilde{\mathbf{a}}_n, t_n\right] \\
\tilde{\mathbf{a}}^{(2)} &= \tilde{\mathbf{a}}_n + \Delta t \tilde{\mathcal{D}}\left[\tilde{\mathbf{a}}^{(1)}, t_{n+1}\right] \\
\tilde{\mathbf{a}}_{n+1} &= \left(\tilde{\mathbf{a}}^{(1)} + \tilde{\mathbf{a}}^{(2)}\right)/2
\end{aligned}$$

Including the interaction picture transforms, based at t_n, one calculates:

$$\begin{aligned}
\bar{\mathbf{a}} &= \mathcal{P}\left(t_{n+1}, t_n\right) \cdot \mathbf{a}_n \\
\mathbf{a}^{(1)} &= \mathcal{P}\left(t_{n+1}, t_n\right)\left(\mathbf{a}_n + \Delta t \cdot \mathcal{D}\left[\mathbf{a}_n, t_n\right]\right) \\
\mathbf{a}^{(2)} &= \bar{\mathbf{a}} + \Delta t \mathcal{D}\left[\mathbf{a}^{(1)}, t_{n+1}\right] \\
\mathbf{a}_{n+1} &= \left(\mathbf{a}^{(1)} + \mathbf{a}^{(2)}\right)/2.
\end{aligned} \tag{9.9}$$

9.3.6. RK4: fourth order Runge-Kutta

This is a fourth order Runge-Kutta method using an interaction picture. It is convergent to fourth order in time for non-stochastic equations, but for stochastic equations it can be more slowly convergent than the midpoint method. It requires four half-length IP transforms per step ($ipsteps = 2$). To get the next time point, one calculates four

derivatives sequentially:

$$\begin{aligned}
\bar{\mathbf{a}} &= \mathcal{P}\left(\frac{\Delta t}{2}\right)\cdot[\mathbf{a}_n] \\
\mathbf{d}^{(1)} &= \frac{\Delta t}{2}\mathcal{P}\left(\frac{\Delta t}{2}\right)\cdot\mathcal{D}\left[\mathbf{a}_n, t_n\right] \\
\mathbf{d}^{(2)} &= \frac{\Delta t}{2}\mathcal{D}\left[\bar{\mathbf{a}}+\mathbf{d}^{(1)}, t_{n+1/2}\right] \\
\mathbf{d}^{(3)} &= \frac{\Delta t}{2}\mathcal{D}\left[\bar{\mathbf{a}}+\mathbf{d}^{(2)}, t_{n+1/2}\right] \\
\mathbf{d}^{(4)} &= \frac{\Delta t}{2}\mathcal{D}\left[\mathcal{P}\left(\frac{\Delta t}{2}\right)\left[\bar{\mathbf{a}}+2\mathbf{d}^{(3)}, t_{n+1}\right]\right] \\
\mathbf{a}_{n+1} &= \mathcal{P}\left(\frac{\Delta t}{2}\right)\cdot\left[\bar{\mathbf{a}}+\left(\mathbf{d}^{(1)}+2\left(\mathbf{d}^{(2)}+\mathbf{d}^{(3)}\right)\right)/3\right]+\mathbf{d}^{(4)}/3
\end{aligned} \tag{9.10}$$

This might seem the obvious choice, having the highest order. However, it can converge at a range of apparent rates, depending on the relative importance of stochastic and non-stochastic terms. Due to its use of differentiability, it may converge more slowly than the midpoint method with stochastic terms present. It is the default for ODE and PDE cases.

9.4. Weighted library

In some types of stochastic equation, there is a weight associated with each trajectory, which is used to weight the probability of the trajectory [96]. This type of equation is sometimes found when dealing with quantum trajectories [64, 97] and feedback [98].

The equations still have the standard form of Eq (2.1), with an extra weight equation, Eq (2.4). However, the results for mean values are weighted by a term $\exp(\Omega(t))$, so that:

$$\langle\mathbf{O}\rangle_\Omega = \frac{\sum_n \mathbf{O}\left(\mathbf{a}^{(n)}\right)\exp\left(\Omega^{(n)}(t)\right)}{\sum_n \exp\left(\Omega^{(n)}(t)\right)}. \tag{9.11}$$

This reduces to the standard expression of Eq (2.3) in the case that $\Omega(t)=0$. To simulate these equations automatically, the weight exponent Ω is integrated as the *last* field in the vector $\mathbf{a}$, which must have at least two components. A nonzero threshold weight, *thresholdw*, must be entered to allow calculation of breeding.

With these changes, averages in each vector ensemble are calculated using Eq (9.11). Before each plotted step in the calculation, a breeding calculation is carried out. There are $p.steps(1)-1$ of these in total. During breeding, any weight such that $\exp\left(\Omega^{(n)}\right) < thresholdw/\langle\exp(\Omega)\rangle$ is removed.

The most probable trajectory is then duplicated to replace the low-weight trajectory. Both exponential weights are halved, so the total weight of the remaining trajectories is unchanged. If they are complex, weights such that $\exp\left(Re\left(\Omega^{(n)}\right)\right) < thresholdw/\langle\exp(Re(\Omega))\rangle$ are removed, and the real weight of the bred trajectory is reduced, which removes any

low-weight trajectories that don't contribute. When used, the internal variable *p.breedw* is set to allow the fraction of trajectories that are bred per step to be monitored. For weighted SPDEs, the spatial weights $\Omega(x_j)$ are summed over space points to obtain Ω.

9.4.1. Example

The following example shows how weights are implemented.

```
function [e] = Weightcheck()
p.name = 'Weightcheck';
p.ensembles = [10000,10,1];
p.fields = 2;
p.points = 6;
p.order = 2;
p.thresholdw = 0.1;
p.diffplot = 1;
p.initial = @(w,p) [1+w(1,:);0*w(2,:)];
p.deriv = @(a,z,p) [-a(1,:)+ z(1,:);-a(2,:)+...
z(2,:)];
p.observe{1} = @(a,p) a(1,:);
p.observe{2} = @(a,p) p.breedw;
p.compare{1} = @(p) exp(-p.t);
p.olabels{1} = '<a>';
p.olabels{2} = '<fractional breeds per step>';
e = xcheck(2,p);
end
```

This algorithm converges with second-order accuracy for this exercise, due to the structure of the equation. The example also demonstrates how to use the *xcheck* function instead of *xspde*, to check convergence.

9.5. Projection library

It is sometimes necessary to constrain an equation to a sub-manifold [62], with an equation of form:

$$\mathbf{f}(\mathbf{a}) = 0, \tag{9.12}$$

where $\mathbf{f}(\mathbf{a})$ is a scalar or vector function that defines the relevant manifold in Euclidean space. The projected SDE then has the form of a Stratonovich SDE, where:

$$\frac{\partial \mathbf{a}}{\partial t} = \mathcal{P}_{\mathbf{a}}^{\parallel}\left[\mathbf{A}[\mathbf{a}] + \underline{\mathbf{B}}[\mathbf{a}] \cdot \mathbf{w}(t)\right], \tag{9.13}$$

where $\mathcal{P}_{\mathbf{a}}^{\parallel}$ is a tangential projection operator at location $\mathbf{a}$ on the sub-manifold, and as usual, $\mathbf{A}$ is a vector, $\underline{\mathbf{B}}$ a matrix and $\mathbf{w}$ is a real Gaussian noise vector, delta-correlated

in time. Similarly, the general stochastic partial differential equation can be written in projected form as

$$\frac{\partial \mathbf{a}}{\partial t} = \mathcal{P}_{\mathbf{a}}^{\|}\left[\mathbf{A}\left[\mathbf{a}\right] + \underline{\mathbf{B}}\left[\mathbf{a}\right] \cdot \mathbf{w}(t,\mathbf{x}) + \underline{\mathbf{L}}\left[\nabla, \mathbf{a}\right]\right]. \tag{9.14}$$

When numerically integrating these, it is also useful to have a normal projection $\mathcal{P}^{\perp}$available. This is used to normally project to the nearest point on the manifold, to eliminate constraint errors. These are solved using functions collected in a projection library, to provide the specialized methods that are needed for this purpose.

The projection library has three predefined algorithms,

- ***Enproj***,
- ***MPproj***,
- ***MPnproj***.

Here the capital E stands for Euler, MP for midpoint. All use tangential projection. The letter *n=normal* indicates if an additional normal projection is used. In all cases, if it is present, a normal projection is used last. The recommended type is ***MPnproj***, due to its much lower errors.

Tangential and normal projections are needed to define the geometry of any sub-manifold. These are input by setting the variable *project* equal to a function handle that defines the projection. These can be user provided if required. There are three different predefined manifold geometry types, which need different inputs, given below.

9.5.1. Calling the project function

The calling arguments for the *project* function are: *(d,a,n,p)*, where d is a vector to be tangentially projected at location a, a is the current (near)-manifold location, n is an option switch, and p is the parameter structure.

The options available in any *project* implementation are defined as:

- *n = 0* returns the tangent vector for testing
- *n = 1* returns the tangential projection of *d* at *a*
- *n = 2* returns the normal projection of *a*, where *d* is not used
- *n = 4* returns the constraint function at *a* for testing

The projections defined in an xSPDE *project* function can be of any type. Arbitrary dimension reduction and manifold geometry is possible. Currently in the examples, dimensionality is reduced by 1, and normal projections use fixed point iterations, defined by *iterproj*.

9.5.2. The predefined manifold geometries

The current manifolds, by setting p.project = @Quadproj ..., are as follows:

1. Quadratic - *Quadproj* - needs: *qcproj* defined by $f = \sum q_{ij} x^i x^j - 1 = 0$
2. Polynomial - *Polproj* - needs: *vcproj* defined by $f = \sum v_i (x^i)^p - 1 = 0$
3. Catenoid - *Catproj* - uses fixed coefficients defined by $f = (x_1)^2 + (x_2)^2 - (sinh(x_3))^2 - 1 = 0$

Any other manifold can be used by replacing these predefined manifolds with an appropriate *project* function.

9.6. Time-step discretization errors

To check convergence, xSPDE defualt settings will repeat the calculations twice for checking time-steps, and many times more in stochastic cases to estimate sampling errors. Since the checks make xSPDE slower, they can be turned off, but then there are no error-estimate. Whatever the application, error-estimates useful, and generally should be used.

If the errors are too large relative to the application, you should decrease the time-steps or increase the number of samples. Which is needed depends on the type of error.

Errors caused by the finite time-domain step-size are checked automatically, since $p.checks(1) = 1$ is the default option. If $p.checks = 0$ is used, there is no time-domain error check.

Errors due to a finite step-size are estimated by running a check simulation with half the initial step-size and the same random sequence, extrapolating to zero step-size if $order > 0$ is specified. The program returns an error bound as the difference of the two most accurate results. Any 2D output graph plots error-bars if $checks = 1$ was specified, provided they are large enough to plot.

RMS output error summaries are also reported in the text outputs. Even more error information is abailable if p.verbose=1 is specified. Individual time-step error bounds, $e\,(o)$ are given in the output data, and the plots give $\bar{o} \pm e\,(o)$.

Error-bars below a minimum relative size compared to the vertical range of the plot, specified by the graphics variable *minbar*, are not plotted. The default for this is $minbar = 0.01$. All error bars are calculated individually for each type of data average. Minbar is a cell array that can can be set for each type of average or graph. If the cell argument is omitted, it applies globally. Error estimates are also given for functional transforms of averages.

If the errors are too large, one can either increase the *points*, which gives more plotted points and lower errors, or increase the *steps,* which reduces the step size without changing the data resolution. The default algorithm and extrapolation order can also be changed. Error bars on graphs can be removed by setting $checks = 0$ or increasing *minbar*.

Discretization errors caused by the finite spatial lattice are not currently checked in the xSIM code. They must be checked by comparing results with different transverse lattice ranges and step-size. Similarly, errors from discrete probability bin sizes are not checked.

If computed, the discretization error is included in the graphical data outputs for all observables. It is accessed by setting the last index for the output data equal 2. The raw discretization error is generally a very cautious estimate, and may overestimate the errors. This estimate can be improved using extrapolation, explained next.

9.6.1. Extrapolation

xSPDE can use extrapolation to improve convergence, which requires input of the method *order*. If this is non-zero, and *checks* are set to 1 to allow successive inte-

gration with different step-sizes, the output of all data graphed will be extrapolated by assuming the method has the specified order. To implement extrapolation and obtain a less conservative mean and error-bar result, set $p.order > 0$. Note that this value is user-defined.

Although convergence rates are somewhat problem-dependent, all xSPDE methods will return their theoretical convergence order for deterministic and stochastic calculations respectively. To extrapolate using these theoretical orders, specify $p.order = -1$, which gives the method order. The deterministic order is used if there is one ensemble.

Extrapolation is valuable for improving the accuracy of a differential equation solver. It is valid for small time-steps. Suppose an algorithm has a correct solution R_0, but returns a numerical result R with an error order n. For small step-size, integration results $R(dt)$ with step-size dt have an error of order dt^n, that is:

$$R(dt) = R_0 + e(R) = R_0 + k.dt^n. \tag{9.15}$$

Hence, from two results at different values of dt, differing by a factor of 2, one would obtain

$$\begin{aligned} R_1 &= R(dt) = R_0 + k.dt^n \\ R_2 &= R(2dt) = R_0 + 2^n k.dt^n. \end{aligned} \tag{9.16}$$

The true result, extrapolated to the small-step size limit, is obtained by giving more weight to the fine step-size result, while *subtracting* from this a correction due to the coarse step-size calculation, to cancel the leading error term:

$$R_0 = \frac{[R_1 - R_2 2^{-n}]}{[1 - 2^{-n}]}. \tag{9.17}$$

Thus, if we define a factor ϵ as

$$\epsilon(n) = \frac{1}{[2^n - 1]} = \left(1, \frac{1}{3}, \frac{1}{7} \dots\right), \tag{9.18}$$

the true results are obtained from extrapolation to zero step-size as:

$$R_0 = (1 + \epsilon) R_1 - \epsilon R_2. \tag{9.19}$$

The built-in algorithms have an order as ordinary differential equation integrators of 1, 1, 2, 2, 2, 4 respectively and will converge to this order at small step-sizes. Weak first order convergence is always obtainable for these single noise-step SDE methods [31]. Second order weak convergence is obtained in some cases with RK4 algorithms.

Higher order convergence for the raw data is not guaranteed for the built-in SDE algorithms. The algorithms used do **not** always converge to the standard ODE order when used for stochastic equations. Hence extrapolation to higher than first order should be used with caution in stochastic calculations, unless more complex methods are used [29].

9.6.2. Extrapolated error-bars

If extrapolation is used, the error bar half-size is the difference of the best raw estimate and the extrapolation. Extrapolated results are usually inside those given by the error-bars, however, note that:

- **extrapolation with too high an order may under-estimate error bars**
- **extrapolation with too low an order reduces the accuracy**

A conservative order estimate of *order* = 1 can be used for all SDE and SPDE cases, although there are higher order methods available. This gives an extrapolated weak order of 2 for stochastic cases. One can set *order* = 0 to remove the default, or use a higher order if preferred, although, as explained above, it requires some caution. For an ODE or PDE the usual deterministic order should be used. For the default RK4 deterministic method, *order* = 4. All orders are improved by one with extrapolation.

High-order convergence *without* extrapolation can also be obtained, either in special cases using the xSPDE methods, or by adding user-specified techniques. The xSPDE libraries can be readily extended by the user to include these, through defining a modified *method* function appropriately.

9.7. Statistical errors

Sampling error estimation in xSIM uses three different techniques.

- xSIM uses sub-ensemble averaging, requiring high-level ensembles.
- For probability estimates, a Poissonian sampling error is used, based on counts.
- If there is a comparison probability, this is used for sampling error estimates.

This procedure leads to reliable sampling error estimates, and makes efficient use of the vector instruction sets used by Matlab. Ensembles are specified in three levels. The first, *ensembles(1)*, is called the number of samples for brevity. All computed quantities returned by the ***observe*** functions are first averaged over the samples, which are calculated efficiently using a parallel vector of trajectories. By the central limit theorem, these low-level sample averages are distributed as a normal distribution at large sample number.

Next, the sample averages are averaged again over the two higher level ensembles, if specified. This time, the variance is accumulated. The variance of these distributions is used to estimate a standard deviation in the mean, since each computed quantity is now a normally distributed result. This method is applied to all the observables. The two lines generated represent $\bar{o} \pm \sigma(o)$, where o is the observe function output, and σ is the standard deviation in the mean.

Here, *ensembles(2)* specifies ensembles computed in series. The highest level ensemble, *ensembles(3),* is used for parallel simulations. This is faster for a multiple core CPU or when the codes are run in a supercomputing environment, which requires the Matlab

parallel toolbox. Either type of high-level ensemble, or both together, can be used to calculate sampling errors.

If $ensembles(2) > 1$ or $ensembles(3) > 1$, which allows xSPDE to calculate sampling errors, it will plot upper and lower limits of one standard deviation. If the sampling errors are too large, try increasing $ensembles(1)$, which increases the trajectories in a single thread. An alternative is to increase $ensembles(2)$, which is slower, but is only limited by the compute time, or else to increase $ensembles(3)$, which gives higher level parallelization.

Each is limited in different ways: the first by memory, the second by time, the third by the number of cores. Sampling error control helps ensures accuracy.

9.7.1. Sampling error

Quantitative sampling error estimation in xSPDE uses sub-ensemble averaging. Ensembles are specified in three levels, using vector, serial and parallel methods, respectively. The vector ensemble length, *p.ensembles(1)*, is called the number of samples for brevity. All quantities returned by the observe functions are averaged over the samples, which are calculated efficiently using a vector of trajectories.

By the central limit theorem, the sample averages are distributed as a normal distribution at large sample number. Next, the sample averages are averaged over the two higher level ensembles, if specified. The variance of this data is used to estimate a standard deviation in the mean, since each is normally distributed.

The next level, *p.ensembles(2)*, is for serial calculations of ensembles. The highest level ensemble, *p.ensembles(3)*, is used for parallel simulations. This requires the Matlab parallel toolbox. Either type of high-level ensemble, or both together, can be used to calculate sampling errors.

Note that one standard deviation is not a strong bound; errors are expected to exceed this value in 32% of observed measurements. Another point to remember is that stochastic errors are often correlated, so that a group of points may all have similar errors due to statistical sampling.

The statistical error due to finite samples of trajectories is called the sampling error. The RMS value of the relative sampling error for each computed function, normalized by the maximum modulus of the observable, is printed out after each xSPDE simulation. If the expected comparison value is zero, the absolute value is given.

Averages over stochastic ensembles are the specialty of xSPDE, which requires specification of the ensemble size. A hierarchy of ensemble specifications in three levels allows maximum resource utilization, so that:

$$p.ensembles = [ensembles(1), ensembles(2), ensembles(3)] .$$

The local ensemble, $ensembles\,(1)$, gives within-thread parallelism, allowing vector instruction use for single-core efficiency. The serial ensemble, $ensembles\,(2)$, gives the number of independent sub-ensembles of trajectories calculated serially.

The parallel ensemble, *ensembles* (3), gives multi-core parallelism, and requires the Matlab parallel toolbox. This improves speed when there are multiple cores. One should optimally put *ensembles* (3) equal to the available number of CPU cores.

The *total* number of stochastic trajectories or samples is

$$ensembles(1) \times ensembles(2) \times ensembles(3)\,.$$

Either *ensembles*(2) or *ensembles*(3) are required if sampling error-bars are to be calculated, owing to the sub-ensemble averaging method used in xSPDE to calculate sampling errors accurately.

Two lines are graphed for an upper and lower standard deviation departure from the mean. This is only plotted if the total number of serial or parallel ensembles is greater than one, preferably at least 10–20 to give reliable estimates. The sampling error is reasonably accurate, but may underestimate errors for observe function results that have highly non-Gaussian trajectory distributions, especially with asymmetries. These estimates are available for all observables in any dimension. The two lines generated in the graphs represent $\bar{o} \pm \sigma$, where o is the mean output, and σ is the computed standard deviation in the mean.

9.7.2. Comparisons: compare

Every *observe* function can be accompanied by a comparison function, with a function handle *compare*$\{n\}$. This generates a vector of analytic solutions or experimental data-points which is compared to the average of the stochastic results. Results are plotted as additional lines on the two-dimensional graphical outputs, and a summary of comparison differences is printed.

A cell array of functions is used to obtain comparison results. These are calculated from the user-specified ***compare{n}(p)*** handle where the function argument is the parameter structure p, giving a extra dashed line on the two-dimensional graphs. Other graphics options are available as well. These optional comparisons can be input in all dimensions. When there are error estimates, a chi-squared test is carried out to determine if the difference is within the expected step-size and sampling error bars. If the comparison has errors, for example from experimental data, the chi-squared test will include the experimental errors.

9.7.3. Convergence: xcheck

The convergence checker, *xcheck(checks,p),* is designed for use where there are analytic results available for comparisons. This will automatically run xSIM a total of *checks* times, increasing the initial *steps* by 2 after each run, to reduce the step-size by 2. It then runs xGRAPH to display the most accurate result. It prints the time-step, the maximum difference with an input *compare* and the estimated errors found at the relevant point.

Exercise

- **Simulate the Kubo oscillator using the file, *Kubocheck.m*, with xcheck.**

```
function [e] = Kubocheck()
p.name = 'Kubo with convergence checks';
p.ensembles = [1000,10];
p.initial = @(w,p) 1;
p.range = 2;
p.deriv = @(a,xi,p) 1i*xi.*a;
p.observe{1} = @(a,p) real(a(1,:));
p.observe{2} = @(a,p) a(1,:).*conj(a(1,:));
p.olabels = {'<a> ','< a^2> '};
p.xlabels = {'\tau'};
p.compare{1} = @(p) exp(-p.t/2);
p.compare{2} = @(p) 1;
e = xcheck(2,p);
end
```

9.8. Chi-squared estimates

Chi-squared error estimates are reported in cases that have statistical sampling errors and comparison functions. These allow estimates of goodness of fit for probabilities. For N_p independent points graphed or measured, if O_i is an observable with measured mean $\bar{O}_i$ and statistical fluctuations ΔO_i, one has that:

$$\chi^2/N_p = \frac{1}{N_p}\sum_i \frac{\left\langle \left[\left(\bar{O}_i + \Delta O_i\right) - O_i^a\right]^2 \right\rangle}{\sigma_i^2} \tag{9.20}$$

Here σ_i^2 is an estimated variance. Provided that $\left\langle \Delta O_i^2 \right\rangle = \sigma_i^2$ and $\bar{O}_i = O_i^a$, one should obtain the expected result of $\chi^2/N_p \approx 1$. The exact distribution is known in special cases, but this requires that all data is independent and has a Gaussian distribution, which is not the case for stochastic trajectories.

Because of the lack of independence from point to point, these error sums are not identical to Pearson's original definition of χ^2, and therefore should be used with caution. Nevertheless, the definition provides a way of evaluating goodness of fit that is useful.

The value of σ_i^2 is obtained by including *all* known statistical error sources, so

$$\sigma_i^2 = \sum_{n=1}^{2} \left(\sigma_i^{(n)}\right)^2. \tag{9.21}$$

where:

1. If higher ensembles are used, the estimated σ_i^2 includes numerical sampling errors.
2. If comparisons have known statistical errors, these are included as well.

9.8.1. Probability comparisons

Comparisons of trajectory probabilities and analytic probabilities do not always result in perfect agreement. This is because the limitations of memory and simulation time mean that trajectories have to be binned, which leads to an additional discretization error. Note that xSPDE approximates the comparison analytic probability of a bin by the central bin value of the probability, which is the simplest procedure.

To explain this, comparisons of probabilities ought to use the average probability density over the bin, which is different from the central value. Suppose one has a comparison distribution $p^a(x)$. Using Simpson's rule, the average analytic probability density integrated over a bin size Δx is approximately:

$$\begin{aligned} p_o^a &= \frac{1}{\Delta x}\int_{x_0-\Delta x/2}^{x_0+\Delta x/2} p^a(x)dx \\ &\approx \frac{1}{6}\left[4p^a(x_0) + p^a\left(x_0+\frac{\Delta x}{2}\right) + p^a\left(x_0-\frac{\Delta x}{2}\right).\right] \end{aligned} \tag{9.22}$$

This is equivalent to a cubic polynomial fit. It can be used to improve the analytic binning comparisons. It is especially important for multi-dimensional comparisons. It results in 9 distinct terms for two dimensions. This correction should be inserted manually in the comparison functions.

9.8.2. Scaling of χ^2 errors

Because chi-squared probability tests are sensitive, it helps to understand how they scale with bin-size. With N_s total samples, the estimated probability P_i in a bin with probability density $p(\mathbf{a})$ and sampled counts of N_i is given by $P_i = N_i/N_s = p_i A$ for a bin b_i with area A, where:

$$p_i = \frac{1}{A}\int_{b_i} p(\mathbf{a})\, dA \tag{9.23}$$

The Poissonian variance of the counts in the bin is $\langle \Delta N_i\rangle = \langle N_i\rangle$. The expected probability variance is therefore

$$\left\langle \Delta P^2\right\rangle = \left\langle \Delta N_i^2/N_s^2\right\rangle = \langle N_i\rangle /N_s^2. \tag{9.24}$$

Let $\langle N_i\rangle = N_i^a$, the analytic or expected count number. The expected probability density variance at a point is therefore

$$\left\langle \Delta p_i^2\right\rangle = \left\langle \Delta N_i^2/A^2N_s^2\right\rangle = N_i^a/A^2N_s^2 = p_i^a/AN_s. \tag{9.25}$$

Here p_i^a is the analytic or comparison probability density, and $\left\langle \Delta p_i^2\right\rangle^a = p_i^a/AN_s$ is the expected analytic variance. The χ^2 variable, that follows the Pearson χ^2 distribution, is defined as follows:

$$\chi^2/N_p = \frac{1}{N_p}\sum_i \frac{\left\langle [p_i - p_i^a]^2\right\rangle}{\left\langle \Delta p_i^2\right\rangle} \tag{9.26}$$

Here, p_i^a is obtained by integrating over the i-th probability bin. It can be estimated by using the central value, $p_i^a \approx p\left(\mathbf{a}_i\right)$, although cubic interpolation is more precise.

This could lead to a fixed error in the analytic probability density p_i^a, so $p_i^a \to p_i^a + \epsilon_i$, possibly localized to some fraction of bins f which may change with the bin size. Suppose, for simplicity, that ϵ is due to an integration error in integrating the exact distribution or any other error in the 'exact' distribution, and it does not change with changes to the bin area A.

From the definition of χ^2, if the generated samples have negligible step-size errors:

$$\chi^2/N_p = \frac{1}{N_p}\sum_i \frac{\left\langle \left[\left(p_i^a + \Delta p_i\right) - p_i^a - \epsilon_i\right]^2 \right\rangle}{\left\langle \Delta p_i^2 \right\rangle} \tag{9.27}$$

For simplicity, if we consider the large sample limit with uniform probabilities,

$$\chi^2/N_p = 1 + \frac{f\epsilon^2}{\langle \Delta p^2 \rangle} = 1 + \frac{f\epsilon^2 A N_s}{p^a} \tag{9.28}$$

Increasing the bin area A will increase χ^2/N_p above its usual value of *1* by an amount proportional to A. This is simply because smaller bins have less intrinsic accuracy, due to a larger sampling error. As a result, it is often preferable to use more accurate probability estimates with larger bins having more counts, since these are much more sensitive to effects like this.

Often, simulated and comparison graphs may appear identical visually, but even if they have small errors they may still be very significant. Such comparison binning errors can be reduced by using cubic spline interpolations, as explained above.

9.9. Error outputs

There are six types of data outputs: data, step errors, sampling errors, comparisons, comparison systematic errors, and comparison random errors. Summaries of this will appear in the printed outputs, with greater details if *p.verbose>0* is chosen. Step errors and sampling errors, as well as comparison data are stored in the output data arrays.

9.9.1. Numerical error outputs

The last data index c is used to obtain errors and comparisons in data outputs. To obtain comparison data, a comparison function is defined for each output function. This can include, for example, experimental data, experimental errors or exact analytic comparisons where they are available.

1. Means are in $c = 1$ data, except if *scatters>1,* which gives individual trajectories.
2. If *checks>0*, all the step errors are in $c = 2$ data.
3. If $ensembles(2, 3) > 1$, the sampling errors are in $c = 3$ data.

4. Comparison values from *compare* functions are in $c = 4$ data.
5. Comparison systematic errors can be included in $c = 5$ data.
6. Comparison statistical errors can be included in $c = 6$ data.

9.9.2. Graphical error outputs

These are explained in detail in the xGRAPH reference section.

1. Mean values or trajectories are graphed as separate data lines.
2. Step errors generate graph error bars
3. Sampling errors are graphed as parallel solid lines
4. Dashed lines indicate comparison values from *compare* functions.
5. Comparison systematic errors give additional error bars
6. Comparison statistical errors can be included as parallel lines

Because multiple errors can generate very complex graphs, there is additional control of error bar generation, explained in the xGRAPH reference section. One can also obtain difference graphs with comparisons, which allow errors to be examined more closely, and error bars can be combined in different ways.

Graphics data is only available for two-dimensional graphs, and is subject to selection using the *axes* inputs.

9.9.3. Printed error outputs

Printed error summaries are generated for each data output if $p.verbose > 0$. The defaults are root mean square (RMS) and maximum errors, all normalized. Normalization is by the modulus of the largest data. If available, the largest comparison values is used. If it is zero or p.relerr = 0, then no normalization is carried out.

After computing RMS values for each data output, a second RMS average is taken over all totals, weighting each total equally, and including all functions and sequence datasets where there are nonzero errors. Data with no errors, below a tolerance of 10^{-10}, are not included in the mean RMS total errors for each category.

There is a final RMS average taken over the step, sampling and comparison totals. This ignores categories with no errors. This printout occurs even with verbose = 0, to allow a rapid comparison in case there are unexpected errors, which might require a new simulation with more steps or random trajectories.

Printed errors are summarized in three main categories

1. Discretization or step errors
2. Sampling errors

3. Comparison or difference errors

Comparison data may not be available over an entire lattice. If this is the case, the *axes* point selections can be used to restrict the relevant datas points used for these comparisons. This also applies to the goodness of fit and error-vector outputs, since they make use of comparison data where it is available.

9.9.4. Goodness of fit (χ^2)

The χ^2 statistics are obtained by normalizing the comparison squared differences by the sum of squares of all the data and comparison errors at that point. These are summed over every data point with relevant data, and the number of relevant data points, k, is stored. The ratio of χ^2/k should be order 1 for statistical errors.

These are summarized for each functional data output type, as well as giving rise to an error total.

9.9.5. Error vector output

When used as a function call in batch mode, the first type of data returned by xSIM is a six-component error vector. This can be used for summarizing error data in a batch job, to determine if a specified error-threshold is reached, to allow an iterative increase in the number of time-steps or trajectories.

The error-vector components are all RMS averages:

1. Total error overall, including step, discretization and comparisons
2. Total step-size error
3. Total sampling error
4. Total comparison error
5. Total χ^2/k goodness of fit
6. Simulation elapsed time

9.9.6. Error summaries

There are six types of data outputs: data, errors, comparisons and comparison errors. Summaries will appear in the printed outputs, depending on the verbosity setting. Step errors and sampling errors, as well as comparison data are stored in output data arrays. These are also available graphically in two-dimensional graphs.

10. API reference and extensibility

This chapter gives a reference guide to the xSPDE parameters and functions.

10.1. Overview

Simulations carried out by xSPDE are performed by xSIM, then graphed by xGRAPH. Input parameters come from an **input** sequence of parameter structures, while output is saved in a **data** array, and optionally in data files. During the simulation, global averages are calculated for time-step and sampling errors, togther with comparisons. When completed, timing and errors are printed.

10.1.1. Output data storage and batch jobs

An xSPDE session can either run simulations interactively, described in section 6, or else using a function file called a project file. In either case, the Matlab path must include the xSPDE folder. For generating graphs automatically, the script input or project function should end with the combined function **xspde**.

Alternatively, it can be useful to divide xSPDE into its simulation function, xSIM, and its graphics function, xGRAPH, to allow graphs to be made at a later time from the simulation. In this case the function *xsim* runs the simulation, and *xgraph* makes the graphs. The two-stage option is better for running batch jobs which you can graph at a later time.

10.1.2. Batch input template

To create a data file, you must enter the filename when running the simulation, using the $p.file = filename$ input. A typical xSPDE project function of this type, where all the data is stored is as follows:

```
function e = project.m
p.[label1] = [parameter1];
p.[label2] = ...;
p.file = '[myfile].mat'
[e,~,p] = xsim(p);
xgraph(p.file);
end
```

Alternatively, for an interactive session one can use the commands:

```
...
[e,data,p] = xsim(p);
xgraph(data,p);
...
```

This is specially useful if one wishes to have direct access to the data and graphics options, with possible multiple trials. When preparing a project file using the editor, click on the Run arrow above the editor window to run the job.

A batch job workflow is as follows:

- Create the metadata *p*, including a file name, eg, *p.file='myfile.mat'*.
- Change the Matlab directory path to your preferred directory.
- Run the simulation with *[e,data, p] = xsim(p)*, or just *xsim(p)*.
- Run *xgraph(p.file)*, and the data will be graphed.
- Alternatively, *xgraph(p.file,p)* allows you to change the inputs in the structure *p*.
- Graph outputs can be stored using the *p.saveeps=1* and/or *p.savefig=1* options.

You can use either Matlab (.mat) or standard HDF5 (.h5) file-types for data storage. If raw data is generated it will be stored too, but the files can be large. For stored graphics files the options are encapsulated postscript (.eps) files or Matlab graphics (.fig) files, obtained using the graphics input switches *p.saveeps* and/or *p.savefig*.

10.2. Input, output and logic

To explain xSPDE in full detail,

- Simulation parameters are stored in the ***input*** list.
- This describes a sequence of parameter structures, so that ***input=p1,p2,....***
- Each structure ***p1,p2,...*** generates an output which is the input of the next.
- The main simulation function is called using ***xsim(input).***
- The RMS errors and integration time are returned in the ***error*** vector
- Parameters including defaults are returned in the ***output*** cell array.
- Averages are recorded sequentially in the ***data*** cell array.
- Raw trajectory data is optionally stored in the ***raw*** cell array.

The sequence *input* defines a sequence of individual simulations, with parameters that specify the simulation functions and give the equations and observables. If there is only one simulation, just one data structure is needed, without a cell array. In addition, xSPDE can generates graphs with its own graphics program, xGRAPH.

10.2.1. xSPDE

The control program, *xspde*, calls the *xsim* integration and *xgraph* graphics functions successively

$$\textbf{xspde} \rightarrow \begin{cases} \textbf{xsim}\ (simulations) \\ \textbf{xgraph}\ (graphics) \end{cases}$$

For convergence checking, a useful alternative to xspde which repeats the calculation *checks* times while halving the time-step each time, and reports the resulting errors for averaged observables, is:

- xcheck (checks,p)

10.2.2. xSIM

The integration function, *xsim*, generates all data. It first carries out elementary checks in *xpreferences* and constructs the grid of lattice points in *xlattice*. Then it generates the nested ensembles in *xensemble*, and integrates each subensemble using *xpath*. The output data is written to files, if required, in *xwrite*.

$$\begin{aligned} \textbf{xsim} &\rightarrow \textbf{xpreferences} \rightarrow \textbf{xlattice}\ (checks\, inputs) \\ &\rightarrow \textbf{xensemble} \leftrightarrow \textbf{xpath} \leftrightarrow \textbf{xdata}\ (simulates) \\ &\rightarrow \textbf{xwrite}\ \ (stores\, data) \end{aligned}$$

10.2.3. Applications

The parameters that xSIM uses are divided into applications for ease of use. Almost all parameters have default values. The SDE parameters are common to all applications, but the default values may be changed in more specialized cases. Defaults are defined through *preference* functions that are included in each application folder. Parameters are shared between the applications where this is meaningful.

Current application folders are as follows:

SDE Stochastic differential equation data and methods

SPDE Partial differential equation extensions and grids.

PROJECTIONS This is the projective library, used to solve projected SDE/SPDEs

QUANTUM Stochastic Schrödinger and master equations, including logic gates

All applications use a common definition of cell arrays of integration variables, and cell arrays of output averages. In all cases, a single variable, vector or array can be used instead of a multicomponent cell array. All data outputs are xGRAPH compatible, except for *raw* trajectory outputs that need to be further processed if graphs are needed.

10.2.4. User functions

The xSIM input objects include parameters and functions, with an extensible architecture. All xSIM functions are modular and replaceable. This is as easy as just defining a new function handle to replace the default value.

There are two types of functions:

- *User* functions define the equations, and have default values. The defaults are usually obtained by adding 'x' in front of the name. In the special case of *method*, the default depends on the problem.
- *Helper* functions usually start with *'x'*. In some cases these are defaults for user functions. In all cases they have well-defined roles, like the reserved functions in C, Python, Matlab or Julia.
- All arguments in square brackets are optional, but may be needed only in specific cases.
- The last argument, *p,* is the parameter structure.

For example, to define your own integration function, include in the xSPDE/xSIM input the line:

```
p.method = @Mystep;
```

Next, include anywhere on your Matlab path the function definition, for example:

```
function a = Mystep(a,w,p)
% a = Mystep(a,w,p) propagates a step my way.
..
a = ...;
end
```

10.3. xSIM Parameters

Simulation parameters are stored in a parameter structure which is passed to the *xsim* program. Constants can be included, but must not be reserved names. Names starting with a capital letter like 'A...' - except the reserved '*D*' for derivatives - are always available. Globals are incompatible with the Matlab parallel toolbox. Graphics data is stored for the graphics program to use.

Standard inputs have default values, which are user-modifiable through the *xpreferences* function. Defaults can be checked by including the input *verbose* = 2. All the inputs are part of a structure passed to xSPDE. If a cell array of multiple structures are input, these are executed in sequence, with the output of the first simulation passed to the second, then the third, and so on.

Library functions inputs do not have defaults, as these are subject to change.

Label	Default value	Description
version	*'xSIM4.xx'*	Current version number
name	*"*	Simulation name
dimensions	1	Space-time dimensions
fields	[1, ...]	Internal stochastic field dimensions
backfields	0	Number of backward fields
auxfields	0	Auxiliary field dimensions
ranges	[10, ..]	Range of coordinates in *[t,x,y,z,..]*
origins	[0,..]	Origin of coordinates in *[t,x,y,z,..]*
points	[51,...	Output lattice points in *[t,x,y,z,..]*
noises	*[1, 0]*	Number of noise fields in *[x,k]*
inrandoms	*[1, 0]*	Initial random fields in *[x,k]*
ensembles	*[1, 1, 1]*	Size of *[vector, serial, parallel]* ensembles
steps	*1*	Integration steps per output point
iterations	*4*	Maximum implicit or midpoint iterations
order	*1*	Extrapolation order: *depends on the method*
checks	*[1,0,0..]*	Check errors for time and space grids: 0 or 1
seed	*0*	Seed for random number generator
file	*"*	File-name: *'f.mat'* = Matlab, *'f.h5'* = HDF5
boundaries{*n*}	[0, 0; 0, 0]	Boundary: '-1,0,1'=Neum, periodic, Dirichlet boundary.
binranges{*n*}	{*0,0,...*}	Observable binning ranges for probabilities
cutoffs{*n*}	0	Lower graph cutoff for chi-squared estimates
mincount	0	Lower count cutoff for chi-squared estimates
ipsteps	2	IP transforms per time-step: *depends on the method*
numberaxis	0	If 1, forces use of numerical axis labels
verbose	0	0 for brief, 1 for informative, 2 for full output
$A, B, C, \ldots$	-	User specified static parameters
transforms	{*[0 0 0 0],..*}	Fourier transforms in [t,x,y,z,..] per observable
f*transforms*	{*[0 0 0 0],..*}	Fourier transforms in [t,x,y,z,..] per function
rawdata	0	Raw data switch: 1 for raw output
scatters	{*0,..*}	Specify to obtain scatter plots, not averages
octave	*0*	Force octave syntax: 1 for octave
thresholdw	0	Threshold for weighted simulation breeding
qcproj	-	Quadratic projection coefficients
vcproj	-	Vector projection coefficients

10.3.1. Parameter reference

10.3.1.1. auxfields{c}

Default: *0*

These are real or complex auxiliary fields stored at each lattice point, specified using *define*. They are useful for input/output spectral calculations, and can be functions of

the noise. Like fields, there can be several of these, defined in a cell array.

Examples: *p.auxfields = 2* ,*p.auxfields = {1,2}*

10.3.1.2. axes{n}

Default: *{0,0,0,..}*

Gives the axis points used for comparisons in the n-th output function, in each dimension. For each function, the axes can be individually specified in each dimension. Each entry value is a vector range for a particular dimension, for *d=1,...p.dimension*s. Thus, *5* gives the fifth point only in that dimension, and an input *1:4:41* plots every fourth point. Zero or negative values are shorthand: *-1* generates a default point at the midpoint, *-2* the endpoint, and *0* is the default value that gives the vector for the every axis point. This data is also used to control graphics outputs. It can be input separately for the graphs if required.

Example: *p.axes{4} = {1:2:10,0,0,-1}*

10.3.1.3. backfields{c}

Default: *0*

The optional input ***backfields*** is the number of backward-time stochastic fields that are integrated, as part of the overall vector of integrated *fields* components. Requires a forward-backward method like *MPfb.*

Example: *p.backfields = 2*

10.3.1.4. binranges{n}

Default: {}

Nested cell array, *binranges*$\{n\}\{m\}$, that defines the probability plotted for observable n. If null or zero, the mean of the observable is calculated as usual. The second cell index, $m = 1, \ldots M$, corresponds to the line index returned by the corresponding n-th *observe* function. When nonzero, the probability of the n-th observable is calculated and plotted according to the specified vector of axis points. This sets extra dimensions in the data, depending on the range of m values, with $[o_1, o_2, \ldots o_K]$, being the start and end of each of the bins used to accumulate probabilities. The $k-th$ bin is centered at $(o_k + o_{k+1})/2$. In this version of xSPDE, each bin must have the same width for an observable and line number. The output is the average probability density versus the (vector) value of the observable. Hence M extra output dimensions are added to the generated probability data.

Example: *p.binranges{n}{1} = {-5:0.1:5,-2:0.1:2}*

10.3.1.5. boundaries{c,d}

Default: *[0, 0]*

Cell array for type of spatial boundary conditions used, set for each dimension and field component independently, and used in the equation solutions. The cell index is $dir = 2, 3, ..$, indicating the dimension. The boundary conditions are defined as a matrix. The first index is the field index i and the second index the boundary j, with $j = 1$ for the lower and $j = 2$ for the upper boundary. The options are $b = -1, 0, 1$.

- The default option, or 0, is periodic.
- If -1, Robin/Neumann boundaries are used, with derivatives set to prescribed values.
- If 1, Dirichlet boundaries are used, with fields set to prescribed values.

In the current code, only default boundaries are available using spectral (*linear*) methods. Using arbitrary non-periodic boundaries *requires* the use of finite difference derivatives, without the option of an interaction picture derivative. In such general cases, arbitrary boundary values are set by *boundfun(a,d,p)*. If the cell index c is omitted, the first cell is used.

Example: *p.boundaries{d} = [-1,1;0,0;1,-1]*

10.3.1.6. C...

The starting letter C is reserved to store user-specified constants and parameters. It is passed to user functions and can be any data. All inputs — including C data — are copied into the stored data files via the lattice structure p, to give a permanent record of simulation parameter values along with the output data.

Most other capital letters are available, unless reserved for specific method functions.

Example: *p.Constant = 2*pi*

10.3.1.7. checks

Default: *1*

This defines if a repeat integration is carried out for error-checking purposes. If *p.checks* = 0, there is one integration, with no checking at smaller time-steps. For error checking, set *p.checks = 1*, which repeats the calculation at half the time-step — but with identical noise — to obtain error bars. This is the default value, taking three times longer overall, but with increased accuracy and error-estimates.

Also see the *order* parameter, below.

Example: *p.checks = 0*

10.3.1.8. dimensions

Default: *1*

This is the space-time dimension for an SPDE. If omitted, *dimensions=1*, giving an SDE. It is arbitrary apart from the obvious memory requirements at large dimensionality.

Example: *p.dimensions = 4*

10.3.1.9. ensembles

Default: *[1, 1, 1]*

Number of independent stochastic trajectories simulated. This has three levels to maximize efficiency. The first is within-thread parallelism, allowing vector instructions. The second gives a number of independent trajectories calculated serially. The third gives multi-core parallelism and requires the Matlab parallel toolbox. Either *p.ensembles(2)* or *p.ensembles(3)* are required to obtain sampling error-bars. The total number of stochastic trajectories or samples is $ensembles(1) \times ensembles(2) \times ensembles(3)$. The second and third *ensembles* cannot be changed during a sequence of simulations.

Example: *p.ensembles = [1000,100,10]*

10.3.1.10. fields

Default: *1*

These are real or complex variables stored at each lattice point that are the independent variables for integration. The fields are vectors that can have any number of components and any number of dimensions. The *fields* input is the number of real or complex components that are initialized by the *initial* function and integrated using the deriv derivative. In some cases arrays can be used, or cell arrays of multiple named fields. See the specific method for details.

Example: *p.fields = {2,[3,3]}*

10.3.1.11. file

Default: ' '

Matlab or HDF5 file name for output data. Includes all data and parameter values, including raw trajectories if $p.rawdata = 1$. If not needed just omit this. A Matlab filename should end in .mat, while an HDF5 file requires the filename to end in .h5. For a sequence of inputs, the filename should be given in the first structure of the sequence, and the entire sequence is stored. This cannot be changed for successive parts of the overall sequence.

Example: *p.file = 'file-name'*

10.3.1.12. ftransforms{n}

Default: *transforms*{*n*}

Cell array defining the Fourier transform switches for output *n*. There is one *ftransform* vector per output function. The *n*-th flag indicates a Fourier transform if it is set to one, and none if set to zero. The default value is the *observe* transform switch. If there are more functions than *observe* handles, the additional transform switches default to zero.

This is to identify transformed outputs. It is needed if there are multiple outputs generated from one transformed observe function. Otherwise, the default is completely adequate.

Example: *p.ftransforms*{*n*} *= [1,0,0,1]*

10.3.1.13. inrandoms{n}

Default: noises

This gives the number of initial random fields generated per lattice point in coordinate and momentum space. Set to zero (*p.inrandoms* = 0) for no random fields. Random fields can be delta-correlated in x-space or in k-space. The second input is the dimension of random fields that are delta-correlated in momentum space. It can be left out if zero. The Fourier-space random variance is modified by the filter function. This takes the initial random fields in Fourier space and returns a filtered version, which is inverse Fourier transformed before use. The first noise index, *p.inrandoms(1)*, indicates how many independent random fields delta-correlated in space are generated, while *p.inrandoms(2)* indicates how many additional random fields are Fourier-transformed, filtered and then inverse Fourier transformed. These are additional random fields, so the total is *p.inrandoms(1)+p.inrandoms(2)*. The filtered random inputs have a finite correlation length.

Example: *p.inrandoms = [2, 0]*

10.3.1.14. ipsteps

Default: 1 for *Euler*, *Implici*t and *RK2*; 2 for *MP, MPadapt* and *RK4; 0 otherwise*

This specifies the number of interaction picture time-steps needed in an integration time-step. Default values are specified in *method*. Can always be changed for custom integration methods. This must be initialized if a non-standard integration method is used that requires an interaction picture, and the relevant data isn't returned by *method*.

Example: *p.ipsteps = 1*

10.3.1.15. iterations

Default: 4

For iterative algorithms like the implicit midpoint method, the iteration count is set here, typically around 3-4. Will increase the integration accuracy if set higher, but it may be better to increase steps if this is needed. With non-iterated algorithms, this input is not used. Also used to specify the iterations in projection methods.

Example: *p.iterations = 3*

10.3.1.16. name

Default: ' '

Name used to label simulation, usually corresponding to the equation or problem solved. This can be removed from graphs using *headers* equal to a single blank space when running *xgraph*.

Example: *p.name = 'your project name'*

10.3.1.17. noises

Default: *fields (1)*

This gives the number of stochastic noises generated per lattice point, in coordinate and momentum space, respectively. Set to zero ($noises = 0$) for no noises. This is the number of rows in the noise-vector. Noises can be delta-correlated in x-space or in k-space. The second input is the dimension of noises in k-space. It can be omitted if zero. This allows use of finite correlation lengths, by including a frequency filter function that is used to modify the noise in Fourier-space.

The Fourier-space random variance is defined by the filter function. This takes the noises in Fourier space and returns a filtered version, which is inverse Fourier transformed before use. The first noise index, $noises(1)$, indicates how many independent noise fields are generated, while $noises(2)$ indicates how many noises are Fourier-transformed, filtered and then inverse Fourier transformed to give correlations. These are extra noises, so the total is $noises(1) + noises(2)$. Filtered noises have a finite correlation length.

Example: *p.noises = [2,4].*

10.3.1.18. order

Default: 0

This is the extrapolation order, which is only used if $p.checks = 1$. The program uses the estimated convergence order to extrapolate to zero step-size, with reduced errors. If

p.order = 0, no extrapolation is used, which is the most conservative input. The specific default order returned by the *method* can be used if one specifies *p.order* = -1.

The extrapolation order cannot be changed during a sequence. The default deterministic orders of the six preset methods used *without* stochastic ensembles are:

1 for *Euler* and *Implicit;*

2 for *RK2*, *MP* and *MPadapt*;

4 for *RK4*.

Example: *p.order = 0*

10.3.1.19. origins

Default: *[0, -p.ranges/2]*

This displaces the graph origin for each simulation to a user-defined value. If omitted, all initial times in a sequence are zero, and the space origin is set to *-p.ranges/2* to give results that are symmetric about the origin. As an example, for the x-dimension, the problem is solved on an interval of $x = [O_2, O_2 + R_2]$, with a default origin of $-R_2/2$, so that $x = [-R_2/2, R_2/2]$. There is no cell index used.

Example: p.origins = [0,-20,-20]

10.3.1.20. points{n}

Default: *[51, 35, ..., 35]*

The rectangular lattice of points plotted for each dimension and field cell n, are defined by a vector giving the number of points in each dimension. The default values are given as a guide for initial calculations. Large, high dimensional lattices take more time to integrate. Increasing points improves graphics resolution and gives better accuracy in each relevant dimension as well, but requires more memory.

Cells for n >1 can be reduced to singleton dimensions to treat boundary fields, but the smallest space-steps used in the integrations are defined relative to *points{1}*. Speed when using spectral methods is improved when the lattice points are a product of small prime factors. In order to discretize the problem, the p_i lattice *points* are fitted into the range R_i so that $dx_i = R_i/(p_i - 1)$, ie:

$$x_i = O_i + (i - 1)dx_i \,. \tag{10.1}$$

Example: *p.points = [30,40,40]*

10.3.1.21. ranges

Default: *[10, 10, ...]*

Each lattice dimension has a coordinate range. The default value is 10 in each dimension. In the temporal graphs, the first coordinate is plotted over $0 : p.ranges(1)$. All other coordinates are plotted over $-p.ranges(n)/2 : p.ranges(n)/2$. The starting value in any dimension can be changed using the *origins* variable. This is not a cell array, since the ranges are the same for all field cells (see: *points*).

Example: *p.ranges = [1, 10]*

10.3.1.22. rawdata

Default: *0*

Flag for storing raw trajectory data. If this flag is turned on, raw trajectories are stored in memory. The raw data is returned in function calls and also written to a file on completion, if a file-name is included.

Example: *p.rawdata = 1*

10.3.1.23. relerr

Default: *1*

Flag for normalising the error data. If *p.relerr = 1* then all errors are normalised either by the maximum output value, or else by the maximum comparison value, if there is one. If *p.relerr = 0* then the absolute error values are output, without normalisation.

Example: *p.relerr = 0*

10.3.1.24. rmserr

Default: *1*

Flag for averaging the error data. If *p.rmserr = 1* then all errors are calculate as RMS averages over the space and time grid of the output values. If *p.rmserr = 0* , then the error outputs are the maximum values, not the space-time averages.

Example: *p.rmserr = 0*

10.3.1.25. scatters{n}

Default: 0

Cell array that defines the number of scatter trajectories plotted for observable n. If absent or zero, the mean of the observable is calculated as usual. If nonzero, a set of s observables that correspond to independent stochastic fields are accumulated, with no averaging. This cannot be combined with probabilities or with parallel ensembles. There must be at least s trajectories in *ensembles(1)*, otherwise the number of stored trajectories is reduced.

Example: *p.scatters{n} = 20*

10.3.1.26. seed

Default: *0*

Random noise generation seed, for obtaining reproducible noise sequences. Set to unique and distinct values for the different parallel ensembles. Used if $p.noises > 0$ or $p.inrandoms > 0$.

Example: *p.seed = 42*

10.3.1.27. steps

Default: *1*

Number of time-steps per plotted point. The total number of integration time-steps in a simulation is therefore *p.steps*×*(p.points(1)-1)*. Thus, steps can be increased to improve the accuracy, but gives no change in graphics resolution. Increasing the steps will give a lower time-discretization error.

Example: *p.steps = 1, 2, ...*

10.3.1.28. transforms{n}

Default: *[0,0,..]*

Cell array defining the Fourier transforms used for an observable n. There is one transform vector per observable. The n-th flag indicates a Fourier transform on the n-th axis if set to one, starting with the time axis. The default value is zero, indicating no transform. The normalization of the Fourier transform is such that the $k = 0$ value in momentum space corresponds to the integral over space with a factor of $1/\sqrt{2\pi}$ in each transformed dimension. The Fourier transform that is graphed has $k = 0$ as the central value. The default is no Fourier transform. Must be set for any functional transform of a Fourier observable, to give the correct graph axes.

Example: *p.transforms{n} = [1,0,0,1]*

10.3.1.29. verbose

Default: 0

Print flag for output information while running xSIM. Print options are:

- Brief if *verbose = 0*: Additionally prints the final, total integration errors
- Informative if *verbose = 1*: Also prints the individual function RMS errors and progress indicators
- Full if *verbose = 2*: Prints everything, including the internal parameter structure data.

In summary, if *verbose = 0*, most output is suppressed except the final data, while *verbose = 1* displays a progress report, and *verbose = 2* additionally generates a readable summary of the parameter input as a record.

Example: *p.verbose = 2*

10.3.1.30. version

Default: '*xSIM4*'

Sets the current version number of the simulation program. There is no need to input this except for project documentation for a customized version.

Example: *p.version = 'current version name'*

10.3.2. User-defined functions.

These functions define the stochastic problem. The three most important ones are given in boldface. These are generated automatically by the Quantum application, to simplify the user inputs and interface. Their calling arguments, and purpose, are:

Label	Arguments	Purpose
initial{n}	(z, p)	**Functions to initialize fields**
deriv{n}	$(a, ..w, ..p)$	**Total stochastic derivatives**
observe{n}	(a, p)	**Observable functions**
derivA$\{n\}$	(a, p)	Drift derivative term
derivB$\{n\}$	(a, p)	Noise derivative term
linear $\{n\}$	(p)	Linear derivative function
transfer $\{n\}$	$(a0, z, p)$	Transfer inside a sequence
method	(a, w, p)	Algorithm defining a time-step*
output$\{n\}$	(o, p)	Output function
compare$\{n\}$	(p)	Function for differences and χ^2
define $\{n\}$	(a, w, p)	Defines an auxiliary field value
boundfun	(a, c, d, p)	Boundary function
project	(d, a, n, p)	Defines projections
firstfb	$(a0, nc, p)$	First forward-backward path

*In all cases except for *method,* the calling variables are a list of field and noise arrays. The method function inputs cell arrays of fields and noises, and a parameter structure. It outputs a field cell array.

If cell arrays have more than one member, then $(a, w, p) \to (a, b, c, ..w, x, y, ..p)$, where a, b, c are the fields and w, x, y, are the noises. The cell array of *deriv*, *initial*, or *transfer* functions must be as large as the cell array of integrated fields.

10.3.3. Integrals and derivatives

For details of the internal integration and differentiation functions that can be used in deriv, observe and define see section 10.6.20 and sections 9 and 9. All xSPDE internal functions are capitalized. They are:

Label	Arguments	Purpose
Ave	$(a, [av,]p)$	Averages over a spatial lattice
D1	$(a, [dir,]p)$	First derivative
D2	$(a, [dir,]p)$	Second derivative
Int	$(a, [dx \text{ or } dk], p)$	Integrates over space or momentum

- For Int, one can integrate either with respect to dx or dk, in either ordinary space or momentum space, by changing the second argument passed to $xint$, but the transformation choice must be chosen using transforms.
- For integration in momentum space, fields that are passed to Int are transformed only if the *observe* function is used with Fourier transforms selected using *transforms.*
- For integrating functions like *function*$\{n\}$ with transforms, the transform flags *transforms*$\{n\}$ should be used both for the function and any *observe* averages

used, but the data is *not* Fourier transformed after averaging.

10.3.4. Extensible functions

Extensible functions define the numerical methods used. They use a similar pattern of *(fields..,noises.., parameters)*. For generality, these all pass and return cell arrays of fields and noises.

They all have defaults, and needn't be input in user code when the default available is used. Any compatible user function can be employed instead. If required, use the followiing syntax:

```
p.method = @My_extended_method;
```

.

The system default values don't usually have to be changed unless required.

Label	Standard Value	Arguments	Purpose
method	@$MP, RK4$	(a, w, p)	Algorithm defining a time-step
grid	@xgrid	(p)	Grid calculator for the lattice
prop	@xprop	(a, p)	Interaction picture propagator
propfactor	@xpropfactor	(nc, p)	Propagator array calculation
randomgen	@xrandom	(p)	Initial random generator
noisegen	@xnoise	(p)	Noise generator

10.3.5. SDE methods table

For details of the internal methods available, see section 10.6.20 and sections 9 and 9. All xSIM internal method functions are capitalized. Currently only the MP method is available for jump processes as well as SDEs.

They are:

Label	Arguments	Purpose
*Euler	(a, w, p)	Euler algorithm
MP	(a, w, p)	Midpoint algorithm
MPadapt	(a, w, p)	Midpoint adaptive algorithm
RK2	(a, w, p)	Runge-Kutta (2) algorithm
RK4	(a, w, p)	Runge-Kutta (4) algorithm
**Implicit*	(a, w, p)	Implicit or time-reversed

All standard methods can use the *xprop* interaction picture propagator, which also projects onto boundaries. They can all normalise quantum wavefunctions and density matrices if $p.quantum > 1$, and can treat vectors, arrays and cells. The MP and RK methods are intended for Stratonovich equations.The '*' methods are for Ito equations, while '**' methods are for time-reversed Ito equations.

In general, the input and output,'a' is a cell array of fields. The fields themelves can be scalars, vectors or tensors. These can have definitions that include spatial indices. However, there also are special cases:

- Field tensors can't be integrated in space as well as time, although this will change in future.
- A weak, second order Ito method, RKWP21 is available for scalar ODEs, and extensions are planned.
- Currently, quantum fields and non-quantum fields can't be mixed, but this will be extended.

10.3.6. Projection methods

More advanced methods are also available:

Label	Arguments	Purpose
Catproj	(d, a, n, p)	Catenoid projector
Quadproj	(d, a, n, p)	General quadratic projector
Polproj	(d, a, n, p)	Diagonal polynomial projector
Enproj	(a, w, p)	Euler normal projection method
MPproj	(a, w, p)	Midpoint projection method
MPnproj	(a, w, p)	Midpoint normal projection method

- Projection algorithms with a '*proj*' suffix require a *project* function.
- The *method* functions take cell inputs and outputs.
- The projectors take individual arrays as inputs and outputs.

10.4. xSIM exported data

The following table show how xSPDE output data is stored, which helps customize and extend the code. There are several different types of arrays used. Averages are generated from the observe functions, *p.observe*. These are modified, if required, by user functions *p.output*, and exported as graphics data. The exported data has additional sequence and check indices.

The internal averages and the exported graphics data are as follows:

Label	Indices	Description
av	$\{n\}(\ell, \mathbf{j})$	Internal averages
d	$\{s\}\{n\}(\ell, \mathbf{j}, c)$	Graph data

Here:

- s is the sequence index
- n is the graph index
- ℓ is the graphics line index
- j_1 is the time index
- $\mathbf{j} = j_1, j_2, \ldots j_d$ is the space-time index
- c is the check index

10.4.1. Check index uses

There are multiple uses for the last index, c. It can be omitted if needed. If present, it stores data for errors and comparisons. This is indicated by the input parameter field $p.errors > 0$, which is the index of the largest error field. If there are no parameters, or $p.errors = 0$, there is no error or comparison index. The standard value that xSIM outputs is $p.errors = 3$.

When the check index present, the index values are defined as follows:

$c = 1$ for the average of the n-th output function

$c = 2$ for the time-step error,

$c = 3$ for the sampling error.

$c = 4$ for (optional) comparisons

$c = 5$ for (optional) systematic comparison errors

$c = 6$ for (optional) statistical comparison errors

If xGRAPH is used with data from an other source, with no simulation error fields, but with comparisons, then one simply puts $p.errors = 1$, or if there is just one input error field $p.errors = 2$.

10.4.2. Comparisons

For every type of observation in xSIM, the observe function can be accompanied by a comparison function, *compare(p)*. This generates a vector of analytic solutions or experimental data which is compared to the stochastic results. Results are plotted as additional lines on the two-dimensional graphical outputs, and comparison differences can be graphed in any dimension.

Comparisons are possible for either moments or probabilities, and can be input in any number of dimensions. When there are error estimates, a chi-squared test is carried out to determine if the difference is within the expected step-size and sampling error bars. If the comparison has errors, for example from experimental data, the chi-squared test will include the experimental errors.

Comparison data can be added to the graphics files from any source. It must match the corresponding space-time lattice or probability bins that are in the graphed data. Note that the *compare* functions are specified during the simulation. The graphics code does not generate comparison data, as it is dedicated to graphics, not to generating data.

10.5. QUANTUM parameters

The QUANTUM parameters are identical to the xSIM parameters, with additional functions and methods. Currently only one cell-array index is available.

There are three switchable options that can be chosen:

Label	Value	Purpose
quantum	$0, 1, 2$	Use wave-functions (1), or density matrices (2)
sparse	$0, 1$	Use functional (0) or sparse (1) operators
jump	$0, 1$	Use continuous (0) or jump (1) methods

Wave-functions are stored in a packed, one-dimensional form with sparse operators, in a packed, two-dimensional form with density matrices, and in a multidimensional array with functional operators. Sparse operators usually give faster results, but require greater overall memory storage for larger Hilbert spaces.

For operators with two mode indices, the second mode index can be omitted if identical to the first. Hermitian conjugate operators are returned if the mode index is negative.

10.5.1. Bosonic operator table

Label	Inputs	Output(s)
a	(m, psi)	$\hat{a}_m \left\|\psi\right\rangle$
$a2$	(m, psi)	$\hat{a}_m^2 \left\|\psi\right\rangle$
n	$([m_1 \left(, m_2\right)], psi)$	$\hat{a}_{m_1}^\dagger \hat{a}_{m_2} \left\|\psi\right\rangle$

10.5.2. Qubit and Pauli spin operators

Label	Inputs	Output(s)
sx	(m, psi)	$\hat{\sigma}_m^x \left\|\psi\right\rangle$
sy	(m, psi)	$\hat{\sigma}_m^y \left\|\psi\right\rangle$
sz	(m, psi)	$\hat{\sigma}_m^z \left\|\psi\right\rangle$
$sx2$	$([m_1 \left(, m_2\right)], psi,)$	$\hat{\sigma}_{m_1}^x \hat{\sigma}_{m_2}^x \left\|\psi\right\rangle$
$sy2$	$([m_1 \left(, m_2\right)], psi)$	$\hat{\sigma}_{m_1}^y \hat{\sigma}_{m_2}^y \left\|\psi\right\rangle$
$sz2$	$([m_1 \left(, m_2\right)], psi)$	$\hat{\sigma}_{m_1}^z \hat{\sigma}_{m_2}^z \left\|\psi\right\rangle$

10.5.3. Quantum logic gate operators

Label	Inputs	Output(s)
ha	(m, psi)	$h\,\|\psi\rangle$
ph	(m, psi)	$p\,\|\psi\rangle$
$p8$	(m, psi)	$t\,\|\psi\rangle$
cx	$([m_1\,(, m_2)], psi,)$	$cx\,\|\psi\rangle$

10.6. Function reference

10.6.1. User function reference

The following user-defined function inputs define the differential equation that is integrated or solved. They are specified in an xSPDE/xSIM input file using *p.(fun) = @(Myfun)*, either as inline or externally defined functions. Externally defined functions must be in the same file as the input parameters, or on the execution path.

10.6.2. boundfun(a, c, d, p)

Default: *xboundfun()*

The boundary function *boundfun(a,c,d,p)* is called for specified boundary conditions for field cell c in the d-th dimension. This returns the boundary values used for the fields or their first derivatives in space dimension $d > 1$, as an array indexed as $b(f, \mathbf{i}, e)$ in the standard way. Here f is the field index, $\mathbf{i} \equiv [j_2, \ldots j_d]$ are the space indices, and e is the ensemble index.

Only two values are needed for j_d, which is the index of the dimension whose boundary values are specified. These are $j_d = 1, 2$, for the lower and upper boundary values, which are either field values or derivatives. Boundary values may be constant or a function of the fields a and space-time $t, \mathbf{x}$.

If boundary values have stochastic values which are calculated only once, they must be initialized. To allow for this, *boundfun(a,c,d,p)* is initially called with time $t = origins(1) - 1$, and with the input field a set to random values from *randomgen,* which are independent of those that initialize the field at $t = origins(1)$.

They are reproducible for different *check* cycles, to allow noise-independent error-checking. The initial results for the boundaries are stored in an array *boundval{c,d}* for later use by *boundfun.*

The default boundary value is zero, or equal to *boundval* if it is specified initially. It is automatically set by the default boundary function *xboundfun(a,c,d,p).*

10.6.3. compare{n}(p)

Default: *compare{n}= []*

This is for comparisons to experimental or analytic data. The output is an array with $d + 2$ dimensions. The first dimension is the line index, the next d dimensions are time

and space, while the last index is an error index. This can have up to two additional entries for systematic and/or statistical error bars in the comparison data, from analytic or experimental results. Error-bars are optional if not available.

10.6.4. define(a{:},w{:}, p)

Default: *xdefine()*

Calculates a list of auxiliary fields, which are combinations of fields and noises. If used they are accessed in *observe* functions as part of the input list, after the propagating fields. These are used in spectral calculations. They enable access to noise fields, which are needed in quantum input-output calculations. The default, *xdefine(),* sets the auxiliary fields to zero.

10.6.5. deriv(a{:},w{:},p)

Default: *deriv()= 0*

This defines the stochastic time derivative, given the current field cells a, delta-correlated noise terms w, and parameters p. It is defined explicitly in (5.15). This is the right-hand-side of (2.1) or (5.1), *without* the linear term if it is specified separately. In the case of multiple cell calculations, this user defined function must return a full list of all propagating derivative terms in the form of *[da{1}, da{2},..]*.

10.6.6. firstfb(a0,nc,p)

Default: *xfirstfb()*

Returns the zero-th order field estimates in a forward-backward iteration. Here nc is the time-step check index. This is needed because the number of time-points to be initialized depends on nc. The default function is *xfirstfb*, which sets each field in either direction equal to its initial value at the time boundaries, given by $a0$. Other estimates may give faster convergence.

10.6.7. grid(p)

default *xgrid*

Calculates the spatial grid for specialized purposes like non-uniform grids. The default, *xgrid*, returns a homogeneous rectangular grid in both ordinary and momentum space, as part of the parameter structure p. Grids are removed from stored data.

10.6.8. initial{c}(rv, p)

Default: *xinitial()*

This is used to initialize each field cell integration in time. It is a user-defined function which can involve random numbers for an initial probability distribution. This creates a stochastic field on the spatial lattice. The returned first dimension is *p.fields*(1). The initial Gaussian random field variable, *rv*, has unit variance if dimension is 1 or else is delta-correlated in space, with variance $1/p.dv = 1/(dx_2...dx_d))$ for d space-time dimensions. If *inrandoms* is given in the input parameter structure, *rv* has a first dimension of *inrandoms(1) + inrandoms(2)*. If not specified, the default for *inrandoms* is *noises*. The default function is *xinitial,* which sets fields to zero. The function can be either a cell array of initial functions, or a single function if there is just one cell.

10.6.9. linear{c}(p)

Default: *xlinear()*

A cell array of user-defined linear response functions. It is a vector for an SDE or ODE. For an SPDE or PDE, it includes transverse derivatives in space, returning linear coefficients L in FFT/DST/DCT space, which are assumed diagonal in the field index. These are functions of differential terms *Dx, Dy, Dz*, which correspond to $\partial/\partial x$, $\partial/\partial y$, $\partial/\partial z$, respectively. Each component has a dimension the same as the coordinate lattice. For axes that are numbered, use *D{2}, D{3}* etc. The default, *xlinear,* sets L to zero. The function can be either a cell array of linear functions, or a single function if there is just one cell.

10.6.10. method(a, w, p)

Default: *@MP* (stochastic); *@RK4* (deterministic)

GIves the integration method for the field cell array a, noise cell array w, parameters p. It returns the new field cell array. It uses the current reduced step in time p.dtr and current time p.t. This function can be set to any of the predefined stochastic integration routines provided with xSPDE, described in the Algorithms section. User-written functions can also be used. The default deterministic method, *RK4*, is a fourth-order interaction picture Runge-Kutta. The default stochastic method, *MP*, is an interaction picture midpoint integrator which is used if *ensembles* is not *[1,1,1]*.

10.6.11. nfilter{n} (w,p)

Default: *xnfilter()*

Returns the $n-th$momentum-space filter function for the propagation noise terms in momentum-space. Each component has an array dimension the same as the random noises in momentum space, that is, the return dimension is *[noises{n}(2), d.lattice]*.

10.6.12. noisegen(p)

Default: *xnoisegen(p)*

Generates arrays of noise terms for each point in time. The default, *xnoisegen()* returns *noises(1) + noises(2)* Gaussian real noises that are delta-correlated in time, space and momentum space, unless *nfilter* is used to modify momentum space correlations.

10.6.13. observe{n}(a..., p)

Default: *xobserve{1}=@(a,p) a*

Cell array of function handles that take the current field(s) and returns an observable o. Note the braces for cell arrays! One can input these as *p.observe{n} = @(a,p) f(a,p)*. An omitted function less than the maximum index is replaced by the default, which is the first vector *a* of real field amplitudes.

10.6.14. output{n}(o,p)

Default: *@(o,p) o{n}*

This is a user-defined cell array of output functions of the *observe* results after averaging over *ensembles(1)*, possibly involving combinations of several observed averages. The input to the n-th output function is the cell array of all averages, and the output is the data for the n-th graph. This function is compatible with all error estimates. The default values generate all the *observe* averages that are in the data.

The output data formatof the output functions is an array with $d+1$ dimensions. The first dimension is the line index, the next d dimensions are time and space.

The xSIM program augments the outputs with columns of errors and comparison data, if available, before graphing.

10.6.15. prop(a, p)

Default: *xprop()*

Returns the fields propagated for one step in the interaction picture, given an initial field a, using the propagator array. The time-step used in propagator depends on the input time-step, the error-checking and the algorithm. The default, *xprop*, takes a Fourier transform of **a**, multiplies by propfactor to propagate in time, then takes an inverse Fourier transform.

10.6.16. propfactor(nc, p)

Default: *xpropfactor()*

Returns the interaction picture propagator used by the prop function. The time propagated is a fraction of the current integration time-step, *dt*. It is equal to $1/ipsteps$ of the integration time-step. It uses data from the **linear** function to calculate this.

10.6.17. randomgen(p)

Default: *xrandom()*

Generates a cell array of initial random fields v to initialize the fields simulated. The default, **xrandomgen**, returns Gaussian real fields that have *inrandoms{n}(1)* components delta-correlated in space, with *inrandoms{n}(2)* delta-correlated in momentum space. The default uses a user-defined cell array, *rfilter{n}*, of filter functions, to modify correlations in momentum space, if specified.

10.6.18. rfilter{n}(w, p)

Default: *xrfilter()*

Returns the momentum-space filter function for the momentum-space random terms. Each component has an array dimension the same as the input random fields in momentum space, that is, the return dimension of cell n is *[inrandoms{n}(2),... nlattice]*.

10.6.19. transfer{c}(a0{:},v{:},p)

Default: *xtransfer()*

This function initializes sequential simulations, where the previous field *a0* can be used as an input to the next stage in the integration sequence. The default, *xtransfer()*, takes each output, *a0{c}* of the previous simulation to initialize the field *a{c}*. Otherwise, this function is identical to *initial()*.

10.6.20. Internal function reference

The following xSIM predefined functions are available to define the differential equations and averages. They all start with a capital letter. Algorithms are documented in section 9. Fields can be differentiated or integrated only in space, observables in space or time.

10.6.21. Ave(o[, av], p)

This function takes a field or observable and returns an average over one or more dimensions. The input includes an optional averaging switch *av*. If $av(j) > 0$, an average is taken over dimension j. If the *av* vector is omitted, the average is taken over all space directions.

10.6.22. Bin(o[, dx], p)

The *Bin* function takes a field o and returns probabilities on space axes that are defined by a vector dx. This allows binning of position probabilities if the observable is a mean position that is plotted on an axis. If j is the first index with $dx(j) > 0$, the binning is taken over dimension j. The results returned are the probability of o in the

bin, normalized by $1/dx\,(j)$. If the input array is Fourier transformed, by using the transforms attribute in the observe function, then one must set $dx(j) = p.dk(j)$ for transformed dimensions j. If the dx vector is omitted, or a scalar dx is used, the binning is over the first space direction.

10.6.23. D1(a[, d,ind,c], p)

Takes a scalar or vector field a and returns a derivative in dimension d using finite differences. Set $d = 2$ for an x-derivative, $d = 3$ for a y-derivative, etc. The default value is $d = 2$. If the dimension is input, an index list *ind* can be included to take a derivative of one component or of a specified list. If omitted, derivatives of all components are returned.

Boundary values are stored in *p.boundval*, and are needed for Neumann/Robin boundaries. Hence, in multicell computations, if a is from a cell index $c > 1$, the cell index c must be included to identify which boundary value to use. If there are Neumann/Robin boundaries, the entire field a must be input unless all boundary values are the same.

For other types of boundaries, the cell index is not needed, and D1 can differentiate a single field component without having to identify the component. The method is of second order in the space step. It is used in the deriv, observe and output functions, with automatic compensation for the prsence/absence of a time index.

For Dirichlet boundaries, the derivatives are ambiguous at the boundaries, and a periodic derivative is returned. This is not needed for time-evolution, as the boundary value overrides it.

10.6.24. D2(a[, d,ind,c], p)

This takes a scalar or vector field a and returns the second derivative in dimension d. Other properties are the same as *D1()*. The method is of second order in the space step, except at a Neuman/Robin boundary, where the boundary result is of first order.

10.6.25. Int(o[, dx, bounds], p)

This function takes any vector or scalar field or observable and returns a space integral over selected dimensions with vector measure *dx*. If $dx(j) > 0$, dimension j is integrated. Time integrals are only possible for observables. Space dimensions are labelled from *j = 2,3,...dimensions*. To integrate over the lattice, set *dx = p.dx*, otherwise set *dx(j) = p.dx(j)* for integrated dimensions and *dx(j) = 0* for non-integrated dimensions.

If the input array is Fourier transformed by using the *p.transforms* attribute, one must set *dx(j) = p.dk(j)* for transformed dimensions *j*, to get correct results. If the *dx* vector is omitted, the integral is over all available space dimensions, assuming no Fourier transforms. The optional input *bounds* is an array of size *[p.dimensions,2]*, which specifies lower and upper integration bounds in each direction. This is only available if *dx* is input. If omitted, integration is over the whole domain.

10.7. Internal parameters

Knowing the details of array indexing inside xSPDE isn't usually necessary. Yet it becomes important if you want to write your own functions to extend xSPDE, interface xSPDE with other functions, or read and write xSPDE data files with external programs. It also helps to understand how the program works.

10.7.1. Array tables

There are two main internal xSPDE arrays:, *fields* labelled a and output *data* labelled d. The *fields* contain stochastic variables, the *data* contains the averaged outputs and errors estimates.

Important array and index definitions are:

Label	Indices	Description
a	$\{n_1\}[f, \mathbf{i}, e_1]$	Stochastic field array
v	$\{n_1\}[m_1, \mathbf{i}, e_1]$	Initial random variable array
w	$\{n_1\}[m_2, \mathbf{i}, e_1]$	Noise field array
$r\{2\}$,$k\{2\}$....	$(1, \mathbf{i}, 1)$	Numbered space/momentum coordinates
x,y,z,kx,ky,kz	$(1, \mathbf{i}, 1)$	Labelled space/momentum coordinates
o	$\{n_2\}(\ell, \mathbf{j})$	Cell array of all observed averages
$data$	$\{s\}\{n_2\}(\ell, \mathbf{j}, c)$	Cell array of output data with checks
raw	$\{s, c, h\}\{n_1\}(f, \mathbf{j}, e_1)$	Raw trajectories
$points$	$[pt_1, pt_2 \ldots pt_d]$	Vector of lattice sizes
$ensembles$	$[h_1, h_2, h_3]$	Vector of ensemble sizes

Here:

- s is the sequence index
- f is the field internal index
- $\mathbf{i}$ is the space index
- e_1 is the first ensemble index
- c is the check index for errors and comparisons
- $\mathbf{m}$ is the random or noise index
- $\mathbf{j} = [j_1, \mathbf{i}]$ is the space-time index
- n_1 is the cell index of a computational field or noise
- n_2 is the cell index of an observe and/or output function
- ℓ is the line index of an output

- e is the high-level ensemble index (combines e_2, e_3 indices)

When fields are passed to *observe* or to *raw* outputs, the defined auxiliary fields are included as well. Apart from the internal field dimension(s), the common dimensionality for internal arrays used in computations is $[d.space, ensembles(1)]$. The number of points in $d.space$ can be changed depending on the cell index, for different integrated fields.

10.7.2. Simulation data in xSIM

In xSIM, the space-time dimension d is unlimited. xGRAPH can plot up to three chosen axes. All fields are stored in cell arrays that contain real or complex numerical arrays. Average results are stored are stored in cell arrays of real numerical arrays, usually of rank $2 + d$, although this can change in special cases like the plot of a probability, which requires extra axes.

The array index ordering in xSPDE integrated fields is $\{n_1\}(\boldsymbol{f}, \mathbf{i}, e_1)$, where:

- The internal cell index n_1 labels distinct integrated variables.
- The internal field index $\boldsymbol{f}$, is a field index or indices, not including auxiliary fields
- The next $d - 1$ indices are $\mathbf{i}$, which is a space index with no time index.
- The last is an ensemble index e_1, to store low-level parallel trajectories.

The array index ordering in graphical averaged data is $(\ell, \mathbf{j}, c)$where:

- The first index is a line index ℓ.
- The next d indices are $\mathbf{j} = [j_1, \ldots j_d] = [j, \mathbf{i}]$, for time *and* space.
- The last is a check index c, for comparisons and errors.

Stored data uses heterogenous cell arrays to package numerical arrays with additional high level indices. The first cell index is the sequence index, s. Inside each sequence, data cell arrays have a graph index n. This distinguishes the different averages generated for output graphs and data. Raw data has cell indices for the sequence, time-step and high level ensembles.

In summary, the xSPDE internal arrays are as follows:

- **Field** arrays $a\{n_1\}(\boldsymbol{f}, \mathbf{i}, e)$ - these have a field index, a space index and low-level ensemble index e.
- **Auxiliary** arrays $a_x\{n_1\}(\boldsymbol{f}, \mathbf{i}, e)$ - these are appended to the field cells for raw data and observables.
- **Random** and **noise** arrays $w\{n_1\}(m, \mathbf{i}, e)$ - these are initial random fields or noise fields. The first index may have a different range to the field index.

- **Coordinate** arrays $x(1, \mathbf{i})$ - these contain the coordinates at grid-points, with labels x, y, z, and $j_1 = 1$. Numeric labels $x\{l\}$ are used for $d > 4$, where $l = 2, \ldots d$. The same sizes are used for:
  - momentum coordinates kx, ky, kz (alternatively $k\{2\}, k\{3\}, \ldots$)
  - spectral derivative arrays Dx, Dy, Dz (alternatively $D\{2\}, D\{3\}, \ldots$) .
- **Raw data** arrays $r\{s, c, e\}\{n_1\}(\boldsymbol{f}, \mathbf{j}, e_1)$ - these are cell arrays of generated trajectories, including integrated and defined field values. They are optional, as they use large amounts of memory. These are saved in cell arrays with indices s for the sequence, c for the time-step error-check and h for high level ensemble index. The cell indices are:
  - $s = 1, \ldots S$ for the sequence number,
  - $c = 1, 2, 3..$ for the error-checking step used: first fine, then coarse in each dimension checked.
  - $e = 1, \ldots ensembles(2) * ensembles(3)$ for a high level parallel and serial ensemble index.
- **Observe** arrays $o\{n_2\}(\ell, \mathbf{j})$ - these are generated in xSIM by the observe functions, then used to store generated average data at all time points. The cell index n is the *observe* index, which indexes overs the observe functions.The internal index ℓ is a *line* index generated by an observe function.
- **Data** arrays $d\{s\}\{n_2\}(\ell, \mathbf{j}, c))$ - these store the final results. The $\mathbf{j}$ indices may be Fourier indices if transforms are specified, and may incude extra axes for probabilities.
  Check indices are used for error estimates and comparisons, where $c = 1$ for the average, $c = 2$ for the total step error, and $c = 3$ for the sampling error. The total step error is a composite of all step errors that are checked.
  If there is comparison data, it uses $c = 4$ up to $c = 6$, to allow for any error bars.
  The output data uses cell indices $\{s\}$ for the *sequence* index, and $\{n_2\}$ for the *data* index. This has a default of the index of the *observe* function.
  If this data is modified by an xSIM *output* function, the data index equals the relevant output function index.

10.7.3. Internal parameter table

The internal parameter structures in xSPDE are available to the user if required. Internally, all xSPDE parameters are stored in the parameter structures passed to functions. This includes the data given above from the input structures. In addition, it includes the computed parameters given below, which includes internal array dimensions.

Data in $k-$space is stored in two alternative lattices, each having their own axis vectors. The propagation grid is used while propagating, and is compatible with numerical FFT conventions where the first index value is $k = 0$. The graphics grid is centered around $k = 0$, and is used for graphics and data storage, following scientific conventions.

For more than four total dimensions, the spatial grid, momentum grid and derivative grid notation of t, x, y, z, ω, kx, ky, kz and Dx, Dy, Dz is changed to use numerical labels that correspond to the dimension numbers, i.e., $D\{2\}, \ldots D\{d\}$, $r\{1\}, \ldots r\{d\}$, $k\{1\}, \ldots k\{d\}$.

Numeric dimension labeling can also be used even for lower dimensionality if preferred.

Label	Type	Typical value	Description
t, x, y, z	array	-	Space-time grid of t, x, y, z
ω, kx, ky, kz	array	-	Frequency-momentum grid of k_x, k_y, k_z
Dx, Dy, Dz	array	-	Derivative grid of D_x, D_y, D_z
$r\{1\}, \ldots r\{d\}$	array	-	Space-time grid of $r_1, \ldots r_d$
$k\{1\}, \ldots k\{d\}$	array	-	Graphics momentum grid of $k_1, \ldots k_d$
$D\{2\}, \ldots D\{d\}$	array	-	Derivative grid of $D_2, \ldots D_d$
dx	vector	*[0.2,..]*	Steps in $[t, x, y, z]$
dk	vector	*[0.61,....]*	Steps in $[\omega, k_x, k_y, k_z]$
dt	double	*0.2000*	Output time-step
dtr	double	*0.1000*	Computational time-step
v	real	*1*	Spatial lattice volume
kv	real	*1*	Momentum lattice volume
dv	real	*1*	Spatial cell volume
dkv	real	*1*	Momentum cell volume
xc{d}	cells of vectors	*[-5,... 5]*	Coordinate axes in t, x, y, z
kc{d}	cells of vectors	*[-5,..5]*	Graphics axes in$[\omega, k_x, k_y, k_z]$
kcp{d}	cells of vectors	*[0,...]*	Propagation axes in$[\omega, k_x, k_y, k_z]$
s.dx	double	1	Initial stochastic normalization
s.dxt	double	*3.1623*	Propagating stochastic normalization
s.dk	double	1	Initial k stochastic normalization
s.dkt	double	*3.1623*	Propagating k stochastic normalization
nspace	integer	35	Number of spatial lattice points
nlattice	integer	3500	Total lattice: *ensembles(1) x n.space*
ncopies	integer	20	*ensembles(2) x ensembles(3)*
inrandoms	vector	[2,0]	Number of initial random fields
noises	vector	[2,0]	Number of noise fields
d.space	vector	*[35, 35]*	Space dimensions: [points(2), points(3), ...]
d.lattice	vector	*[1, 1]*	Lattice dimensions: [d.space, ensembles(1)]
d.a	vector	*[1, 1]*	Dimensions for a field
d.r	vector	*[1, 1]*	Dimensions for coordinates
d.fields	vector	*[1, 1]*	Dimensions for a field (including time)
d.aplus	vector	*[1, 1, 1]*	Dimensions for integrated plus defined fields
d.k	vector	*[0, 1, 1]*	Dimensions for noise transforms
d.obs	vector	*[1, 35]*	Dimensions for observations
d.data	vector	*[1, 35, 3]*	Dimensions for average data
d.raw	vector	*[1, 51, 35, 100]*	Dimensions for raw data

10.8. xGRAPH overview

The graphics function provided is a general purpose multidimensional batch graphics code, xGRAPH, which is automatically called by xSPDE when xSIM is finished. The results are graphed and output if required. Alternatively, xGRAPH can be replaced by another graphics code, or it can be used to process the data generated by the xSIM function at a later time.

The *xgraph* function call syntax is:

- ***xgraph (data [,input])***

This takes simulation *data* and *input* cell arrays, then plots graphs. The *data* should have as many cells as there are *input* cells, for sequences.

If *data = 'filename.h5'* or *'filename.mat'*, the specified file is read both for *input* and *data*. Here *.h5* indicates an HDF5 file, and *.mat* indicates a Matlab file.

When the *data* input is a filename, parameters in the file can be replaced by new *input* parameters that are specified. Any stored *input* in the file is then overwritten when graphs are generated. This allows graphs of data to be modified retrospectively, if the simulation takes too long to be run again in a reasonable timeframe.

10.8.1. Parameter and data structures

This is a batch graphics function, intended to process quantities of graphics data, input as a cell array of multi-dimensional data. Theoretical and/or experimental data is passed to the graphics program, including the complete *data* cell array and a cell array of graphics parameters for plotting each graph.

To explain xGRAPH in full detail,

- Data to be graphed are recorded sequentially in a cell array, with *data*={*d1,d2,...*}.
- Graphics parameters including defaults are given in the *input* cell array.
- This describes a sequence of graph parameters, so that *input*={*p1,p2,...*}.
- For a one member sequence, a dataset and parameter structure can be used on its own.
- Each dataset and parameter structure describes a set of graphs.

The data input to *xGRAPH* can either come from a file, or from data generated directly with *xSIM*. The main graphics data is a nested cell array. It contains several numerical graphics arrays. Each defines one independent set of averaged data, the observed data averages, stored in a cell array indexed as $data\{s\}\{n\}(\ell, \mathbf{j}, c)$. To graph these also requires a corresponding cell array of structures of graphics parameters.

The output is unlimited, apart from memory limits. The program also generates error comparisons and chi-squared values if required. The data structure for input is as follows:

1. The input *data* is a cell array of *datasets,* which can be collapsed to a single dataset
2. The *parameters* are also a cell array of parameter structures, which can be collapsed to one structure
3. The *dataset* is a cell array of multidimensional *graphs*, each with arbitrary dimensionality.
4. The first or *line* index of each graph array allows multiple lines, with different line-styles
5. The last or *check* index of each graph array is optionally used for error and comparison fields.
6. Each *graph* array can generate multiple graphic plots, as defined by the parameters.

10.8.2. xGRAPH structure

The graphics function, *xgraph*, plots the simulation data. The general structure is:

$$\begin{aligned}\textbf{xgraph} &\rightarrow \textbf{xgpreferences}\ (checks\, inputs)\\ &\rightarrow \textbf{xmultigraph} \leftrightarrow \textbf{xreduce} \leftrightarrow \textbf{xcompress}\ (structures\, data\, arrays)\\ &\rightarrow \textbf{ximages} \rightarrow \textbf{xtransverse} \rightarrow \textbf{xplot3} \rightarrow \textbf{xplot2}\ (graphs\, all\, data)\end{aligned}$$

Most graphics functions simply work, but two important functions are listed below for reference.

10.8.3. xgraph(data,input)

The *xgraph* function graphs multidimensional data files.

- Input: graphics data cells *data*, input parameter cells *input*.
- Output: graphs, displayed and/or stored as *eps* or *fig* files.
- If no numeric *data* present, reads data from a file named *data*.
- If *data* is present but without any *input* parameters it plots using default parameters.
- First data dimension is the line index, last dimension are the error-bars and comparisons
- Needs: x*read, xmakecell, xgpreferences, xmultiplot*

10.8.4. xgpreferences (input,oldinput)

The *xgpreferences* function sets default values for graphics inputs.

- Input: *input* cell array and optionally previous inputs from a datafile, *oldinput.*
- Note that each cell array is a sequence of graphics parameter structures
- Output: the updated plus default graphics parameters
- Called by: *xgraph*
- Needs: *xprefer*, *xcprefer*

10.8.5. Parameter table

The complete cell array of the simulation data is passed to the *xGRAPH* program, along with graphics parameters for each observable, to create an extended graphics data structure. Graphics parameters have default values which are user-modifiable by editing the *xgpreferences* function.

Some input parameters are global parameters for all graphs. However, most *xGRAPH* parameters are cell arrays indexed by graph index. These graphics parameters are individually set for each output that is plotted, using the cell index $\{n\}$ in a curly bracket. If present they replace the global parameters like labels.

If a graph index is omitted, and the parameter is not a nested array, the program will use the same value for all graphs. The *axes*, *glabels, legends, lines, logs,* and *xfunctions* of each graph are nested cell arrays, as there can be any number of lines and axis dimensions. In the case of the *logs* switch, the observable axis is treated as an extra dimension.

The plotted result can be an arbitrary function of the generated average data, by using the optional input *gfunction.* If this is omitted, the generated average data that is input is plotted.

Comparisons are plotted if present in the input data indexed by the last or check index c, with $c > errors$, where $errors = 3$ is the usual maximum value.

A table of the graphics parameters is given below.

Label	Default value	Description
axes{*n*}	{0,..}	Points plotted for each axis
chisqplot{*n*}	0	Chi-square plot options
cutoff	1.e-12	Global lower cutoff for chi-squares
cutoffs{*n*}	*cutoff*	Probability cutoff for n-th graph
diffplot{*n*}	0	Comparison difference plot options
errors	0	Index of last error field in *data*
esample{*n*}	1	Size and type of sampling error-bar
font{*n*}	18	Font size for graph labels
gfunction{*n*}	@(d,˜) d{n}	Functions of graphics data
glabels{*n*}	{*'t' ,'x' ,'y' ,'z'*}	Graph-specific axis labels
graphs	$[1 : max]$	Vector of all the required graphs
gsqplot{*n*}	0	G-square (likelihood) plot options
headers{*n*}	”	Graph headers
images{*n*}	0	Number of movie images
imagetype{*n*}	0	Type of 3D image
klabels	{*'\omega' ,'k_x' ,'k_y' ,'k_z'...*}	Global transformed axis labels
legends{*n*}	{'label1',..}	Legends for multi-line graphs
limits{*n*}	{*[lc1,uc1],[lc2,uc2]*}	Axis limits, first lower then upper
linestyle{*n*}	{*'-'*,..}	Line styles for multiline 2D graphs
linewidth{*n*}	*0.5*	Line width for 2D graphs (in points)
logs{*n*}	{0,..}	Axis logarithmic switch: 0 linear, 1 log
minbar{*n*}	*0.01*	Minimum relative error-bar
mincount	10	Global counts for chi-square cutoffs
name	”	Global graph header
olabels{*n*}	*'a_1'*	Observable labels
pdimension{*n*}	3	Maximum plot dimensions
saveeps	0	Switch, set to 1 to save eps files
savefig	0	Switch, set to 1 to save figure files
scale{*n*}	1	Scaling: Counts/ probability density
transverse{*n*}	0	Number of transverse plots
xfunctions{*n*}	{*@(t,˜) t,@(x,˜) x,..*}	Axis transformations
verbose	0	0 for brief, 1 for informative, 2 for full output
xlabels	{*'t' ,'x' ,'y' ,'z'...*}	Global axis labels
octave	0	0 for Matlab, 1 for octave environment

- Up to 6 types of input data can occur, including errors and comparisons, indexed by the last index. The original mean data always has $c = 1$. If there are no errors or comparisons, one graph is plotted for each dimensional reduction.
- The input data has up to two error bars (I and II), and optional comparisons also with up to two error bars.
- Type I errors labeled $c = 2$ have standard vertical error bars. Type II errors labeled

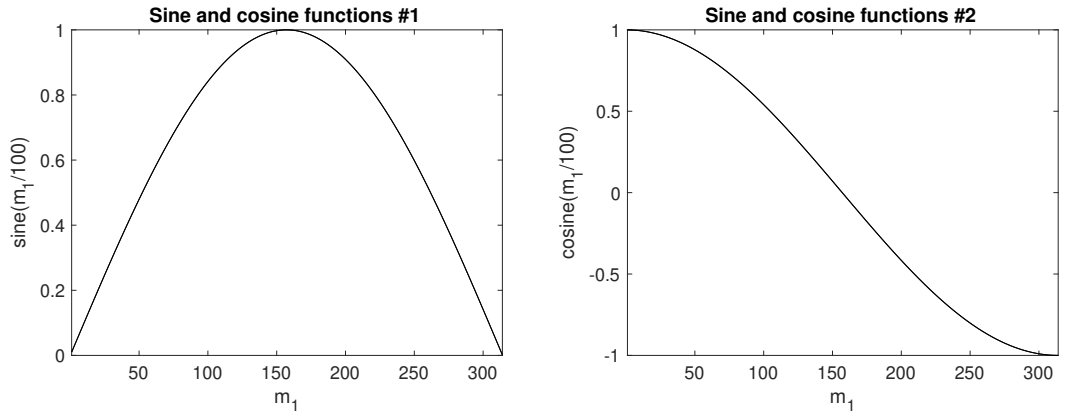

Figure 10.1.: *Example: xgraph output of two plots.*

$c = 3$, which are usually standard deviation errors from sampling, have two solid lines.

- If *esample* = -1, both error bars are combined and the RMS errors are plotted as a single error bar.
- If $diffplot > 0$, differences are plotted as unnormalized ($diffplot = 1$), or normalized ($diffplot = 2$) by the total RMS errors. If $diffplot = 3$, raw comparison data is plotted.
- When differences are plotted, the total comparison errors are treated as type I error bars, while total simulation errors are treated as type II errors with parallel lines in the graphs, in order to distinguish them.

A detailed description of each parameter is listed in Sec (10.9).

10.8.6. Example

A simple example of data and input parameters, but without errors or comparisons is as follows

```
p.name = 'Sine and cosine functions';
p.olabels = {'sine(m_1\pi/100)','cosine(m_1\pi/100)'};
data = {sin([1:100*pi]/100),cos([1:100*pi]/100)};
xgraph(data,p);
```

Note that in this case the default setting of *p.errors=0* is used, with no check index used in the data arrays, because these are simple graphs without error-bars or comparisons.

10.8.7. xGRAPH data arrays

The data input to *xGRAPH* can come from a file, or from data generated directly from any compatible program.

The data is stored in a cell array *data* with structure:

$$data\{s\}\{n\}(\ell, \mathbf{j}, c)$$

Each member of the outer cell array $data\{s\}$ defines a number of related sets of graphical data, all described by common parameters $input\{s\}$. Comparisons and errors are plotted if there are errors and comparison data in the input, indexed by c. This generates comparison plots, as well as error totals and χ- squared error estimate when there are statistical variances available.

An individual member of $data\{s\}\{n\}$ is a multidimensional array, called a *graph* in the xSPDE User's guide. For each *graph*, multiple different plots with different dimensionality can be obtained from the dataset $data\{s\}\{n\}$, either through projections and slices or by generating additional data defined with graphics functions. Either or both alternatives are available.

Note that:

- If a sequence has one member, the outer cell array can be omitted.
- In this simplified case, if there is only one *graph* array, the inner cell array can be omitted.

The graphics data for a single dataset is held in a multidimensional real array, where:

- ℓ is the index for lines in the graph. Even for one line, the first dimension is retained.
- $\mathbf{j} = j_1, \ldots j_d$ is the array index in each dimension, where $d \geq 1$.
- Averages in momentum space have the momentum origin as the central index.
- If integrals or spatial averages are used, the corresponding dimension has one index $j_d = 1$.
- With probabilities, extra dimensions are added to $\mathbf{j}$ to store the bin indices.
- c indexes error-checks and comparisons. If not present, omit $p.errors$ and the last dimension.
- If $c > p.errors$, the extra fields are comparison inputs, where $p.errors$ is the largest data index.

When the optional comparison fields are used, an input parameter *errors* is required to indicate the maximum error index, to distinguish data from comparisons. Parameter

structures from xSIM have $errors = 3$ set to allow for both sampling errors and discretization errors. If this is omitted, the default is $errors = 0$, which implies that there is no error or comparison data

If $errors > 0$, the last index can have larger values with $c > errors$, for comparisons. The special case of $errors = 1$ is used if the data has no error bars, but there are comparisons in the data. Larger indices are used to index the comparison data, which can also have two types of errors. The largest usable last index is $errors + 3$.

It is possible to directly plot the *raw* data using xGRAPH. One can even combine the raw data with a graphics parameter input. But since the raw data has no error estimates - it is raw data - one must set $p.errors = 0$, since the xsim output parameters have a normal setting of $p.errors = 3$. This will give a single trajectory.

However, the raw data from a simulation typically includes many trajectories if $ensembles(1) > 0$. One must select particular trajectory datasets from the raw cell array, to plot just one.

10.8.8. Input parameters and defaults

A sequence of graph parameters is obtained from inputs in a cell array, as *input* = {*in1, in2, ...*}. The input parameters of each simulation in the sequence are specified in a Matlab structure. The inputs are numbers, vectors, strings, functions and cell arrays. All metadata has preferred values, so only changes from the preferences need to be input. The resulting data is stored internally as a sequence of structures in a cell array, to describe the simulation sequence.

The graphics parameters are also stored in the cell array *input* as a sequence of structures *p.* This only need to be input when the graphs are generated and can be changed at a later time to alter the graphics output. A sequence of simulations is graphed from *input* specifications.

If there is one simulation, just one structure can be input, without the sequence braces. The standard way to input each parameter value is:

$$p.label = parameter$$

The standard way to input a function handle is:

$$p.label = @function$$

The inputs are scalar or vector parameters or function handles. Quantities relating to graphed averages are cell arrays, indexed by the graph number. The available inputs, with their default values in brackets, are given below.

Simulation metadata, including default values that were used in a particular simulation, can be included in the input data files. This is done in both the *.mat* and the *.h5* output files generated by xSIM, so the entire graphics input can be reconstructed or changed.

Parameters can be numbers, vectors, strings or cell arrays. Conventions that are used are that:

- All input parameters have default values
- Vector inputs of numbers are enclosed in square brackets, *[...]*.
- Cell arrays of strings, functions or vectors are enclosed in curly brackets.
- Vector or cell array inputs with only one member don't require brackets.
- Incomplete parameter inputs are completed with the last used default value.
- Function definitions can be handles pointing elsewhere, or defined inline.

If any inputs are omitted, there are default values which are set by the internal function *xgpreferences*. The defaults can be changed by editing *xgpreferences*.

In the following descriptions, *graphs* is the total number of graphed variables of all types. The space coordinate, image, image-type and transverse data can be omitted if there is no spatial lattice, that is, if the dimension variable is set to one.

For uniformity, the graphics parameters that reference an individual data object are cell arrays. These are indexed over the graph number using braces {}. If a different type of input is used, like a scalar or matrix, xSPDE will attempt to convert the type to a cell array.

Axis labels are cell arrays, indexed over dimension. The graph number used to index these cell arrays refers to the data object. In each case there can be multiple generated plots, depending on the graphics input.

10.8.9. Cascaded plots

The xGRAPH function generates a default range of graphs, but this can be modified to suit the user. In the simplest case of one dimension, one graph dataset will generate a single plot. For higher dimensions, a cascade of plots is generated to allow visualization, starting from 3D movies, then 3D static plots and finally 2D slices. These can also be user modified.

Note that for all probabilities, the plot dimension is increased by the bin range dimensionality.

10.8.10. Plot dimensions

The *pdimension* input sets the maximum plotted dimensions. For example, $pdimension\{1\} = 1$ means that only plots vs r_1 are output for the first function plotted. Default values are used for the non-plotted dimensions, unless there are axes specified, as indicated below.

The graphs cascade down from higher to lower dimensions, generating different types of graphs. Each type of graph is generated once for each function index.

10.8.11. Plot axes

The graphics axes that are used for plotting and the points plotted are defined using the optional *axes* input parameters, where $axes\{n\}$ indicates the n-th specified graph or set of generated graph data.

If there are no *axes* inputs, or the *axes* inputs are zero - for example, $axes\{1\} = \{0, 0, 0\}$ - only the lowest dimensions are plotted, up to *3*. If either the data or *axes* inputs project one point in a given dimension, - for example, $axes\{1\} = \{0, 31, -1, 0\}$, this dimension is suppressed in the plots, which reduces the effective dimension of the data - in this case to two dimensions.

Examples:

- $axes\{1\} = \{0\}$ - For function 1, plot all the first dimensional points; higher dimensions get defaults.
- $axes\{2\} = \{-2, 0\}$ - For function 2, plot the maximum value of r_1 (the default) and all higher-dimensional x-points.
- $axes\{3\} = \{1 : 4 : 51, 32, 64\}$ - For function 3, plot every 4-th x_1 point at x_2 point 32, x_3 point 64
- $axes\{4\} = \{0, 2 : 4 : 48, 0\}$ - For function 4, plot every x_1 point , every 4-th x_2 point, and all x_3-points.

Points labelled -1 indicates a default 'typical' point, which is the midpoint. If one uses -2, this is the last point.

Lower dimensions are replaced by corresponding higher dimensions if there are *dimensions* or *axes* that are suppressed. Slices can be taken at any desired point, not just the midpoint. The notation of $axes\{1\} = \{6 : 3 : 81\}$, is used to modify the starting, interval, and finishing points for complete control on the plot points.

The graphics results depend on the resulting **effective** dimension, which is equal to the actual input data dimension unless there is an *axes* suppression, described above. Since the plot has to include a data axis, the plot itself will usually have an extra data axis.

One can plot only three axes directly using standard graphics tools. The strategy to deal with the higher effective dimensionality is as follows. For simplicity, "time" is used to label the first effective dimension, although in fact any first dimension is possible:

dimensions = 1 For one lattice dimension, a 2D plot of observable *vs t* is plotted, with data at each lattice point in time. Exact results, error bars and sampling error bounds are included if available.

dimensions = 2 For two lattice dimensions, a 3D image of observable *vs x,t* is plotted. A movie of distinct 2D graphic plots is also possible. Otherwise, a slice through $x = 0$ is used tp reduce the lattice dimension to 1.

dimensions = 3 For three lattice dimensions, if *images* > 1, a movie of distinct 3D graphic images of observables are plotted as *images* slices versus the first plot dimension. Otherwise, a slice through the chosen point, is used at the highest dimension to reduce the lattice dimension to 2.

dimensions = 4,5.. For higher lattice dimensions, a slice through a chosen point, or the default midpoint is used to reduce the lattice dimension to 3.

As explained above, in addition to graphs versus x_1 the **xGRAPH** function can generate *images* (3D) and *transverse* (2D) plots at specified points, up to a maximum given by the number of points specified. The number of these can be individually specified for each graph number. The images available are specified as *imagetype*= $1, \ldots 4$, giving:

1. 3D perspective plots (Matlab *surf* - the default)
2. 2D filled color plots (Matlab *contourf*)
3. contour plots (Matlab *contour*)
4. pseudo-color plots (Matlab *pcolor*)

Error bars, sampling errors and multiple lines for comparisons are only graphed for 2D plots. Error-bars are not plotted when they are below a user-specified size, with a default of 1% of the maximum range, to improve graphics quality. Higher dimensional graphs do not output error-bar data, but they are still recorded in the data files.

10.8.12. Probabilities and parametric plots

Probability data can be input and plotted like any other data. It is typically generated from simulation programs using the *binranges* data for binning. It is plotted like any other graph, with any dimension, except that the total dimension is extended by the number of variables or lines in the *observe* function.

10.8.13. Chi-squared plots

In addition the program can make a χ^2 plot, which is a plot of the χ^2 comparison with a comparison probability density against space and/or time. This allows a test of the simulated data against a known target probability distribution, provided that the following input data conditions are satisfied:

- The input data dimension exceeds the p.*dimensions* parameter,
- The switch p.*chisqplot* is set to 1or 2, and
- The input data includes comparison function data.

The χ^2 plots, depending on *p.chisqplot* are:

1. a plot of χ^2 and k, where k is the number of valid data points,

2. a plot of $\sqrt{2\chi^2}$ and $\sqrt{2k-1}$, which should have a unit variance.

Here, for one point in space and time, with m bins, N_j counts per bin and E_j expected counts:

$$\chi^2 = \sum_{j=1}^{m} \frac{(N_j - E_j)^2}{E_j}. \tag{10.2}$$

The number k is the number of valid counts, with $N_j, E_j > mincount$. This is partly determined from the requirement that the probability count data per bin is greater than the *p.mincount* parameter. The default is set to give a number of samples > 10. The program prints a summary that sums over of all the χ^2 data.

The $p.scale\{n\}$ parameter gives the number of counts per bin at unit probability density. This is needed to set the scale of the χ^2 results, ie, $N_j = scale\{n\} \times p_j$, where p_j is the probability density that is compared and plotted in the simulation data. Note that a uniform bin size is assumed here, to give a uniform scaling.

10.8.14. Comparisons with variances

It can be useful to compare two probability distributions with different variances. For one point in space and time, with m bins, p_j probability density and e_j expected probability density,

$$\chi^2 = \sum_{j=1}^{m} \frac{(p_j - e_j)^2}{\sigma_j^2 + \sigma_{e,j}^2}. \tag{10.3}$$

In this case, σ_j^2 and $\sigma_{e,j}^2$ are the sampling errors in the simulation data and comparison data, so that built-in error fields in the data are used to work out the χ^2 results. This option is chosen if $p.scale\{n\} = 0$, and the cutoff for the data is then specified so that $p_j, e_j > p.cutoffs\{n\}$. This only has a χ^2 distribution if points are independent.

10.8.15. Maximum likelihood

It is also possible to plot the G^2 or maximum likelihood plot of the data, which is an alternative means to compare distributions, where

$$G^2 = 2\sum_{j=1}^{m} N_j \ln\left(N_j/E_j\right). \tag{10.4}$$

The expected values E_j are automatically scaled so that $\sum N_j = \sum E_j$,with the same minimum count cutoff that is used for the χ^2 data. The result is similar to the χ^2 results. It is obtained if p.*gsqplot* is set to 1 or 2 and requires for the input that $p.scale\{n\} > 0$. It is sometimes regarded as a preferred method for comparisons.

10.8.16. Parametric plots

Any input dataset can be converted to a parametric plot, where a second data input is plotted along the horizontal axis instead of the time coordinate. It is also possible to substitute a second data input for the x-axis data if a parametric plot in space is required instead. This allows visualization of how one type of data changes as a function of a second type of data input.

The two datasets that are plotted must have the same number of lines, that is, the first index range should be the same, in order that multiple lines can be compared. This is achieved where required using the *p.scatters* input in the simulation code. The details of the parametric plot are specified using the input:

$$p.parametric\{n\} = [n1, p2] \tag{10.5}$$

Here n is the graph number which is plotted, and must correspond to an input dataset. The number $n1$ is the graph number of the observable that is plotted on the horizontal axis, ignoring functional transformations. The second number is the axis number where the parametric value is substituted, which can be the time (axis 1) or the x-coordinate (axis 2), if present.

In all cases the vertical axis is used to plot the original data. The specified horizontal axis is used for the parametric variable. Only vertical error-bars are available. An example is given in xAMPLES/SDE_1/SHO, which is a noise-driven harmonic oscillator, with several lines plotted of x vs y.

10.9. xGRAPH Parameter reference

10.9.1. axes{n}

Default: {*0,0,0,..*}

Gives the axis points plotted for the n-th plotted function, in each dimension. Each entry value is a vector range for a particular plot and dimension. Thus, *p = 5* gives the fifth point only, and a vector input *p = 1:4:41* plots every fourth point. Single points generate graphics projections, allowing the other dimensions to be plotted. Zero or negative values are shorthand. For example, *p = -1* generates a default point at the midpoint, *p = -2* the endpoint, and *p = 0* is the default value that gives the vector for the every axis point. For each graph type, i.e. *n=1,..graphs* the axes can be individually specified in each dimension, *d=1,..dimension*s. If more than three axes are specified to be vectors, only the first three are used, and others are set to default values in the plots.

Example: *p.axes{4}* = {*1:2:10,0,0,-1*}

10.9.2. diffplot{n}

Default: *0*

Differences are plotted as a comparison dashed line on $2D$ plots as a default. Otherwise, a separate difference plot is obtained which is unnormalized (*diffplot = 1)*, or normalized (*diffplot = 2)* by the total RMS errors. If *diffplot = 3*, the comparison data is plotted directly as an additional graph.

Example: *p.diffplot{3} = 2*

10.9.3. errors

Default: *0*

Indicates if the last index in the graphics input data arrays is used for error-bars and/or comparisons. Should be set to zero if there is no error or comparison data. If non-zero, this will give the highest last index used for errors. The standard *xsim* output sets $p.errors = 3$ automatically. As a special case, $p.errors = 1$ is used to indicate that there is comparison data but no error data.

If $p.errors > 0$, the data indexed up to $p.errors$ gives the data, then a maximum of two types of error bars. Up to three further index values, up to $p.errors+3$, are available to index all comparison data and its error fields. The maximum last index value used is 6.

Example: *p.errors = 2*

10.9.4. esample{n}

Default: *1*

This sets the type and size of sampling errors that are plotted. If *esample = 0*, no sampling error lines are plotted, just the mean. If $esample = -n$, $\pm n\sigma$ sampling errors are included in the error-bars. If $esample = n$, separate upper and lower $\pm n\sigma$ sampling error lines are plotted. In both cases, the magnitude of esample sets the number of standard deviations used.

Example: *p.esample{3} = -1*

10.9.5. font{n}

Default: *18*

This sets the default font sizes for the graph labels, indexed by graph. This can be changed per graph.

Example: *p.font{4}=18*

10.9.6. functions

Default: number of functional transformations

This gives the maximum number of output graph functions and is available to restrict graphical output. The default is the length of the cell array of input data. Normally, the default will be used.

Example: *p.functions = 10*

10.9.7. glabels{n}

Default: *xlabels* or *klabels*

Graph-dependent labels for the independent variable labels. This is a nested cell array with first dimension of *graphs* and second dimension of *dimension*s. This is used to replace the global values of *xlabels* or *klabels* if the axis labels change from graph to graph, for example, if the coordinates have a functional transform. These can be set for an individual coordinate on one graph if needed.

Example: *p.glabels{4}{2} = 'x^2'*

10.9.8. graphs

Default: observables to plot

This gives the observables to plot. The default is a vector of indices from one to the length of the cell array of observe functions. Normally not initialized, as the default is used. Mostly used to reduce graphical output on a long file.

Example: *p.graphs = 10*

10.9.9. gtransforms{n}

Default: [0,0,...]

This switch specifies the Fourier transformed graphs and axes for graphics labeling. Automatically equal to *ftransforms* if from an earlier xSIM input, but can be changed. If altered for a given graph, all the axis Fourier switches should be reset. This is ignored if there is no *dimensions* setting to indicate space dimensions.

Example: *p.gtransforms{1} = [0,0,1]*

10.9.10. headers{n}

Default: *”*

This is a string variable giving the graph headers for each type of function plotted. The default value is an empty string. Otherwise, the header string that is input is used. Either is combined with the simulation name and a graph number to identify the graph. This is used to include simulation headers to identify graphs in simulation outputs. Graph headers may not be needed in a final published result. For this, either edit the graph, or use a space to make plot headers blank: *p.headers*{*n*} = ’ ’, or *p.name* = ’ ’ .

Example: *p.headers*{*n*} = *’my_graph_header’*

10.9.11. images{n}

Default: *0*

This is the number of 3D, transverse o-x-y images plotted as discrete time slices. Only valid if the input data dimension is greater than 2. If present, the coordinates not plotted are set to their central value when plotting the transverse images. This input should have a value from zero up to a maximum value of the number of plotted points. It has a vector length equal to *graphs.*

Example: *p.images*{*4*} = *5*

10.9.12. imagetype{n}

Default: *1*

This is the type of transverse o-x-y movie images plotted. It has a vector length equal to *graphs.*

- *imagetype* = *1* gives a perspective surface plot
- *imagetype* = *2*, gives a 2D plot with colors
- *imagetype* = 3 gives a contour plot with 10 equally spaced contours
- *imagetype* = 4 gives a pseudo-color map

Example: *p.imagetype*{*n*} = *1, 2, 3, 4*

10.9.13. klabels

Default: {*’\omega’, ’k_x’, ’k_y’, ’k_z’*}“ *or* “{*’k_1’, ’k_2’, ’k_3’, ’k_4’,...*}

Labels for the graph axis Fourier transform labels, vector length of *dimension*s. The numerical labeling default is used when the “*p.numberaxis*“ option is set. Note, these are typeset in Latex mathematics mode! When changing from the default values, all the required new labels must be set.

Example: *p.klabels*= {*’\Omega’, ’K_x’, ’K_y’,*}

10.9.14. legends{n}

Default: {",",}

Graph-dependent legends, specified as a nested cell array of strings for each line.

Example: *p.legends{n} = {labels(1), ..., labels(lines)}*

10.9.15. limits{n}

Default: {*0,0,0,0; ...*}

Graph-dependent limits specified as a cell array with dimension *graphs*. Each entry is a cell array of graph limits indexed by the dimension, starting from $d = 1$ for the time dimension. The limits are vectors, indexed as 1,2 for the lower and upper plot limits. This is useful if the limits required change from graph to graph. If an automatic limit is required for either the upper or lower limit, it is set to *inf*.

An invalid, scalar or empty limit vector, like [0,0] or 0 or [] is ignored, and an automatic graph limit is used.

Example: *p.limits{n} = {[t1,t2],[x1,x2],[y1,y2] ...,}*

10.9.16. linestyle{n}

Default: {*'-k','--k',':k','-.k','-ok','--ok',':ok','-.ok','-+k','--+k'*}

Line types for each line in every two-dimensional graph plotted. If a given line on a two-dimensional line is to be removed completely, set the relevant line-style to zero. For example, to remove the first line from graph 3, set p.linestyle{3} ={0}. This is useful when generating and changing graphics output from a saved data file. The linestyle uses Matlab terminology. It allows setting the line pattern, marker symbols and color for every line. The default lines are black (*'k'*), but any other color can be used instead.

The specifiers must be chosen from the list below, eg, '-ok', although the marker can be omitted if not required.

- Line patterns: '-' (solid), '–' (dashed), ':' (dotted) ,'-.' (dash-dot)
- Marker symbols: '+','o','*','.','x','s','d','^','v','>','<','p'
- Colors: 'r','g','b','c','m','y','k','w'

Example: *p.linestyle{4} = {'-k','--ok',':g','-.b',}*

10.9.17. linewidth{n}

Default: 0.5

Line width for plotted lines in two-dimensional graphs. For example, to make the lines wider in graph 3, set p.linewidth{3} =1. This is useful for changing graphics output appearance if the default lines are too thin.

Example: *p.linewidth{n} = 1*

10.9.18. minbar{n}

Default: {*0.01, ...*}

This is the minimum relative error-bar that is plotted. Set to a large value to suppress unwanted error-bars, although its best not to ignore the error-bar information! This can be changed per graph.

Example: *p.minbar{n} = 0*

10.9.19. name

Default: ''

Name used to label simulation graphs, usually corresponding to the equation or problem solved. This can be removed from individual graphs by using *headers{n}* equal to a single blank space. The default is a null string. To remove all headers globally, set *name* equal to a single blank space: *name = ' '*.

Example: *p.name = 'Wiener process simulation'*

10.9.20. olabels{n}

Default: *'a'*

Cell array of labels for the graph axis observables and functions. These are text labels that are used on the graph axes. The default value is *'a_1'* if the default observable is used, otherwise it is blank. This is overwritten by any subsequent label input when the graphics program is run:

Example: *p.olabels{4} = 'v'*

10.9.21. parametric{n}

Default: *[0,0]*

Cell array that defines parametric plots, for each graph number. The first number is the graph number of the alternative observable plotted on the horizontal axis. The second number is the axis number where the parametric value is substituted, which can be the time (axis 1) or the x-coordinate (axis 2), if present.

If both are zero, the plot against an independent space-time coordinate is calculated as usual. If nonzero, a parametric plot is made for two-dimensional plots. In all cases the vertical axis is used to plot the original data. The specified horizontal axis is used for the parametric variable. Only vertical error-bars are available. Can be usefully combined with *scatters{n}* to plot individual trajectories, but the number of scatters should be the same in each of the two graphs that are parametrically plotted against each other.

Example: *p.parametric{n} = [p1,p2] >= 0*

10.9.22. pdimension{n}

Default: *3*

This is the maximum plotted space-time dimension for each plotted quantity. The purpose is eliminate unwanted graphs. For example, it is useful to reduce the maximum dimension when averaging in space. Higher dimensional graphs are not needed, as the data is duplicated. Averaging can be useful for checking conservation laws, or for averaging over homogeneous data to reduce sampling errors. All graphs are suppressed if it is set to zero. Any three dimensions can be chosen to be plotted, using the *axes* parameter to suppress the unwanted data points in other dimensions.

Example: *p.pdimension{4} = 2*

10.9.23. saveeps

Default: 0

If set to 1, all plots are saved to the current folder as .eps files, numbered consecutively. It is best to use the *close all* command first to remove unwanted displayed xFIGURES, before running *xgraph* with this option.

Example: *p.saveeps =1*

10.9.24. savefig

Default: 0

If set to 1, all plots are saved to the current folder as .fig files, numbered consecutively. It is best to use the *close all* command first to remove unwanted displayed xFIGURES, before running *xgraph* with this option.

Example: *p.savefig =1*

10.9.25. transverse{n}

Default: *0*

This is the number of 2D transverse images plotted as discrete time slices. Only valid if *dimensions* is greater than 2. If present, the y, z-coordinates are set to their central values when plotting transverse images. Each element can be from 0 up to the number of plotted time-points. The cell array has a vector length equal to *graphs*.

Example: *p.transverse{n}= 6*

10.9.26. verbose

Default: 0

Print flag for output information while running xGRAPH. Print options are:

- Minimal if *verbose = -1*: Prints just the start-up time and hard error messages
- Brief if *verbose = 0*: Additionally prints the final, total chi-squared errors where present
- Informative if *verbose = 1*: Also prints the graph progress indicators
- Full if *verbose = 2*: Prints everything including the internal parameter structure data.

In summary, if *verbose = 0*, most output is suppressed except the final data, *verbose = 1* displays a progress report, and *verbose = 2* additionally generates a readable summary of the graphics parameter input.

Example: *p.verbose = 0*

10.9.27. xlabels

Default: {*'t', 'x', 'y', 'z'*} or {*'x_1', 'x_2', 'x_3', 'x_4'*,...}

Global labels for the independent variable labels, vector length equal to *dimension*s. The numerical labeling default is used when the *numberaxis* option is true. These are typeset in Latex mathematics mode. When changing from the default values, all the required new labels must be set.

Example: *p.xlabels* = {*'tau'*}

10.9.28. gfunction{n} (d,p)

This is a cell array of graphics function handles. Use when a graph is needed that is a functional transformation of the observed averages. The default value generates the *n-th* graph *data* array directly from the *n-th* input *data*. The input is the data cell array for all the graphs in the current sequence number with their graph parameters x, and the output is the *n-th* data array that is plotted.

An arbitrary number of functions of these observables can be plotted, including vector observables. The input to graphics functions is the observed data averages or functions of averages in a given sequence, each stored in a cell array $d\{n\}(\ell, \mathbf{j}, c)$. If there are more graphics functions than input data cells, this generate additional data for plotting.

10.9.29. xfunctions{n} {nd} (ax,p)

This is a nested cell array of axis transformations. Use when a graph is needed with an axis that is a function of the original axes. The input is the original axis coordinates, and the output is the new coordinate set. The default value generates the input axes. Called as *xfunctions{n}{nd}(ax,p)* for the *n*-th graph and axis direction *dir*, where *ax* is a vector of coordinates for that axis.There is one graphics function for each separate graph dimension or axis. The default value is the coordinate vector *xk{nd}* stored in the input parameter structure p, or else the relevant index if *xk{nd}* is omitted.

11. Examples and batch testing

A variety of examples are given in the xAMPLES folder distributed with xSPDE. These can all be run using *Batchtest.m*, which has a typical runtime of $50 - 100s$, and runs 35 different case studies. This shows your distribution is intact. All the graphs produced are deleted. It lists the different examples available, some of which are given below.

The batch testing code will run each different example sequentially. It prints the RMS relative errors for the step-size, sampling and difference error, as well as the total RMS error combining all three, the chi-square error normalised by the number of points, and the timing. The geometric mean of the 35 RMS total errors is computed as a benchmark.

As Matlab random noise is reproducible with a fixed seed, this geometric mean error is fixed. The total is printed to more than six decimals for verification, and an error is indicated if it varies by a factor of more than $\pm 10^{-3}$. Due to different random noise algorithms used in some Octave versions, the Octave error may vary by up to $\pm 20\%$.

11.1. SDE examples

11.1.1. Kubo

This solves a multiplicative SDE with initial condition $a(0) = 1$ and:

$$\frac{\partial a}{\partial t} = iaw(t)\,. \tag{11.1}$$

The function uses the RK4 algorithm together with both vector and series ensembles, then stores the computed averages with a comparison of the variance and an exact solution,

$$\langle a^n \rangle = e^{-tn^2/2}. \tag{11.2}$$

```
function [e] = Kubo()
p.name = 'Kubo oscillator';
p.ensembles = [1000,8];
p.method = @RK4;
p.initial = @(w,p) 1;
p.deriv = @(a,w,p) 1i*w.*a(1,:)  ;
p.file = 'Kubo.mat';
p.observe{2} = @(a,p) a.^2;
p.olabels{2} = {'<a^2>'};
p.compare = {@(p) exp(-p.t/2),@(p) exp(-2*p.t)};
e = xsim(p);
p2.name = 'Kubo oscillator edited title';
xgraph(p.file,p2);
end
```

Notes

- The algorithm is changed from the default to RK4.
- The data is stored to 'Kubo.mat'.
- This is re-read and edited using a second parameter structure, p2.

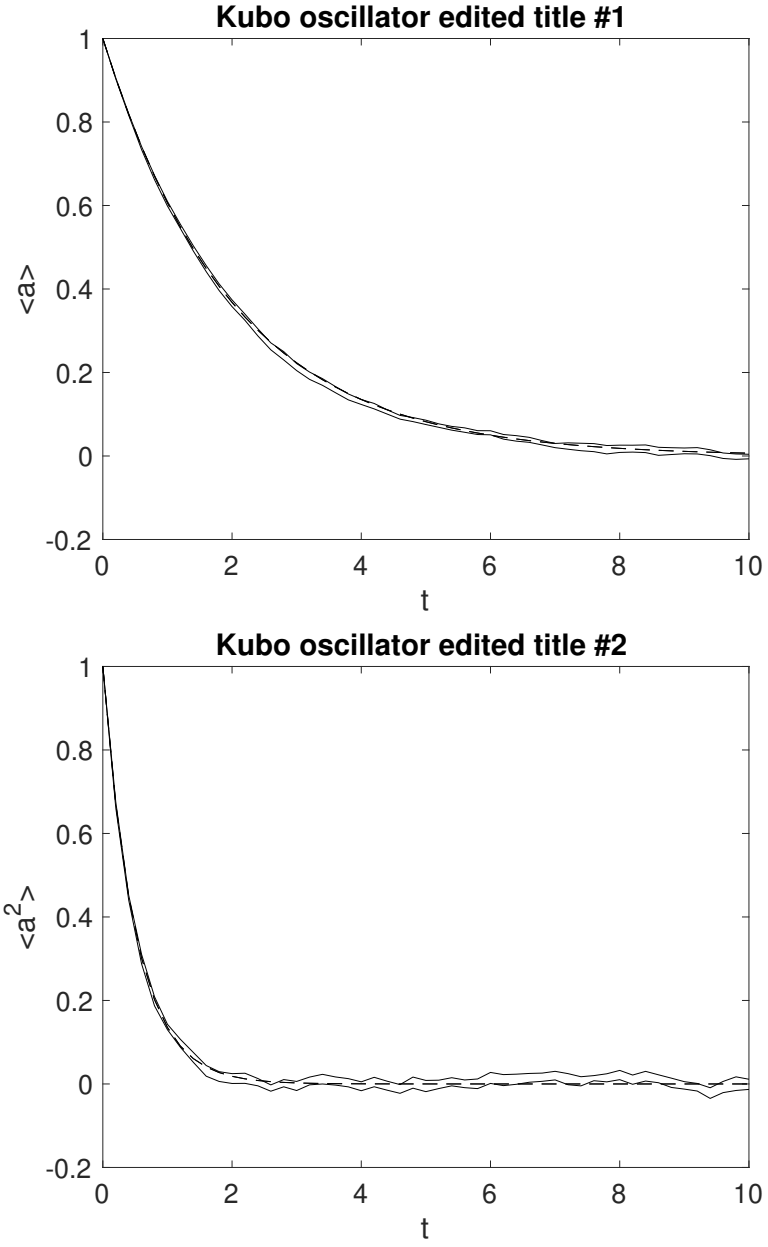

Figure 11.1.: *Example: Kubo oscillator. The graph shows the sampling error-bars as two parallel lines. The discretization error-bars are less than the minimum, and are not shown.*

11.1.2. Loss/Gain with noise

This solves an SDE with a complex Gaussian distributed initial condition having $\left\langle |a(0)|^2 \right\rangle = 1$ and a sequence of SDE equations, such that

$$\frac{\partial a}{\partial t} = \begin{cases} -a + w_1(t) + iw_2(t) & 0 < t < 4 \\ a + w_1(t) + iw_2(t) & 4 < t < 8 \end{cases}. \tag{11.3}$$

The computed variance is compared with an exact solution,

$$\left\langle a^2 \right\rangle = \begin{cases} 1 & 0 < t < 4 \\ 2e^{2(t-4)t} - 1 & 4 < t < 8 \end{cases}. \tag{11.4}$$

.

```
function [e] = Gain()
p.name = 'Loss with noise';
p.ranges = 4;
p.noises = [2,0];
p.ensembles = [10000,1,10];
p.initial = @(w,~) (w(1,:)+1i*w(2,:))/sqrt(2);
p.deriv = @(a,w,p) -a + w(1,:)+1i*w(2,:);
p.observe = {@(a,~) a.*conj(a)};
p.olabels = {'|a|^2'};
p.compare = {@(p) 1};
p2 = p;
p2.steps = 2;
p2.name = 'Gain with noise';
p2.deriv = @(a,w,~) a + w(1,:)+1i*w(2,:);
p2.compare = {@(p) 2*exp(2*(p.t-4))-1};
e = xspde({p,p2});
end
```

Notes

- Low and high level parallel ensembles optimize use of multi-core vector hardware.
- Two distinct simulations are run in series, with a change in the equation.
- The simulation name is changed in sequence 2, to distinguish the graphical outputs

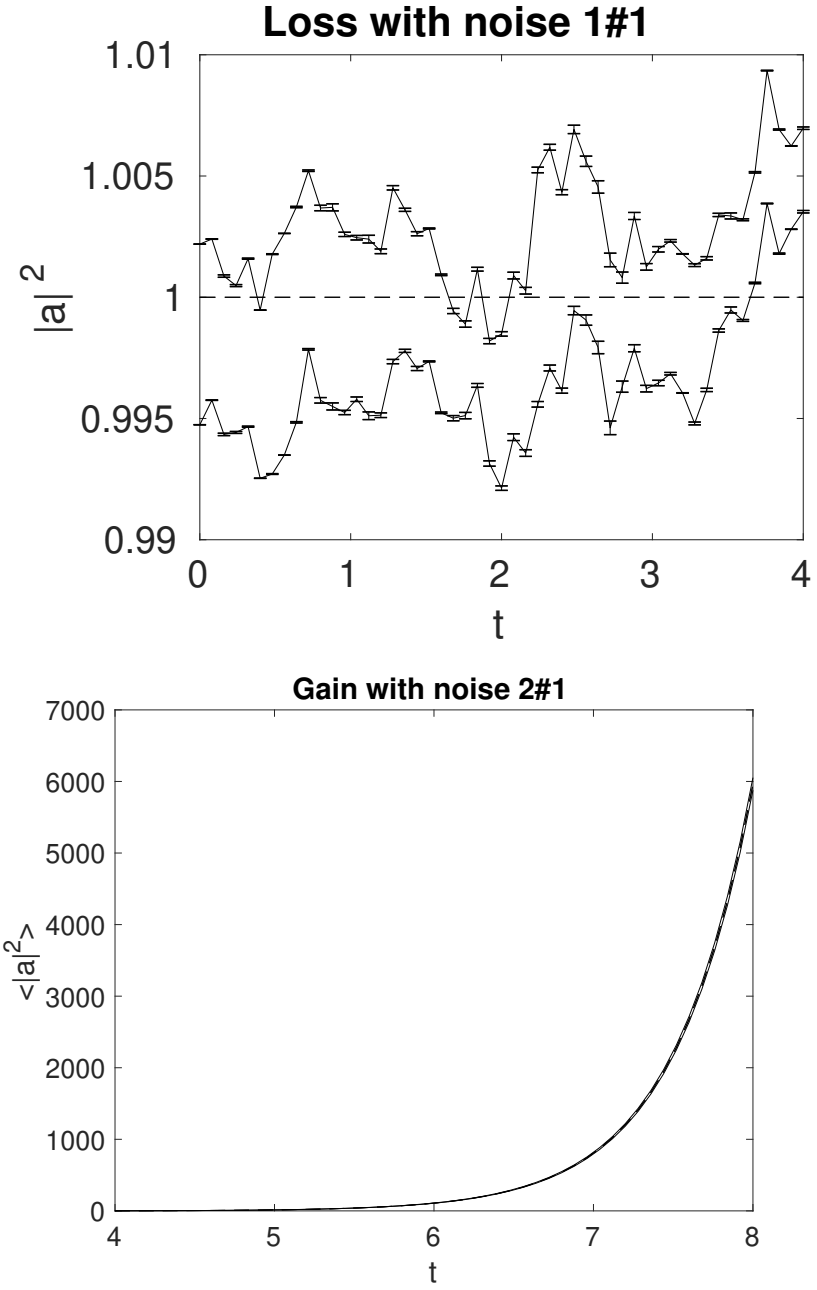

Figure 11.2.: *Top figure: amplitude squared with loss balanced by noise. Bottom figure, amplitude squared with gain. Graphs show excellent agreement with theory up to the sampling errors of less than* ± 0.005 *in the initial phase, shown by the parallel lines, with step errors of order* ± 0.001 *indicated by error-bars.*

11.2. Spectral examples

11.2.1. Equilibrium

This solves an SDE with a complex Gaussian initial condition having $\left\langle |a(0)|^2 \right\rangle = 1$ and:

$$\frac{\partial a}{\partial t} = -a + w_1(t) + iw_2(t)\,. \tag{11.5}$$

The equation is such that the initial distribution is also the equilibrium probability distribution. The computed ordinary and spectral variances are compared with exact solutions and graphed, where

$$\lim_{t\to\infty} \left\langle |a(t)|^2 \right\rangle = 1.$$
$$\left\langle |a(\omega)|^2 \right\rangle = \frac{T}{\pi\left(1+\omega^2\right)}. \tag{11.6}$$

```
function [e] = Equilibrium()
p.name = 'Equilibrium spectrum';
p.points = 101;
p.ranges = 100;
p.seed = 241;
p.noises = [2,0];
p.ensembles = [100,5];
p.initial = @(w,~) (w(1,:)+1i*w(2,:))/sqrt(2);
p.deriv = @(a,w,~) -a + w(1,:)+1i*w(2,:);
p.observe{1} = @(a,~) a.*conj(a);
p.observe{2} = @(a,~) a.*conj(a);
p.transforms = {0,1};
p.olabels = {'|a(t)|^2','|a(\omega)|^2'};
p.compare = {@(p) 1, @(p)p.ranges(1)./(pi*(1+p.w.^2))};
e = xspde(p);
end
```

Notes

- A fixed random seed is input using the *p.seed* parameter.
- The *p.transforms* cell array gives a Fourier transform for *p.observe*{*2*} only.
- A small number of ensembles and time-steps is used to improve error visibility.

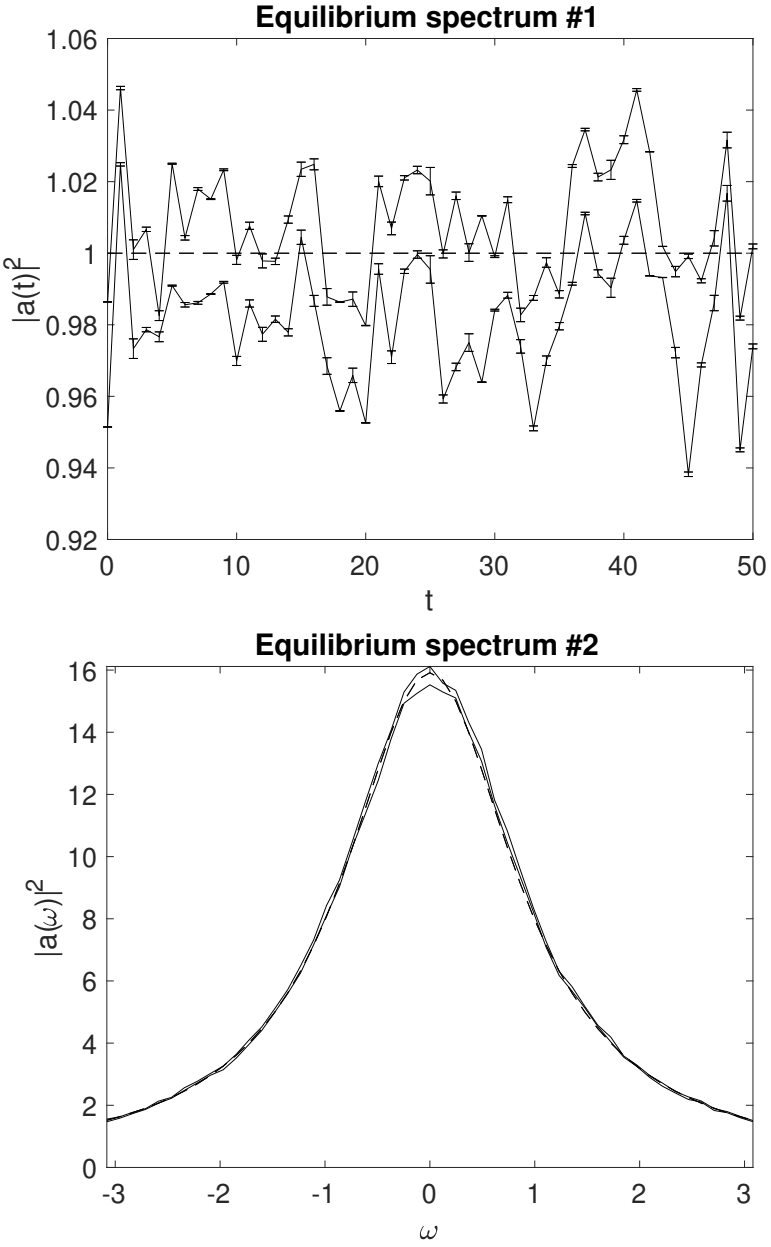

Figure 11.3.: *Top figure: Mean amplitude squared, showing invariant behavior with time, apart from sampling errors. Bottom figure: Mean spectrum as a function of frequency. The dashed lines are exact results, solid lines are upper and lower sampling error bounds* ($\pm\sigma$)*, from sampling the stochastic equations, the error-bars are errors due to the step-size. Error bars are less than the minimum size for graphics display in the bottom figure.*

11.2.2. Quantum

This solves an SDE for a quantum harmonic oscillator in the (truncated) Wigner phase-space calculus. It is initialized as a vacuum state, corresponding to a complex Gaussian initial condition having $\left\langle |a\,(0)|^2 \right\rangle = 1$. It is subject to vacuum noise, here realized by the auxiliary field a_{in}. An output field is given through the input-output relations and is realized by the auxiliary field a_{out}.

$$\begin{aligned} \frac{\partial a}{\partial t} &= -a + \sqrt{2}a_{in}. \\ a_{in} &= \frac{1}{2}\left(w_1(t) + iw_2(t)\right) \\ a_{out} &= \sqrt{2}a - a_{in} \end{aligned} \tag{11.7}$$

The computed spectral variances are compared with exact solutions and graphed, where:

$$\begin{aligned} \frac{2\pi}{T}\left\langle |a\,(\omega)|^2 \right\rangle &= \frac{1}{(1+\omega^2)}. \\ \left\langle |a_{in}\,(\omega)|^2 \right\rangle &= \frac{1}{2} \\ \left\langle |a_{out}\,(\omega)|^2 \right\rangle &= \frac{1}{2}. \end{aligned} \tag{11.8}$$

Notes

- Demonstrates how to include defined fields
- There are 4 steps per point, to give better accuracy due to finite steps
- The observe functions are all transformed, and include defined fields.

```
function e = Quantum()
p.name = 'Quantum harmonic oscillator spectrum';
p.points = 160;
p.steps = 4;
p.ranges = 120;
p.fields = 1;
p.auxfields = 2;
p.noises = 2;
p.ensembles = [400,1,12];
p.initial = @(w,~) (w(1,:)+1i*w(2,:))/(2);
p.a1 = @(w) (w(1,:)+1i*w(2,:))/2;
p.deriv = @(a,w,~) -a(1,:)+sqrt(2)*p.a1(w);
p.define = @(a,w,p) [p.a1(w);sqrt(2)*a(1,:)-p.a1(w)];
T = @(p) p.ranges(1);
p.observe{1} = @(a,p) (2.*pi/T(p))*a(1,:).*conj(a(1,:));
p.observe{2} = @(a,p) (2.*pi/T(p))*a(2,:).*conj(a(2,:));
p.observe{3} = @(a,p) (2.*pi/T(p))*a(3,:).*conj(a(3,:));
p.transforms = {1,1,1};
p.olabels{1} = '|a(\omega)|^2';
p.olabels{2} = '|a_{in}(\omega)|^2';
p.olabels{3} = '|a_{out}(\omega)|^2';
p.compare{1} = @(p) 1./(1+p.w.^2);
p.compare{2} = @(p) 0.5;
p.compare{3} = @(p) 0.5;
e = xspde(p);
end
```

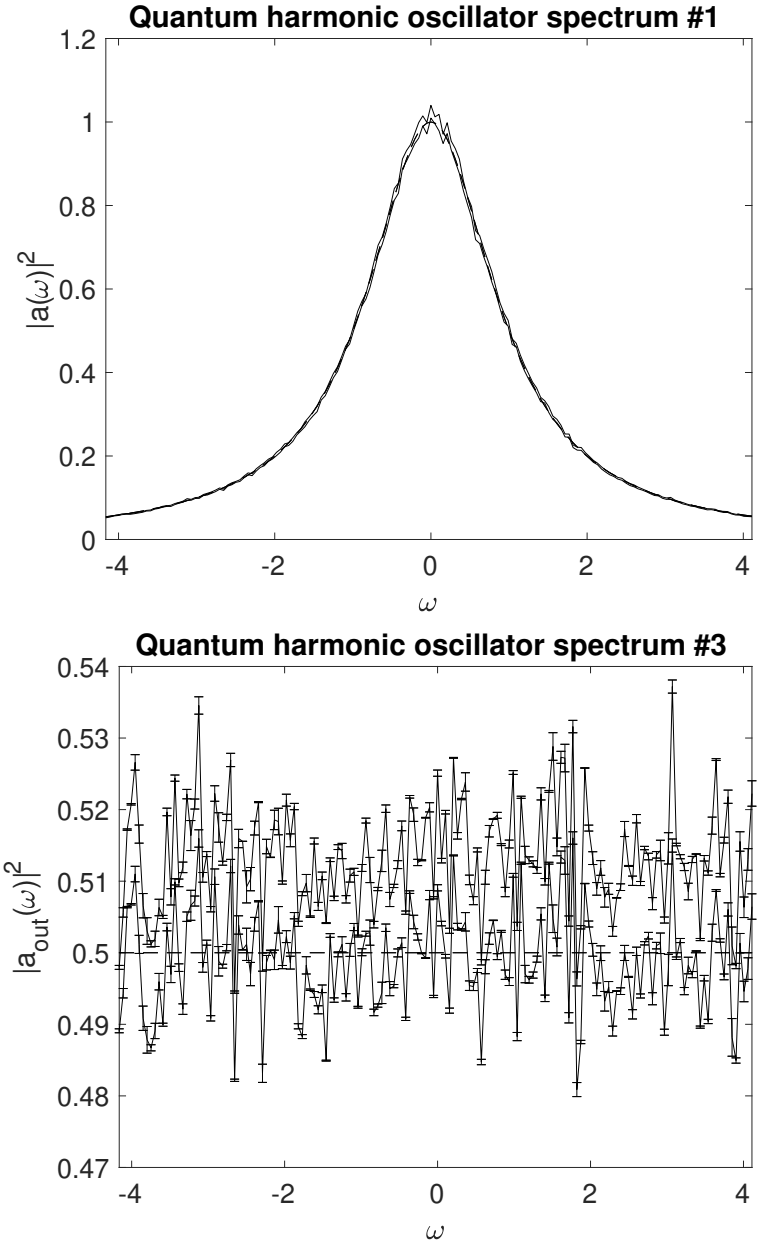

Figure 11.4.: *Top figure: Spectral density of the quantum state. Bottom figure: Spectral density of the output field. The solid lines indicate upper and lower sampling error bounds ($\pm\sigma$), from sampling the stochastic equations. The dashed lines are exact results, the error-bars indicate step-size errors. Error bars are less than the minimum size for display in the top figure.*

11.3. Probability examples

11.3.1. Probability density, Wiener process

Solves an SDE with an initial condition $\langle a(0)\rangle^2 = \frac{1}{4}$ and

$$\dot{a} = w(t)\,. \tag{11.9}$$

Records the probability density and compares this with an exact solution:

$$\begin{aligned} P(x,t) &= \frac{1}{\sqrt{2\pi\sigma^2(t)}} e^{-\frac{x^2}{2\sigma^2(t)}} \\ \sigma^2(t) &= \frac{1}{4} + t\,. \end{aligned} \tag{11.10}$$

Notes

- The script outputs a 3D plot of $P(x,t)$, together with the time evolution of $P(0,t)$
- There are 5 "transverse" plots of transient probabilities at intermediate times.
- Legends are plotted to identify the simulated and the analytic comparison lines.

```
function e = Wienerprob()
p.name = 'Wiener SDE distribution';
p.noises = 1;
p.points = 10;
p.ensembles = [10000,10];
p.initial = @(v,p) v/2;
p.sig = @(p) .25 + p.r{1};
p.deriv = @(a,w,p) w;
p.observe{1} = @(a,p) a;
p.compare{1} = @gaussprob;
p.transverse{1} = 5;
p.olabels{1} = 'P(x)';
p.binranges{1} = {-5:0.25:5};
p.legends{1} = {'Sampled P(x,\tau) \pm \sigma',...
'Exact P(x,\tau)'};
p.xlabels = {'\tau','x'};
e = xspde(p);
end
%
function p = gaussprob(p)
p = exp(-(p.r{2}.^2)./(2*p.sig(p)))./sqrt(2*pi*p.sig(p));
end
```

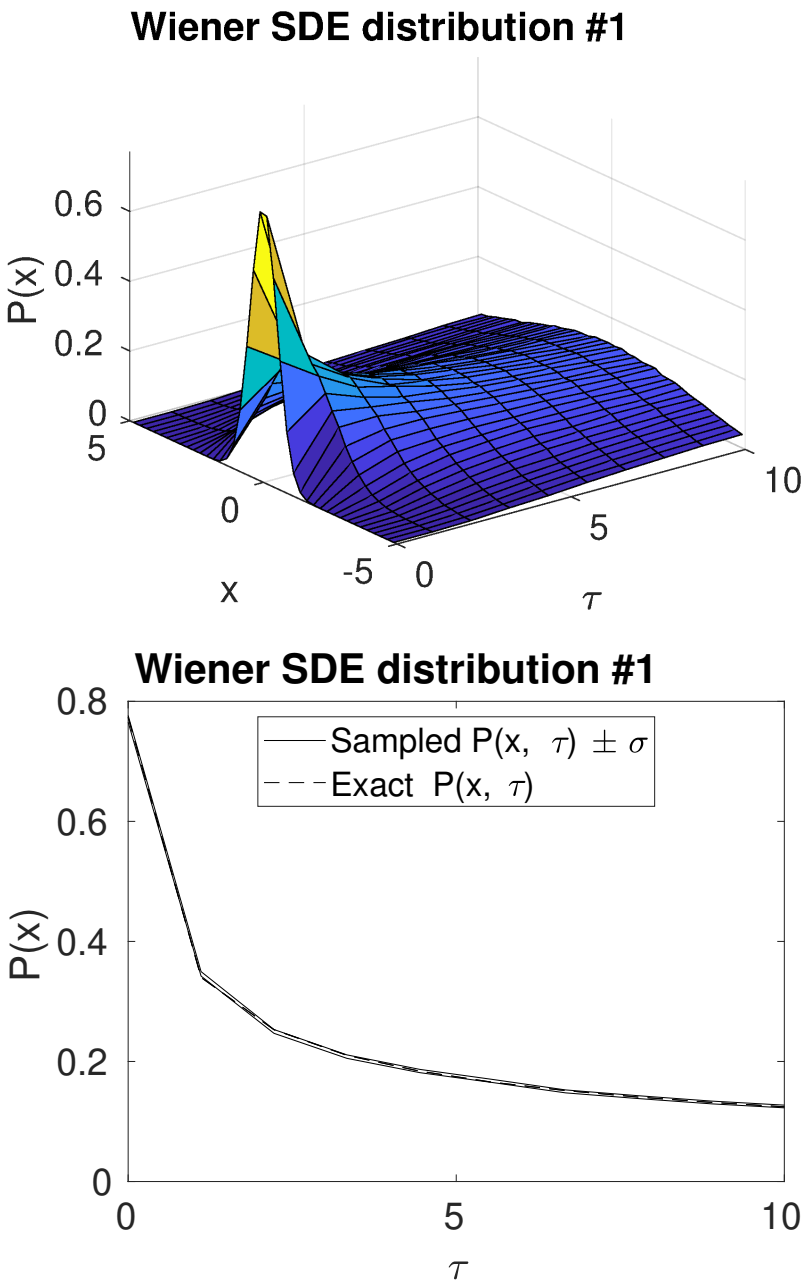

Figure 11.5.: *Top figure: 3D plot of the computed probability density of the simulated Wiener process as a function of time (τ) and "position" (x). Bottom figure: Time evolution of the computed probability density for $x = 0$. The solid lines indicate upper and lower sampling error bounds, while the dashed line indicates theoretical predictions.*

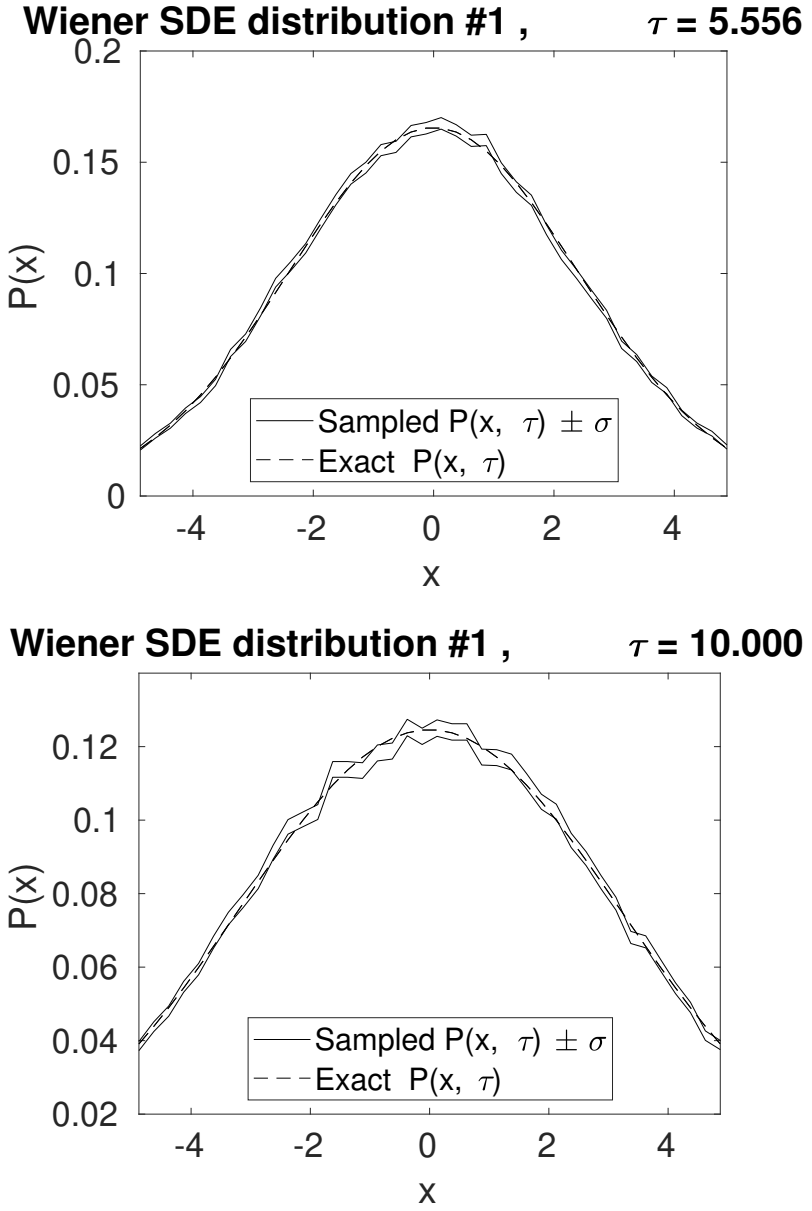

Figure 11.6.: *Top and bottom figure: Computed probability densities of the simulated Wiener process at* $\tau = 5.556$ *and* $\tau = 10$*, respectively. In total, 5 of these transverse plots are generated, however, only 2 are presented here.*

11.4. SPDE examples

11.4.1. Nonlinear Schrodinger equation with Neumann boundary conditions

This solves a (1+1)-dimensional PSDE with an initial condition of $a\left(t=0,x\right)=sech\left(x\right)$ and

$$\frac{\partial a}{\partial t} = i\cdot\left(a\cdot\left(\left|a\right|^2-\frac{1}{2}\right)+\frac{1}{2}\frac{\partial^2 a}{\partial x^2}\right). \tag{11.11}$$

The solution is subject to Neumann boundary conditions with boundary values at zero

$$\frac{\partial a}{\partial x}\left(t,\pm x_m\right) = 0. \tag{11.12}$$

The equation is a deterministic nonlinear Schrodinger equation, which applies to nonlinear optics, Bose-Einstein condensates and plasma physics. The observables are $o_1\equiv\left|a\right|^2$ and $o_2\equiv\int_{-x_m}^{x_m}\left|\frac{\partial}{\partial x}a\right|^2 dx$.

Notes

- The boundary conditions are specified with *p.boundaries{2}*, which is the x-dimension.
- The integration differential dx does not have to be entered, as this is the default.
- Three transverse graphs were specified, but they aren't reproduced here.
- As there is only one field, which is the default, this does not need to be given.
- Since there is no noise, the default integration method was RK4.

```
function [e] = SolitonDerivN()
p.dimensions = 2;
p.points = [101,101];
p.ranges = [10,15];
p.initial = @(v,p) sech(p.x);
p.observe{1} = @(a,p) a.*conj(a);
p.observe{2} = @(a,p) Int(abs(D1(a,2,p)).^2,p);
p.olabels = {'|a|^2','\int |da/dx|^2 dx'};
p.name = 'NLS soliton:spectral method + Neumann';
p.boundaries{2} = [-1,-1];
p.transverse = {3};
p.deriv = @(a,~,p) 1i*a.*(conj(a).*a);
p.linear = @(p) 0.5*1i*(p.Dx.^2-1);
e = xspde(p);
end
```

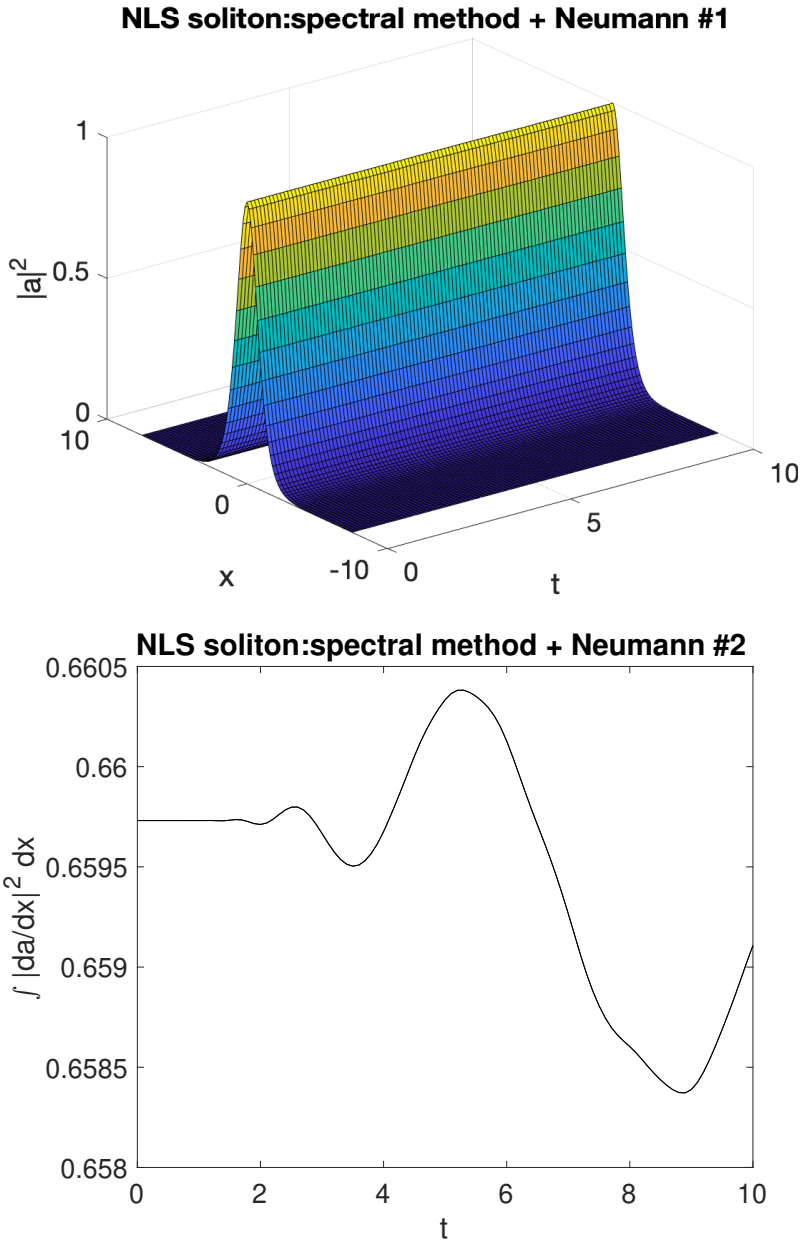

Figure 11.7.: *Top figure: Evolution of the field modulus squared of an NLS soliton with Neumann boundaries.*
Bottom figure: Evolution of the integrated modulus squared of the gradient for an NLS soliton with Neumann boundaries, showing how the reflected fields at the boundaries change the result even though this is not readily visible above.

11.4.2. Planar noise growth

This solves a (1+2)-dimensional PSDE describing the growth of noise in a planar vector field with a diffraction term giving rise to noise dispersion. There are 240 trajectories in the total ensemble. The equation is:

$$\frac{\partial \mathbf{a}}{\partial t} = \frac{i}{2}\left(\frac{\partial^2}{\partial x^2} + \frac{\partial^2}{\partial x^2}\right)\mathbf{a} + \eta\left(t, x\right) . \tag{11.13}$$

The initial conditions are that $\mathbf{a} = \left(\mathbf{v}_x + i\mathbf{v}_y\right)/\sqrt{2}$, where:

$$\left\langle v_i\left(\mathbf{x}\right) v_j\left(\mathbf{x}'\right)\right\rangle = \delta\left(\mathbf{x} - \mathbf{x}'\right)\delta_{ij} \tag{11.14}$$

the noise correlations are that $\eta = \left(\mathbf{w}_x + i\mathbf{w}_y\right)/\sqrt{2}$, where:

$$\left\langle w_i\left(\mathbf{r}\right) w_j\left(\mathbf{r}'\right)\right\rangle = \delta\left(t - t'\right)\delta_{ij}\left(\mathbf{x} - \mathbf{x}'\right) \tag{11.15}$$

The solution has periodic boundary conditions. The noise correlations for the second field are specified in momentum space. As there are no filters specified, the noise terms are delta-correlated in both momentum ($\mathbf{k}$) and in space (x). The exact results for comparison for the correlations within each field are similar in position and momentum space:

$$\begin{aligned}\left\langle \left|a_i\left(t, \mathbf{x}\right)\right|^2\right\rangle &= \left(1 + t\right)/\Delta A_x. \\ \left\langle \left|a_i\left(t, \mathbf{k}\right)\right|^2\right\rangle &= \left(1 + t\right)/\Delta A_k.\end{aligned} \tag{11.16}$$

Here, $\Delta A_{x,k}$ is the area of a lattice cell in space or momentum space respectively. This is $\Delta A_x = 1/49$ for the parameters used here. On integration, the correlation is proportional to N_s, the number of points in the spatial lattice, which is $35^2 = 1225$ for the spatial lattice used here:

$$\int \left\langle \left|a_i\left(t, \mathbf{x}\right)\right|^2\right\rangle d\mathbf{x} = \int \left\langle \left|a_i\left(t, \mathbf{k}\right)\right|^2\right\rangle d\mathbf{k} = N_s\left(1 + t\right). \tag{11.17}$$

Notes

- All three types of ensemble are used
- The much lower sampling error after integration is evident in the graphs
- Spatially resolved graphs show larger sampling errors
- The integration method is mid-point, as it is stochastic.
- Two k-space noises are specified, but they aren't filtered.

- Under these conditions, x-space and k-space noise are identical.

```
function [e] = Planar()
p.name = 'Planar noise growth';
p.dimensions = 3;
p.fields = 2;
p.ranges = [1,5,5];
p.points = 10;
p.noises = [2,2];
p.ensembles = [10,2,12];
p.initial = @Initial;
p.deriv = @D_planar;
p.linear = @Linear;
p.observe{1} = @(a,p) Int(a(1,:).*conj(a(1,:)),p);
p.observe{2} = @(a,p) Int(a(2,:).*conj(a(2,:)),p.dk,p);
p.observe{3} = @(a,p) real(Ave(a(1,:).*conj(a(2,:)),p));
p.observe{4} = @(a,p) a(2,:).*conj(a(2,:));
p.transforms = {[0,0,0],[0,1,1],[0,1,1]};
p.olabels{1} = '<\int|a_1(x)|^2 d^2x>';
p.olabels{2} = '<\int|a_2(k)|^2 d^2k>';
p.olabels{3} = '<< a_1(k)a^*_2(k)>>';
p.olabels{4} = '<|a_2(x)|^2>';
p.compare{1} = @(p) (1+p.t)*p.nspace;
p.compare{2} = @(p) (1+p.t)*p.nspace;
p.compare{3} = @(p) 0.0;
e = xspde(p);
end

function a0 = Initial(v,~)
a0(1,:)  = (v(1,:)+1i*v(2,:))/sqrt(2);
a0(2,:)  = (v(3,:)+1i*v(4,:))/sqrt(2);
end

function da = D_planar(~,w,~) %%Derivatives
da(1,:)  = (w(1,:)+1i*w(2,:))/sqrt(2);
da(2,:)  = (w(3,:)+1i*w(4,:))/sqrt(2);
end

function L = Linear(p)
lap = p.Dx.^2+p.Dy.^2;
L(1,:)  = 1i*0.5*lap(:);
L(2,:)  = 1i*0.5*lap(:);
end
```

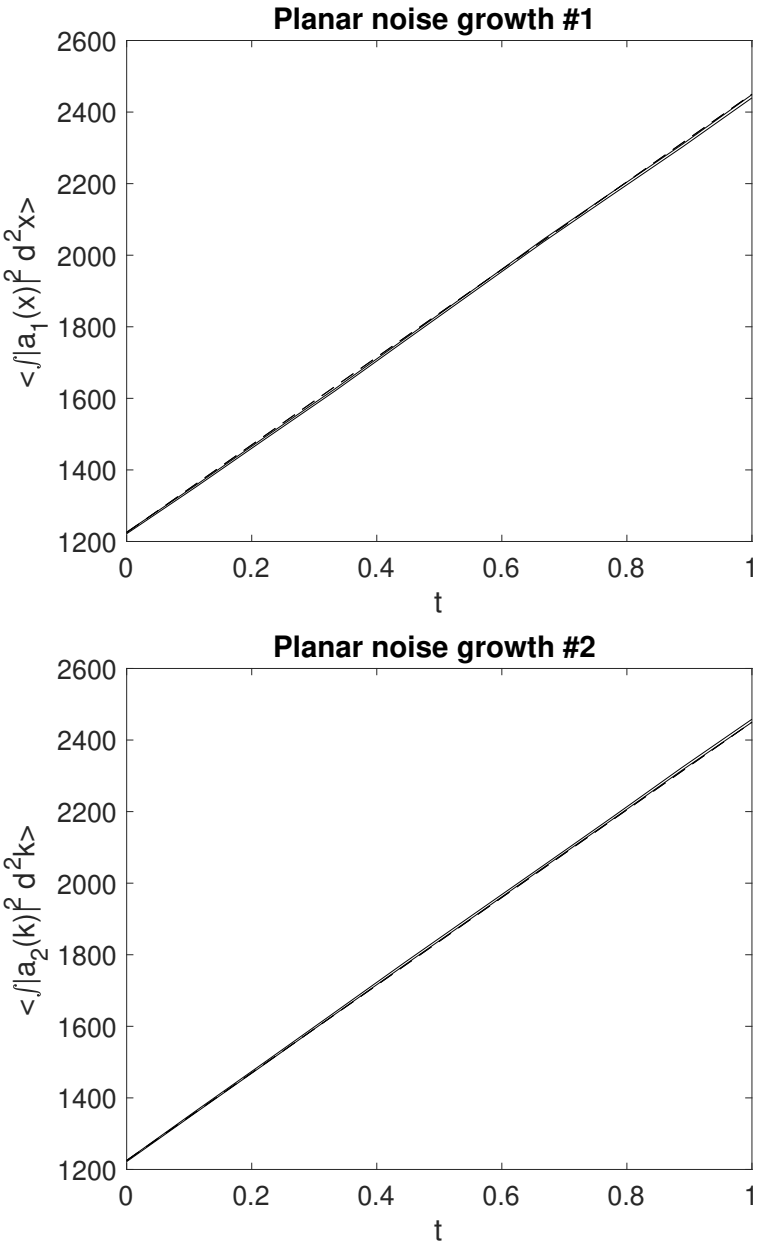

Figure 11.8.: *Top and bottom figure: Time evolution of the integrated modulus square of the first and second field, respectively. The solid lines indicate upper and lower bounds of the stochastic error, which the dashed lines indicate theoretical predictions.*

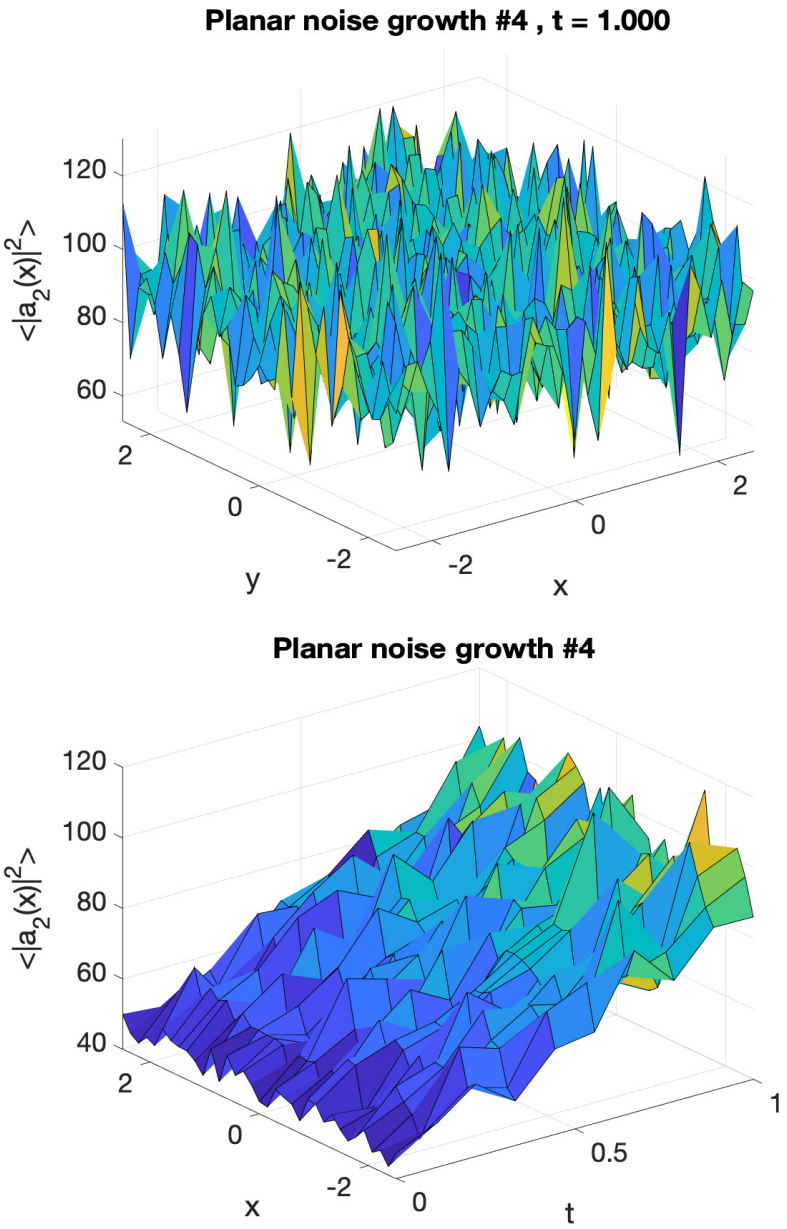

Figure 11.9.: *Top figure: 3D plot of the modulus square of a_2 at $t = 1$ as a function of x and y. Bottom figure: 3D plot of the modulus square of a_2 for $y = 0$ as a function of x and t.*

11.4.3. Gross-Pitaevskii equation with vortex formation

This solves a (1+2)-dimensional PDE called the Gross-Pitaevskii equation. In addition to the standard GPE terms, it includes the vortex forming term $(\mathbf{x} \times \nabla) a$. There is just one ensemble member, to demonstrate how a single trajectory can be imaged. The equation is:

$$\begin{aligned} \frac{\partial a}{\partial t} &= \left(\frac{1}{2} \nabla^2 a - \left\| \left(\left(V(\mathbf{x}) + 200 |a|^2 \right) + 0.6i \cdot (\mathbf{x} \times \nabla) \right) a \right\| \right) \\ V(\mathbf{x}) &= 0.35 \left(x^2 + y^2 \right) \\ \|b(\mathbf{x})\| &= \frac{b(\mathbf{x})}{\int |b|^2 d\mathbf{x}} . \end{aligned} \tag{11.18}$$

Here,$\|\cdot\|$ is the normalized derivative and $\times$ indicates the two-dimensional cross-product. The system is initialized as

$$a(t = 0, \mathbf{x}) = 0.1 \cdot \exp(-V(\mathbf{x})) . \tag{11.19}$$

Notes

- This is a deterministic partial differential equation case
- The 15 intermediate *steps* used are necessary to reduce integration errors
- The trap potential is an inline function, and is not a parameter
- Normalization is used because otherwise particle number is not conserved
- The output includes transverse *images* to show how the vortices develop
- Different *imagetypes* are used to show different 3D features

```
function [e] = GPEvortex2D()
p.name = 'GPEvortex2D';
p.dimensions = 3;
p.fields = 1;
p.points = [50,40,40];
p.ranges = [15,16,16];
p.steps = 15;
g = 200;
om = 0.6;
L = @(a,p) 1i*(p.x.*D1(a,3,p)-p.y.*D1(a,2,p));
V = @(p) 0.35*(p.x.^2+p.y.^2);
p.initial = @(v,p) 0.1*exp(-V(p));
rho = @(a) g*conj(a).*a;
p.deriv = @normda;
p.da1 = @(a,w,p) -a.*(V(p)+rho(a))+om*L(a,p);
p.linear = @(p) 0.5*(p.Dx.^2+p.Dy.^2);
p.observe{1} = @(a,p) a(1,:).*conj(a(1,:));
p.observe{2} = @(a,p) a(1,:).*conj(a(1,:));
p.images = {2,2};
p.imagetype = {1,2};
p.olabels = {'|a|^2','|a|^2'};
e = xspde(p);

function b = normda(a,w,p)
% b = NORMDA(a,z,p) is a normalized derivative
% Takes a derivative and returns a normalized step
b = a+p.da1(a,w,p)*p.dtr;
norm = sqrt(Int(abs(b).^2,p.dx,p));
b = (b./norm-a)/p.dtr;
end
end
```

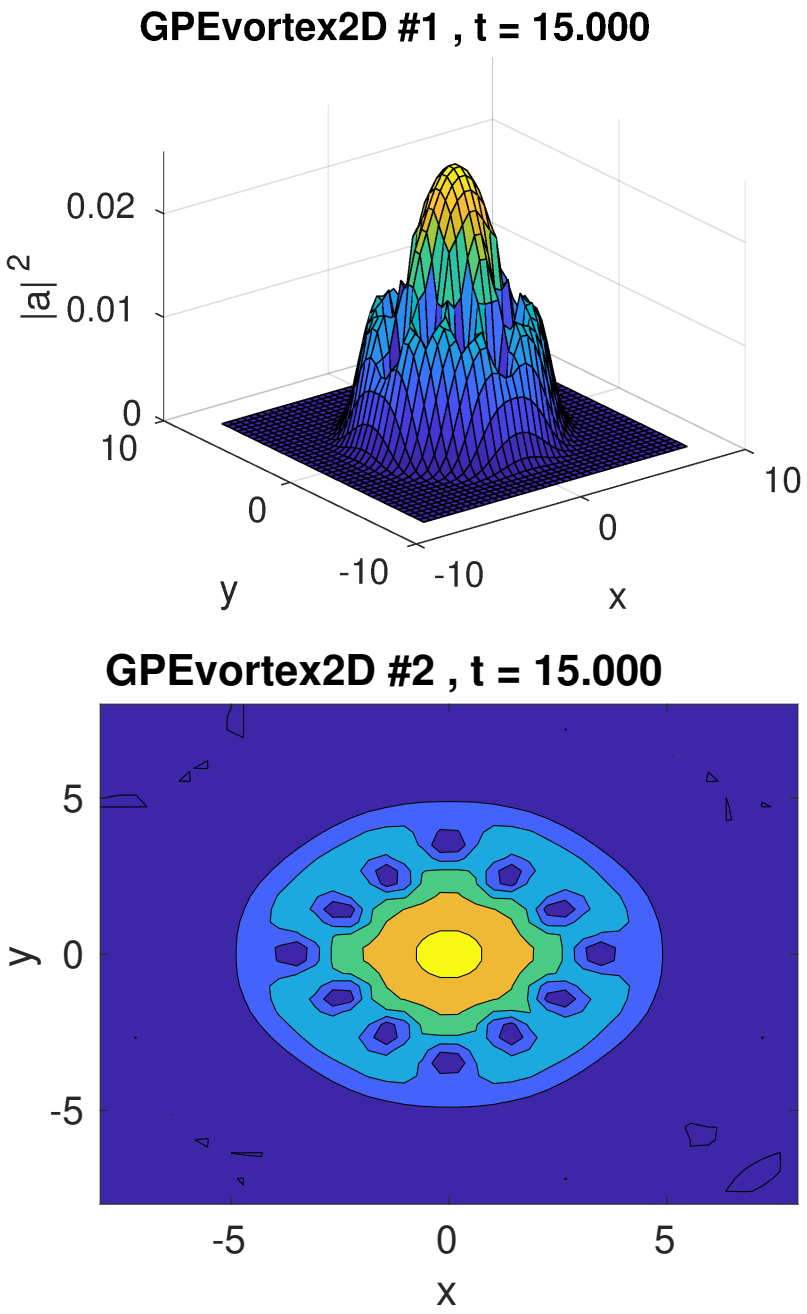

Figure 11.10.: *Top and bottom figure: The computed solution for* $|a|^2$ *at* $t = 15$ *as a function of* x, y *as a 3D plot (top) and as a color map (bottom).*

11.4.4. Heat equation with non-periodic boundaries

This example solves a (1+1)-dimensional PDE with an initial condition of $\mathbf{a}(t=0,x) = \mathbf{f}(x)$ and

$$\frac{\partial \mathbf{a}}{\partial t} = \frac{\partial^2 \mathbf{a}}{\partial x^2}. \tag{11.20}$$

The solution is subject to either periodic boundary conditions or Dirichlet and/or Neumann with boundary values at zero, so that $a(t, \pm x_m) = 0$ or $\partial a/\partial x\,(t, \pm x_m) = 0$. Each component has different combinations of boundary types. Using spectral methods the solutions here are exact, up to round-off errors of order 10^{-15}, and are also much faster than with finite differences, which is demonstrated in the example.

In all cases the grid range is from $x = 0$ to $x = \pi$, and the time duration is from $t = 0$ to $t = 4$. In the examples, the spectral propagation error is reduced by more than 10^{10} and the time is reduced by a factor of 20 compared to the finite-difference methods. The periodic method has boundaries just outside the grid as explained in.

Dirichlet-Dirichlet The exact solution has the form:

$$a = \sum_{n=1}^{2} S_n \sin(nx)\, e^{-n^2 t}. \tag{11.21}$$

Suppose that

$$a(x,0) = 1 - 2x/\pi + 4\sin(x) + \sin(2x), \tag{11.22}$$

and

$$a_x(-\pi/2) = 2 - 4e^{-t} - e^{-4t}$$
$$a_x(\pi/2) = +4e^{-t} + e^{-4t}$$

For this case:

$$a(x,t) = 1 - 2x/\pi + 4\sin(x)\, e^{-t} + \sin(2x)\, e^{-4t}. \tag{11.23}$$

Neumann-Neumann with $a(0) = a(\pi) = 0$, then the exact solution has the form:

$$a = \sum_{n=0}^{\infty} C_n \cos(nx)\, e^{-n^2 t}. \tag{11.24}$$

Suppose that

$$a(x,0) = 5 + 4\cos(x) + \cos(2x), \tag{11.25}$$

For this case:

$$a(x,t) = 5 + 4\cos(x)\, e^{-t} + \cos(2x)\, e^{-4t}. \tag{11.26}$$

Dirichlet-Neumann Here $a(0) = a_x(\pi) = 0$, then the exact solution has the form:

$$a = \sum_{n=1}^{\infty} S_n \sin\left((2n-1)x/2\right) e^{-(2n-1)^2 t/4}. \tag{11.27}$$

Suppose that

$$a(x,0) = 4\sin\left(x/2\right) + \sin\left(3x/2\right), \tag{11.28}$$

For this case:

$$u(x,0) = 4\sin\left(x/2\right) e^{-t/4} + \sin\left(3x/2\right) e^{-9t/4}. \tag{11.29}$$

Neumann-Dirichlet Here $a_x(0) = a(\pi) = 0$, then the general solution has the form:

$$a = \sum_{n=1}^{\infty} C_n \cos\left((2n-1)x/2\right) e^{-(2n-1)^2 t/4}. \tag{11.30}$$

Suppose that

$$a(x,0) = 4\cos\left(x/2\right) + \cos\left(3x/2\right). \tag{11.31}$$

For this case:

$$a(x,t) = 4\cos\left(x/2\right) e^{-t/4} + \cos\left(3x/2\right) e^{-9t/4}. \tag{11.32}$$

Periodic Here $a(0) = a(\epsilon\pi)$, where $\epsilon = N/\left(N-1\right)$ accounts for the periodic boundaries being outside the grid range, then the general solution has the form:

$$\begin{aligned} a = &\sum_{n=1}^{\infty} S_n \sin\left(2nx\right) e^{-4n^2 t/\epsilon^2} \\ &+ \sum_{n=0}^{\infty} C_n \cos\left(2nx\right) e^{-4n^2 t/\epsilon^2}. \end{aligned} \tag{11.33}$$

Suppose that

$$a(x,0) = 2 + \cos\left(2x/\epsilon\right) + \sin\left(4x/\epsilon\right). \tag{11.34}$$

For this case:

$$u(x,0) = 2 + 2\cos\left(2x/\epsilon\right) e^{-4t/\epsilon^2} + \sin\left(4x/\epsilon\right) e^{-16t/\epsilon^2}. \tag{11.35}$$

Notes

- This is another deterministic pde case, although noise can be added
- Different boundary conditions apply to each component
- Sequential integration is used, but the initial condition is just recycled.
- In *p1*, the 40 intermediate *steps* are necessary to reduce finite-difference errors

```
function [e] = Boundaries()
p.dimensions = 2;
p.points = [51,51];
p.order = 0;
p.verbose = 1;
p.fields = 5;
p.ranges = [4,pi];
p.origins = [0,0];
p.initial = @heat_in;
p.observe = {@(a,p) a(1,:),@(a,p) a(2,:),@(a,p) a(3,:)...
@(a,p) a(4,:),@(a,p) a(5,:)};
p.compare = {@heat_1,@heat_2,@heat_3,@heat_4,@heat_5};
p.diffplot = {1,1,1,1,1};
p.olabels = {'a, DD','a, NN','a, DN','a, ND','a, PP'};
p.name = 'Heat test, spectral';
p.boundaries{2}= [1,1;-1,-1;1,-1;-1,1;0,0];
p.linear = @(p) p.Dx.^2;
p1 = p;
p1.linear = @(p) [];
p1.deriv = @(a,w,p) D2(a,2,p);
p1.steps = 40;
p1.transfer = @(~,p,~,~) heat_in(0,p);
p1.name = 'Heat test, finite diffs';
e = xspde({p,p1});
end

function a = heat_in(~,p)
a(1,:)  = 4*sin(p.x)+sin(2*p.x);
a(2,:)  = 5+4*cos(p.x)+cos(2*p.x);
a(3,:)  = 4*sin(p.x/2)+sin(3*p.x/2);
a(4,:)  = 4*cos(p.x/2)+cos(3*p.x/2);
a(5,:)  = 2+cos(2*p.x/1.02)+sin(4*p.x/1.02);
end

function o = heat_1(p)
o = 4*sin(p.x).*exp(-p.t)+sin(2*p.x).*exp(-4*p.t);
end
function o = heat_2(p)
 o = 5+4*cos(p.x).*exp(-p.t)+cos(2*p.x).*exp(-4*p.t);
end
function o = heat_3(p)
 o = 4*sin(p.x/2).*exp(-p.t/4)+sin(3*p.x/2).*exp(-9*p.t/4);
end
function o = heat_4(p)
 o = 4*cos(p.x/2).*exp(-p.t/4)+cos(3*p.x/2).*exp(-9*p.t/4);
end
function o = heat_5(p)
o = 2+cos(2*p.x/1.02).*exp(-4*p.t/1.02^2)+...
sin(4*p.x/1.02).*exp(-16*p.t/1.02^2);
end
```

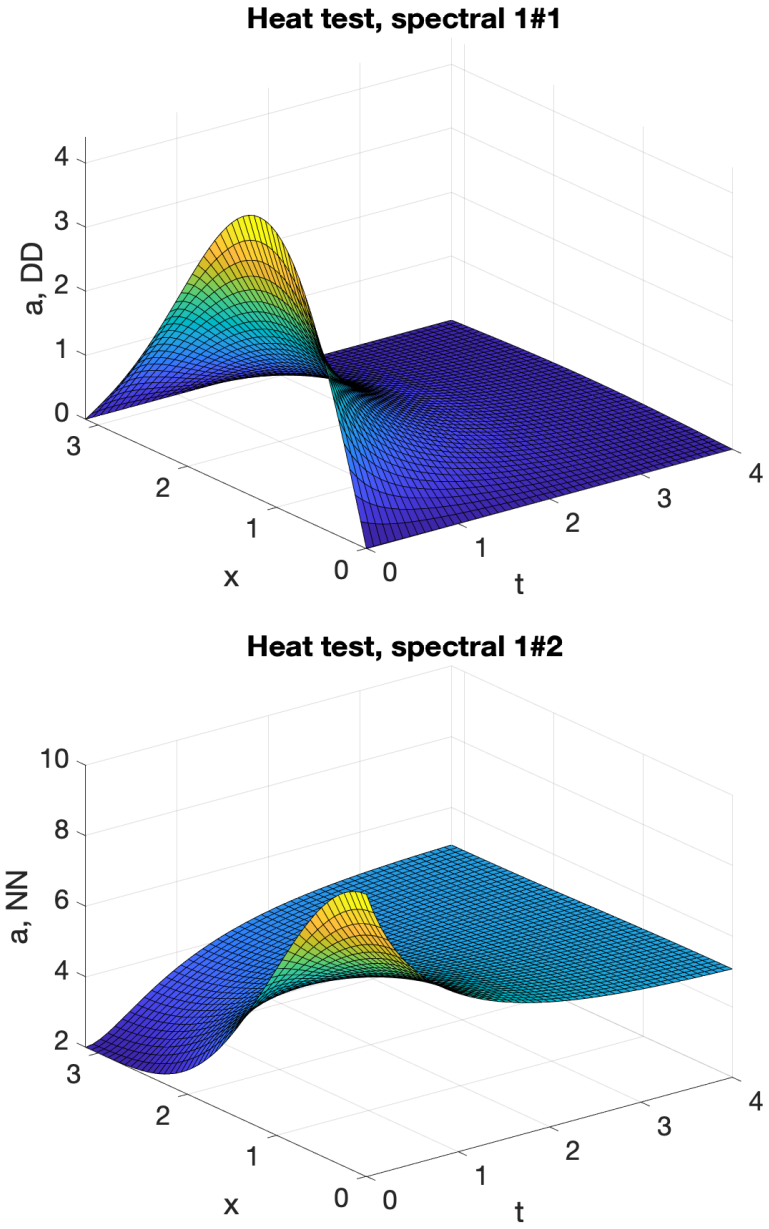

Figure 11.11.: *Top figure: Spectral solution for a as a function of time and position with Dirichlet-Dirichlet boundaries. Bottom figure: Plot of the solution with Neumann-Neumann boundaries.*

11.4.5. Peregrine solitary wave with arbitrary boundary conditions

Peregrine solitary waves are models for isolated large ocean waves. They are modeled as solutions to a (1+1)-dimensional PDE,

$$\frac{\partial a}{\partial t} = i \cdot \left(a \cdot |a|^2 + \frac{1}{2} \frac{\partial^2 a}{\partial x^2} \right) . \tag{11.36}$$

The Peregrine solution on an infinite domain is:

$$a = e^{it} \left(\frac{4\,(1+2it)}{1+4\,(t^2+x^2)} - 1 \right) . \tag{11.37}$$

In the example, this is solved using finite boundary conditions, with initial values and boundary values that correspond to the exact solution.

Notes

- The boundary conditions are specified with *p.boundaries{2},* which is the x-dimension.
- Four different boundary conditions are specified for a four component field.
- Spectral methods are used for accuracy
- No noise is included in the example below, but it can be added
- The boundary values are time-dependent, and are specified with *p.boundfun*
- For improved stability, the integration method is the semi-implicit **MP** method.

Errors

The reported errors in this example are reduced using second order extrapolation, by specifying *p.order =2.* This gives the following RMS average errors for the output intensity, averaged over all four cases:

- Step=0.000621
- Diff=0.00019

The 'Step' error is from subtracting the most accurate global results computed from lower accuracy results. With extrapolation specified in this case, the most accurate results are the extrapolated results, and the less accurate ones are at half the specified time-step. This is averaged over all space-time points, and normalised by the maximum intensity of $|a|^2 = 9$.

Similarly, the 'Diff' error error is from comparing the most accurate global results with the analytic solution. This demonstrates a typical behaviour found in this type of error analysis, where the time-step error is an upper bound to the true error. Due to error propagation, the maximum error occurs at large times, and is greater than the RMS error by about 10×in this case.

All four boundary types used give similar results and errors.

```
function e = Peregrine()
% e = Peregrine() tests xSPDE for a nonlinear Schroedinger equn.
% Using NN,DD,DN,ND boundary values with a spectral method
% Uses time dependent boundary values for a peregrine solution
p.dimensions = 2;
p.noises = 1;
p.fields = 4;
p.order = 2;
p.ranges = [10,10];
p.origins = [-5,-5];
p.points = [51,161];
p.method = @MP;
p.olabels = {'|a|^2 , DD','|a|^2 , NN','|a|^2 , DN','|a|^2 , ND'};
p.boundaries{2} = [1,1;-1,-1;1,-1;-1,1];
p.boundfun = @boundval;
sol = @(p) abs(per(p.x,p.t).^2);
p.initial = @(~,p) per(p.x,p.origins(1))+zeros(4,1,1);
p.compare = {@(p) sol(p),@(p) sol(p),@(p) sol(p),@(p) sol(p)};
p.observe = {@(a,p) a(1,:),@(a,p) a(2,:),...
@(a,p) a(3,:),@(a,p) a(4,:)};
p.output = {@(o,p) abs(o{1}).^2,@(o,p) abs(o{2}).^2,...
@(o,p) abs(o{3}).^2,@(o,p) abs(o{4}).^2};
p.name = 'Peregrine solution';
p.steps = 20;
p.deriv = @(a,w,p) 1i*a.*((conj(a).*a));
p.linear = @(p) 0.5*1i*p.Dx.^2;
e = xspde(p);
end

function [p,varargout] = per(x,t)
% Generates peregrine solutions with alpha = 1/2, beta = A0 = 1

p = exp(1i*t).*(4*(1+2*1i*t)./(1+4.*(t.^2+x.^2))-1);
if nargout == 2
dp = -8*x.*exp(1i*t).*(4*(1+2*1i*t)./(1+4.*(t.^2+x.^2)).^2);
varargout{1} = dp;
end

end
function bound = boundval(~,~,~,p)
% Generates nonzero, time dependent boundary values
[p,dp] = per(p.origins(2),p.t);
bound = {p,p;dp,-dp;p,-dp;dp,p};
end
```

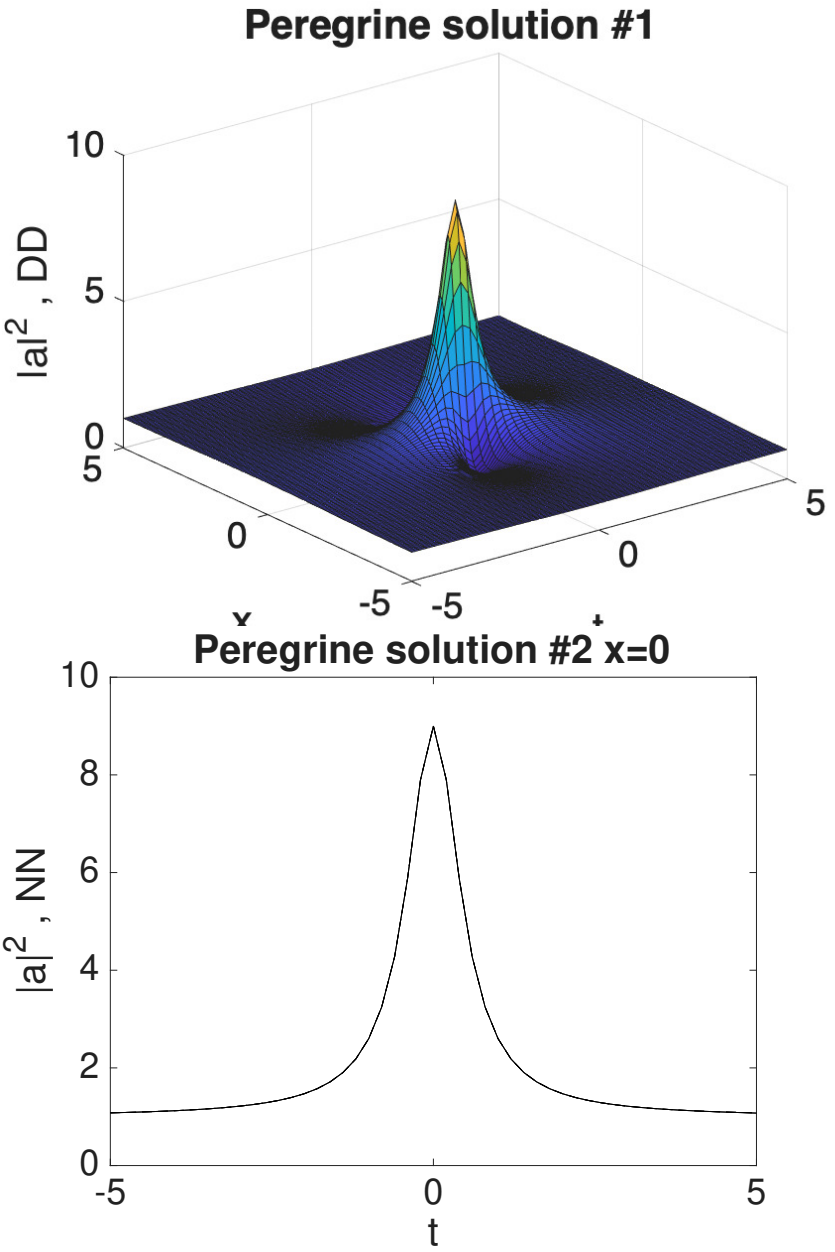

Figure 11.12.: *Top figure: Peregrine solution with Dirichlet-Dirichlet boundaries in space-time.*
Bottom figure: Peregrine solution with Neumann-Neumann boundaries at $x = 0$.

11.5. Projection examples

11.5.1. SDE with catenoid projection

This solves an SDE with 3 field variables $\mathbf{a} = (a_1, a_2, a_3)^T$. The Stratonovich diffusion equation is

$$\frac{\partial \mathbf{a}}{\partial t} = \mathcal{P}_{\mathbf{a}}^{\parallel}[\mathbf{w}] \,, \tag{11.38}$$

where $\mathcal{P}_{\mathbf{a}}^{\parallel}[\cdot]$ indicates a projected onto the surface of a catenoid manifold defined by

$$f = x_1^2 + x_2^2 - \sinh^2(x_3) - 1 = 0 \,. \tag{11.39}$$

The initial condition is given by $\mathbf{a}(o) = (1, 0, 0)^T$. Here $\mathbf{w} = (w_1, w_2, w_3)^T$ consists of 3 independent noise variables

Notes

- This is a projected sde case
- The Euclidean distance from the initial point is computed
- This is compared with the predicted analytic value $\langle R^2 \rangle = 2t$.

```
function [e] = Catenoid
p.name = '3D Catenoid diffusion';
p.iterproj = 3;
p.X0 = [1,0,0]';
p.fields = 3;
p.ranges = 5;
p.points = 51;
p.ensembles = [400, 10];
p.compare{2} = @(p) 2*p.t;
p.deriv = @(a, w, p) w;
p.initial = @(w, p) p.X0;
p.observe{2} = @(a, p) sum((p.X0-a).^2,1);
p.diffplot{2} = 1;
p.function{1} = @(o, p) o{2}.^2;
p.olabels = {'\langle R^2 \rangle^2','\langle R^2 \rangle'};
p.project = @Catproj;
p.method = @MPnproj;
e = xspde(p);
end
```

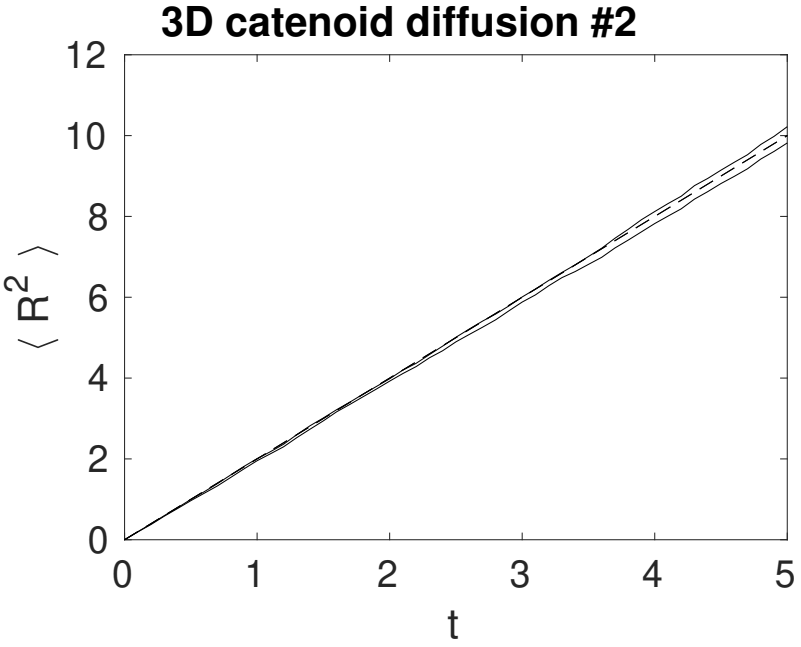

Figure 11.13.: *Computed time evolution of the catenoid squared Euclidean diffusion distance* $|\mathbf{x}_0 - \mathbf{x}(t)|^2$*, where* $\mathbf{x}_0 = (1, 0, 0)^T$*, as a function of time. The solid lines indicate the stochastic error bounds while the dashed line indicates the theoretical prediction.*

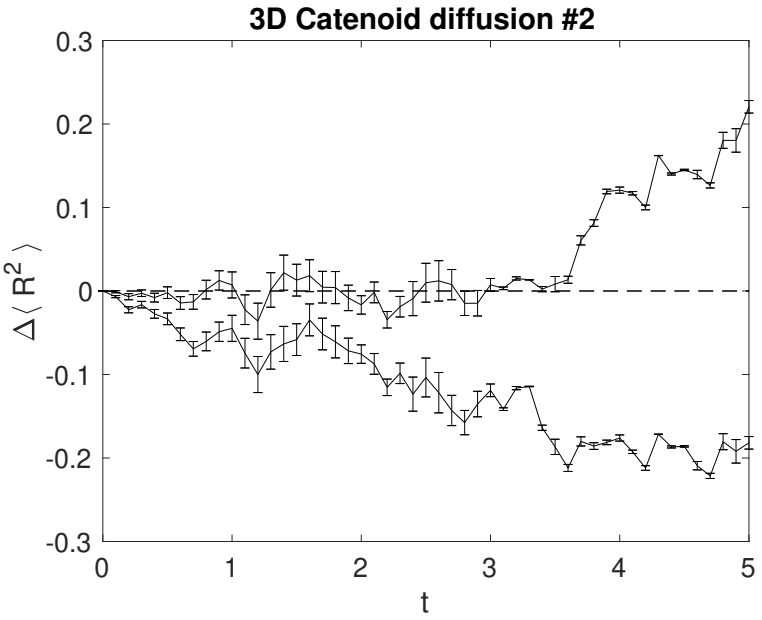

Figure 11.14.: *Differences between the computed time evolution of the catenoid squared Euclidean distance* $|\mathbf{x}_0 - \mathbf{x}(t)|^2$ *and the exact result. The solid lines indicate the stochastic error bounds, error-bars are the time-step errors, while the dashed line indicates the theoretical prediction.*

11.6. Quantum examples

11.6.1. Linear decay, complex SSE

This solves a standard Lindblad master equation for linear decay with initial condition $\psi_j = \delta_{Nj}$ and $L = \sqrt{\gamma}a$, $\hat{H} = \hat{a}^\dagger \hat{a}$; for $N = 6$, $\gamma = 0.25$:

$$\dot{\rho} = -i[\hat{H}, \rho] + 2L\rho L^\dagger - L^\dagger L\rho - \rho L^\dagger L$$

The corresponding Stratonovich SSE is given by:

$$\frac{d}{dt}|\Psi\rangle = -i\hat{H}|\Psi\rangle + \left[\left\langle L^\dagger L\right\rangle_\Psi - L_m^\dagger L_m + \left(\sqrt{2}\xi + 2\left\langle L^\dagger\right\rangle_\Psi\right)(L - \langle L_m\rangle)\right]|\Psi\rangle$$

where:

$$\left\langle \xi_j(t)\,\xi_j^*\left(t'\right)\right\rangle = \delta_{kj}\delta\left(t - t'\right).$$

The function uses the MPS algorithm together with the SSE derivative, and compares it with the solution that

$$\langle \hat{n}\rangle = \langle \hat{n}(0)\rangle\, e^{-2t\kappa}.$$

Both the sparse and functional methods give identical results.

Sparse operator method

```
function [e] = SSElinsp
%Uses SSE for linear decay with sparse methods
p.name = 'SSE-sparse decay, N=6 initially';
p.N = 6;
p.nmax = p.N+1;
p.ranges = 2;
p.a = mkbose(p);
p.quantum = 1;
p.sparse = 1;
p.ensembles = [100,1, 10];
p.gamma{1} = @(p)0.25;
p.compare{1} = @(p) p.N*exp(-2*p.t*p.gamma{1});
p.L{1} = p.a;
p.H = @(p)p.a{1}'*p.a{1};
p.diffplot = 1;
p.initial = @(w,p) [0,0,0,0,0,0,1]';
p.expect{1} = @(p) p.a{1}'*p.a{1};
p.olabels = {'\langle N \rangle','\langle N \rangle'};
e = xsde(p);
end
```

With the sparse method, the function 'mkbose' is used to create the operator matrix cell array '*p.a*', before it is used. These are only generated as needed. For large numbers of modes they can use a large amount of storage, even though they are sparse matrices. The use of p.L{1} indicates the first decay type is a linear loss, but there could be other dissipative processes as well.

The use of *p.quantum=1* shows that it is a stochastic wavefunction problem, while *p.sparse=1* indicates the use of sparse matrices.

Function operator method

```
function [e] = SSElin
%Uses an SSE to solve for a linear decay
p.name = 'SSE linear decay, N=6 initial photons';
p.N = 6;
p.nmax = p.N+1;
p.ranges = 2;
p.quantum = 1;
p.ensembles = [100, 10];
p.gamma{1} = @(p) 0.25;
p.H = @(psi,p) n(1,psi);
p.compare = @(p) p.N*exp(-2*p.t*p.gamma{1});
p.L{1} = @a;
p.diffplot = 1;
p.initial = @(w,psi) [0,0,0,0,0,0,1]';
p.expect = @(psi,p) n(1,psi);
p.olabels = {'\langle N \rangle'};
e = xsde(p);
end
```

With the function method, the function '*mkbose*' is not required. Instead, the effect of the operators is obtained through a function call to the handle '*@a*' . For large numbers of modes this method uses a reduced amount of memory as there is no stored matrix involved in this case.

One cannot simply write *p.H=@n* here, because the Hamiltonian is a function of the wavefunction *psi* and the parameters *p,* while the number operator is a function of the mode number and the wavefunction. For Linblad operators, these arguments are inserted automatically.

The flag *p.diffplot =1* is used by the graphics code to create a plot of the difference between the comparison solution and the simulation.

Note that one can determine the relative size of the sampling errors and step-size errors from the difference plot, although these are also printed out.

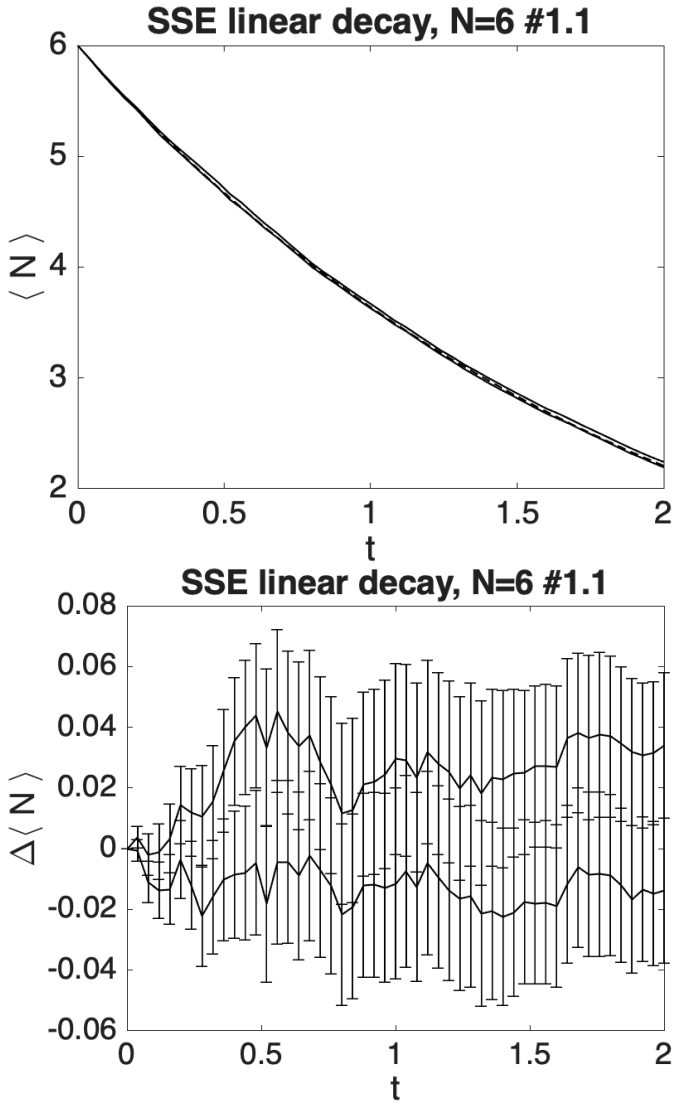

Figure 11.15.: *Example: Linear decay, including a comparison with the exact result, below. The graph shows the sampling error-bars as two parallel lines. The discretization error-bars are less than the minimum, and are not shown.*

11.6.2. Time-dependent decay, real SSE

This solves a Lindblad master equation for linear time-dependent decay with two modes. and real noises, corresponding to homodyne detection. The initial condition is $\psi_j = \delta_{Nj}$ and $L_1 = a$, for $\boldsymbol{N} = [3, 6]$.

The decay rates are:

$$\gamma_1 = [0.5, 1] * t$$

As above, the sparse and functional methods give identical results, but the sparse method is faster. For comparison purposes, the following results are expected:

$$\boldsymbol{N} = [3e^{-t^2/2}, 6e^{-t^2}]$$

Sparse operator method

```
function e = SSElin2spr
%Uses a sparse SSE to solve for a linear two-mode decay
p.name = 'SSE sparse real, N = 3,6';
p.N = 3;
p.Om = 1;
p.noises = 4;
p.ranges = 2;
p.nmax = [p.N+1,2*p.N+1];
p.a = mkbose(p);
p.quantum = 1;
p.sparse = 1;
p.ensembles = [100,1,10];
p.theta{1} = [1,1];
p.gamma{1} = @(p) [0.5,1]*p.t;
p.L{1} = p.a;
p.H = @(p) p.Om*(p.a{1}'*p.a{1}+p.a{2}'*p.a{2});
p.initial = @(~,p) kron([0,0,0,1],[0,0,0,0,0,0,1])';
p.expect{1} = @(p) p.a{1}'*p.a{1};
p.expect{2} = @(p) p.a{2}'*p.a{2};
p.compare{1} = @(p) p.N*exp(-p.t.^2/2);
p.compare{2} = @(p) 2*p.N*exp(-p.t.^2);
p.diffplot = {1,1};
p.olabels = {'< n_1 >','< n_2 >'};
e = xsde(p);
end
```

The use of *p.quantum=1* shows that it is a stochastic wavefunction problem, while *p.sparse=1* indicates sparse matrices, and *p.alpha* = {*[1,1]*} specifies that all channels have real noises.

Function operator method

```
function e = SSElin2r
%Uses a non-sparse SSE to solve for a linear two-mode decay
p.name = 'SSE, N = 3,6';
p.N = 3;
p.Om = 1;
p.ranges = 2;
p.nmax = [p.N+1,2*p.N+1];
p.quantum = 1;
p.ensembles = [100, 10];
p.gamma{1} = @(p)[0.5,1]*p.t;
p.theta{1} = [1,1];
p.L{1} = @a;
p.H = @(psi,p) p.Om*(n(1,psi)+n(2,psi));
p.initial = @(~,p) kron([0,0,0,1]',[0,0,0,0,0,0,1]);
p.expect{1} = @(psi,p) n(1,psi);
p.expect{2} = @(psi,p) n(2,psi);
p.compare{1} = @(p) p.N*exp(-p.t.^2/2);
p.compare{2} = @(p) 2*p.N*exp(-p.t.^2);
p.olabels = {'n_1','n_2'};
e = xsde(p);
end
```

With the function method, the function '*mkbose*' is not required. Instead, the effect of the operators is obtained through a function call to the handles '*@a*' and '*@a*2' . For large numbers of modes this method uses a reduced amount of memory as there is no stored matrix involved in this case.

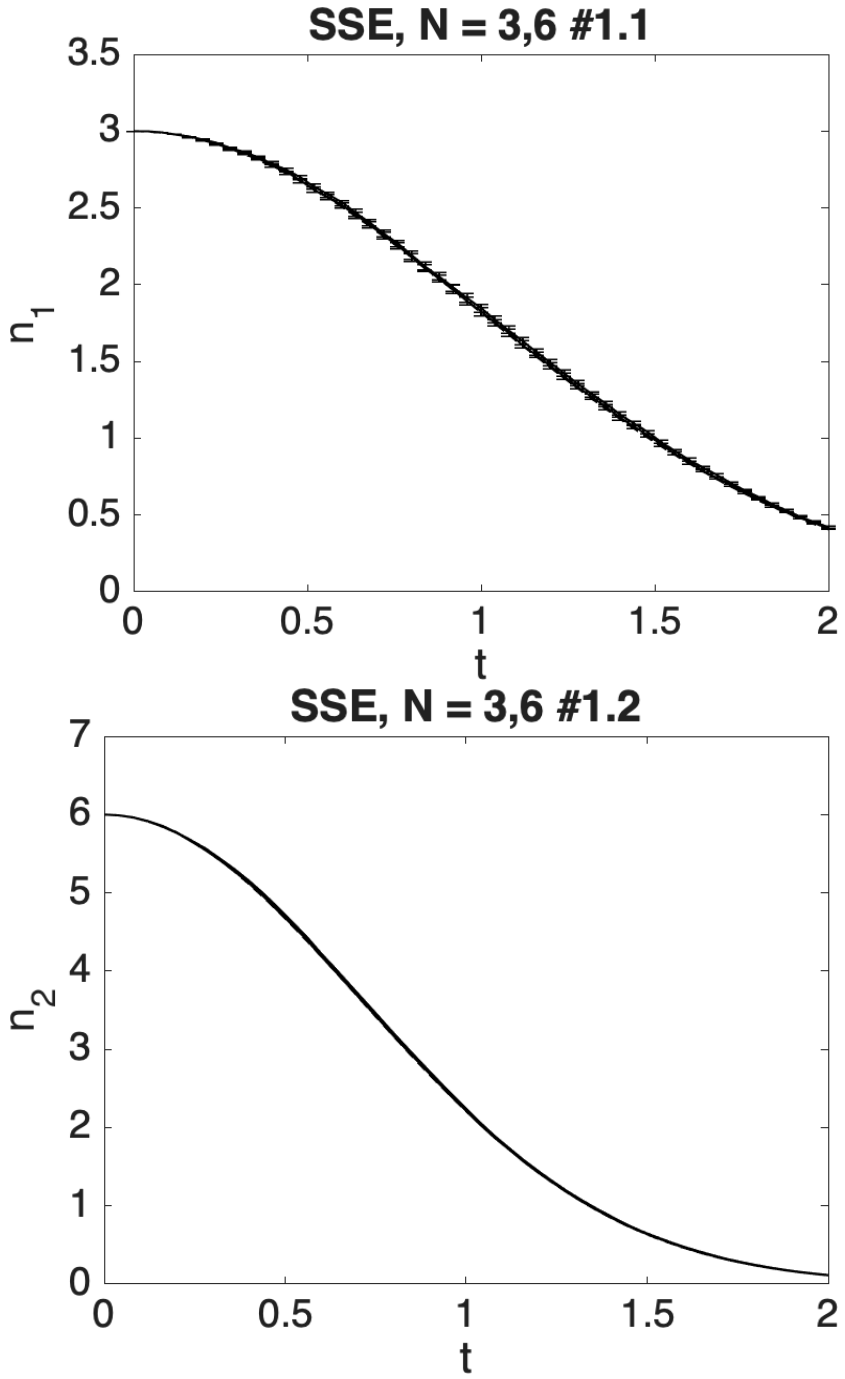

Figure 11.16.: *Example: SSE linear decay, with a time-dependent decay rate.. Top graph has* $N = 3$ *, lower graph has* $N = 6$.

11.6.3. Nonlinear decay, real SSE

This solves a Lindblad master equation for nonlinear decay with two modes and two decay channels. The initial condition is $\psi_j = \delta_{Nj}$ and $L_1 = a$, $L_2 = a^2$, for $N = [3, 6]$.

The decay rates are:

$$\gamma_1 = [0.01, 0.01]$$
$$\gamma_2 = [.5, .25],$$

The function uses the MPS algorithm with the SSE derivative, and has real noise terms. The sparse and functional methods give identical results, but the sparse method is faster.

Sparse operator method

```
function e = SSEnonlin2spr
%Uses a real sparse SSE to solve for nonlinear two-mode decay
p.name = 'Real sparse SSE, M=2, N=3,6';
p.nmax = [4,7];
p.steps = 8;
p.a = mkbose(p);
p.a2 = mkbose(1:2,2,p);
p.ensembles = [10,10,10];
p.quantum = 1;
p.sparse = 1;
p.gamma = {@(p)[0.01,0.01],@(p)[.5,.25]};
p.theta = {[1,1],[1,1]};
p.L = {p.a,p.a2};
p.initial = @(~,p) kron([0,0,0,1],[0,0,0,0,0,0,1])';
p.expect{1} = @(p) p.a{1}'*p.a{1};
p.expect{2} = @(p) p.a{2}'*p.a{2};
p.olabels = {'n_1','n_2'};
e = xsde(p);
end
```

With the sparse method, the function 'mkbose' is used twice to create the operator matrix cell array '*p.a*', and '*p.a*2' before they are used.

The use of *p.quantum=1* shows that it is a stochastic wavefunction problem, while *p.sparse=1* indicates sparse matrices, and *p.alpha* = {*[1,1],[1,1]*} specifies that all channels have real noises.

Function operator method

```
function e = SSEnonlin2r
%Uses an SSE to solve for a linear two-mode decay
p.name = 'Real nonlinear SSE, 2-modes, N = 3,6';
p.nmax = [4,7];
p.steps = 8;
p.ensembles = [10,10,10];
p.quantum = 1;
p.gamma = {@(p)[0.01,0.01],@(p) [.5,.25]};
p.L = {@a,@a2};
p.theta = {[1,1],[1,1]};
p.initial = @(~,p) kron([0,0,0,1]',[0,0,0,0,0,0,1]);
p.expect{1} = @(psi,p) n(1,psi);
p.expect{2} = @(psi,p) n(2,psi);
p.olabels = {'n_1','n_2'};
e = xsde(p);
end
```

With the function method, the function '*mkbose*' is not required. Instead, the effect of the operators is obtained through a function call to the handles '@a' and '@a2' . For large numbers of modes this method uses a reduced amount of memory as there is no stored matrix involved in this case.

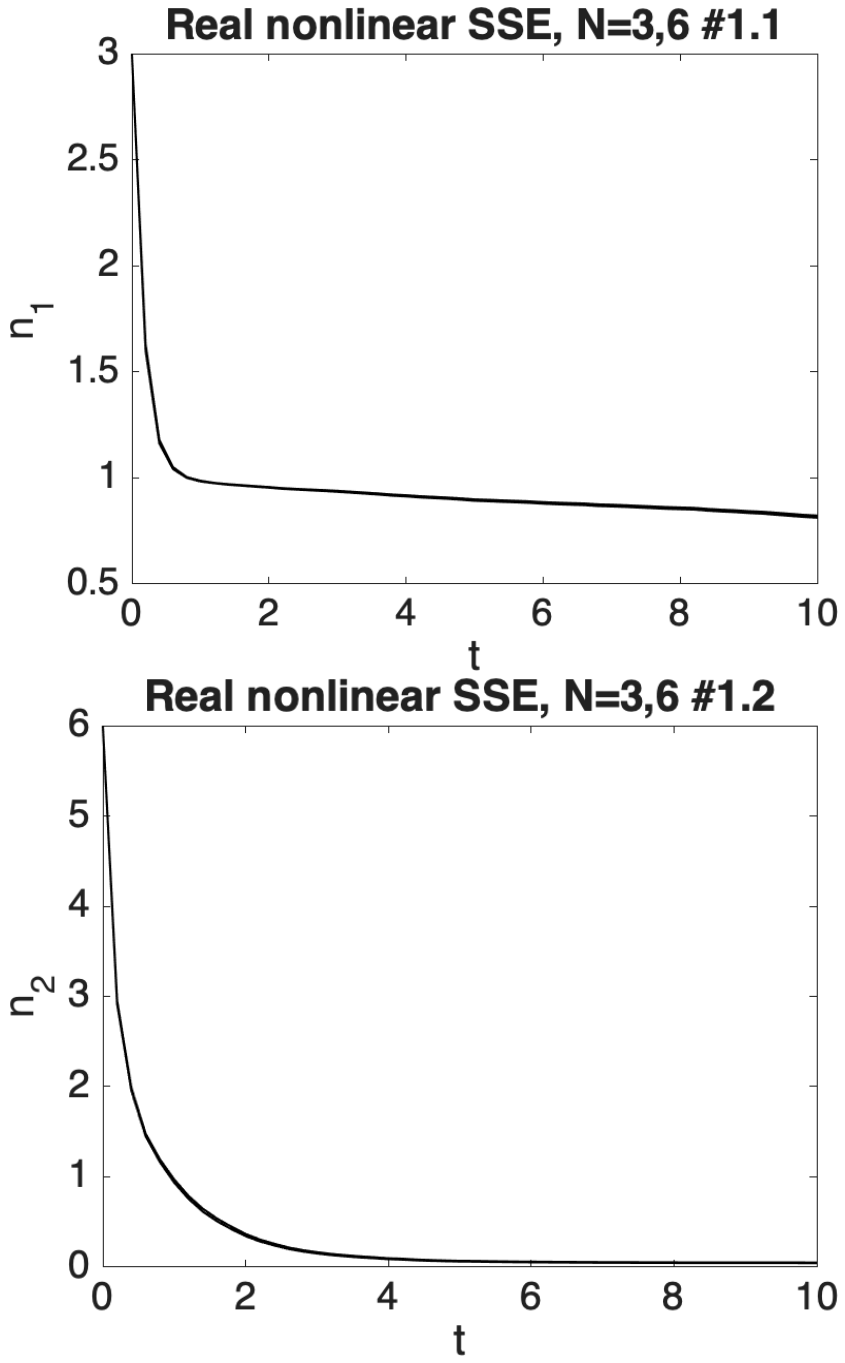

Figure 11.17.: *Example: SSE nonlinear decay, with a small linear decay., real noise and either odd or even number starting points.Top graph has* $N = 3$ *, lower graph has* $N = 6$.

Acknowledgements

We would like to thank the many users and researchers whose feedback was invaluable, including Rodney Polkinghorne, Simon Kiesewetter, Bogdan Opanchuk, King Ng, Alex Dellios, Run Yan Teh, Manushan Thenabadu, Margaret Reid, Jesse van Rhijn and Thomas Rodriguez. This work was funded through the Australian Research Council Discovery Project scheme under Grants DP180102470 and DP190101480. The authors also wish to thank NTT Research and the Templeton Foundation for their financial and technical support.

Bibliography

[1] C. W. Gardiner, *Stochastic Methods: A Handbook for the Natural and Social Sciences*, Springer-Verlag, Berlin, Heidelberg, ISBN 978-3-540-70712-7 (2009). 1, 2.1, 2.2, 2.5, 2.10, 3.3, 4.4

[2] P. D. Drummond and M. Hillery, *The Quantum Theory of Nonlinear Optics*, Cambridge University Press, ISBN 9780511783616, doi:10.1017/CBO9780511783616 (2014). 1, 2.1, 2.9, 2.10, 4.1, 4.4, 6.8.5

[3] P. Langevin, *Sur la théorie du mouvement brownien*, C. R. Acad. Sci. (Paris) **146**, 530 (1908). 1, 2.1

[4] I. Karatzas and S. Shreve, *Brownian motion and stochastic calculus*, doi:10.1007/978-1-4612-0949-2 (1991). 1, 2.1

[5] P. Glasserman, *Monte Carlo Methods in Financial Engineering*, Springer, reprint edn., ISBN 978-0-387-00451-8, doi:10.1007/978-0-387-21617-1 (2010). 1

[6] B. Opanchuk, R. Polkinghorne, O. Fialko, J. Brand and P. D. Drummond, *Quantum simulations of the early universe*, Annalen der Physik **525**(10-11), 866 (2013), doi:10.1002/andp.201300113. 1

[7] K. L. Ng, R. Polkinghorne, B. Opanchuk and P. D. Drummond, *Phase-space representations of thermal bose–einstein condensates*, Journal of Physics A Mathematical General **52**(3) (2019), doi:10.1088/1751-8121/aaeeb1. 1

[8] V. Ramesh, K. Peters and S. Rodriguez, *Arcsine laws of light*, arXiv preprint arXiv:2208.07432 (2022). 1

[9] K. Peters and S. Rodriguez, *Limit cycles and chaos induced by a nonlinearity with memory*, The European Physical Journal Special Topics **231**(3), 247 (2022), doi:10.1140/epjs/s11734-021-00407-3. 1

[10] R. Y. Teh, S. Kiesewetter, M. D. Reid and P. D. Drummond, *Simulation of an optomechanical quantum memory in the nonlinear regime*, Phys. Rev. A **96**, 013854 (2017), doi:10.1103/PhysRevA.96.013854. 1

[11] R. Y. Teh, *Quantum correlations in mesoscopic systems*, Ph.D. thesis, Swinburne University of Technology (2018). 1

[12] S. Kiesewetter and P. D. Drummond, *Phase-space simulations of feedback coherent ising machines*, Optics Letters **47**(3), 649 (2022), doi:10.1364/ol.434114. 1

[13] R. Teh, S. Kiesewetter, P. D. Drummond and M. Reid, *Creation, storage, and retrieval of an optomechanical cat state*, Physical Review A **98**(6), 063814 (2018), doi:10.1103/physreva.98.063814. 1

[14] K. Dechoum, L. Rosales-Zárate and P. D. Drummond, *Critical fluctuations in an optical parametric oscillator: when light behaves like magnetism*, JOSA B **33**(5), 871 (2016), doi:10.1364/josab.33.000871. 1

[15] P. D. Drummond and B. Opanchuk, *Truncated wigner dynamics and conservation laws*, Physical Review A **96**(4), 043616 (2017), doi:10.1103/physreva.96.043616. 1

[16] B. Opanchuk and P. D. Drummond, *One-dimensional bose gas dynamics: Breather relaxation*, Phys. Rev. A **96**, 053628 (2017), doi:10.1103/PhysRevA.96.053628. 1

[17] P. Drummond, *Higher-order stochastic differential equations and the positive wigner function*, Physical Review A **96**(6), 062104 (2017), doi:10.1103/physreva.96.062104. 1

[18] K. L. Ng, B. Opanchuk, M. Thenabadu, M. Reid and P. D. Drummond, *Fate of the false vacuum: Finite temperature, entropy, and topological phase in quantum simulations of the early universe*, PRX Quantum **2**(1), 010350 (2021), doi:10.1103/prxquantum.2.010350. 1

[19] R. R. Joseph, J. van Rhijn and P. D. Drummond, *A hybrid projection algorithm for stochastic differential equations on manifolds*, arXiv preprint arXiv:2112.03391 (2021). 1

[20] P. D. Drummond, *Time evolution with symmetric stochastic action*, Physical Review Research **3**(1), 013240 (2021), doi:10.1103/physrevresearch.3.013240. 1

[21] P. D. Drummond and B. Opanchuk, *Initial states for quantum field simulations in phase space*, Physical Review Research **2**(3), 033304 (2020), doi:10.1103/physrevresearch.2.033304. 1

[22] K. L. Ng, B. Opanchuk, M. D. Reid and P. D. Drummond, *Nonlocal pair correlations in a higher-order bose gas soliton*, Physical review letters **122**(20), 203604 (2019), doi:10.1103/physrevlett.122.203604. 1

[23] J. Busink, P. Ackermans, K. Cognee and S. Rodriguez, *Stochastic light in a cavity: A brownian particle in a scalar potential?*, arXiv preprint arXiv:2107.01414 (2021). 1

[24] K. Peters, Z. Geng, K. Malmir, J. Smith and S. Rodriguez, *Extremely broadband stochastic resonance of light and enhanced energy harvesting enabled by memory effects in the nonlinear response*, Physical Review Letters **126**(21), 213901 (2021), doi:10.1103/physrevlett.126.213901. 1

[25] K. J. Peters and S. R. Rodriguez, *Exceptional precision of a nonlinear optical sensor at a square-root singularity*, Physical Review Letters **129**(1), 013901 (2022), doi:10.1364/np.2022.nptu4f.3. 1

[26] S. Kiesewetter, R. Polkinghorne, B. Opanchuk and P. D. Drummond, *xspde: Extensible software for stochastic equations*, SoftwareX **5**, 12 (2016), doi:10.1016/j.softx.2016.02.001. 1

[27] S. Kiesewetter, R. R. Joseph and P. D. Drummond, *xspde3: Extensible software for stochastic ordinary and partial differential equations*, SciPost Physics Codebases p. 017 (2023). 1

[28] P. D. Drummond and I. K. Mortimer, *Computer simulations of multiplicative stochastic differential equations*, J. Comput. Phys. **93**, 144 (1991), doi:10.1016/0021-9991(90)90131-j. 1, 2.2, 3.3

[29] P. E. Kloeden and E. Platen, *Numerical Solution of Stochastic Differential Equations*, Springer-Verlag, Berlin, doi:10.5194/gmd-2016-45-rc1 (1992). 1, 9.6.1

[30] M. J. Werner and P. D. Drummond, *Robust algorithms for solving stochastic partial differential equations*, J. Comput. Phys. **132**, 312 (1997), doi:10.1006/jcph.1996.5638. 1, 5.5

[31] K. Burrage, P. Burrage, D. J. Higham, P. E. Kloeden and E. Platen, *Comment on "numerical methods for stochastic differential equations"*, Physical Review E **74**(6), 068701 (2006), doi:10.1103/physreve.74.068701. 1, 9.6.1

[32] J. W. Eaton, *Gnu octave and reproducible research*, Journal of Process Control **22**(8), 1433 (2012), doi:10.1016/j.jprocont.2012.04.006. 1

[33] G. Collecutt and P. D. Drummond, *xmds: extensible multi-dimensional simulator*, Computer physics Communications **142**(1-3), 219 (2001), doi:10.1016/s0010-4655(01)00309-5. 1

[34] G. R. Dennis, J. J. Hope and M. T. Johnsson, *Xmds2: Fast, scalable simulation of coupled stochastic partial differential equations*, Computer Physics Communications **184**(1), 201 (2013), doi:10.1016/j.cpc.2012.08.016. 1

[35] N. Wiener, *Generalized harmonic analysis*, Acta mathematica **55**(1), 117 (1930), doi:10.1007/bf02546511. 2.1

[36] K. Itô and H. P. McKean, *Diffusion processes and their sample paths: Reprint of the 1974 edition*, Springer Science & Business Media, doi:10.1007/978-3-642-62025-6 (1996). 2.1

[37] R. L. Stratonovich, *On the theory of non-equilibrium random processes*, Soviet Physics JETP **11**(3) (1960). 2.1, 3.3

[38] N. G. Van Kampen, *Stochastic Processes in Physics and Chemistry*, North Holland, 3rd edn., ISBN 978-0444529657 (2007). 2.1

[39] F. C. Klebaner, *Introduction to stochastic calculus with applications*, World Scientific Publishing Company, doi:978-1848168329 (2012). 2.1

[40] L. Arnold, *Stochastic differential equations: theory and applications*, Folens Publishers, reprint edn., doi:10.1002/zamm.19770570413 (1992). 2.1, 2.2

[41] R. Graham, *Path integral formulation of general diffusion processes*, Zeitschrift für Physik B Condensed Matter **26**(3), 281 (1977), doi:10.1007/BF01312935. 2.1.1

[42] P. D. Drummond, *Forward, backward, and weighted stochastic bridges*, Phys. Rev. E **96**, 042123 (2017), doi:10.1103/PhysRevE.96.042123. 2.1.1

[43] D. J. Higham and P. E. Kloeden, *Numerical methods for nonlinear stochastic differential equations with jumps*, Numerische Mathematik **101**(1), 101 (2005). 2.3

[44] H. Risken, *The Fokker-Planck Equation*, Springer-Verlag, Berlin, 2nd edn., doi:10.1007/978-3-642-61544-3 (1996). 2.5

[45] J. W. Cooley and J. W. Tukey, *An algorithm for the machine calculation of complex fourier series*, Mathematics of computation **19**(90), 297 (1965), doi:10.2307/2003354. 2.8.1

[46] B. Opanchuk, L. Rosales-Zárate, R. Y. Teh, B. J. Dalton, A. Sidorov, P. D. Drummond and M. D. Reid, *Mesoscopic two-mode entangled and steerable states of 40 000 atoms in a Bose-Einstein-condensate interferometer*, Phys. Rev. A **100**, 060102 (2019), doi:10.1103/PhysRevA.100.060102. 2.9, 4.1

[47] B. Opanchuk, L. Rosales-Zárate, M. D. Reid and P. D. Drummond, *Robustness of quantum fourier transform interferometry*, Optics letters **44**(2), 343 (2019), doi:10.1364/OL.44.000343. 2.9, 4.1

[48] E. Schrödinger, *The constant crossover of micro-to macro mechanics*, Naturwissenschaften **14**, 664 (1926). 2.9, 4.1

[49] E. Wigner, *On the Quantum Correction For Thermodynamic Equilibrium*, Phys. Rev. **40**, 749 (1932), doi:10.1103/PhysRev.40.749. 2.9, 4.1

[50] J. E. Moyal, *Quantum mechanics as a statistical theory*, Mathematical Proceedings of the Cambridge Philosophical Society **45**(01), 99 (1949), doi:10.1017/S0305004100000487. 2.9, 4.1

[51] R. J. Glauber, *Coherent and incoherent states of the radiation field*, Phys. Rev. **131**, 2766 (1963), doi:10.1103/PhysRev.131.2766. 2.9, 4.1

[52] W. H. Louisell, *Quantum statistical properties of radiation*, Wiley, New York, ISBN 978-0471523659 (1973). 2.9, 4.1, 6.8.2

[53] C. W. Gardiner and P. Zoller, *Quantum noise: a handbook of Markovian and non-Markovian quantum stochastic methods with applications to quantum optics*, Springer Science & Business Media, ISBN 978-3-540-22301-6 (2004). 2.9, 2.11, 4.1, 4.6, 6.8.2, 6.8.5

[54] H. J. Carmichael, *Statistical methods in quantum optics 1. Master Equations and Fokker-Planck Equations.*, Springer, Berlin, ISBN 978-3-540-54882-9, doi:https://doi.org/10.1007/978-3-662-03875-8 (2002). 2.9, 4.1, 6.8.2

[55] J. F. Corney and P. D. Drummond, *Gaussian quantum operator representation for bosons*, Phys. Rev. A **68**, 063822 (2003), doi:10.1103/PhysRevA.68.063822. 2.9, 4.1

[56] P. A. M. Dirac, *On the analogy between classical and quantum mechanics*, Rev. Mod. Phys. **17**, 195 (1945), doi:10.1103/RevModPhys.17.195. 2.9, 4.1

[57] P. D. Drummond and C. W. Gardiner, *Generalised P-representations in quantum optics*, J. Phys. A **13**, 2353 (1980), doi:10.1088/0305-4470/13/7/018. 2.9.1

[58] S. J. Carter, P. D. Drummond, M. D. Reid and R. M. Shelby, *Squeezing of quantum solitons*, Phys. Rev. Lett. **58**, 1841 (1987), doi:10.1103/PhysRevLett.58.1841. 2.9.2, 4.3

[59] P. P. Deuar and P. D. Drummond, *Gauge P representations for quantum-dynamical problems: Removal of boundary terms*, Phys. Rev. A **66**(3), 033812 (2002), doi:10.1103/PhysRevA.66.033812. 2.9.2, 4.3

[60] M. J. Steel, M. K. Olsen, L. I. Plimak, P. D. Drummond, S. M. Tan, M. J. Collett, D. F. Walls and R. Graham, *Dynamical quantum noise in trapped bose-einstein condensates*, Phys. Rev. A **58**, 4824 (1998), doi:10.1103/PhysRevA.58.4824. 2.9.2, 4.3

[61] S. Kiesewetter, Q. Y. He, P. D. Drummond and M. D. Reid, *Scalable quantum simulation of pulsed entanglement and einstein-podolsky-rosen steering in optomechanics*, Phys. Rev. A **90**, 043805 (2014), doi:10.1103/PhysRevA.90.043805. 2.11, 4.6

[62] R. R. Joseph, J. van Rhijn and P. D. Drummond, *Midpoint projection algorithm for stochastic differential equations on manifolds*, Physical Review E **107**(5) (2023), doi:10.1103/physreve.107.055307. 3.3, 3.3, 9.5

[63] J. Gambetta and H. M. Wiseman, *Non-markovian stochastic schrödinger equations: Generalization to real-valued noise using quantum-measurement theory*, Phys. Rev. A **66**, 012108 (2002), doi:10.1103/PhysRevA.66.012108. 3.3.1

[64] J. Dalibard, *Wave-function approach to dissipative processes in quantum optics*, Physical Review Letters **68**(5), 580 (1992), doi:10.1103/PhysRevLett.68.580. 3.4.3, 9.4

[65] H. Quastel, Jand Spohn, *The one-dimensional kpz equation and its universality class*, Journal of Statistical Physics **160**(4), 965 (2015), doi:https://doi.org/10.1007/s10955-015-1250-9. 5.1

[66] C.-H. Lam and F. G. Shin, *Improved discretization of the kardar-parisi-zhang equation*, Physical Review E **58**(5), 5592 (1998), doi:10.1103/PhysRevE.58.5592. 5.1

[67] P. D. Drummond and A. D. Hardman, *Simulation of Quantum Effects in Raman-Active Waveguides*, Europhys. Lett. **21**, 279 (1993), doi:10.1209/0295-5075/21/3/005. 5.5

[68] W. Bao and J. Shen, *A fourth-order time-splitting laguerre–hermite pseudospectral method for bose–einstein condensates*, SIAM Journal on Scientific Computing **26**(6), 2010 (2005), doi:10.1137/030601211. 5.5.1

[69] P. B. Blakie and M. J. Davis, *Projected gross-pitaevskii equation for harmonically confined bose gases at finite temperature*, Phys. Rev. A **72**, 063608 (2005), doi:10.1103/PhysRevA.72.063608. 5.5.1

[70] A. Jentzen and P. E. Kloeden, *The numerical approximation of stochastic partial differential equations*, Milan Journal of Mathematics **77**, 205 (2009), doi:https://doi.org/10.1007/s00032-009-0100-0. 5.5.1

[71] M. Frigo and S. G. Johnson, *FFTW: An adaptive software architecture for the FFT*, In *Proc. 1998 IEEE Intl. Conf. Acoustics Speech and Signal Processing*, vol. 3, pp. 1381–1384. IEEE, doi:10.1109/ICASSP.1998.681704 (1998). 5.7.1

[72] M. Frigo and S. G. Johnson, *The design and implementation of FFTW3*, Proceedings of the IEEE **93**(2), 216 (2005), doi:10.1109/JPROC.2004.840301, Special issue on "Program Generation, Optimization, and Platform Adaptation". 5.7.1

[73] J. Crank and P. Nicolson, *A practical method for numerical evaluation of solutions of partial differential equations of the heat-conduction type*, In *Mathematical proceedings of the Cambridge philosophical society*, vol. 43, pp. 50–67. Cambridge University Press, doi:10.1017/S0305004100023197 (1947). 5.10.2

[74] F. Black, *The pricing of commodity contracts*, Journal of Financial Economics **3**(1), 167 (1976), doi:https://doi.org/10.1016/0304-405X(76)90024-6. 6.8.4

[75] P. Drummond, K. McNeil and D. Walls, *Non-equilibrium transitions in sub/second harmonic generation*, J. Mod. Opt. **28**(2), 211 (1981), doi:10.1080/713820226. 6.8.5

[76] F.-X. Sun, *Schrödinger cat states and steady states in subharmonic generation with kerr nonlinearities*, Physical Review A **100**(3) (2019), doi:10.1103/PhysRevA.100.033827. 6.8.5

[77] F.-X. Sun, Q. He, Q. Gong, R. Y. Teh, M. D. Reid and P. D. Drummond, *Discrete time symmetry breaking in quantum circuits: exact solutions and tunneling*, New Journal of Physics **21**(9), 093035 (2019), doi:10.1088/1367-2630/ab3f5e. 6.8.5

[78] L. A. Lugiato, C. Oldano, C. Fabre, E. Giacobino and R. J. Horowicz, *Bistability, self-pulsing and chaos in optical parametric oscillators*, Il Nuovo Cimento D **10**(8), 959 (1988), doi:10.1007/bf02450197. 6.8.5

[79] Z. Leghtas, S. Touzard, I. M. Pop, A. Kou, B. Vlastakis, A. Petrenko, K. M. Sliwa, A. Narla, S. Shankar, M. J. Hatridge, M. Reagor, L. Frunzio *et al.*, *Confining the state of light to a quantum manifold by engineered two-photon loss*, Science **347**(6224), 853 (2015), doi:10.1126/science.aaa2085. 6.8.5

[80] A. Marandi, Z. Wang, K. Takata, R. L. Byer and Y. Yamamoto, *Network of time-multiplexed optical parametric oscillators as a coherent ising machine*, Nature Photonics **8**(12), 937 (2014), doi:10.1038/nphoton.2014.249. 6.8.5

[81] P. L. McMahon, A. Marandi, Y. Haribara, R. Hamerly, C. Langrock, S. Tamate, T. Inagaki, H. Takesue, S. Utsunomiya, K. Aihara, R. L. Byer, M. M. Fejer *et al.*, *A fully programmable 100-spin coherent ising machine with all-to-all connections*, Science **354**(6312), 614 (2016), doi:10.1126/science.aah5178. 6.8.5

[82] T. Inagaki, Y. Haribara, K. Igarashi, T. Sonobe, S. Tamate, T. Honjo, A. Marandi, P. L. McMahon, T. Umeki, K. Enbutsu, O. Tadanaga, H. Takenouchi *et al.*, *A coherent ising machine for 2000-node optimization problems*, Science **354**(6312), 603 (2016), doi:10.1126/science.aah4243. 6.8.5

[83] P. D. Drummond, *Quasiprobability methods for nonlinear chemical and optical systems*, Physical Review A **24**(2), 914 (1981), doi:10.1103/PhysRevA.24.914. 6.8.5

[84] P. Kinsler, *Critical fluctuations in the quantum parametric oscillator*, Physical Review A **52**(1), 783 (1995), doi:10.1103/PhysRevA.52.783. 6.8.5

[85] S. Kiesewetter, *Pulsed entanglement of two optomechanical oscillators and furry's hypothesis*, Physical Review Letters **119**(2) (2017), doi:10.1103/PhysRevLett.119.023601. 6.8.5

[86] M. D. Reid, *Demonstration of the einstein-podolsky-rosen paradox using nondegenerate parametric amplification*, Physical Review A **40**(2), 913 (1989), doi:10.1103/PhysRevA.40.913. 6.8.5

[87] M. D. Reid, *Correlations in nondegenerate parametric oscillation: Squeezing in the presence of phase diffusion*, Physical Review A **40**(8), 4493 (1989), doi:10.1103/PhysRevA.40.4493. 6.8.5

[88] L. Rosales-Zárate, *Probabilistic quantum phase-space simulation of bell violations and their dynamical evolution*, Physical Review A **90**(2) (2014), doi:10.1103/PhysRevA.90.022109. 6.8.5

[89] M. D. Reid, *Quantum probabilistic sampling of multipartite 60-qubit bell-inequality violations*, Physical Review A **90**(1) (2014), doi:10.1103/PhysRevA.90.012111. 6.8.5

[90] A. Scott, F. Chu and D. McLaughlin, *The soliton: A new concept in applied science*, Proceedings of the IEEE **61**(10), 1443 (1973), doi:10.1109/proc.1973.9296. 8.10.3

[91] C. W. Gardiner and M. J. Davis, *The stochastic gross–pitaevskii equation: II*, Journal of Physics B: Atomic, Molecular and Optical Physics **36**(23), 4731 (2003), doi:10.1088/0953-4075/36/23/010. 8.10.5

[92] R. Courant and D. Hilbert, *Methods of mathematical physics: partial differential equations*, vol. 2, John Wiley & Sons, ISBN 978-0471504399 (2008). 8.10.6

[93] P. W. Anderson, *Absence of diffusion in certain random lattices*, Physical Review **109**(5), 1492 (1958), doi:10.1103/PhysRev.109.1492. 8.10.7

[94] J. Billy, V. Josse, Z. Zuo, A. Bernard, B. Hambrecht, P. Lugan, D. Clément, L. Sanchez-Palencia, P. Bouyer and A. Aspect, *Direct observation of anderson localization of matter waves in a controlled disorder*, Nature **453**(7197), 891 (2008), doi:10.1038/nature07000. 8.10.7

[95] A. S. Pikovsky, *Destruction of anderson localization by a weak nonlinearity*, Physical Review Letters **100**(9) (2008), doi:10.1103/PhysRevLett.100.094101. 8.10.7

[96] S. Kiesewetter, *Coherent ising machine with quantum feedback: The total and conditional master equation methods*, Physical Review A **106**(2) (2022), doi:10.1103/PhysRevA.106.022409. 9.4

[97] H. J. Carmichael, *Quantum trajectory theory for cascaded open systems*, Physical Review Letters **70**(15), 2273 (1993), doi:10.1103/PhysRevLett.70.2273. 9.4

[98] M. R. Hush, S. S. Szigeti, A. R. R. Carvalho and J. J. Hope, *Controlling spontaneous-emission noise in measurement-based feedback cooling of a bose–einstein condensate*, New Journal of Physics **15**(11), 113060 (2013), doi:10.1088/1367-2630/15/11/113060. 9.4